Analyzing the boundary conditions of the innovative technique of agitation dredging, the Tiamat

Sterre Neumann

TU Delft Delft University of Technology

Port of Rotterdam

Delft University of Technology

Port of Rotterdam

Analyzing the boundary conditions of the innovative technique of agitation dredging, the Tiamat

Author:
Sterre Neumann (4483030)

May 2023

Committee
Dr. Alex Kirichek, TU Delft (Chair)
Dr. ir. Sierd de Vries, TU Delft
Andre van Hassent, Port of Rotterdam

Abstract

Sedimentation is a common issue in navigating through channels, berths and anchorages of many ports and harbors. In order to address this issue, maintenance dredging can be done in three different ways; relocating of the sediments, keeping the sediments in place, or dredging with nature and using the natural currents to remove sediment. Trailing Suction Hopper Dredging (TSHD) is currently the preferred method for dredging and relocating sediment, however, this method is both costly and time-consuming. As a result, more nature-based solutions are becoming attractive, like the Water Injection Dredger (WID). The Underwater Plough (UWP) is another commonly used method usually for dealing with irregularities in the seabed. Harwich Haven Authority has recently developed a new dredging technique called the Tiamat, this is a new agitation dredging method and a potential environmentally friendly solution. The Tiamat employs a water injection technique to dredge sediment from the seabed. The system injects water into the seabed to fluidize the sediments and then uses a suction pump to bring the sediment plume higher in the water column, such that it can be carried away by the natural currents.

To ascertain the boundary conditions for the Tiamat, tests were conducted at three locations in the Port of Rotterdam, each with different sediment classifications (cohesive and non-cohesive), current strengths (high and low), and depths. Because the Tiamat was developed by the Harwich Haven Authority, it was expected that the Tiamat would perform optimally in areas with strong currents and cohesive sediment at moderate depths. In order to evaluate the performance of the Tiamat, two other dredging techniques - WID and UWP - were tested alongside the Tiamat in these areas.

The results of the pilots and monitoring indicated that the boundary conditions for the Tiamat are primarily influenced by the depth, currents, and sediment characteristics. The depth is limited by the length of the discharge pipe. The Tiamat has the highest production rate in cohesive sediments, as production rates tend to be lower in coarser sand sediments due to their higher tendency to settle. For non-cohesive sediments, a highly energetic river with strong currents is necessary to achieve a certain sediment transport distance.

In order to estimate the performance of the Tiamat, the dredging technique is compared with the WID and UWP. Different parameters such as turbidity, sediment transport, development of the top sediment layer, depth limitations, the production rate in different grain sizes, fuel consumption and costs are compared and discussed.

Preface

This report is my master thesis on 'Analyzing the boundary conditions of the innovative technique of agitation dredging, the Tiamat', which performs a research about the Tiamat and compares this agitation dredging method with the Water Injection Dredger and the Underwater Plough. It has been written as a result of my graduation project which finishes the Master of Hydraulic Engineering at the Faculty of Civil Engineering and Geosciences at the Delft University of Technology. This study was initiated by the Port of Rotterdam, as part of the PRISMA program.

I would like to express my gratitude to my graduation committee. Andre van Hassent as my daily supervisor at the Port of Rotterdam, Alex Kirichek as the committee chair and Sierd de Vries. All have provided me with feedback and support. I would also like to thank my colleagues at the Dredging and Construction department at the Port of Rotterdam and especially my colleagues in the Survey department. In addition, I would like to thank Deltares, where I could conduct tests in the laboratory.

Sterre Neumann
Rotterdam, May 2023

Contents

1 Introduction

This chapter provides a brief introduction to the research topic. Starting, in section 1.1, with some background information and the problem definition in section 1.2. Section 1.3, introduces the location for the research, the Port of Rotterdam. Followed by the introduction of three different dredging methods and their working principles; the Underwater Plough in section 1.4, the Water Injection Dredger in section 1.5 and the Tiamat in section 1.6. Findings about previous pilots with the Tiamat, conducted at Harwich Haven are described in section 1.7. At the end of this chapter, the research questions are formulated in section 1.8, followed by the document outline of this thesis in section 1.9.

1.1 Background

Sedimentation is a common issue in the channels, berths and anchorages of many ports and harbors. Sedimentation happens as water-carrying eroded materials slow down, causing the materials to settle out of the water column and on the bottom surface. As a result, the depth of water available for navigation tends to decrease, necessitating dredging to maintain safe passage for ships. Due to this maintenance dredging is needed in ports and harbors. Maintenance dredging refers to the regular removal of accumulated sediment from the beds to preserve the intended depth. This process is necessary to ensure safe and efficient navigation for vessels using these facilities (EL-Hattab, 2014). Maintenance dredging can be done in three different ways; relocation of the sediments to another area, keeping the sediments in place or dredging with nature and using the natural currents to remove the sediment.

Nowadays, Trailing Suction Hopper Dredging (TSHD) is the preferred technique for dredging and relocating sediment (Kirichek et al., 2018b). This dredging technique is designed to remove sediment from the bottom of waterways using a suction pipe, next the sediment will be transferred into a hopper located on board of the vessel. When the hopper is full, the dredger transports the material to a designated disposal site, where it can be safely disposed of. However, since maintenance dredging must be carried out frequently, this method is both costly and time-consuming (IADC, 2014). As a result, Water Injection Dredging (WID) is one of the agitation dredging methods that has gained popularity in recent years. WID is a hydrodynamic dredging technique, its origins are rooted in the Dutch company Koninklijke Volker Stevin (Bergs & Bossinade, 2000). The WID method has proven successfully implemented across various ports. Over recent years, WID vessels have undergone significant advancements. Notably, the latest technological developments in heave compensation and dynamic positioning have enabled highly pre-programmed and efficient dredging operations (Dredgepoint, 2021). Furthermore, the water jetting system has undergone improvements through the integration of a new design that allows for more precise and powerful water jets. As a result, the dredging process has become more effective and efficient. Additionally, to enhance the sustainability of the WID method, the WID vessels have been made hybrid (Redactie Scheepsbouw, 2021). Another dredging method used is an underwater plough (UWP), particularly when there are irregularities present in the seabed. The concept of the UWP was already there around 1970. Since then, the UWP had significant improvements. One of the key innovations has been the integration of advanced technology such as GPS and computerized control systems. With these systems more precise positioning and control of the plough can be achieved, resulting in a more efficient and effective dredging process. This is why this method is still used in various

ports to remove compacted sediments which are difficult to remove (European Patent Office, 1998). But as the popularity of nature-based solutions is growing (Institute for Water Education, 2023) is there a new agitation dredging method, the Tiamat, as a potential nature-based solution. The Tiamat system has been developed by the Harwich Haven Authority and is patented for its unique approach. Unlike other techniques that simply inject water into bottom sediments to fluidize the sediments, the Tiamat system also raises the sediment plume higher in the water column, so currents can take them offshore, thereby is the goal reducing costs and emissions. This could be achieved if Harwich Haven Authority could reduce the use of the TSHD by utilizing Tiamat for dredging. The Tiamat application has already been tested at Harwich Haven and has yielded positive results; but the system is still being improved. Nevertheless, Harwich Haven has already expressed satisfaction with the performance of the Tiamat system (Simpson & Vural, 2022).

1.2 Problem definition

The current method of maintenance dredging requires a significant amount of operational hours and must be conducted with minimal disruption to other vessels in the port. Nevertheless, the used dredging methods are costly and time-consuming. Consequently, costs and production rates are important factors for maintenance dredging in ports. When conducting dredging activities, other factors must be taken into account as well, including water quality (turbidity) and ensuring the nautical guaranteed depth (NGD). To ensure the NGD the nautical bottom (yield stress and nautical density) are needed (PIANC, 2014). For a busy and dynamic port, vessels frequently need to navigate in and out of the area, making these factors critical for dredging operations. Additionally, most ports have a natural environment, including the presence of sea creatures and other wildlife, this is an essential consideration for maintaining healthy water quality. This means that there needs to be a good balance between dredging, maintaining the water quality, and the need to maintain safe and efficient navigation within the port. Also with the current developments, the CO_2 emissions need to be reduced, hence fuel consumption is also an important factor for maintenance dredging. Subsequently, for all these factors, the work that the dredging equipment can do is also important, this depends on its performance at different depths, sediment transport and in which sediments the dredging equipment is productive.

Therefore, alternative dredging methods are being considered with the potential to reduce CO_2 emissions as sediments do not need to be transported via vessel to the disposal location, as, for instance, with the TSHD. However, it remains to be seen if the Tiamat can be applied to different ports as it is currently optimized for use at Harwich Haven Authority. To optimize the Tiamat method for various ports, several factors such as sediment properties, dredging-induced turbidity, nautical density, yield stress, currents and varying depth must be considered. Therefore, it is important to determine what the boundary conditions of the Tiamat are in order to work productively. Additionally, the dredging technique should aim to achieve high production rates, minimize fuel consumption and decrease overall costs.

The Tiamat is not tested in other ports yet. Furthermore, there has been no comparative analysis between the Tiamat and the WID technique or other dredging equipment, for example, the UWP, in the same port. In order to evaluate the performance of Tiamat, it is necessary to conduct a comprehensive comparison of dredging techniques. A comparative comparison can be conducted

by assessing various factors including sediment characteristics, sediment transport, top sediment layers, varying depths, production rates, fuel consumption and costs.

1.3 Port of Rotterdam

In recent years, the amount of dredged material in the port of Rotterdam has increased. This is due to two reasons: the larger container ships (Sánchez et al., 2020) and the siltation upstream (Cox et al., 2020). The Port of Rotterdam is situated in the estuary of the Rhine, Meuse and Scheldt rivers, and is affected by the North Sea's tidal regime (Gandrass & Salomons, 2001). Consequently, the Port of Rotterdam is a tide-dominated port, wherein tides play a crucial role in determining the water level and current flow patterns. In such ports, the rise and fall of the tides have a significant impact on the sediment transport, navigational depth and access to the port (Wells, 1995). In the Port of Rotterdam the tide can vary up to 2 meters and the tidal currents can be powerful, especially in narrow parts of the port (Tiessen et al., 2016). Additionally, the Port of Rotterdam is in the transition zone between a maritime environment and a river environment. Therefore, the harbor is influenced by the river and the sea, leading to the sedimentation of both fluvial and marine types of deposited sediments (Kirichek et al., 2018b). The amount of dredged material is already increased by 4 million m^3 since 2011. In figure 1 the increase in dredging volumes can be found (Kirichek et al., 2018b). With these developments of increasing container ships, the demand for an increase in dredged material would continue like this for the next few years (Bhonsle, 2022).

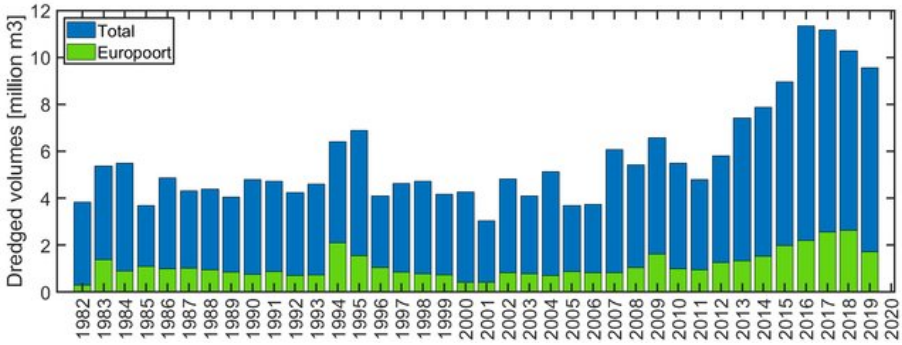

Figure 1: Dredged sediment volumes in the Port of Rotterdam from 1982 until 2020. The blue bars are the total dredged volumes in millions m^3 (Kirichek & Rutgers, 2020).

Another problem for the Port of Rotterdam is that approximately 20 % of the CO_2 emissions in the Netherlands are coming from fossil fuel activities in the Port of Rotterdam (Organization & the Ecoports Foundation, 2020). This situation could potentially pose a long-term issue as the Port of Rotterdam has established emission goals for the future. The goal is already to emit 75% less CO2 in 2025 and 90% less in 2030 than in 2019. This must be a reduction of 45% by 2030 in the use of fuels (especially in dredging and earthmoving) (Ganic, 2022). The CO_2 emissions in 2019 were 25.4 MTonnes and the CO_2 emissions in 2021 were 22.4 MTonnes (Safety4Sea, 2022). Therefore, also for the Port of Rotterdam, more nature-based solutions have become increasingly important (Institute for Water Education, 2023). Due to the fact that dredging has also many impacts on

water quality and nature, leading to climate change (Wasserman et al., 2016).

As a result, the Port of Rotterdam is a good location to test the Tiamat application and determine the boundary conditions of the Tiamat. As the Tiamat is invented in Harwich Haven the different parameters are important. Harwich Haven Authority is a port located between two estuaries and the North Sea; between the Stour estuary and the Orwell estuary. The location of the port in relation to these estuaries has a significant influence on the dynamics of the port, specifically the tidal currents. Despite the notable impact of tides on the water exchange, other non-tidal factors such as sedimentation and wind patterns play a crucial role in shaping the estuarine conditions. Therefore, Harwich Haven Authority is classified as a semi-tide dominated estuary (Spearman & Benson, 2022). Because the agitation dredging technique depends on the currents is this an important difference with the Port of Rotterdam. The Port of Rotterdam relies on the tidal action of the North Sea but also the conditions of the Rhine and the Meuse (Gandrass & Salomons, 2001). Another important difference between the ports is the sediment characteristics and the depths. These parameters are just as important for the Tiamat application to work.

By analyzing the variations in the ports and the distinct features across different areas within the Port of Rotterdam, it is possible to establish the boundary conditions of the Tiamat.

1.4 The Underwater Plough (UWP)

The UWP is still being used today in the Port of Rotterdam. The plough is usually used to perform relatively small dredging operations and for maintenance dredging in tidal basins where amounts of natural sedimentation accumulate. The sediments will be displaced to deeper areas within the port basin. The plough is also used in places where other dredging equipment does not have access, then the material is pushed to one side where it can be further removed by other dredging equipment. This is a less suitable method for environmentally sensitive operations because there is no perfect control over the transport and relocation process.An advantage of this method is that it is low in cost and the material will stay in the natural processes. Overall, the UWP is a versatile and effective dredging technique that is used in a variety of marine environments to maintain navigation channels and ports, as well as to support offshore construction projects (Laboyrie et al., 2018). The working principle of the UWP is that the UWP has pulled over the bottom with a tugboat. There is a cutting device in front of the plough, the sediments that were cut by the device remain in front of the frame and are pushed forward until the device is full or until the sediments reach suspension, where the currents are strong enough to carry away the loosened material. If the material remains in front of the device, it will fall into deeper areas when it is released. Because the plough cut layers in the bottom there will be a turbidity cloud close to the bed. The output rate of an UWP can be up to 2000 m^3/hr (Laboyrie et al., 2018).

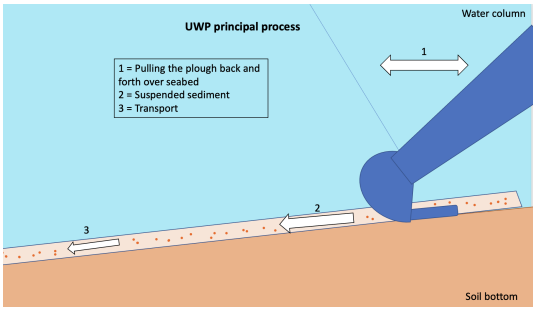

Figure 2: The principle of UWP. Phase 1 is pulling the plough back and forth over the bottom sediments, phase 2 is suspended sediments near the bed and phase 3 is the transport zone.

In figure 2, the different phases are illustrated. The plough is pulled over the bed, phase 1, and the sediments are in suspension in phase 2. In phase 3 the sediments can be transported.

1.5 The Water Injection Dredger (WID)

The principle of WID is that the water injects into the soil at low pressure of 1 to 1.5 bar, this is done with a dredger which can be adjusted close to the bottom surface (Welp et al., 2017). This happens in injection phase number 1 of figure 3. On the dredging vessel, there is a barge with pumps and a manifold. On the beam, there are a couple of nozzles lined up horizontally over an equal distance from the jet, the range of the nozzles can vary between 10 to 15 nozzles. Now that the sediment is mixed with water, fluidization, the strength between the sediment particles is destroyed (Hales, 1995). The suspended sediments have a higher density than the surrounding water. This happens in transition zone 2 of figure 3. In the second stage, swirling up occurs in a hydraulic jump, where the volume of the density current increases and the flow velocity decreases (Kortmann, 1994a). Next, the mix can be transported horizontally due to a gravity-driven density current and this current depends on the tide, the wave and the river currents (Hales, 1995). This happens in the transport zone, number 3, of figure 3. The horizontal displacement can occur due to the combined forces of a pressure difference in the water and the gravitational force. This flow is driven to deeper areas (IADC, 2013).

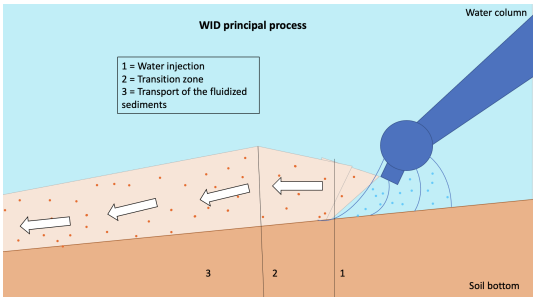

Figure 3: The principle of WID. Phase 1 is the water injection zone, phase 2 is the transition zone and phase 3 is the transport zone.

The balance between injection force, local currents, gravity, and friction forces determines the behavior of a density current (Sigwald et al., 2015). This is shown in figure 4. The behavior of the density current is important for the travel distance of the sediments.

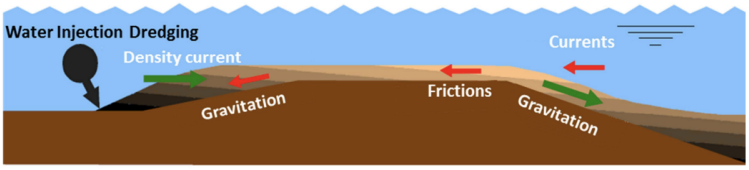

Figure 4: Forces that influence the movement of the density current during WID. (Sigwald et al., 2015)

The vertical travel distance is limited and the sediments tend to form a density current close to the seabed without being suspended in the water column. For the horizontal travel distance, various factors, such as sediment density and composition, bottom morphology, and slope, influence the ultimate distance traveled during transport. Another factor for the horizontal travel distance is the currents, the direction and the velocity (Sigwald et al., 2015). When the WID was invented, a major advantage was that it did not require sediments to be put into the hopper. However, the limitation is that the disposal location should not be far from the dredging location (Verhagen, 2000).

The output rate of the WID depends on the location and the soil characteristics. So in favorable circumstances, the output rate can be higher and in unfavorable circumstances, the output rate can be lower. But the output rates up to 4000 m^3/hr are recorded. The output rate depends on the type of sediment and the current velocity (Laboyrie et al., 2018).

1.6 The Tiamat

The Tiamat is a type of agitation dredging that uses natural currents to transport the sediments further away. The Tiamat application consists of 3 different pumps, as illustrated in figure 5; two water injection pumps located on the sides, which are sourced from Damen DOP 150, and a large central pump, which is a DOP 350. The Damen DOP 150 dredging pump is capable of producing 400 m^3/hr, while the Damen DOP 350 has a significantly higher production capacity of 2400 m^3/hr (Damen, 2022). The two pumps situated on either side of the Tiamat are designed to inject water, whereas the larger central pump serves as a suction pump. All of these pumps are hydraulic pumps, with the power source located on the deck of the vessel. The machine is held on the winch wire of the vessel and it will use the crane on the vessel to rise and lower the hydraulics. This setup offers a significant advantage for the Tiamat, as it can be used on any workboat equipped with a winch and lifting frame (Spearman & Benson, 2022). The illustration of the Tiamat can be found in figure 5, the Tiamat framework has a front plate that conceals the water injection pump beneath it, protecting the nozzles and the pump from potential damage. The Tiamat also features an intake and an outlet located at the end of the framework. The Tiamat uses water from its surrounding environment during two intakes to inject it back into the bottom. At the front of the Tiamat, there is a knife plate, which is capable of slicing through the sediment on the bottom and separating it

into layers. The nozzles situated above the knife plate have been optimized, with the angle of the nozzles adjusted to protrude slightly outwards, rather than straight downwards.

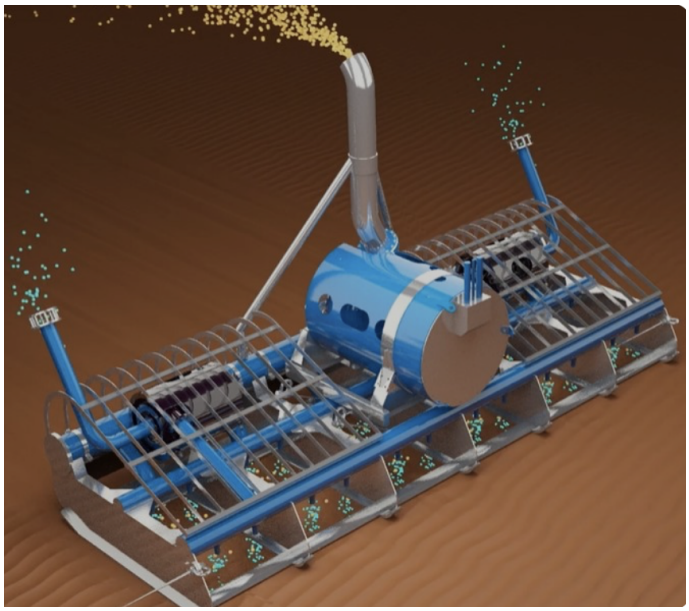

Figure 5: Illustration of the Tiamat system (HHA, 2021).

The Tiamat also injects water into the bottom sediments, like the WID. One main distinction between the Tiamat and the WID pertains to their sediment-handling capabilities. Specifically, the Tiamat is capable of resuspending and pumping sediment in such a way that allows it to be transported by tidal currents. As a result of the height at which the sediment plume is raised above the seabed, will lead to the dispersion of the sediments. This is illustrated in the animation in figure 6. For the Tiamat system, the water intake process is phase 1, which involves utilizing two water inlets to draw water from the surrounding area. The next step is phase 2, during which water is injected into the bottom sediments after the bottom sediments are cut into layers with the knife plate in front of the Tiamat. In phase 3, the sediment dispersion happens, the diluted sediments are transported to a higher part of the water column by means of a discharge pipe and a suction pump located in the center of the Tiamat.

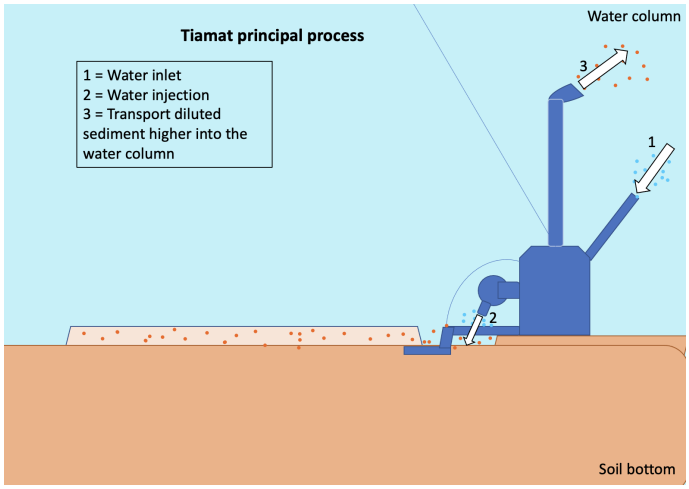

Figure 6: Illustration of the Tiamat system. With phase 1, the water inlet from the surrounding area. Phase 2, is water injection into the sediments with the two water injection pumps and nozzles above the knife plate. And phase 3 is the transportation of the diluted sediments to higher parts of the water column with the use of the discharge pipe and the suction pump.

1.7 Previous pilot tests with the Tiamat in Harwich

The Tiamat application was invented in Harwich and the design of the Tiamat was done in the Netherlands. After designing the Tiamat, the application was tested in Harwich with four trials. For the first pilot trial, turbidity was measured on the bottom of the harbor with sensors in a fixed location, so that turbidity was measured near the bottom. The monitoring time was a couple of months during different dredging operations, so the data could be compared.

First, when the monitoring started, there was no dredging activity in the pilot area. Subsequently, the monitoring was conducted during the deployment of the trailing suction hopper dredger (TSHD). Next, there was another period of a few weeks during which no dredging equipment was in operation. Subsequently, the monitoring was conducted during the operation of the Tiamat dredging vessel, followed by another monitoring phase with no dredgers. This setup with pilot weeks enabled them to evaluate the impact of both dredging equipments on the turbidity. The outcomes of the study were dependent on the composition of sediment present on the bottom, for Harwich, the bottom consists of 90 percent of cohesive sediment and 10 percent non-cohesive sediment (Spearman & Benson, 2022). This means that the results can differ for other harbors. Nevertheless, the results of the turbidity measurements were not desirable for Harwich, they could not detect the plume during monitoring because the plume behind the machine spreads out very quickly. The turbidity levels detected by the monitor sensors were within the range of natural variations and were no longer distinguishable. Stormy weather changes were observed during the monitoring, but they could not tell when the different dredging methods were used.

During the second pilot, Harwich Haven Authority placed turbidity monitors on the research boat

to monitor turbidity levels, while also using the Multibeam Echosounder to assess turbidity. This monitoring approach proved effective and therefore, this method of turbidity measuring is still being used. The monitoring process involves several steps, beginning with the use of an ADCP Backscatter to track the sediment plume. This is followed by Rheotune, density probing, grab sampling, and a particle size distribution (PSD) (Simpson & Vural, 2022).

With this information, Harwich Haven Authority came up with a production rate. The production rate is larger than a typical TSHD productivity per cycle, which is 4,5 hours for this location. This conclusion is only based on data from Harwich Haven Authority (Spearman & Benson, 2022). Based on the different pilot weeks, Harwich has determined that the Tiamat will be more productive when the use of the Tiamat increases. This is due to the bottom sediments being less stiff and more conducive to water injected when used more often.

Currently, the Tiamat is used for maintenance dredging. However, a hopper is required to collect the coarser sediments as the Tiamat does not work optimally at Harwich in coarser sediments.

1.8 Research questions

Further research needs to be done into the Tiamat system. Therefore, the objective of the study can be summarized in the following research questions.

RQ1: What boundary conditions are most suitable for the Tiamat application for tide-dominated ports taking into account factors such as sediment characteristics, sediment transport, turbidity, top sediment layer, different depths, production rate and fuel consumption?

RQ2: How does the Tiamat perform compared to the Water Injection Dredging (WID) and the Underwater Plough (UWP) taking into account factors such as sediment characteristics, sediment transport, turbidity, different depths, production rate, fuel consumption and costs?

RQ3: How is the fuel consumption from the dredging vessels for the long term using the Tiamat compared to using the WID and UWP and how can the production of the Tiamat be improved?

The main objective of this thesis is to get a better understanding of Tiamat application as agitation dredging compared to WID and the UWP.

1.9 Document outline

Chapter 1 gives the introduction for the thesis including the problem definition and the research question. Next, chapter 2 describes the methodology of the research which includes the monitoring tools, the locations for the pilots, and the maintenance dredging methods. In chapter 3, the results for the Tiamat, WID, and UWP are presented, along with initial findings. The sections are categorized into the seven key factors used to compare the maintenance dredging methods, namely sediment transport, turbidity, top sediment layer, depth, production rate, fuel consumption, and

costs. Subsequently, the discussion in chapter 4, where the results, assumptions and limitations of this research are discussed. Followed by the conclusion chapter, where the answers to the research questions are described, this is chapter 5. The final chapter, chapter 6, the recommendations for further research.

2 Methodology

This chapter provides the methodology for monitoring the effect of maintenance dredging carried out with the Tiamat, WID and UWP. The method chosen to establish the boundary conditions of Tiamat involves conducting pilot weeks and monitoring activities. First, in section 2.1, the monitoring tools are presented. With the data of these monitoring tools, the results can be extracted. Second, in section 2.2, the locations of the pilots are described with the properties for each location, this can be used to determine the boundary conditions of the three different dredging methods. After this, in section 2.3, the details of the vessels and the equipment used for the Tiamat, WID and UWP for maintenance dredging pilots are discussed. Section 2.4, gives a brief summery of this chapter in a table. Subsequently, the methods and equations for data processing and estimation of production rates for selected maintenance methods are described in appendix II.

2.1 Monitoring tools

This research involves surveys conducted before, during, and after the dredging process. The focus is not limited to the dredging process itself, and the properties linked to this but also includes other factors such as the extent of sediment transport, the level of turbidity during dredging, the impact on the particle size distribution of the bottom sediments, the depth of the Tiamat, and the impact of dredging on the top layer of sediment at the bottom. To be able to identify this, there will be monitoring during, before and after dredging. This section explains the monitoring tools used for the pilot weeks and where the data is used for. After the description of the different tools, the monitoring plan is presented.

2.1.1 Overview monitoring tools

Table 1 provides an overview of the monitoring tools used during this research, along with the corresponding output generated by each tool.

Tool	**Output**	**Unit**
Multibeam	Water-mud level	m
Silas	100 Pa, 1030 kg/m^3 and 1200 kg/m^3 levels	m
Rheotune	Vertical density and yield stress profiles	Pa, g/L
Swift Turbidity	Turbidity	NTU
ADCP Backscatter	Path of the plume	
Silt profiler	Turbidity and density profile	kg/m^3
Malven Mastersize 2000	Particle size distribution	percentage per μm grain size

Table 1: Monitoring tools used for the pilots with the outputs.

2.1.2 Multibeam echosounder

The new multibeam echosounder has more than a thousand beams and swath opening angles until 160 degrees. The three main types of multibeam echosounder are bathymetry, backscatter and

water column. Bathymetry is the measure of the water depth, this is calculated by the travel time of the acoustic pings. This depends on the sound speed which is needed for the total water column, this can be done with two methods. The first method is called the CTD probe, this device measures the conductivity, the temperature and the pressure. After this, the temperature, depth and salinity are determined and used for the sound speed. The second method is a device that emits a pulse of sound that is reflected to the transducer, measuring the speed of the sound. The backscatter is the intensity of the return signal. This is thus carried out on the part of the sound signal which, after interacting with the seabed and scattering, scatters back in the direction from which it came, in the direction of the sonar. The water column is the total time the ping travels through the water column. The multibeam echosounder uses the principle of acoustic beamforming, so it concentrates on the emission of sound and the reception of sound reflected from the seabed. Because of this principle, the depth and backscatter measurements are known to have come from a specific location. This is why for this method, Multibeam Echosounder, the speed of sound in the ocean is important and this depends on the water temperature, the depth and the salinity (Koop, 2022).

The Teledyne Reson SeaBat T50R Multibeam Echosounder is used for the pilot. The Multibeam Echosounder is capable of determining the depth before dredging, after dredging and during the monitoring weeks. By comparing the depth data before and after dredging, the production rate can be calculated. Additionally, by analyzing the depth measurements during the monitoring period, it is possible to determine the amount of time required for the sediments to settle back.

2.1.3 Silas

The Silas Software offers a comprehensive range of capabilities, from deep penetration to ultra-high resolution. This high-resolution geophysical sub-bottom profiling and imaging software is used in marine geophysical surveys. It is designed to process and interpret acoustic data collected by sub-bottom profilers, which are used to create images of the sediment and rock layers beneath the seafloor (StemaSystems, 1990). The SILAS software is to look for the nautical bottom that is derived from the DensX or the RheoTune and the acoustic data measured by the beam echo-sounder (Kirichek et al., 2018b). The meaning of the nautical bottom is the level at which the physical characteristics of the bottom reach a critical limit beyond which contact with the keel of a vessel results in damage or unacceptable effects on steerability and maneuverability (PIANC, 1997). This depth usually depends on the nautical density, 1200 g/L, within the liquid mud layer. It also depends on the yield strength of the top layer sediments. The reason for this is that navigation through channels and harbors often has a liquid mud layer, which is characterized by low density and weak yield strength (de Boer & Werner, 2016).

Thus, during the pilot, the Silas is used to create a ground map, detect nautical depth, and ascertain the mud layer. The Silas used for the pilot is the Stema Silas: Odom CV200 processor with a 24 kHz transducer.

2.1.4 Rheotune

The RheoTune is a device that is designed to measure the viscosity of fluids. It is a small instrument that uses a vibrating wire sensor on a winch to determine the dynamic viscosity of a fluid (StemaSystems, 2020). This application correlates amplitudes, which are generated by mechanical

vibrations at resonant frequencies, with data sets on density or yield strength from (semi-) fluid muds (Kirichek & Rutgers, 2020). The output of the Rheotune is an in-situ output with a vertical yield stress profile and a vertical density profile.

Thus, for the pilot, the Rheotune is used to determine the development of the mud layer before, during and after dredging. The Stema Rheotune is used for the pilot.

2.1.5 Swift Turbidity

The Swift Turbidity Meter is a compact and portable instrument that uses the winch of the boat to be lowered into the water. The Swift Turbidity meter is designed on a basic optical principle consisting of a light-emitting diode and a photodiode, so the device consists of a sensor and a led. The amount of scattered light is directly related to the turbidity of the water, with higher turbidity resulting in more light scattering. The Swift integrates the physics of optics and electronics with simple mathematical applications for data analysis (Omar & Jafri, 2010). With this technique, the device can measure turbidity levels between 0 and 2000 NTU. NTU is short for Nephelometric Turbidity Unit and is a measure of the turbidity of a liquid (Valeport, 2022).

During the pilot, the Swift Turbidity is used at certain points to make vertical depth profiles of the turbidity. The Valeport Swiftplus Turbidity is used for the pilot.

2.1.6 ADCP Backscatter

The ADCP Backscatter is a feature of an Acoustic Doppler Current Profiler (ADCP) device that measures the strength of an acoustic signal that is reflected to the instrument by particles in the water. When ADCP Backscatter was designed, it was intended to measure velocity profiles (Manik et al., 2020). Additionally, to measure the water velocity, ADCPs can also measure the backscatter of the acoustic signal, which is related to the amount and size of particles in the water. This can be used to estimate the concentration of suspended sediment (Holdaway et al., 2000). Before using the ADCP Backscatter, the ADCP Backscatter needs to be calibrated. This can be done 1 meter above the bottom.

For the pilots, the ADCP Backscatter is only used to follow the sediment plume and to determine how far the sediment plume could come within the natural variations. This means that the objective of using the ADCP Backscatter was to determine the maximum distance over which the sediment plume can be detected and tracked. The Teledyne RDI WHN workhorse 600 kHz sentinal ADCP is used for the pilot.

2.1.7 Silt profiler

The Silt profiler device comprises two optical backscatter sensors with varying ranges of suspended particulate matter (SPM) concentrations, a transmission probe that measures the highest SPM concentrations, a conductivity sensor that computes salinity after adjusting for temperature and pressure, a chlorophyll sensor that measures fluorescence, a pressure sensor, a temperature sensor, and three Niskin water samplers. This instrument was designed for measuring the concentration and size distribution of suspended particles in water. The Silt Profiler with OBS works by using a

laser to illuminate particles in the water and then measuring the amount of light that is scattered back by those particles (Borst et al., 2013). The OBS gives a vertical profile in the water and the Niskin bottles collect samples. After analyzing the water samples the vertical OBS profile will be calibrated.

During the pilots, the Silt profiler is used to calibrate the ADCP Backscatter to determine the concentration of the sediment plume.

2.1.8 OSR

OSR is short for "Operationeel Stromingsmodel Rotterdam". The OSR model has 2 submodels; the 2DH OSR-Haven-model and the 3D OSR-NSC-model (Deltares, 2015). This model can make a map of currents and water levels at a highly detailed scale. The results of the model are used to support port authorities in ensuring ships enter and exit ports safely (Svasek, 2007).

Before the pilot, the OSR-model is employed to compute the velocities across the water column and determine the length of the discharge pipe of the Tiamat. After the pilots the OSR-model is used to generate a map of velocities in the waterway at a specific depth, in order to estimate if the sediments can be transported further by the currents.

2.1.9 Malvern Mastersizer 2000

The Malvern Mastersizer 2000 is a software-controlled plug-and-play dispersion units to deliver the optimal sample presentation necessary for the production of reliable, comparable and high-quality results time after time. The Malvern Master 2000 is a device that is commonly used for particle size distribution (PSD) analysis. It is a laser diffraction instrument that measures the size distribution of particles in a sample by passing a laser beam through the sample and detecting the scattered light at various angles. The resulting data can be used to determine the size distribution of the particles in the sample, as well as other parameters such as particle shape and concentration (Malvern Instrument, 2005).

This is used before and after dredging for the PSD of the locations.

2.1.10 AsteRx-U Marine and iXblue

The AsteRx-U is used on board for navigation. It is a multi-frequency Global Navigation Satellite System (GNSS) receiver. So this device is used for the positioning of the vessel (Septentrio, 2019). Another device on board is the iXBlue, which is an internal navigation system. It provides important position and time data without depending on easily disrupted GNSS signals (Lagaillarde, 2022).

This is useful for the pilots because the areas for the pilot and the points for monitoring are all made and then sent to the surveyor vessel. With this equipment the locations and areas can be used.

2.1.11 Monitoring plan

The week before the Tiamat, the "zero situation" is determined. And this is done again for the WID and UWP pilot week. In figure 7 the table with the monitor plan can be found.

Week	41	42	43	44	45	46	47	48	49	50	51	52	1	2	3	4	5	6	7	8	9
Day	0	1	7	14	21	28	35	42	49	56	63	70	77	84	91	98	105	112	119	126	133
Multibeam		Tiamat						WID									Plough				
SILAS		Tiamat						WID									Plough				
Swift turbidity		Tiamat						WID									Plough				
RheoTune		Tiamat						WID									Plough				
ADCP Backscatter		Tiamat						WID									Plough				
Slib sampler		Tiamat						WID									Plough				
Silt profiler		Tiamat						WID									Plough				
Malven Mastersizer 2000		Tiamat						WID									Plough				

Figure 7: The monitoring plan for this research. The blue section corresponds to the monitoring plan for Tiamat, the orange section represents the monitoring plan for WID, and the yellow section pertains to the monitoring plan for UWP.

The blue boxes in the table indicate monitoring for the Tiamat areas, the red boxes indicate monitoring for the WID areas and the yellow boxes indicate monitoring for the UWP area. However, during week 47, monitoring for all the areas, for the WID and the Tiamat, is done.

2.2 Locations for the maintenance pilot weeks with the Tiamat, WID and UWP

For the selection of suitable locations, an analysis of the Port of Rotterdam area was conducted, focusing on several crucial factors, including current patterns, water depths, sediment characteristics of the bottom and the impact of vessel traffic on the surrounding currents and overall area. Furthermore, the possibility of the fluid mud layer in the area being dispersed throughout the port was considered a significant factor in this analysis. To justify this requirement, a sediment dispersion map was used as a starting point for the assessment of spreading sediment in the water (Royal Haskoning DHV, 2022). This map can change every year; most the tests will be conducted in 2022, so this map is a good reflection. Because the Tiamat involves the suction of sediments from the bottom and subsequent dispersal of the sediments throughout the water column, the mentioned sediment dispersion map is important for this type of dredging. This is also important because permits are needed for this pilot and this will be their first question on the formats. Another essential map for the selection of the locations is the depth map. The chosen locations need to have different water depths to enable testing across a range of depths (PortMaps, 2022). Additionally, the current profiles of the port are made because the sediments must be carried away with the currents for the Tiamat system to work. Therefore, these maps are also used for choosing the locations (Port of Rotterdam, 2022). In addition to the factors previously mentioned, minimizing uncertainty during the pilot is another critical factor for choosing the location. Because the hindrance can significantly impact the quality and accuracy of monitoring data. Therefore, selecting locations with reduced vessel activity is another factor for choosing the locations.

Based on the information and maps referenced above, a series of locations have been selected for the pilots. The specific locations are identified as follows:

- Koolekade (Port of Rotterdam)
- Estuary of the 2e Petroleumhaven (Port of Rotterdam)
- Europahaven (Port of Rotterdam)
- Strandhafen (Port of Hamburg)

The following sections provide a comprehensive overview of the locations involved in the pilots. For additional information regarding the timing of the pilot, please refer to appendix I, which contains the pilot schedules.

Figure 8: This is a map with an overview of the different locations for the three different dredging methods. The pink dots on the map indicate the locations of the Tiamat pilot, the blue dots indicate the locations of the WID pilot, and the yellow dot corresponds to the location of the UWP pilot.

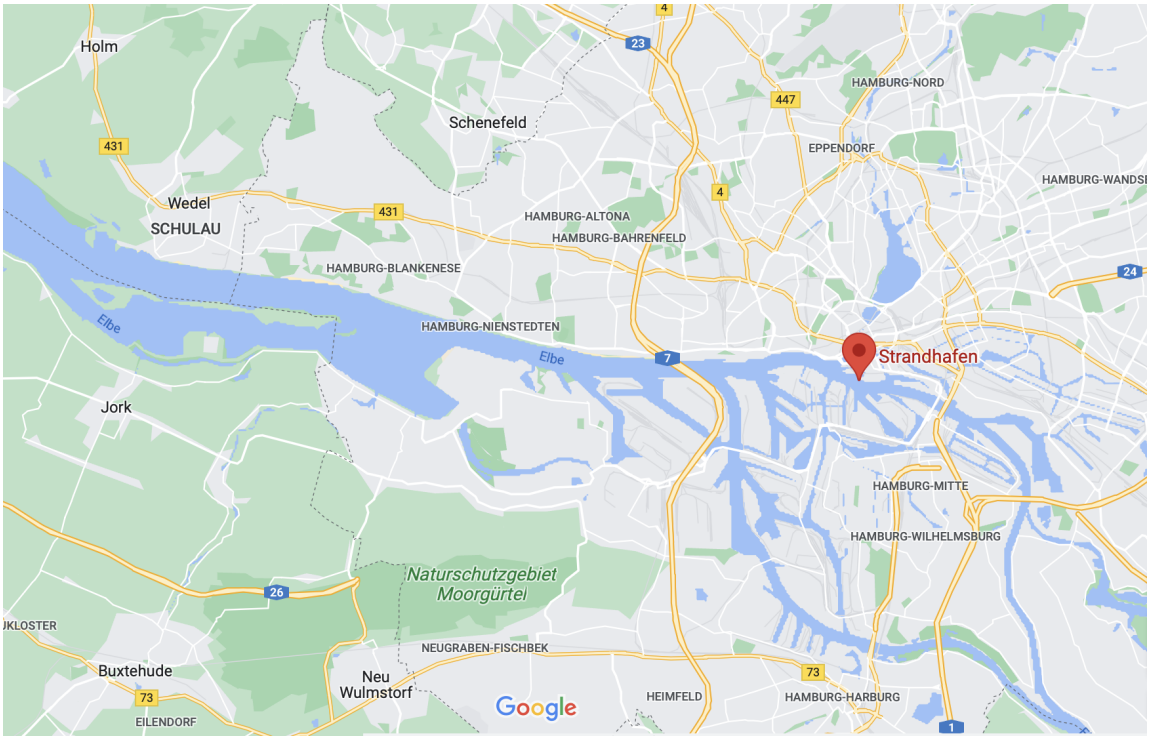

Figure 9: The location for the Tiamat pilot in the Port of Hamburg at the Strandhafen.

In figure 8, an overview is given of the different locations and the different dredging methods for the locations. The locations are chosen to collect data to determine which boundary conditions are most suitable for the use of the dredging methods and in particular the use of the Tiamat. In figure 9, the extra location where the Tiamat is tested is given, this is in the Port of Hamburg at the Strandhafen, therefore these properties are also given in table 2. In table 2, the properties of the different locations can be found. Harwich is also added to the table, because the Tiamat is invented in Harwich, with the information in the table it is easier to compare. The report will utilize abbreviated location names for the remainder of the document. Specifically, EH left and right will refer to Europahaven, KK will stand for Koolekade, PH will represent the estuary of the 2nd Petroleumhaven, and SH will be used for Strandhafen.

Location	Sediment characteristics	Currents	Depth	Salinity
EH left area	Non-cohesive sediment	The lowest current; velocities around 0.1 m/s	Depth around 19 meter with bed level differences	25-30 PSU
EH right area	Non-cohesive sediment	Low current velocity; velocities around 0.22 m/s	Depth around 19 meter	25-32 PSU
KK	Cohesive sediment (with mud layer)	Higher currents; velocities around 0.45 m/s	Depth around 16 meter	5-25 PSU
PH	Cohesive sediment (with the thickest mud layer)	Highest currents; velocities of 0.6 m/s	Depth around 16 meter	3-22 PSU
SH	Cohesive sediment	High currents	Depth around 7 meter	0.5-1 PSU
Harwich	Cohesive sediment	High currents; velocities between 0.05 to 0.9 m/s	Depth around 15 meter	28-33PSU

Table 2: Boundary conditions at selected locations for maintenance pilots.

The differences between the locations are very important; with the differences, the boundary conditions can be determined. The purpose of including table 2 is to highlight the varying conditions at different locations.

2.2.1 Koolekade/2nd Petroleumhaven (Port of Rotterdam)

Harwich Haven Authority, with a depth of approximately 15 meters and a mud layer, closely resembles the sedimentary characteristics of the KK/PH location. Furthermore, the presence of two rivers, the Orwell River and the Stour, at Harwich Haven are most comparable to the waterway and tidal conditions at the KK/PH location. As the Tiamat technology was originally developed and tested in Harwich, it is expected to perform optimally in similar environmental conditions, making the KK/PH location an ideal choice for the pilot, especially for the Tiamat pilot.

The first area, KK, is next to a berth. Due to the unpredictable vessel traffic at the time of testing, it was impractical to conduct the pilot directly in the berth. Therefore, an adjacent area was selected for the pilots. The area is located in a pocket where the seabed on the left side is shallower, providing a realistic representation of how the Tiamat, WID and UWP would operate in a berth. By testing the dredging methods at this location, we can evaluate the performance in an environment where factors such as limited space, potential vessel traffic, and varying seabed conditions play a role.

The second area, PH, is more influenced by currents. There are also a lot of vessels going over the area and the bottom has a thicker mud layer. The potential influence of vessels going over the area was considered. While the presence of ships passing through the area may create some disturbance to the sediment jetted up by the Tiamat.

The dimensions of the areas are 200 meters by 25 meters. This is because turning the vessels take some time, so the idea is to do this as little as possible. In figure 10 the pilot areas for these 2 locations can be found.

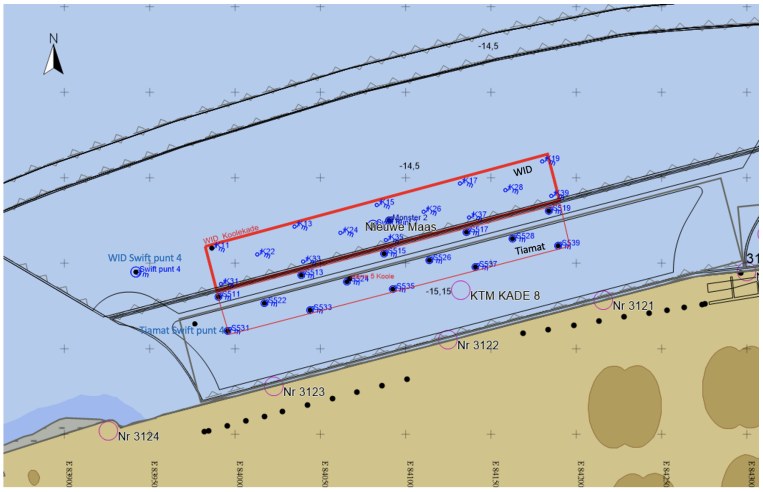

(a) Pilot areas for KK.

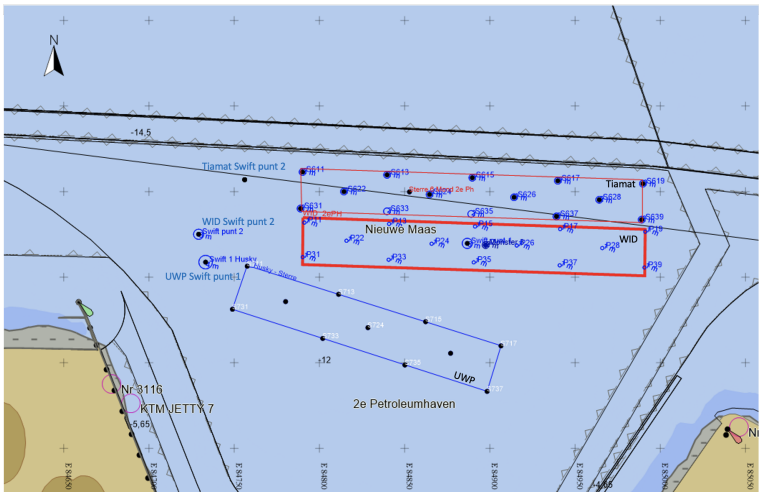

(b) Pilot areas for PH.

Figure 10: The pilot areas at KK and PH for Tiamat, WID and UWP. With the Rheotune points in the pilot areas and the Swift Turbidity points.

Figure 10 displays the designated pilot areas, where the WID pilot areas are positioned adjacent to those of the Tiamat pilot, while the UWP pilot area is adjacent to the WID pilot area. The decision to avoid dredging in the exact same area was made to ensure greater accuracy in comparing sediment characteristics. During the Tiamat pilot, the EH left area was too difficult to dredge for water injection dredging due to sediment classification and low current velocity and is therefore excluded from the other pilots. The presence of too many depth differences in the area combined with insufficient current led to sediment flow toward the nearby area. The UWP will be utilized in the PH location, which is characterized by cohesive sediment. The non-cohesive sediment in EH gives significant challenges in generating a density current using the UWP. The pilot points in the pilot areas are referred to as the Rheotune points with different names, and the Swift Turbidity points are also indicated in figure 10. The Swift Turbidity points are located in the tidal stream near the area.

Based on the results of the PSD, the ideal sediment conditions could be determined for the Tiamat, WID and UWP. First, the reference situation needed to be determined, the PSD of the reference situation can be found in figure 11. For all three methods, a new reference situation is determined. The reference situations can be different due to morphology, channel and currents.

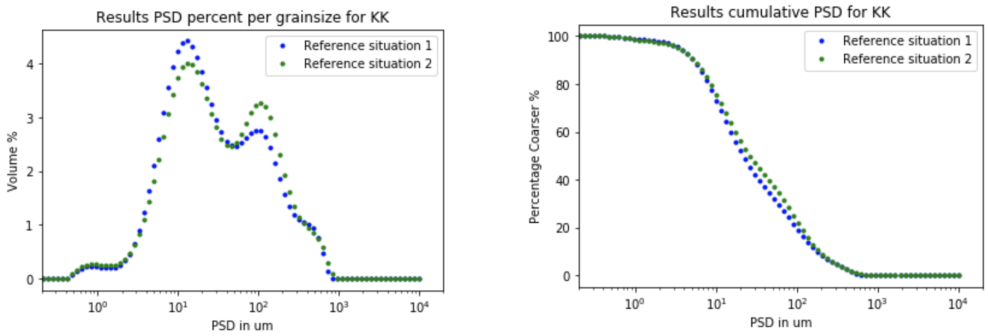

(a) PSD for the reference situations at KK.

(b) Cumulative PSD for the reference situations at KK.

Figure 11: PSD for KK. The blue line represents reference situation 1 and the green line represents the reference situation 2.

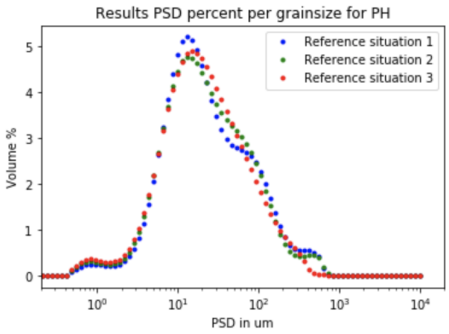

(a) PSD for the reference situations at PH.

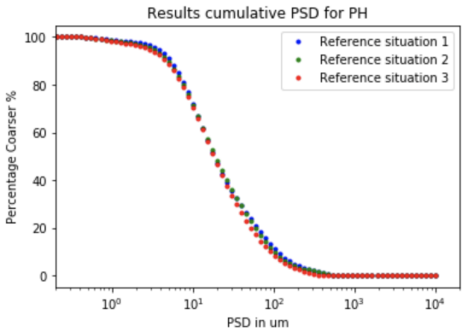

(b) Cumulative PSD for the reference situations at PH.

Figure 12: PSD for PH. The blue line represents reference situation 1, the green line represents the reference situation 2 and the red line represents the reference situation 3.

From figure 12 can be concluded that the three different reference situations are almost the same. The first reference situation is for the Tiamat, the second reference situation is for the WID and the third reference situation is for the UWP.

For the reference situations the D50 is determined; $D50_{KK}$ is 21.5 μm which means medium silt so cohesive sediment. PH has a $D50_{PH}$ of 19.1 μm which means also medium silt so cohesive sediment. More important are the different peaks of the PSD. The peak of the KK is at 14 μm for the first reference situation. The peak for KK for the second reference situation is at 13.18 μm. The peak at PH is at 18 μm, in this area, the thickest mud layer is found.

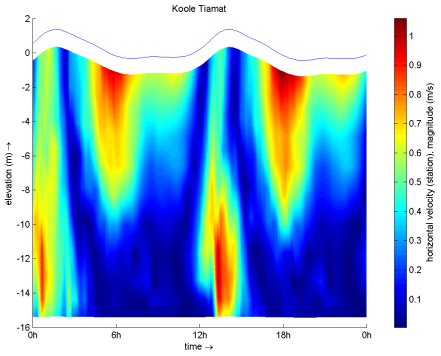

Figure 13: Flow velocities over the water column for the KK and PH location, see figure 8. This particular figure is intended to illustrate a single point in time, encompassing both the incoming and outgoing tide throughout a 24-hour period.

As concluded in figure 13, the highest velocities are in the upper half of the water column. This

is due to the fact that in the Port of Rotterdam, there is a distribution of sweet and saltwater, as well as the marine and river environment of the port. Due to higher salinity levels at the bottom of the water column, there is a greater range of salinity in these areas compared to the higher parts of the water column. The salinity range within KK region falls between 5 and 25 PSU, and, in PH, it varies between 3 and 22 PSU. Figure 13 depicts the water velocity distribution, with the velocities of 1 m/s represented in red.

2.2.2 Europahaven (Port of Rotterdam)

This location has a greater depth, almost 19 meters, with this information the performance in different depths can be determined. The bottom sediment distribution in the area consists primarily of fine sand, with a smaller percentage of mud. This provides an opportunity to evaluate the performance of sediment with varying grain sizes. By testing the technology under different sediment conditions, a better understanding of the capabilities and limitations of the different dredging methods can be gained. Additionally, the currents of this area are different than the currents at the KK/PH location. The currents in EH are influenced by the presence of the Hartelkanaal and Beerkanaal underneath. However, further, into EH, the current velocities are observed to be low. This presents an opportunity to evaluate the optimal current velocity conditions for the Tiamat. By analyzing the current velocities in different areas of the Europahaven, we can determine the most favorable conditions for the Tiamat and WID to perform. Due to the proximity of this location to the sea, the salinity levels are relatively higher, falling within a range of 25 and 32 PSU.

The first area, the one on the right, is next to a berth and closer to the estuary where the currents are around 0.22 m/s. The question is whether it is possible for the sediments to flow to the estuary, if the sediments are there they can be carried with the currents from the Hartelkanaal. If this is not possible the currents can settle down there and then a hopper can pick them up more easily. The second area, the one on the left, has less influence from the currents, the current velocity is around 0.1 m/s. The path to the estuary is longer; the question is whether it is still possible for the sediments to get there or if they settle too quickly. Another feature of this area is that there are depth differences within the area. The question is whether the Tiamat can still suck up the sediments before the WID effect of fluidized sediments operates. The WID principle is that the fluidized sediments flow to the deeper area because of the density current (IADC, 2020). This process is described in subsection 1.5, The Water Injection Dredger (WID). The deeper area is still in this area, so it will be interesting to see how the Tiamat performs in this area. In figure 14 the pilot areas are shown in white. The dimensions are the same as for KK and PH, 200 meters by 25 meters.

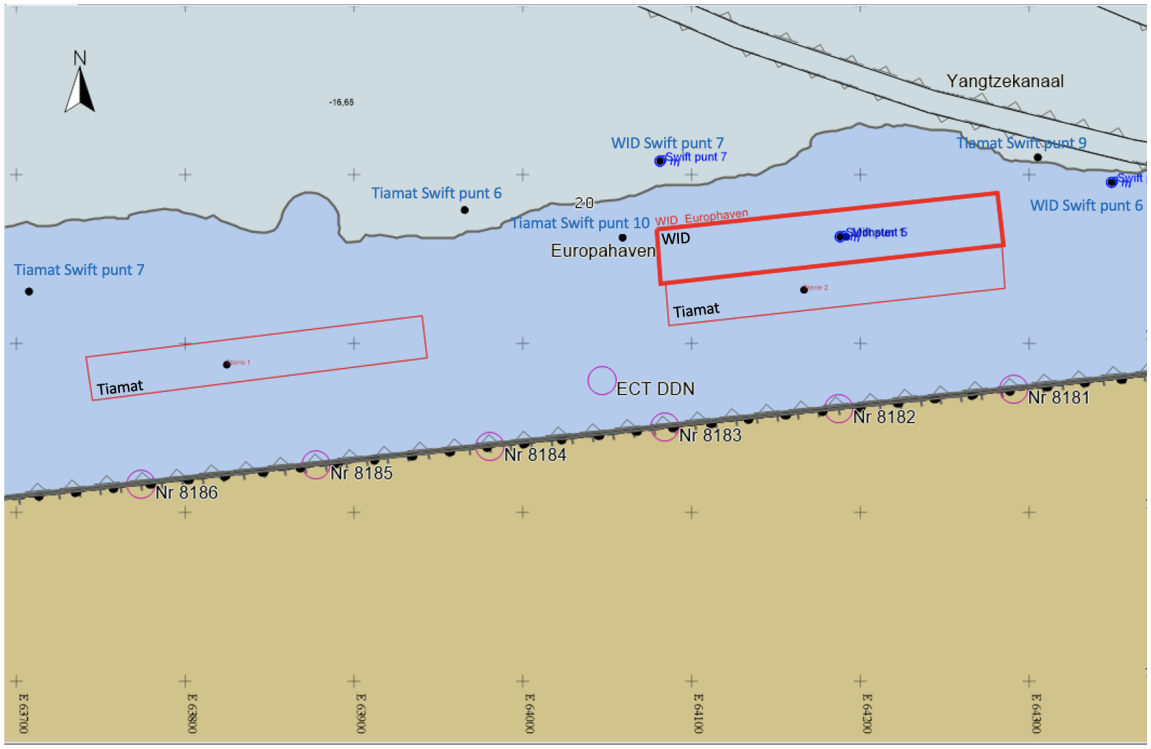

Figure 14: The pilot areas at EH for Tiamat and WID, with the locations of Swift Turbidity.

In figure 14 the areas are displayed. The Swift Turbidity points are also displayed here. For each area in EH, there are two different Swift Turbidity points. One is located in the tidal stream near the area and one is located wider next to the pilot area. The two different reference situations are almost the same. The first reference situation is for the Tiamat and the second reference situation is for the WID.

To determine the optimal sediment for the use of the Tiamat and the WID another PSD is performed for this location, the results are in figure 15.

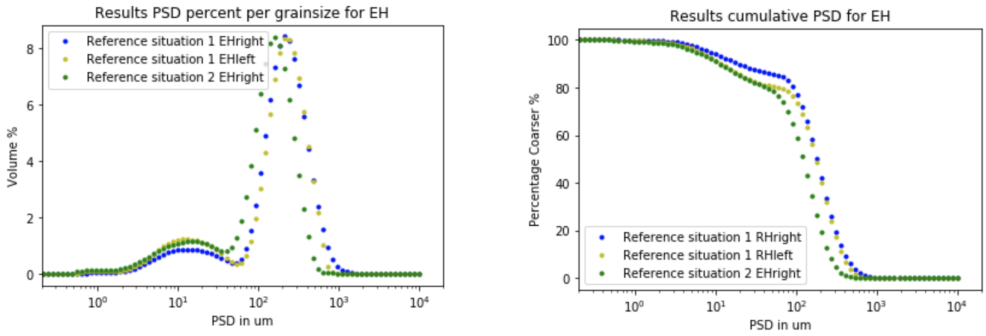

(a) PSD for the reference situations at EH.

(b) Cumulative PSD for the reference situations at EH.

Figure 15: PSD for EH. The blue and yellow lines represent reference situation 1 and the green line represents the reference situation 2.

The D50 is determined out of figure 12; $D50_{EHleft}$ is 177.9 μm this means fine sand so non-cohesive sediment and the $D50_{EHright}$ is 183.4 μm this means also fine sand so non-cohesive sediment. Again, the peaks in the PSD are more important than the D_{50}; the peak of the sediments in EH left and the right area is at 209 μm for the first reference situation. The peak of the sediments for the second reference situation at EH right is at 158.5 μm.

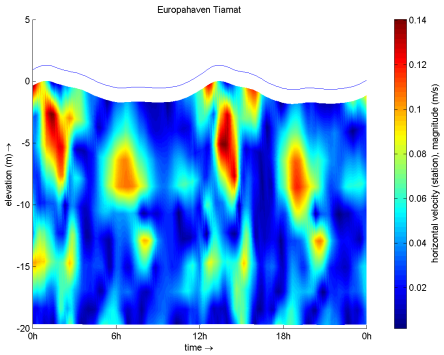

Figure 16: Flow velocities in the water column at EH, see figure 8. This particular figure is intended to illustrate a single point in time, encompassing both the incoming and outgoing tide over the course of a 24-hour period.

In figure 16, the velocities of 0.14 m/s are represented in red, and these are the strongest currents at this location. Near the bed, the velocities are almost zero. Also, recognize the velocities at this location are significantly lower than at the KK and PH looking at both the legend on the right.

2.2.3 Strandhafen (Port of Hamburg)

The last location where only the Tiamat is tested is in the Port of Hamburg at the Strandhafen. In figure 9 an overview of the location is given. This location has a depth of approximately 7 meters. Which is considerably shallower than the Port of Rotterdam, where the depth is twice that of the Port of Hamburg. Additionally, there is minimal salinity in the port of Hamburg. The SH location in Hamburg is characterized by strong currents and medium silt sediments, which means cohesive sediments, making it a suitable location for the implementation of Tiamat, as it shares similar features with Harwich.

2.3 Maintenance equipment

Three different dredging methods will be employed during the pilot weeks. The first method to be used is the Tiamat application, followed by the WID method, and finally the UWP method.

2.3.1 Tiamat

Initially, the length of the discharge pipe for the Tiamat had to be determined for the Port of Rotterdam, taking into account the different depths of EH and KK/PH. As a result, two different lengths were selected. First for KK and PH, the velocity profile over the water column is important and can be found in figure 13. By analyzing the velocity distribution, a 10-meter discharge pipe was found most appropriate to effectively transport sediment through the water column with the currents. With the length of the discharge pipe of 10 meters, the sediments will be spread out on a level of 12 meters above the bottom. For EH, the velocities of 0.14 m/s are represented in red, in figure 16, therefore a discharge pipe of 12 meters is chosen. This will bring the sediments 14 meters above the bottom.

For SH, some changes have been made to the Tiamat. An overview of the different Tiamat applications can be found in figure 17.

(a) Tiamat application for the Port of Rotterdam.

(b) Tiamat application for Hamburg.

Figure 17: The two different Tiamat applications for the Port of Hamburg and the Port of Rotterdam.

Figure 17 shows a notable difference between the Tiamat application from SH and Rotterdam,

particularly in the orientation of the discharge pipe head and the direction of the plume. Another factor that is different for Hamburg compared to Rotterdam is the difference in depth.

Figure 18: The Barney vessel with the Tiamat application, in the Port of Rotterdam.

The boat used for the Tiamat is called the Barney, figure 18. This vessel is used at Rotterdam and at SH. The Barney has a length of 30.02 meters and a with of 13.45 meters (MarineTraffic, 2021). The Tiamat has a width of 8 meters (de Haas, 2022).

2.3.2 WID

The Mersey is used for Water Injection Dredging in the Port of Rotterdam. The biggest difference between the Mersey and the Barney (the vessel with the Tiamat) is that the Mersey has worked in the Port of Rotterdam many times before. So the crew would already know better how to work optimally here and this is a big advantage for the production rate.

Figure 19: One of the Water Injection Dredging vessels used in the Port of Rotterdam, the Mersey (Alamy Stock Photo, 2021).

The vessel used for the pilot, the Mersey is displayed in figure 19. The Mersey has a length of 43.07 meters and a width of 9.7 meters. The WID device has a width of 12 meters (MarineTraffic, 2021).

As already introduced in the introduction section, WID is the method in which water is injected into the soil, this is done by using pumps with a set of nozzles on a horizontal jet bar to spray water at low pressure, 1-1.5 bar, into the seabed (IADC, 2020). The injected water fluidizes the fine sediments creating a density current. This density current, with the sediments in it, moves away from the dredged area under the influence of natural forces. The sediments move to deeper areas or move to high energy environments where the sediments will be part of the natural transport again (Van Oord, 2020). One of the most important differences between the Tiamat and WID is the Tiamat can bring the sediment plume higher up in the water column, dispersion of the sediments, allowing them to be carried away by the currents. The WID application of the Mersey has also the capability to jet sediments up into the water column. This can be achieved by opening two of the nozzles on top of the horizontal bar, which allows water to be jetted up into the water column, the top nozzles are displayed in the sketch of the top view of the WID bar in figure 20. Both nozzles have a diameter of 195 mm. It is not possible to adjust the pressure without also changing the pressure of the nozzles that are directed toward the bed. To regulate the flow, the diameter of the nozzles can be changed. However, changing the diameter will also affect the flow of the nozzles that direct toward the bed. Given that the Port of Rotterdam experiences the highest currents in the upper layer of the water column, it is expected that sediments can be raised to this height and carried away with the currents. This process of water injection dredging is called the agitation function of the WID, which has not been previously tested in the Port of Rotterdam. As such, this technique will be applied only in one of the testing areas, at PH, while the other areas, EH and KK, will be dredged using the standard WID. The results will provide insight into the efficiency of the agitation function in the port of Rotterdam and enable to compare its performance with the standard WID approach.

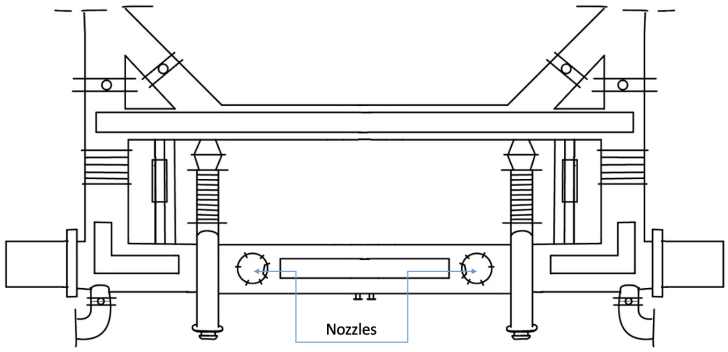

Figure 20: Sketch of the top view of the WID bar. With the nozzles which are opening for the WID with agitation function.

2.3.3 UWP

The method for the UWP used in PH for the pilot, involves using an underwater plough to pull over the bottom and cut the bottom sediments into layers of 10 centimeters, creating a back-and-forth motion that generates a density current. To ensure the removal of sediments from the port, this method can only be performed during an outgoing tide when the currents are strong enough to carry the sediments out. Consequently, the pilot must be executed within a specific time frame. The efficiency of this method in generating a density current has been verified through testing at the Deltares laboratory and has been successfully implemented in the port of Hamburg. However, its effectiveness in the port of Rotterdam is still untested.

The plough boat used in the Port of Rotterdam is called the Husky, figure 21.

Figure 21: Husky, the UWP vessel (MarineTraffic, 2021).

The Husky has a length of 24 meters and a width of 8 meters (van den Bosch, 2023).

2.3.4 Summery

Table 3 gives a brief summary of the different dredging methods, their working principle, and the pilot locations. More details about the different working principles are given more clearly in animation in figures 2, 3 and 6.

Type of dredging	**Working principle**	**Pilot locations**
Tiamat	Sediment dispersal occurs higher in the water column through a suction pump and a discharge pipe. The sediment plume is carried by natural currents.	EH left, EH right, KK, PH and SH
WID	Fluidizes the sediments with a water injection pump and travels with the density current to the deeper areas.	EH right and KK
WID with agitation function	Fluidizes the sediments and jet them up with the two nozzles on top of the WID bar. Allowing them to be carried away with the natural currents.	PH
UWP	Plough is pulling over the bed back and forth trying to create a density current.	PH

Table 3: An overview of the three maintenance dredging equipment and the pilot test locations.

3 Results

This chapter presents the outcomes of the pilot weeks with the three different dredging methods. Several figures are included to depict the results and conclusions are drawn from the data. To answer the research questions and compare the different dredging methods the 7 most important factors for this research are described. First, in section 3.1, the sediment characteristics before and after dredging are described, as well as the distance that these sediments traveled. Second, in section 3.2, the turbidity caused during dredging is described and the time it takes to return to the reference situation after dredging. Subsequently, in section 3.3, the top sediment layer and the development of the density of this layer are discussed. After this, in section 3.4, a comparison is made of the depth profiles before and after dredging and the longitude depth profiles before, after and during the monitoring weeks are shown. These profiles also indicate the sedimentation during the monitoring weeks in the pilot area. Combining these data the production rates can be calculated, in section 3.5, and next the fuel consumption, in section 3.6, and the costs, in section 3.7, per cubic meter of shifted sediment. At the end of this chapter, in section 3.8, there is a brief summary presented in the form of a table that summarizes the results.

3.1 Sediment transport

In order to assess which sediments are most suitable for the dredging methods, a particle size distribution (PSD) analysis will be conducted. The PSD before and after dredging will be plotted on a single graph to compare. The samples before dredging are taken 5 days before dredging and the samples after dredging are taken around 7 days after dredging.

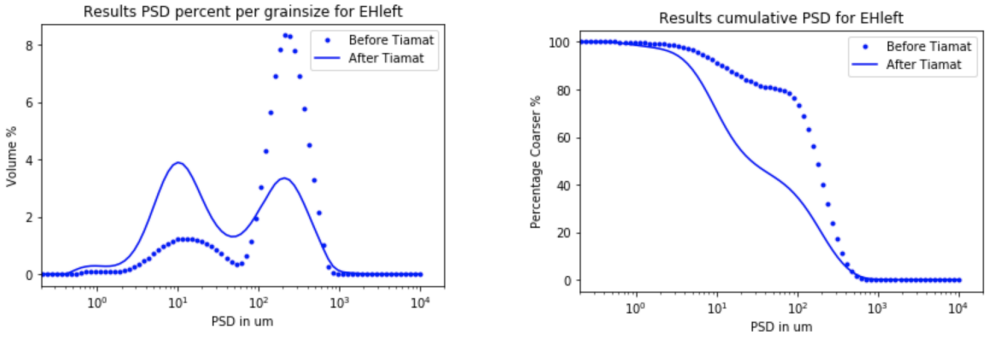

(a) PSD for EH left area.

(b) Cumulative PSD for EH left area.

Figure 22: PSD for EH left area, see figure 8 for the locations. The blue line represents the PSD for the Tiamat. The dashed line represents PSD before dredging and the solid line the PSD after dredging.

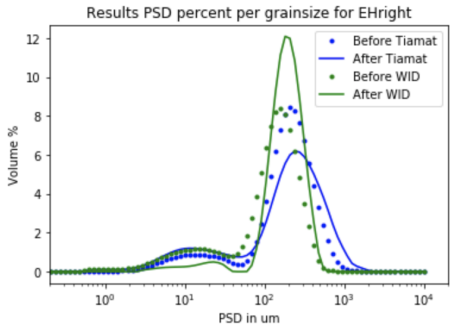

(a) PSD for EH right area.

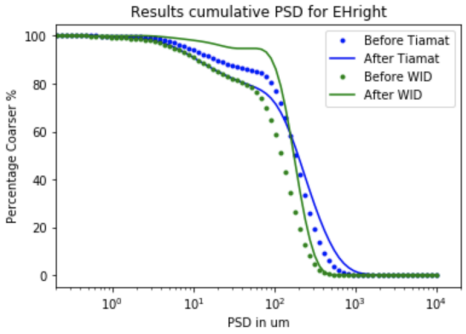

(b) Cumulative PSD for EH right area.

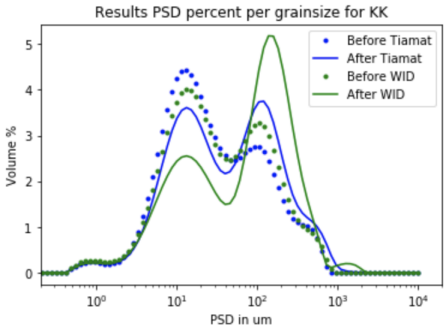

(c) PSD for KK.

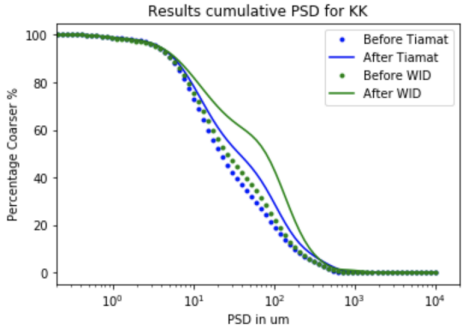

(d) Cumulative PSD for KK.

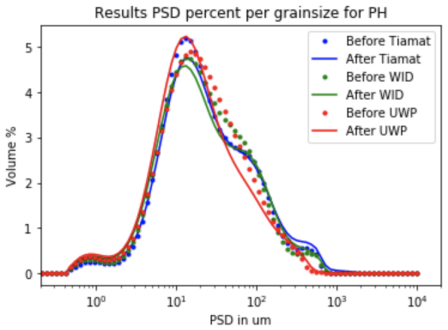

(e) PSD for PH.

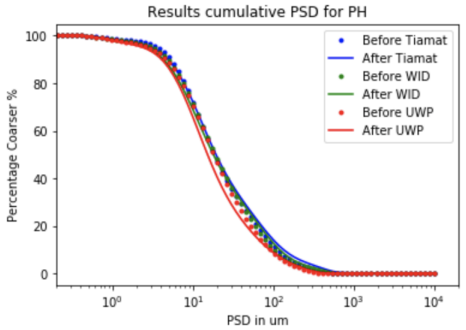

(f) Cumulative PSD for PH.

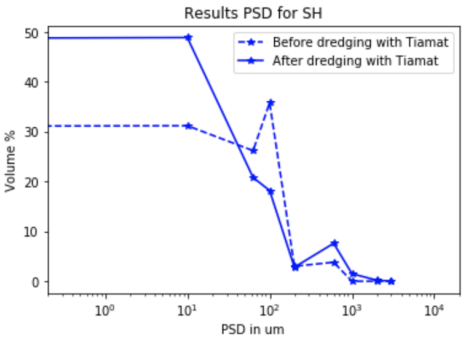

(g) PSD for SH

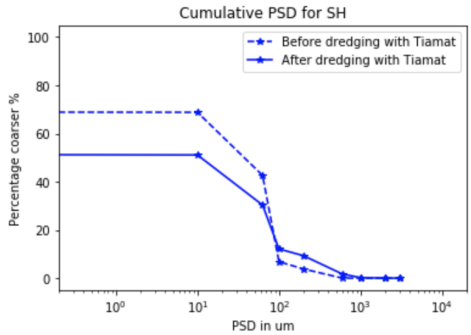

(h) Cumulative PSD for SH.

Figure 23: PSD for EH right, KK, PH and SH, see figures 8 and 9 for the locations. The blue line represents the PSD for the Tiamat, the green line represents the PSD for the WID and the red line represents the PSD for the UWP. The dashed line represents PSD before dredging and the solid line the PSD after dredging.

For the PSD of the Tiamat shown in figure 22a, the peak of the coarser sediment size has decreased and the peak of the finer sediments,13.4 μm, has increased. As obtained from figure 22b, there are fewer coarser sediments than before dredging this is for the location with more bed elevation differences within the area, a greater depth, and non-cohesive sediments. The decreased occurrence of coarse sediments and increase of finer sediments in this particular area may be attributed to bed elevation differences, wherein fluidized sediment flows have caused sediments to relocate from shallower areas towards deeper ones. When Tiamat initially slices through the layers of sediments, the starting depth is the most shallow depth. Subsequently, the water is injected into the sediments and the sediments become fluidized. Because of the bed level elevation within the area and the low currents, these fluidized flows manifest in a downward direction along the slope (Kortmann, 1994b) and settle within the deeper parts of the area. The finer sediments are easier to transport and therefore these finer sediments are displaced in the deeper part of the area, as the sample is taken in the deeper part of the pilot area.

For the PSD of the Tiamat shown in figures 23a and 23b, for non-cohesive sediments and great depth, the peak of the sediment size has shifted slightly, but mainly the top of the peak has become wider. Before using the Tiamat most of the sediments had a size of 209 μm and after dredging most of the sediments have a size of 240 μm. There is also a larger percentage of sediments with a size of 410 μm and greater. Coarser sediments have a tendency to settle faster compared to finer sediments. This faster settling rate results in a shorter distance of travel for the coarser sediments, and some may settle within the same area, leaving the coarser particles behind in the area (Winterwerp & van Kesteren, 2004).

For the PSD of the WID shown in figures 23a and 23b, the peak of the sediment size has shifted slightly, with a notable increase in the quantity of coarser sediment particles and a decrease in the quantity of finer sediments. Before dredging the majority of sediments had a size of 158.5 μm, while after dredging, most sediments had a size of 181.97 μm. Additionally, a larger percentage of sediments with a size of 170 μm or greater were observed after dredging with the WID. During dredging with the WID coarser sediments tend to be left behind and the finer sediments can be transported more easily. Coarser sediments typically have a higher critical shear stress, which means that stronger currents are required to initiate sediment transport (Wilcock, 1994). Therefore the finer sediments are more easily transported. As water is injected into the bottom sediment, the sand and fines become fluidized, resulting in the fine-grained sediments being carried away. This is because the finer sediments can pass between the sand particles when they are fluidized, and transported with the density current. Consequently, there are fewer fine sediments and more coarser sediments after dredging. As a result, the fine-grained sediments are lost at a faster rate, which leads to the seabed becoming even more non-cohesive after repeated use of the WID. This is an important consideration in the production of the WID process for dredging coarser sediments, as higher flow velocities may be required to successfully remove these sediments from a given area. Therefore, the figure suggests that the WID is not able to create a density flow in coarser sediments. The flow velocities generated by the WID process are derived from both the close-to-the-bottom velocities and the density current (Winterwerp et al., 2002). The close-to-bottom velocities are generated by the propeller jets of the WID vessel and the currents already in the water, in this situation, the saltwater current will be dominant, while density currents are created by the sediment in the water flowing downhill due to gravity. These various factors help determine the flow rates

that can mobilize and carry sediments away from the dredging area.

For the PSD of the Tiamat shown in figure 23c, the peak of the coarser sediments has again shifted slightly, and the peak has increased. Nevertheless, the peak of the finer sediments has decreased. The peak of the coarser sediments is shifted from 14 μm to 16.14 μm and note that the peak has increased as well. There is also a larger percentage of sediments with a size of 189 μm and greater. This area is located in a pocket area and there are cohesive sediments with more currents. The Tiamat injects water into the bottom sediments and disperses the sediments higher in the water column. The finer sediments can be carried away with the currents more easily and this will result in a decrease in finer sediments after dredging. But for the coarser sediments, the currents will require more time to move them along, and the coarser sediments are settling faster. Due to the pocket area, the outgoing tidal stream has a shallower depth. As a result, the coarser sediments do not have sufficient time to be transported further before they reach the shallower depth. This causes them to settle back down within the pilot area. This will result in an increase in coarser sediments.

The PSD of the WID shown in figure 23c, indicates that the peak of the coarser sediments has shifted slightly, with a notable increase in the quantity of coarser sediment particles. Before dredging the majority of sediments had a size of 13.18 μm, while after dredging with the WID, most sediments had a size of 138.04 μm. Additionally, out of figure 23d, a larger percentage of sediments between the size of 183 μm and 605 μm were observed after dredging with the WID. The percentage of fine-grained sediments decreases a lot after WID, this is already remarkable for using the WID one time, this means when using the WID more often for this location in a pocket area with cohesive sediments and higher currents, the sediment can become non-cohesive. Due to the fact that the WID is flushing the fine-grained sediments from the bed. It is likely that both sediment characteristics, cohesive and non-cohesive sediments, show a similar conclusion when looking at the PSD since they were both dredged with the normal WID function. As already confirmed the WID works better in fine-grained sediments. This is because fine-grained sediments typically are more easily fluidized and have better transport characteristics compared to coarser-grained sediment. As a consequence of this disparity, the finer sediment fraction is transported to greater distances and more rapidly than the coarser fraction. This can cause the PSD of the sediment bed to become segregated over time as a direct consequence of dredging activities (Kirichek et al., 2021).

The PSD of the Tiamat and the WID shown in figures 23e and 23f show almost the same trend, the PSD before and after dredging show that there was a minimal change in sediment sizes before and after dredging. This location has cohesive sediments, high currents and a medium depth. Also note that the WID dredging method used at this location was different from the normal WID, as the agitation function was also employed. This type of WID is more comparable with the Tiamat dredging method. The suspended sediments jetted upwards until the height is achieved where the currents carry them away. Due to the cohesive sediments and the stronger currents in the higher part of the water column, the sediments are transported out of the area. It is possible that the settling of coarser sediments occurred faster than for the finer sediments outside of the pilot area, which could explain why there was not a significant change observed in the PSD before and after dredging with the WID and the Tiamat. For the Tiamat, it is most likely it works the best under these circumstances because this location was most similar to Harwich Haven. For the WID and the Tiamat, there is a larger percentage of sediments with a size of 192 μm and greater.

Once again, it can be observed in figures 23g and 23h, that after dredging with the Tiamat in SH, there is a higher proportion of coarser sediments and a decrease in finer sediments. There are particularly more coarser sediments with a grain size of 200 μm or larger. Again, for this location, it was easier to transport the finer sediments with the natural currents.

Analyzing the PSD for the UWP shown in figures 23e and 23f, it is observed that the peak of the sediments has increased slightly in amplitude and has also become narrower. The finer particles and flocs on top of the bed are displaced and this will make the PSD more narrow. However, the overall PSD remains relatively unchanged. The sediment peak was observed to be at 13.18 μm both before and after dredging, which can be explained by the action of the UWP that displaces sediments of different sizes by pulling the plough over the bed. Therefore, all the sediments are pulled out of the pilot area.

Analyzing all the PSDs; the sediment peaks for Tiamat were observed to shift towards 195-210 μm, while those for WID shifted towards 190 μm. The WID uses an injection pump which will fluidize the sediments of the bed. The fluidized sediments can travel in the density current to the deeper areas. For the WID with agitation function, the fluidized sediments are also jetted upward, reaching a higher level in the water column than just the bed. The Tiamat has the ability to bring the sediment plume higher in the water column due to the employment of a suction pump and a discharge pipe. Again, there could be concluded that the coarser sediments tend to settle faster and coarser sediments have a higher critical shear stress, it is more difficult to transport the coarser sediments using the Tiamat or WID. This means that for non-cohesive sediments, a highly energetic river is needed to carry the sediments. For the Port of Rotterdam means that the production is significantly lower when using it for coarser sediments. However, this is not a limitation for the UWP, as its plough mechanism is able to displace all sediments irrespective of their size. But by creating the density current with the UWP, finer sediments are needed. This is confirmed with the PSD, the peak for UWP did not exhibit any shift. This means that the Tiamat and the WID do not have a high production rate for bottom sediments with a coarser grain size than 190-210 μm.

For determining where the sediments are going during dredging the ADCP Backscatter is used. The ADCP Backscatter is only used to track the sediment plume until the natural sediment variation and the dredged material can no longer be separated. The objective of using the ADCP Backscatter was to determine the maximum distance over which the sediment plume can be detected and tracked. Figures 24 and 25 have been generated from the ADCP Backscatter data in the current stream profiles for the day of the pilot during the outgoing tide. The corresponding graphs from the ADCP Backscatter can be found in appendix III and more current stream profiles over time can be found in appendix IV.

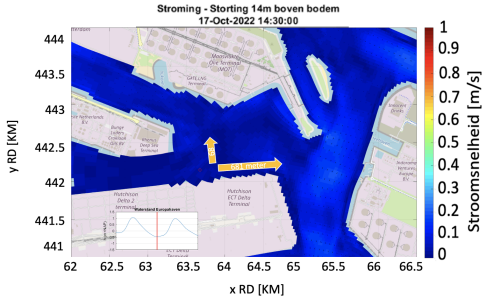

(a) EH left area dredged with the Tiamat; non-cohesive sediments, great depth with different bed elevations and the lowest currents. In the direction of the outgoing tide the sediment plume could be tracked up to a distance of 681 meters, and its width next to the area could be tracked up to 68 meters.

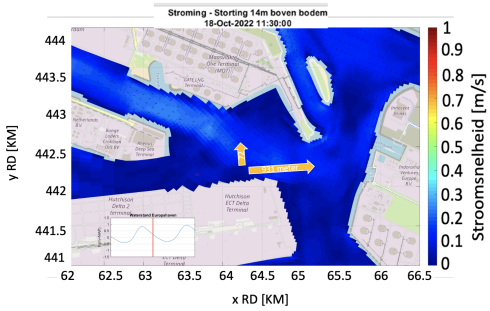

(b) EH right area dredged with the Tiamat; non-cohesive sediments, great depth and the low current velocities. In the direction of the outgoing tide the sediment plume could be tracked up to a distance of 931 meters, and its width next to the area could be tracked up to 72 meters.

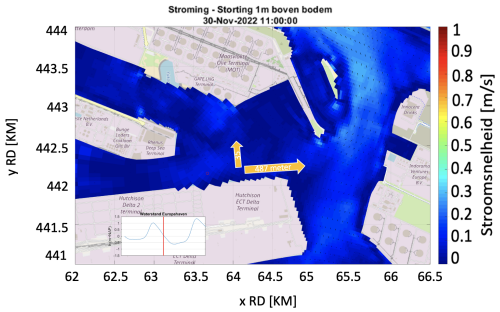

(c) EH right area dredged with WID; non-cohesive sediments, great depth and low current velocities. In the direction of the outgoing tide, the sediment plume could be tracked up to a distance of 487 meters, and its width next to the area could be tracked up to 35 meters.

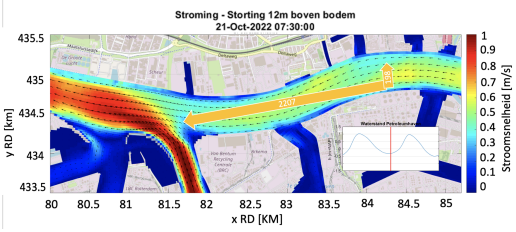

(d) KK dredged with the Tiamat; cohesive sediments, medium depth in a pocket area and high current velocities. In the direction of the outgoing tide, the sediment plume could be tracked up to a distance of 2207 meters, and its width next to the area could be tracked up to 198 meters.

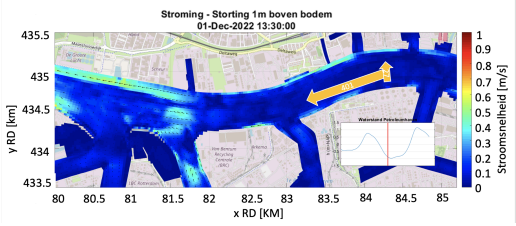

(e) KK dredged with WID; cohesive sediments, medium depth in a pocket area and high current velocities. In the direction of the outgoing tide, the sediment plume could be tracked up to a distance of 401 meters, and its width next to the area could be tracked up to 27 meters.

Figure 24: Path of the sediments plume determined with the ADCP Backscatter data, part 1. The velocity profiles are taken during the pilot and this is after high water, the exact time is displayed in the graph.

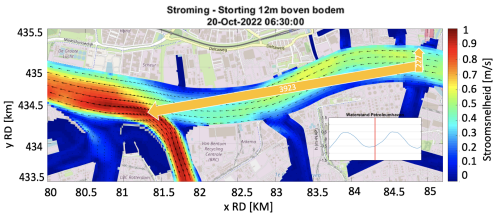

(a) PH dredged with the Tiamat; cohesive sediments, medium depth and high current velocities. In the direction of the outgoing tide, the sediment plume could be tracked up to a distance of 3923 meters, and its width next to the area could be tracked up to 227 meters.

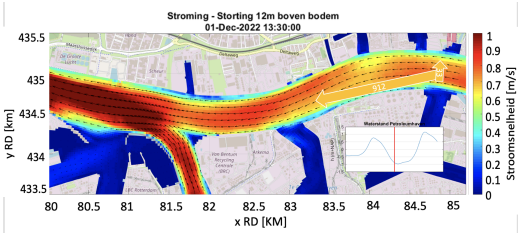

(b) PH dredged with WID with the agitation method; cohesive sediments, medium depth and high current velocities. In the direction of the outgoing tide, the sediment plume could be tracked up to a distance of 912 meters, and its width next to the area could be tracked up to 33 meters.

Figure 25: Path of the sediments plume determined with the ADCP Backscatter data, part 2. The velocity profiles are taken during the pilot and this is after high water, the exact time is displayed in the graph.

As obtained from figure 24a, for the non-cohesive sediments, with great depth with the difference in bed elevation and the lowest current velocities, the sediment plume of the Tiamat could be tracked up to 681 meters away from the pilot area. The width where the sediment plume could still be seen was 68 meters. In order to optimize sediment transport, it is desirable for sediments to be carried toward the Beerkanaal, where currents of 0.25 m/s are present due to the influence of the Hartelkanaal. When the sediments are in the Beerkanaal, they can be transported further out of the port with stronger currents of 0.25 m/s, or they can be picked up with the TSHD more easily. Nevertheless, the sediments transported as a plume are just into the Beerkanaal, when looking into the current profiles there is a dark blue part observed, this means that there are almost no currents there. Given the time, current velocities and sediment characteristics, it is expected that sediment deposition will occur at the beginning of the Beerkanaal, rather than being transported further downstream.

As obtained from figure 24b, for the non-cohesive sediments, with great depth and low current velocities, the sediment plume of the Tiamat could be tracked up to 931 meters away from the pilot area. The width where the sediment plume could still be seen was 72 meters. This can be due to the fact that currents were higher in this area and the difference in elevation within the nearby area was less. As obtained from figure 24c, for the non-cohesive sediments, with a great depth and low current velocities circumstances, the sediment plume of WID could be tracked 487 meters away from the pilot area. The width where the sediment plume could still be seen was 35 meters. With the ADCP Backscatter, it was more difficult to follow the WID sediment plume compared to the Tiamat sediment plume. Due to the blind spot of the ADCP Backscatter 1 meter above the bottom (Dunn & Zedel, 2022). It is again desirable for sediments to be carried towards the Beerkanaal, where 0.25 m/s current velocities are present due to the influence of the Hartelkanaal. For the second day of the Tiamat pilot, 18-10-2022, the current velocities were higher than the first day. The sediment plume is transported into the beginning of the Beerkanaal, where the currents are slightly

higher. This means it is expected that some sediments are transported further away towards the North Sea, but the sediment plume did not reach the middle of the Beerkanaal, where a current velocity of 0.35 m/s is observed, meaning that there are also sediments settled there. For the WID, there is a dark blue spot at the intersection of the EH and the Beerkanaal corresponding with almost no currents. This location is where the sediment plume is primarily transported, indicating sediment deposition. As a result, it is expected that sediment transport out of the port will be minimal.

As obtained from figure 24d, higher flow velocities were observed and there are cohesive sediments, but this location was the pocket area location with the medium depth. Therefore, sediments are assumed to be transported farther away than non-cohesive sediments with low current velocities. For these circumstances and dredging with the Tiamat, the sediment plume could be tracked up to 2207 meters away from the pilot area. The width where the sediment plume could still be seen was 198 meters. There are higher velocities, 1 m/s, at the estuary of the Botlek, therefore it is likely that the ADCP Backscatter could not track the sediments plume anymore within the natural variation. After the Botlek the data reached the maximum turbidity and it dissolved. It is desirable for the sediment plume to reach the estuary of the Botlek, because of the stronger currents of 1 m/s, the sediments can be transported further out of the port with the currents. The sediment plume was noticeable just before the Botlek. Therefore, some of the sediment can be expected to be transported further into the North Sea and some of the sediment precipitated at this location. Obtained from figure 24e, for the cohesive sediments, with a medium depth in the pocket area and high current velocities circumstances, the sediment plume for the WID could be tracked only 401 meters away from the pilot area. And the width where the sediment plume was still noticeable was 27 meters. This is a significantly lower travel distance than with the Tiamat, but note that this data is less reliable. Comparing figures 24d, 24e, 25a and 25b, the conclusion can be made again that the currents higher in the water column are stronger than near the bottom. In this case of cohesive sediments and moderate depth, utilizing the standard WID method is likely to result in sediment movement primarily towards deeper areas, facilitated by the creation of a density current in the water. This movement is expected to occur under conditions of low velocities at the bottom which is the case here.

As obtained from figure 25a, the highest currents were observed at this location. The presence of cohesive sediments at this location and the observed higher flows suggest that sediment transport at this location will be further away than with non-cohesive sediments and low velocities. For these circumstances, the sediment plume of the Tiamat could be tracked up to 3923 meters away from the pilot area. The width where the sediment plume could still be seen was 227 meters. As the circumstances were most similar to the circumstances in Harwich, this location could track the sediment plume the farthest. As it can be observed, there are higher velocities, 1 m/s, at the estuary of the Botlek, therefore it is likely that the ADCP Backscatter could not track the sediments plume anymore within the natural variation. After the Botlek the data reached the maximum turbidity and it dissolved. But for a desirable effect on the transport of the sediments, it would be useful if the sediment plume came at least until the Botlek because the currents are higher after reaching this location. As a result, it is expected that the sediments will be transported by the currents toward the North Sea. For figure 25b, the WID method with the agitation function was used. The ADCP Backscatter followed the WID plume in the higher part of the water column more easily, but at the bottom, it was still difficult. Therefore, for the cohesive sediments, with a medium depth

and high current velocities circumstances dredging with the WID with agitation function, the sediment plume could be tracked up to 912 meters away from the pilot area. The whole waterway has a current velocity of around 1 m/s. These high currents are in the upper part of the water column, where the sediments are being jetted to. This implies that the sediments are likely to be transported to the Botlek intersection. This is further than observed with the ADCP Backscatter. Once they reach this point, the sediments will be carried by stronger currents toward the North Sea. The presence of strong currents in the waterway could explain why the sediments were not observed with the ADCP Backscatter within the natural variation range.

The blind spot of the ADCP Backscatter has also an impact on the WID outcome, as the fluidized sediments are typically found at the bottom. This may explain why it was more difficult to track the WID plume over a longer distance. This is discussed in the discussion section. The sediment plume created with the Tiamat was able to travel the greatest distance, measured with the ADCP Backscatter, likely due to stronger currents in the upper part of the water column and the Tiamat gives an impulse on the sediments. In contrast, WID primarily uses the density current it generates and currents near the bed. As a result, dredging with Tiamat is likely to transport sediments over a greater distance compared to WID and the UWP. Additionally, both the Tiamat and WID are better suited for the transportation of finer sediments, due to the lower threshold of force required for their movement and the settling velocity for coarser sediments (Wilcock, 1994).

Due to this blindspot of 1 meter above the bed, the use of ADCP Backscatter was attempted to use for the UWP pilot as well, but was not successful. (Dunn & Zedel, 2022) Therefore, a combination of swift turbidity data over time, current stream profiles over time and Multibeam Echosounder data before and after dredging as presented in figure 26 were used to determine the location of sediments.

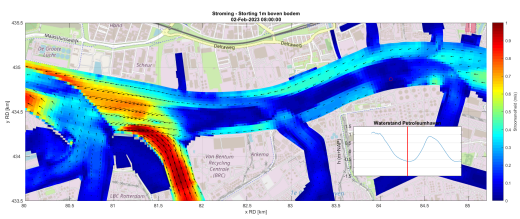

(a) Current profile on 02-02-2023 on a height of 1 meter above the bottom.

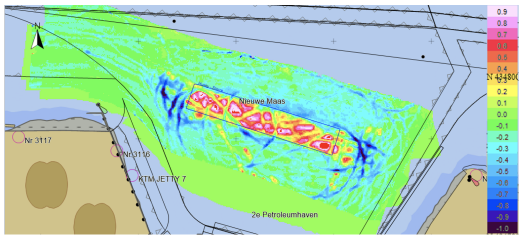

(b) Difference map before and after dredging with the UWP. Yellow, pink and red colors represents where the depth has increased and the blue and green colors represent where the depth has become shallower.

Figure 26: Velocity current map and differences map to determine the sediment transport during the UWP pilot.

The use of UWP resulted in a greater depth in the pilot area, obtained from figure 26. Current stream profiles indicated that sediments transported to the left come to a spot with almost no currents. When a strong enough density current is created with the use of UWP, sediments can

be carried away further to where waterway currents are stronger. Multibeam Echosounder data showed that not all sediments were carried away, resulting in a blue part on the left side of the pilot area. Turbidity measurements over time showed that sediments were also present in a wider area, where currents were stronger, indicating that they were carried away further. Blue parts at the sides of the pilot area were caused by the fact that the surrounding area was dredged and the density current carried sediments to deeper areas at the sides of the pilot area. The blue parts on the right are caused by turning the UWP.

With equations 6,7 and 8, in appendix II, the minimal current velocity for the Tiamat needed for the sediments to go to the higher currents location is calculated, the calculations can be found in appendix VIII. For the non-cohesive sediments and great depth with different bed elevations circumstances the minimal velocity of 5.83 m/s is needed, obtained from the velocity streaming profiles in figure 24a, this velocity is not reached, therefore it is confirmed that the particle did not reach the Beerkanaal. For the non-cohesive sediments and great depth circumstances, the minimal velocity of 4.67 m/s is needed, obtained from the velocity streaming profiles in figure 24b, this velocity is again not reached, therefore it is confirmed that the particles did not reach the whole distance to the middle of the Beerkanaal. For the cohesive sediments and medium depth in the pocket area circumstances, the minimum velocity of 0.074 m/s is needed to reach the Botlek location, obtained from the velocity streaming profiles in figure 24d, this velocity is reached, therefore it is likely that the sediments are taken further with the stronger currents at the estuary of the Botlek. For the area most similar to Harwich, cohesive sediments and medium depth, the minimum velocity of 0.090 m/s is needed to reach the Botlek, obtained from the velocity streaming profiles in figure 25a, this velocity is reached, therefore it is likely that the sediments are taken further with the stronger currents at the estuary of the Botlek. For the boundary conditions of the Tiamat, the sediments must be finer than 195 to 210 μm. The minimal current velocity is also calculated, calculations can be found in appendix VIII. A minimal current velocity for the particles of 195 μm is 0.0030·traveldistance, in the case of the circumstances in EH will be 4.06 m/s. Next, a minimal current velocity for the particles of 210 μm is 0.0034·traveldistance, in the case of EH this will be 4.71 m/s. Again, there can be concluded that strong currents are needed for these coarser-grained sediments, and this is not likely to occur under these circumstances. Therefore the production of the Tiamat will be lower for the sediments with a grain size coarser than 195 μm.

3.2 Turbidity

To monitor the water quality during dredging the turbidity is measured. The turbidity is determined with the Valeport Swift Turbidity. For figures 27, 28, 29, 30, 31 and 32, the "x" means that the dredging is stopped. More turbidity depth profiles can be found in appendix V. The vertical depth profiles of turbidity are presented for different time points: before dredging, minutes after dredging began, and after dredging has stopped and the turbidity has returned to its reference situation. Therefore, the before dredging profiles may not be entirely clear since the after dredging profile is overdrawn over this line.

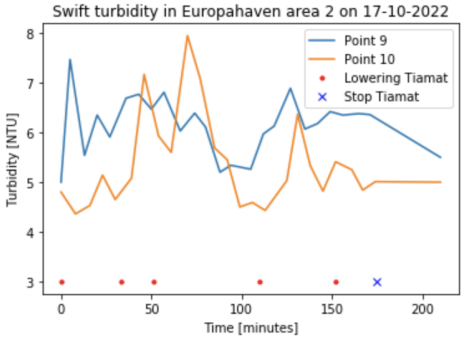

(a) The mean of the turbidity in the water column during dredging with the Tiamat on 17-10-2022. The blue line represents the turbidity at point 9 and the orange line represents the turbidity at point 10.

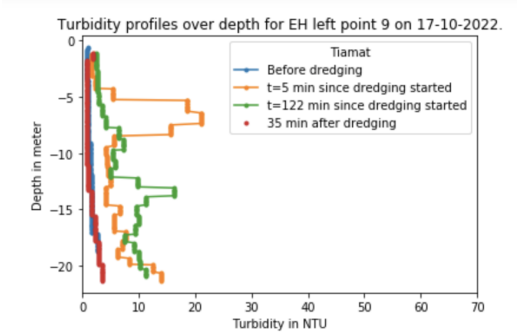

(b) The turbidity over the depth per hour at location 9, the blue line is before dredging, the orange and green lines are minutes after the start of dredging and the red line is 35 minutes after the stop of dredging with the Tiamat on 17-10-2022.

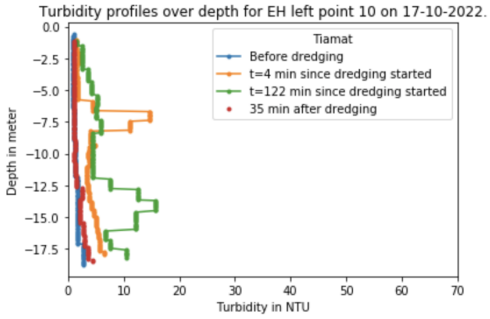

(c) The turbidity over the depth per hour at location 10, the blue line is before dredging, the orange and green lines are minutes after the start of dredging and the red line is 35 minutes after the stop of dredging with the Tiamat on 17-10-2022.

Figure 27: Swift Turbidity data for the non-cohesive sediments, with a great depth and bed elevation differences and the lowest current velocities circumstances.

The Swift Turbidity was located at two different locations, point 9 is located in the outgoing tidal stream and point 10 is located wider near the Tiamat area. These locations for the Swift Turbidity were selected to determine if the sediment plume is being carried by the currents and if it is spreading wider. As obtained from figure 27a, the turbidity in the water column spreads out wider after 50 minutes. But note that this graph is the mean turbidity of the whole water column. In the turbidity depth profile, figures 27b and 27c, the work of the Tiamat is already noticeable after 5 minutes. This can be seen in the graph, the turbidity is higher at the depth of -6.5 meters and again near the bottom. Over time, the turbidity plume may decrease in height over the whole water column,

which may be attributed to the presence of coarser sediment particles that have settled in the water column near the Swift Turbidity location. It takes for the turbidity in the water column to return to the reference situation is 35 minutes for the non-cohesive sediments, with great depth with bed elevation differences and the lowest current velocities circumstances. This is without considering turbidity one meter above the bottom.

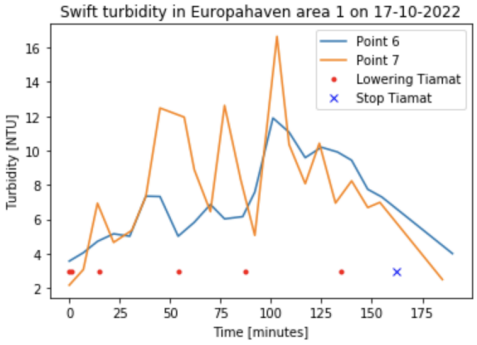

(a) The mean of the turbidity in the water column during dredging with the Tiamat on 17-10-2022. The blue line represents the turbidity at point 6 and the orange line represents the turbidity at point 7.

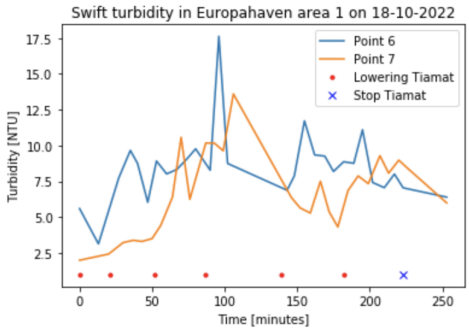

(b) The mean of the turbidity in the water column during dredging with the Tiamat on 18-10-2022. The blue line represents the turbidity at point 6 and the orange line represents the turbidity at point 7.

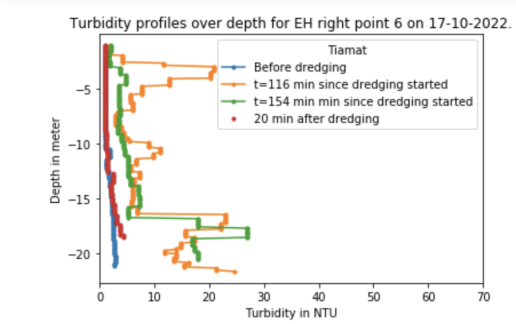

(c) The turbidity over the depth per hour at location 6, the blue line is before dredging, the orange and green lines are minutes after the start of dredging and the red line is 20 minutes after the stop of dredging with the Tiamat on 17-10-2022.

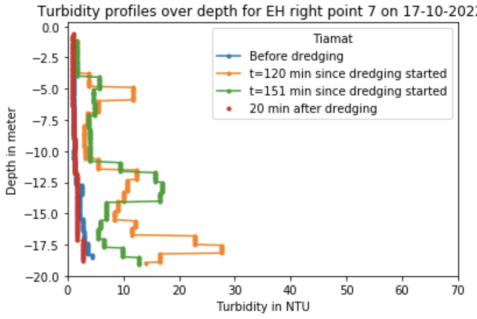

(d) The turbidity over the depth per hour at location 7, the blue line is before dredging, the orange and green lines are minutes after the start of dredging and the red line is 20 minutes after the stop of dredging with the Tiamat on 17-10-2022.

Figure 28: Swift Turbidity data for the non-cohesive sediments, with a great depth and low current velocities circumstances, part 1.

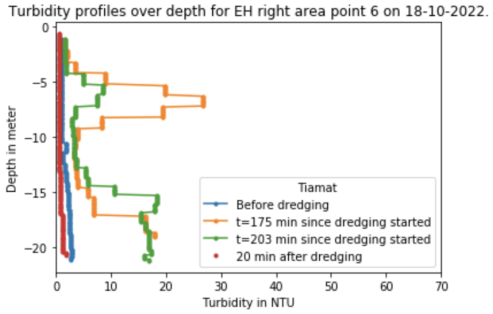

(a) The turbidity over the depth per hour at location 6, the blue line is before dredging, the orange and green lines are minutes after the start of dredging and the red line is 20 minutes after the stop of dredging with the Tiamat on 18-10-2022.

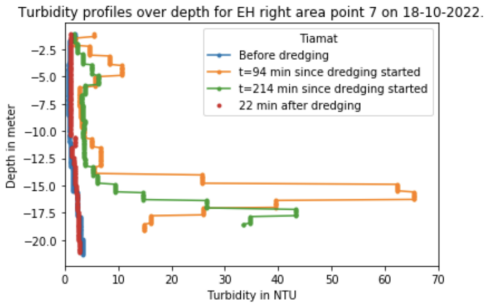

(b) The turbidity over the depth per hour at location 7, the blue line is before dredging, the orange and green lines are minutes after the start of dredging and the red line is 22 minutes after the stop of dredging with the Tiamat on 18-10-2022.

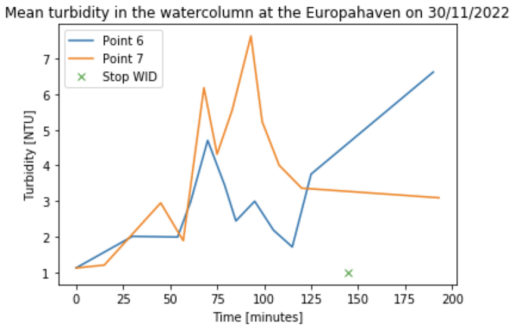

(c) The mean of the turbidity in the water column during dredging with the WID on 30-11-2022. The blue line represents the turbidity at point 6 and the orange line represents the turbidity at point 7.

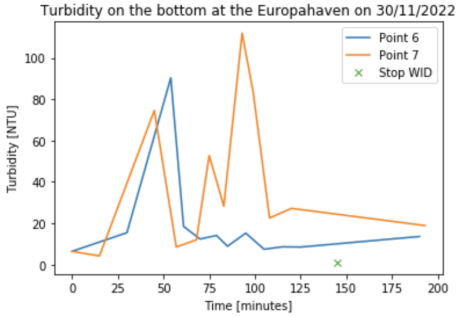

(d) The mean turbidity at the bottom during dredging with WID on 30-11-2022. The blue line represents the turbidity at point 6 and the orange line represents the turbidity at point 7.

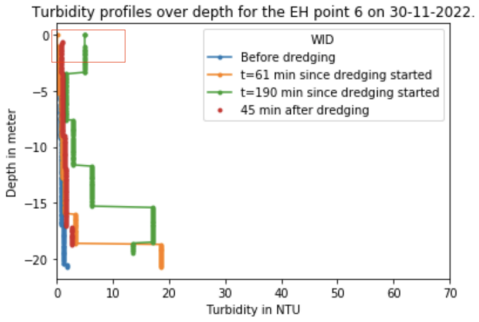

(e) The turbidity over the depth per hour at location 6, the blue line is before dredging, the orange and green lines are minutes after the start of dredging and the red line is 45 minutes after the stop of dredging with the WID on 30-11-2022.

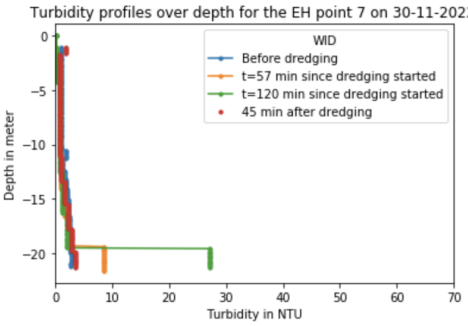

(f) The turbidity over the depth per hour at location 7, the blue line is before dredging, the orange and green lines are minutes after the start of dredging and the red line is 45 minutes after the stop of dredging with the WID on 30-11-2022.

Figure 29: Swift Turbidity data for the non-cohesive sediments, with a great depth and low current velocities circumstances, part 2

The Swift Turbidity is located at two different locations during dredging with the Tiamat and the WID. Point 6, is located in the outgoing tidal stream and point 7 is located wider near the Tiamat area. These locations for the Swift Turbidity were selected to determine if the sediment plume is being carried by the currents and if it is spreading out wider. The depth profile where the work of the Tiamat discharge pipe is best seen is after 100 minutes, observed from figures 28c and 28d; it takes a while for the sediments to flow to location 6 and show a clear profile where the sediments are not settled yet. The turbidity during the first day of dredging is almost the same as the turbidity during the second day of dredging, observed in figures 28a and 28b. The biggest difference between the two days is that on the first day, the turbidity level is greater in the wider area near the Tiamat pilot area, whereas on the second day, the turbidity is higher at the outgoing tidal point. This is also observed in the depth profiles, figures 28c and 28d, the turbidity at the wider location near the Tiamat pilot area is more over the whole depth instead of the clear profile. This is due to the fact that on the second day, the currents were higher. Again, for the second day of the Tiamat pilot, date 18-10-2022, figure 28b, shows that the turbidity spread further into the wide area of the harbor after almost one hour. There are also clear depth profiles during this dredging day, observed in figures 29a and 29b. When the Tiamat disperses its sediment plume in the water column, the turbidity at a certain depth of -6.5 meters increases, but it eventually decreases in height as the sediment settles. The mean turbidity in the water column for these circumstances is higher than for the circumstances with non-cohesive sediments, with great depth with bed elevation differences and the lowest current velocities. It takes for the turbidity in the water column to return to the reference situation 20 minutes for the circumstance of non-cohesive sediments, a great depth and low current velocities after dredging with the Tiamat. This is without considering turbidity one meter above the bottom. This time is shorter than the time required for the circumstances with non-cohesive sediments, with great depth with bed elevation differences and the lowest current velocities, moreover, the turbidity is also higher. This can be explained by the fact that the flow velocities are greater for this area and the other area had more bed elevation differences.

For the WID, it is observed that the turbidity at the bottom was significantly higher than the mean turbidity in the water column, figures 29c and 29d. This observation is likely attributable to a specific cause that the suspended sediments traveling near the bottom instead of being released higher in the water column which happens with the Tiamat. After 70 minutes, the turbidity observed at point 7 was found to be higher than at point 6, as observed in figures 29c and 29d. This can be attributed to the fact that a greater quantity of sediments had become suspended and was no longer being transported solely in the outgoing tidal direction by the density current but spread out wider. After the dredging activities stopped the bottom turbidity at point 6 increased, this is because the density currents and the tidal currents with the sediments are still traveling in the outgoing tidal stream even after dredging. This will stop when the suspended sediments are settled. In the turbidity profiles over the depth during dredging, the turbidity on the bottom can be seen clearly after 30 minutes, observed in figures 29e and 29f. This turbidity is due to fluidizing the bottom sediments and creating turbidity. The 'turbidity' on the top of the water column, in figure 29e indicated with the red column in the graph, is due to the propeller wash of the surrounding vessels. The time it takes for the turbidity to return to the reference situation is 45 minutes after dredging with the WID.

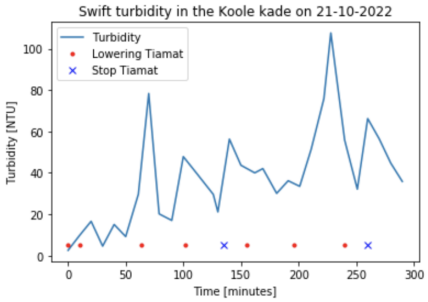

(a) The mean of the turbidity in the water column during dredging with the Tiamat on 21-10-2022.

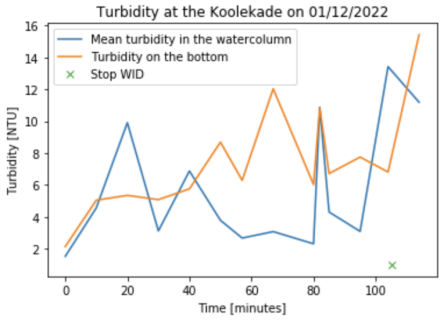

(b) The mean turbidity at the bottom and in the water column during dredging with WID on 01-12-2022. The blue line represents the mean turbidity in the water column and the orange line represents the turbidity at the bottom.

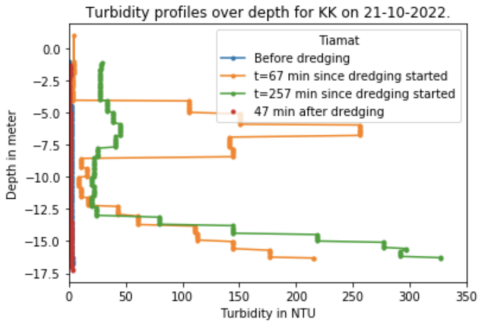

(c) The turbidity over the depth per hour, the blue line is before dredging, the orange and green lines are minutes after the start of dredging and the red line is 47 minutes after the stop of dredging with the Tiamat on 21-10-2022.

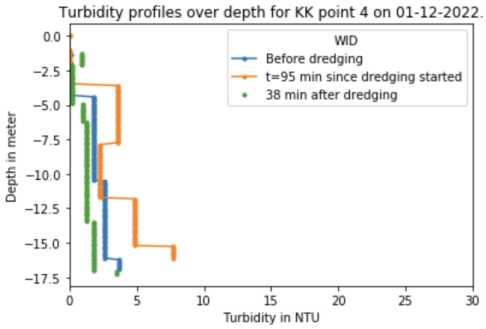

(d) The turbidity over the depth per hour at location 4, the blue line is before dredging, the orange line is minutes after the start of dredging and the green line is 38 minutes after the stop of dredging with the WID on 01-12-2022.

Figure 30: Swift Turbidity data for the cohesive sediments, with a medium depth in the pocket area and high current velocities circumstances.

The Swift Turbidity was only placed at a location in the outgoing tide. The turbidity in these circumstances is much higher than the turbidity for the non-cohesive sediments, great depth and low current circumstances, obtained from figure 30a. It takes for the turbidity in the water column after dredging with the Tiamat to return to the reference situation is 47 minutes for the circumstances of cohesive sediments, medium depth in a pocket area and high currents. This is without considering turbidity one meter above the bottom. This time is longer than it takes in the non-cohesive sediments circumstances. The explanation is that coarser sediments settle faster (Winterwerp & van Kesteren, 2004), in this case the sediments are finer and therefore it takes more time. It takes 49 minutes to get a good view of the work of the Tiamat. In figure 30c, the development of the turbidity is displayed. Initially, the turbidity is at its highest at the height where the Tiamat

releases the sediment plume. However, over time, the sediment settles and the turbidity increases throughout the entire water column. For WID, as observed in figure 30d, this location has the lowest turbidity for the WID. There is also not much difference between the bottom turbidity and the mean turbidity at the water column. As displayed in figure 30d, the turbidity is present throughout the entire water column, and this may be due to the pocket area. When the turbidity is near the bottom it is difficult to be taken out of the pocket area, therefore the turbidity will be more over the entire water column before it is taken away to the deeper area with the density current. An explanation for the lower turbidity in these circumstances compared to the non-cohesive sediments, with great depth and low current velocities circumstances is that this is a pocket area with a shallower depth at the end of the pilot area. The tracks, in appendix IX, show a lower density of dots in the pilot area, which suggests that dredging has not been performed there with many tracks. This could also contribute to lower turbidity. The time it takes for the turbidity after dredging with the WID to return to the reference situation is 38 minutes.

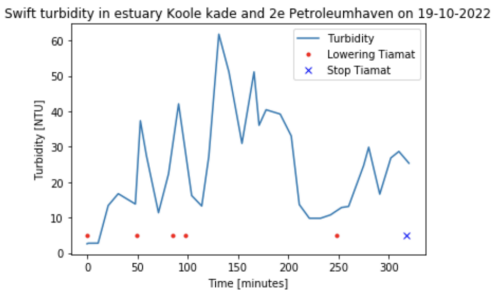

(a) The mean of the turbidity in the water column during dredging with the Tiamat on 19-10-2022.

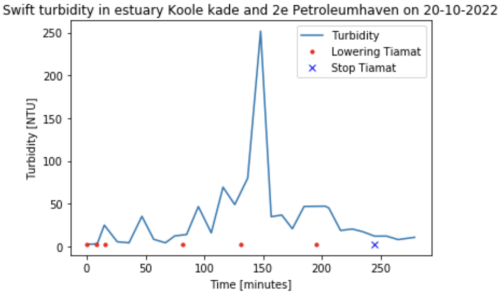

(b) The mean of the turbidity in the water column during dredging with the Tiamat on 20-10-2022.

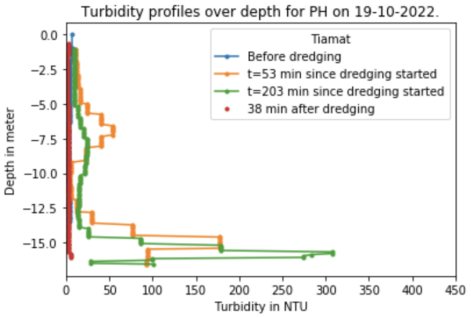

(c) The turbidity over the depth per hour, the blue line is before dredging, the orange and green lines are minutes after the start of dredging and the red line is 38 minutes after the stop of dredging with the Tiamat on 19-10-2022.

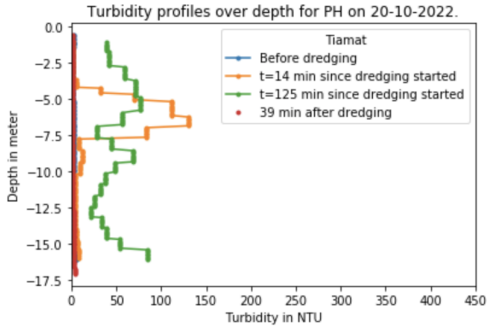

(d) The turbidity over the depth per hour, the blue line is before dredging, the orange and green lines are minutes after the start of dredging and the red line is 39 minutes after the stop of dredging with the Tiamat on 20-10-2022.

Figure 31: Swift Turbidity data for the cohesive sediments, with a medium depth and high current velocities circumstances, part 1.

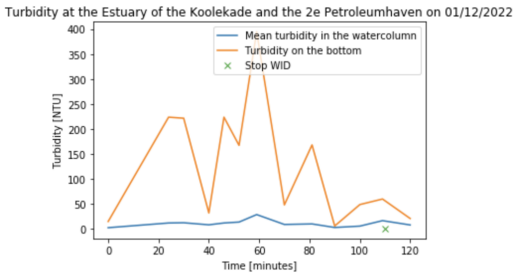

(a) The mean turbidity at the bottom and in the water column during dredging with WID on 01-12-2022. The blue line represents the mean turbidity in the water column and the orange line represents the turbidity at the bottom.

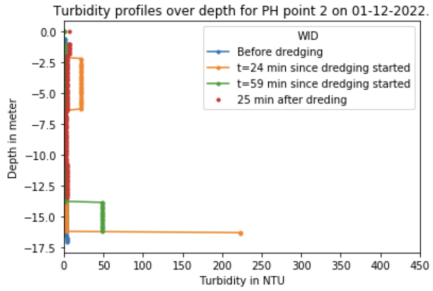

(b) The turbidity over the depth per hour at location 2, the blue line is before dredging, the orange and green lines are minutes after the start of dredging and the red line is 25 minutes after the stop of dredging with the WID with agitation function on 01-12-2022.

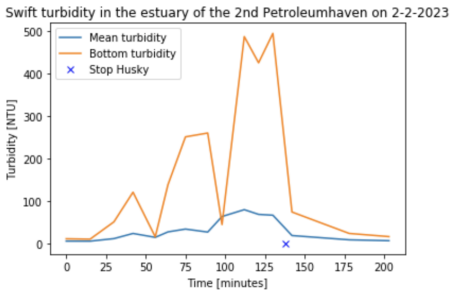

(c) The mean of the turbidity in the water column and at the bottom during dredging with the UWP on 02-02-2023. The blue line represents the mean turbidity in the water column and the orange line the turbidity near the bottom.

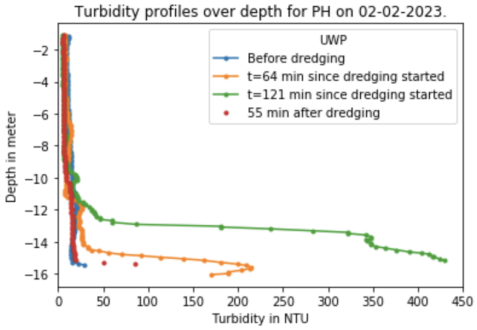

(d) The turbidity over the depth per hour at location 2, the blue line is before dredging, the orange and green lines are minutes after the start of dredging and the red line is 55 minutes after the stop of dredging with the UWP on 02-02-2023.

Figure 32: Swift Turbidity data for the cohesive sediments, with a medium depth and high current velocities circumstances, part 2.

The Swift Turbidity was only located at a location in the outgoing tide for this location. In the turbidity profile over depth, figures 31c and 31d, the work of the Tiamat is already easily noticeable after 14 minutes. As obtained from figures 31a and 31b, the turbidity at this location is much higher than the turbidity for non-cohesive sediment, great depth and low velocity circumstances. On the second day, the Tiamat could be lowered faster because the bottom was less stiff. It takes for the turbidity in the water column after dredging with the Tiamat to return to the reference situation 38 minutes for the circumstances of cohesive sediments, medium depth and high current velocities. This is without considering turbidity one meter above the bottom. This time is lower than for the medium silt sediments with a great depth in a pocket area and high currents. This is

due to the fact that the pocket area is making it more difficult for sediments to flow out. Dredging stops at a time when the tide almost turns from outgoing to incoming, because of this the currents are also less at the end of dredging.

For the WID turbidity, note that the dredging method used at this location was different from the normal WID, as the agitation function was also employed. As observed in figure 32a, the turbidity at the bottom, in comparison to the mean turbidity of the entire water column, may seem counter-intuitive given that the sediments are being jetted upstream. However, it should be noted that the WID affects the suspended bottom sediments once they are injected with water. Although some of the suspended sediments will be carried away by the upstream currents after jetting upstream, there will be more turbidity at the height where the currents are the strongest and where the suspended sediments will be transported. Additionally, some of the coarser sediments will settle more easily, after a while leading to higher turbidity levels in the zone between the WID device and the stronger upper water currents, as observed in the turbidity depth profile in figure 32b. Despite this, the peak turbidity levels remain concentrated at the bottom and at a depth of -4 meters, where the currents are the strongest in the water column for this location. Observed in figure 32b, from the turbidity profile over the depth, it is found that sediments have the potential to be jetted upwards until they reach stronger currents in the upper section of the water column, and this is desirable. The time it takes for the turbidity after dredging with the WID to return to the reference situation is 25 minutes.

For the UWP, it is observed from figure 32c, that the turbidity on the bottom is significantly higher than the mean turbidity in the water column. Due to the physical mechanism of the UWP, pulling the plough over the bed, only the sediment at the bed is disturbed resulting in turbidity near the bottom, this is confirmed by the turbidity profile over the depth, figure 32d. After the stop of dredging with the UWP the turbidity is back to the turbidity at the reference situation within 55 minutes. The turbidity graph displays peaks that correspond to the lowering of the UWP. The initial height of the UWP was at the shallowest depth, resulting in lower turbidity levels at the beginning of the dredging operation.

The reason for the varying turbidity levels among the three methods is due to the height at which the sediments are displaced. With the Tiamat, the turbidity is initially concentrated in the higher part of the water column and near the bed but eventually spreads throughout the entire column. This is because the Tiamat method uses water jets to suspend sediments from the bed and lift them higher into the water column. Over time, some of the sediments settle back down, causing turbidity throughout the whole water column. With the WID, the turbidity is a couple of meters above the bed. This is because the WID fluidizes the sediments and a density current is created and travels near the bed. The UWP, on the other hand, uses a plough to pull back and forth over the bed, which allows water to penetrate between the soil sediments and suspend some of the sediments. However, in this method, most of the turbidity remains concentrated near the bed. Therefore, the turbidity near the bed is the highest for the UWP. Due to these reasons, the time to return to the reference situation for the three dredging methods is also different. The sediments during dredging with the WID are near the bottom this is why the time to return is shorter for cohesive sediments and higher current velocities. But for the non-cohesive sediments and the lower current velocities, the settling time to reach the reference situation is longer for WID compared with the Tiamat due to the presence of low currents near the bed when dredging activity with the WID stopped

and the location where the Swift Turbidity measures. Turbidity measurement for the non-cohesive sediments, with a great depth and low current velocities circumstances, is not influenced by further sediment dispersion because there are almost no currents near the bottom, while after dredging with the Tiamat, the sediment can disperse beyond the measuring point and may not be captured by the Swift Turbidity. This is also discussed in the discussion section. For the UWP it takes the longest time to return to the reference situation as compared to the Tiamat and the WID, due to the presence of a thicker mud layer with a higher concentration of cohesive sediments distributed throughout the depth. The cohesive sediments have a lower settling velocity, resulting in a longer period required to achieve the reference situation.

Normally, the dredging-induced turbidity should not exceed the turbidity (IADC, 2015). For all dredging methods, this will be difficult because there is more turbidity during dredging. The Tiamat causes sediment plumes to rise higher into the water column, resulting in turbidity initially being concentrated near the bed and at the level where the Tiamat is jetting up the sediments. Due to the pressurized injection of water by the Tiamat, with pressure levels of up to 4 bar, a portion of the turbidity will become suspended at elevated depths within the water column. However, as time passes, some of the sediments out of the sediment plume are also settling and the turbidity becomes distributed throughout the entire water column. Minimizing the turbidity can be achieved by using a lower pressure when injecting the sediments with water; with this solution, the suspended sediments will stay near the bottom. Another solution to reduce turbidity is an improvement in the Tiamat application. Currently, the Tiamat uses two side inlet pipes to draw water from the surrounding area during injection, which already contains suspended sediments. By using a water injector to introduce clean water into the sediments, the turbidity can be reduced. The water from the surface can be used, because there are no diluted sediments. An alternative approach could be to extend the inlets to the surface to allow for water intake from the surface. However, this modification would make the Tiamat vulnerable to currents, potentially affecting the results.

3.3 Top sediment layer

Density and strength (yield stress) play a crucial role in soil development over time. During the dredging process of using the Tiamat, the bottom soil is cut into layers, and water is injected. It is expected that this process has a direct impact on the strength of the soil. The strength and density of the soil are measured using the Silas and Rheotune instruments. Because the Rheotune only works in a mud layer the Rheotune is not used in fine sand sediments circumstances. The Rheotune data and the Silas data used can be found in appendix VI.

It can be concluded from the Silas data, appendix VI, that for EH left and right during dredging with the Tiamat and the WID in non-cohesive sediments, with a great depth and low current velocities circumstances the layer in monitor week 1 is smaller than in the weeks after, in monitor week 1 there is no space between the 1030 g/L and 1200 g/L line. In the next monitor weeks, the distance between the lines increases slightly. This can be explained by looking at the PSD before and after dredging with the Tiamat, the coarser sediments remain behind this is why the layer in monitor week 1 is thinner than in monitor week 4 where sediments have already returned. But there is still no mud layer here because of the sediments at this location. For the WID the Silas was also used before and right after the pilot, during the pilot week, the thickness of the layer between the 1030

g/L and 1200 g/L lines is slightly smaller than in the reference situation. However, in monitor week 1, the thickness is reduced again, with almost non-existent thickness. This is because not all of the sediments had settled down after dredging when the Silas was used. Over the next few monitoring weeks, the thickness increases slightly, but only by a few centimeters.

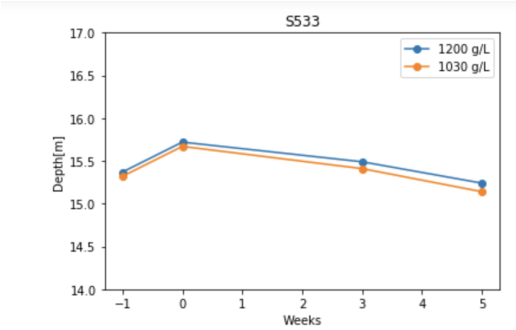

(a) Mud layer developments over time after dredging with the Tiamat for point S533 for the cohesive sediments, with a medium depth in the pocket area and high current velocities circumstances.

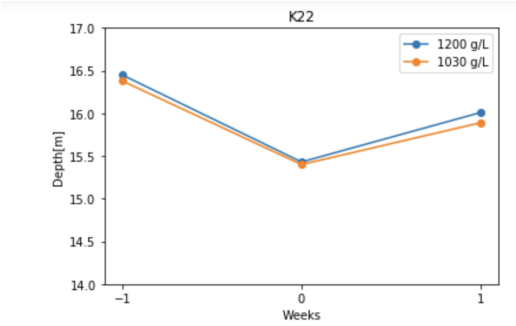

(b) Mud layer developments over time after dredging with the WID for point K22 for the cohesive sediments, with a medium depth in the pocket area and high current velocities circumstances.

Figure 33: The Rheotune data is used for making these graphs. The blue line represents the 1200 g/L line and the orange line represents the 1030 g/L line.

In figure 33, week -1 represents the reference data and week 0 represents the pilot week. After that, weeks represent the monitor weeks. The difference between the points is only a few centimeters but because there is a trend for all the points the data is used. Obtained from the Rheotune data in appendix VI, first, a peak is shown at the Tiamat pilot week. This is because the Rheotune is used after dredging with the Tiamat but not all the sediment has settled yet. Then, at week 1, the sediments are settled down and the density is lower than for the pilot week. Over the next few weeks, the density increases and this is because the mud layer increases. The gap between the blue and orange lines indicates the thickness of the mud layer, which increased further during the monitoring weeks. After dredging with the Tiamat and the WID, a reduction in the thickness of the mud layer has been observed, as the dredging primarily targeted the sediment layer consisting of medium silt. Because the Tiamat system is more productive for cohesive sediments, rather than non-cohesive sediments. The thickness of the mud layer during week 5 has increased in comparison to week 1. The Nautical Guaranteed Depth (NGD) for KK, is -16.15 meters. (PortMaps, 2022) However, Rheotune data obtained during the Tiamat pilot week, which is right after dredging, indicates that the NGD cannot be ensured. The nautical density for vessels to navigate through is 1200 g/L (Kiriche k et al., 2018a) and the boundary is located above a depth of 16.15 meters. In order to mitigate the risk of non-compliance with the NGD, it may be necessary to increase the dredging depth in the future. A fluid mud layer can prove beneficial for dredging purposes as it maintains a density of 1200 g/L or less, ensuring a guaranteed depth for vessels to navigate through. Nevertheless, it was concluded from the Rheotune data that the Tiamat could not be used to create

a fluid mud layer.

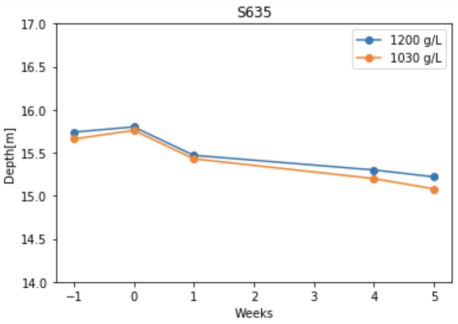

(a) Mud layer developments over time after dredging with the Tiamat for point S635 for the cohesive sediments, with a medium depth and the highest current velocities circumstances.

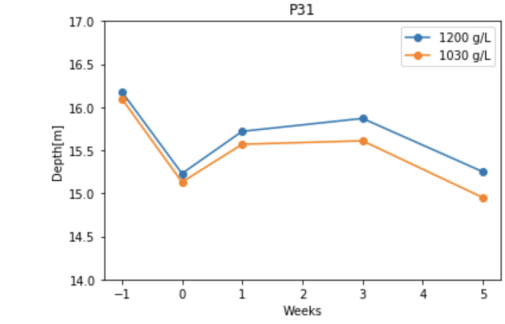

(b) Mud layer developments over time after dredging with the WID for point P31 for the cohesive sediments, with a medium depth and the highest current velocities circumstances.

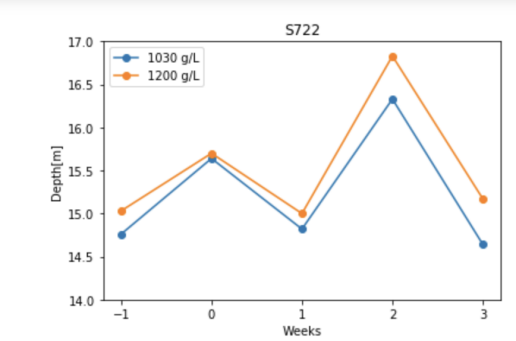

(c) Mud layer developments over time after dredging with the UWP for point S722 for the cohesive sediments, with a medium depth and the highest current velocities circumstances.

Figure 34: The Rheotune data is used for making these graphs. The blue line represents the 1200 g/L line and the orange line represents the 1030 g/L line.

In the Silas data for the Tiamat pilot week, appendix VI, which confirms that the sediments had not yet settled when the Silas was used immediately after dredging. Observed out of figures 34a and 34b, For monitor week 1, the mud layer is really small and reduced compared to the reference situation. But the mud layer increases during the next monitor weeks this is due to sedimentation, which can be confirmed with the depth profiles in the next section. At this location, for Tiamat, WID and UWP, the mud layer increased the most. During the monitoring weeks of the UWP the mud layer increased by almost half a meter. For figure 34c, the bed profiles for week 2 and week 3 differ from those of the other graphs, which can be attributed to different dredging activities in the pilot area. The Nautical Guaranteed Depth (NGD) for PH, is -15.9 meters. (PortMaps, 2022) Rheotune data obtained during the Tiamat pilot week, which is right after dredging, indicates

that the NGD can be ensured. The nautical density for vessels to navigate through is 1200 g/L (Kiriche k et al., 2018a) and the boundary is located beneath a depth of 15.9 meters. For only one point, cannot be guaranteed and this is the turning point of the vessel of the Tiamat. This is due to the sediments falling out of the Tiamat when turning the vessel. For the use of the Tiamat and the WID, the process of jetting water into the bed can impact the strength of the bed. For the Tiamat, the depth of the nautical density increased immediately after dredging, for WID the depth of the nautical density decreased immediately after dredging. This can be due to the difference in technique, for the WID the suspended sediments stay all near the bed while for the Tiamat most of the suspended sediments are brought higher in the water column. Because of the pressured water use the strength of the bed sediments will be reduced. For the UWP this is not happening and the influence on the strength is only on the top layer.

3.4 Depth

The depth profiles and maps play a crucial role in determining the production rates as well as evaluating sedimentation patterns and the effectiveness of the dredging methods in regulating the depth of the water column. In appendix VII the depth over the area before dredging, during the pilot week and for the monitor weeks can be found. Longitudinal profiles of the area were created to facilitate the overview of the figures. These profiles are made from the middle of the dredging area.

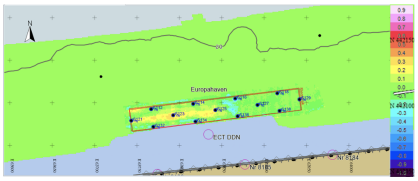

(a) Difference map before and after dredging with the Tiamat for the non-cohesive sediments, with great depth and bed elevation differences and the lowest current velocities circumstances.

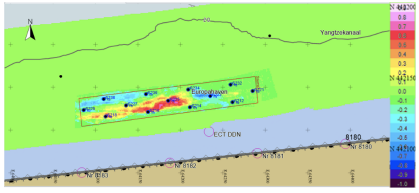

(b) Difference map before and after dredging with the Tiamat for the non-cohesive sediments, with a great depth and low current velocities circumstances.

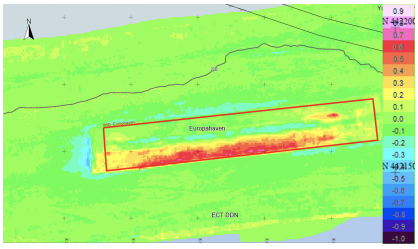

(c) Difference map before and after dredging with the WID for the non-cohesive sediments, with a great depth and low current velocities circumstances.

Figure 35: Map with the differences before and after dredging. Yellow and red colors represent where the depth has increased and the green and blue colors represent where the depth has become shallower.

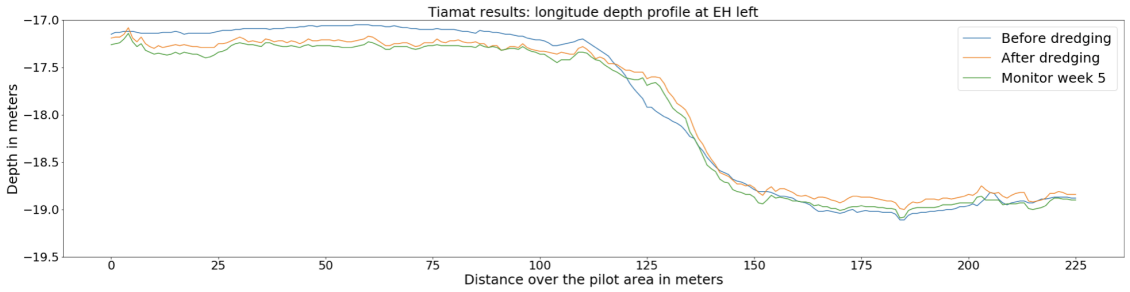

(a) The profile for dredging with the Tiamat in non-cohesive sediments, with great depth and bed elevation differences and the lowest current velocities circumstances. The blue line represents the depth before dredging, the orange represents the depth after dredging, and the green line represents the depth during the monitor weeks.

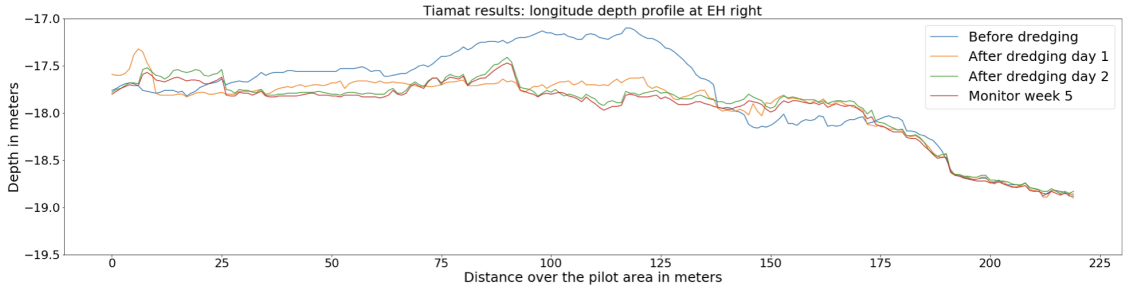

(b) The profile for dredging with the Tiamat in the non-cohesive sediments, with a great depth and low current velocities circumstances. The blue line represents the depth before dredging, the orange and green line represents the depth after dredging, and the red line represents the depth during the monitor weeks.

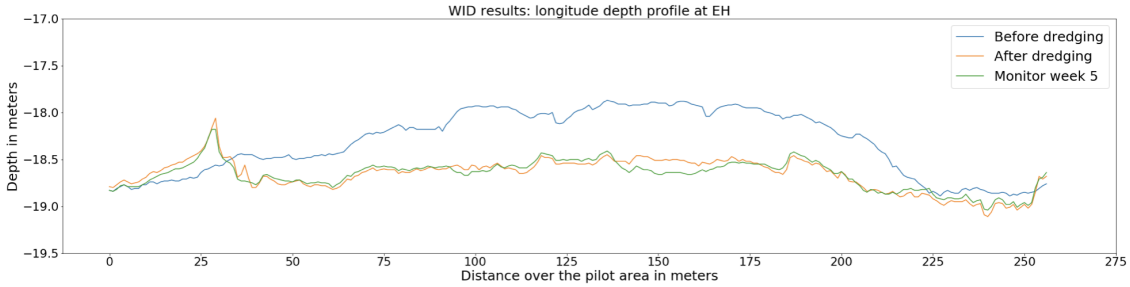

(c) The profile for dredging with the WID in non-cohesive sediments, with a great depth and low current velocities circumstances.The blue line represents the depth before dredging, the orange line represents the depth after dredging, and the green line represents the depth during the monitor weeks.

Figure 36: The longitude depth profiles before dredging, after dredging and for the monitor weeks for different circumstances.

As observed from figures 35a and 36a, in the left part of the area, the depth has increased, but in the right part, the depth has become shallower. This inequality is attributed to the Water Injection Dredging (WID) effect, whereby sediment particles are drawn to the deeper region of the area

(Kortmann, 1994b). Here the currents are weaker than in other areas and the sediment is classified as fine sand and with the combination of lower currents, the sediment particles settle in the deeper region of the area. During the monitor weeks, the depth has not changed much. This can also be explained by the fact that this area has not had many natural currents. This will lead to almost no sedimentation. The currents in this area are mostly created by vessels.

As observed from figures 35b and 36b, the dredging process with the Tiamat occurred over two days. In the right part of the area, an increase in depth is observed, likely resulting from the flattening of the area. Examining the profile indicates that the right section was already at the end depth, explaining the minimal change. Before dredging, a few deeper spots existed in the area, but after dredging, the depth of the area became uniform. Additionally, there are more sediment deposits in the far-left section of the area, which was also the turning point for the Tiamat. The Tiamat must be raised slightly to turn the Barney, which is done at the end of the pilot area. However, sometimes the turning and lifting of the Tiamat occurred within the area, causing some sediment particles to fall out of the Tiamat into the pilot area. The middle section of the area experienced the most significant increase in depth, likely because the Tiamat passed over this part frequently, the tracks of the Tiamat can be found in appendix IX. Already in monitor week 1, the sediment hump is gone. Currents have spread the bottom sediment hump across the area. In addition, the depth did not change much within the 5 monitoring weeks.

As observed in figures 35c and 36c, the area is flattened out again until a certain depth, this is an advantage of WID. After 5 weeks of monitoring the depth has increased slightly. This may have happened because the vessel that was there went out of berth the week after dredging and another vessel went in. The movement of sediments from the berth to areas nearby is attributed to the draught and propellers of the vessel. The propeller jet generates a flow above the seabed that propagates towards the surface and bottom, emanating from the center line. Upon reaching the seabed, the flow transitions to a bottom current, which can cause sediment disturbance if it exceeds the critical shear stress threshold necessary for sediment mobilization (Guarnieri et al., 2021).

As can be concluded from figure 36, there is not much sedimentation in EH during the monitor weeks for both dredging equipment, this can be due to the fact that there are low currents in this area and non-cohesive sediments so it is difficult for the flow to transport the sediments.

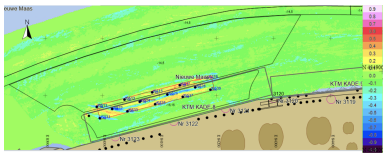

(a) Difference map before and after dredging with the Tiamat for the cohesive sediments, with a medium depth in the pocket area and high current velocities circumstances.

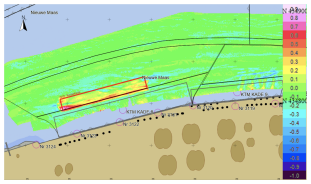

(b) Difference map before and after dredging with the WID for the cohesive sediments, with a medium depth in the pocket area and high current velocities circumstances.

Figure 37: Map with the differences before and after dredging. Yellow and red colors represent where the depth has increased and the green and blue colors represent where the depth has become shallower.

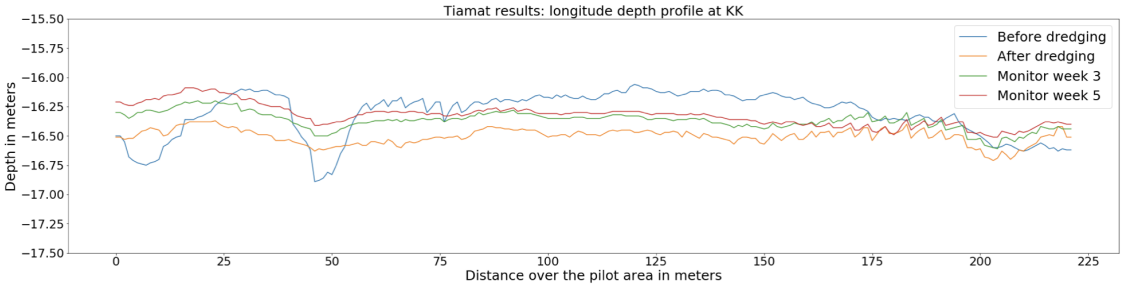

(a) The profile for dredging with the Tiamat in cohesive sediments, with a medium depth in the pocket area and high current velocities circumstances. The blue line represents the depth before dredging, the orange represents the depth after dredging, and the green and red lines represent the depth during the monitor weeks.

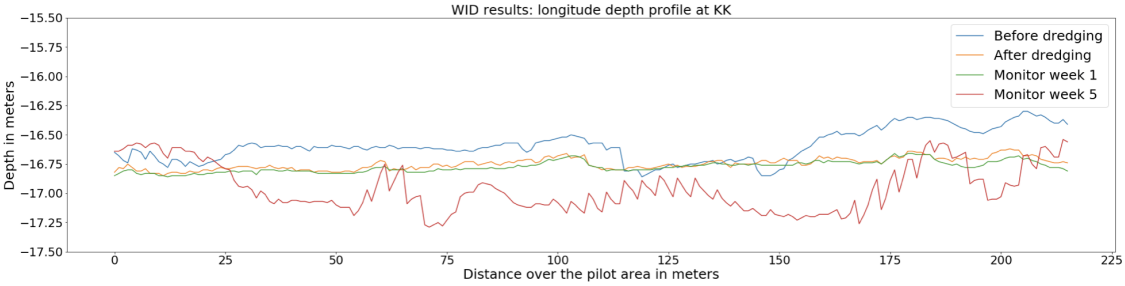

(b) The profile for dredging with the WID in cohesive sediments, with a medium depth in the pocket area and high current velocities circumstances. The blue line represents the depth before dredging, the orange line represents the depth after dredging, and the green and red lines represent the depth during the monitor weeks.

Figure 38: The longitude depth profiles before dredging, after dredging and for the monitor weeks for different circumstances.

As observed in figures 37a and 38a, reveals that there were pits in the area before dredging. After dredging the bottom is flattened with sediments filling the previous pits. This is why in some parts the depth has become shallower in figure 37a. Minimal depth differences are observed in the middle section, likely resulting from settling back at the end of the dredging process. The dredging time was relatively short, just over 4 hours. Also with these circumstances, the turbidity was high, and took longer to return to the reference situation. Additionally, the tide changed slowly after dredging, allowing sediments to settle back into the area. Another reason is that after the dredging day at EH the Tiamat got instructions not to go over the middle all the time. Now the Tiamat went over the sides more often and the depth became shallower in the middle part of the area, this is because some sediments on the side of the Tiamat can fall out. Consequently, the Tiamat must work more precisely because you can see the tracks made. For the monitoring weeks, the depth increased faster than for the fine sand sediments, with a great depth and low current velocities circumstances. This is due to the fact that KK has a busy berth near the pilot area. The vessels going over the area create currents and sediments will shift.

Observed in figures 37b and 38b, reveals by the blue line variations in bottom depth before dredging with the WID. After dredging, the bottom depth has increased and flattened out. However, the presence of blue spots on the sides of the area suggests that sediment has been transported to these locations via the WID process, which entails a density current flowing toward deeper regions. Comparing figures 37a and 37b, it seems that for the area dredged with the WID that the sediments are also settled in the nearby area, concluded out of the blue part in the area. This implies that sediments carried by natural currents and dredged with the Tiamat can travel a greater distance compared to the WID, where they travel with density currents. By analyzing the ADCP Backscatter data, it was observed that the sediment plume of the Tiamat could be tracked further than the fluidized sediments of the WID. Based on this information, it can be concluded that the Tiamat has a greater sediment plume travel distance than the WID. During the monitoring weeks, additional dredging activities were conducted within the pilot area, apparent from the red line that shows peaks indicating a Trailing Hopper Suction Dredger. One of the advantages of the WID method is that it produces a flat bottom surface, in contrast to the peaks of the red and purple line observed from the THSD. However, due to the presence of other dredging activities within the pilot area, monitoring had to be stopped prematurely after three weeks.

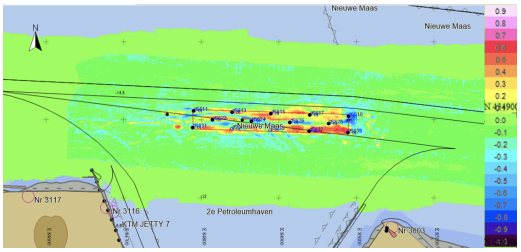

(a) Difference map before and after dredging with the Tiamat for the cohesive sediments, with a medium depth and high current velocities circumstances.

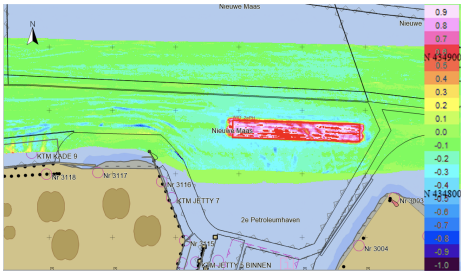

(b) Difference map before and after dredging with the WID for the cohesive sediments, with a medium depth and high current velocities circumstances.

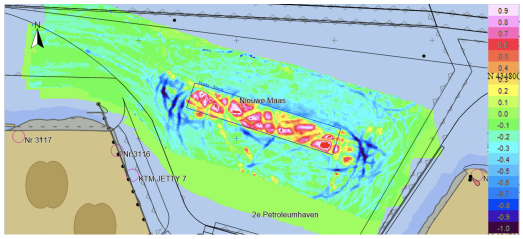

(c) Difference map before and after dredging with the UWP for the cohesive sediments, with a medium depth and high current velocities circumstances.

Figure 39: Map with the differences before and after dredging. Yellow and red colors represent where the depth has increased and the green and blue colors represent where the depth has become shallower.

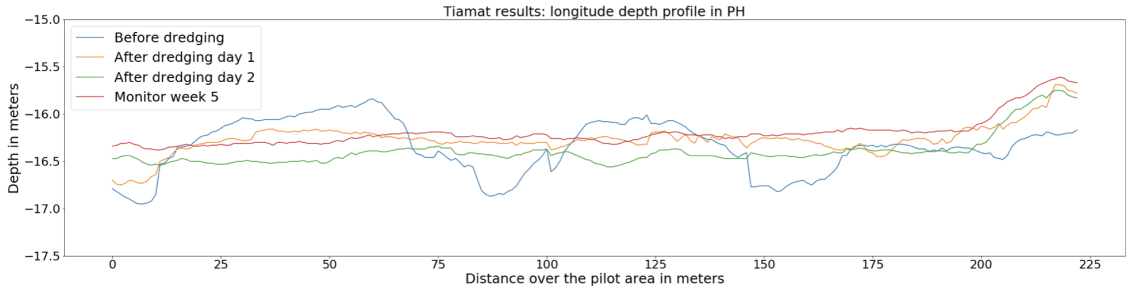

(a) The depth profiles for dredging with the Tiamat in cohesive sediments, with a medium depth and high current velocities circumstances. The blue line represents the depth before dredging, the orange and green line represents the depth after dredging, and the red line represents the depth during the monitor weeks.

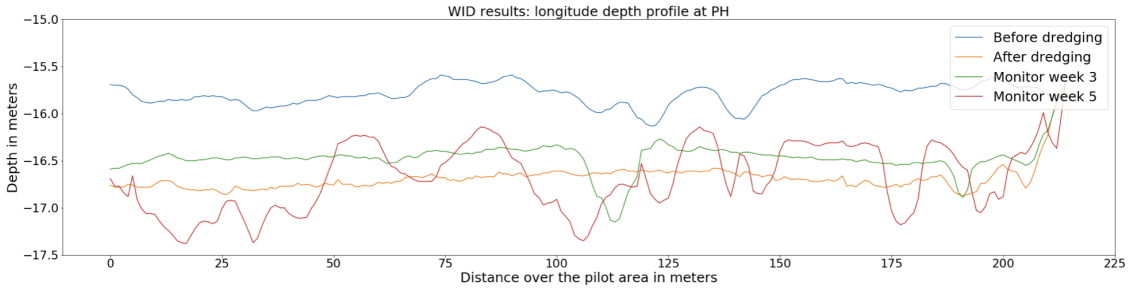

(b) The depth profiles for dredging with the WID in cohesive sediments, with a medium depth and high current velocities circumstances. The blue line represents the depth before dredging, the orange line represents the depth after dredging, and the green and red lines represent the depth during the monitor weeks.

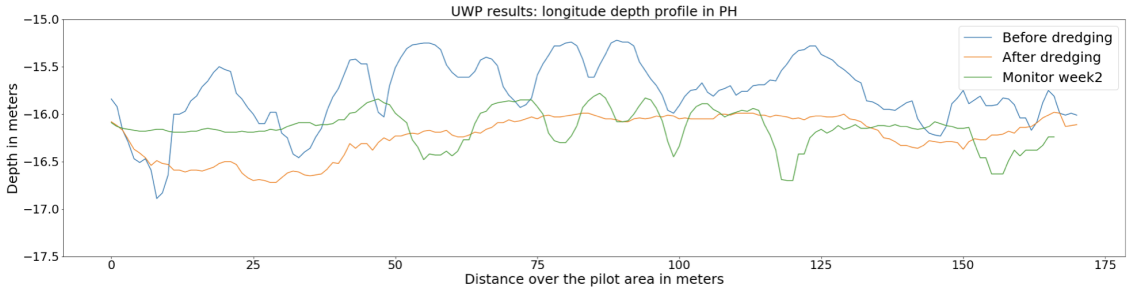

(c) The depth profiles for dredging with the UWP in cohesive sediments, with a medium depth and high current velocities circumstances. The blue line represents the depth before dredging, the orange line represents the depth after dredging, and the green line represent the depth during the monitor weeks.

Figure 40: The longitude depth profiles before dredging, after dredging and for the monitor weeks for different circumstances.

As observed from figures 39a and 40a, with the cohesive sediments, with a medium depth and high current velocities circumstances, the area is dredged the best. This was also expected as the circumstances were most similar to Harwich Haven (Spearman & Benson, 2022). Another reason is that at this location the Tiamat has been dredged for 2 days. As seen in the longitude depth

profiles there are pits before dredging, therefore the blue parts in the area are the pits that are filled with sediments after dredging with the Tiamat because the Tiamat flattens the area. Again, the turning point of the Tiamat is notable at the right end of the area. Observed from the monitor weeks, the depth increased faster than for the non-cohesive sediments, with great depth and low current velocities circumstances. This is influenced by the fact that this is a busy place, meaning that vessels are constantly passing through the area. The location is also in the waterway, which means the currents are high at this location, and a mud layer has been created in this area.

Observed in figures 39b and 40b, the longitudinal depth for the cohesive sediments, with a medium depth and high current velocities circumstances and WID with the agitation function, reveals an increase in depth while the bottom remains flattened. The depths of the monitor weeks closely align with their after dredging positions, the lines indicate that sedimentation is occurring at a relatively slow rate. The pilot area is dominated by red and pink colors, indicating again an overall increase in depth. But again there are more blue parts in the area, meaning that the sediments have settled in the nearby area. With the agitation function, the fluidized sediments are only jetted upwards, not at an angle. This can be the reason for the shorter travel distance. The WID method, with agitation function, was used at this location and was notably successful. However, blue regions are present in the nearby area, which corresponds to locations where after dredging sediment levels are higher than before dredging. This suggests that sediment settling has occurred in these areas. The red line in the longitude depth profile exhibits some irregularities in the form of peaks, which can be explained by additional dredging operations within the pilot area. These activities are also apparent in the maps included in appendix VII.

As observed in figure 39c and 40c, the blue line, the depth before dredging with the UWP, has more depth difference within the area than the orange line, which can be attributed to the Trailing Suction Hopper Dredger used for the previous dredging. After dredging with the UWP the bottom is more flattened out. During the second week of monitoring, additional lines were observed in the Multibeam data within the pilot area, indicating that other dredging activities had taken place.

Analyzing the longitude depth profiles for the three methods, it was observed that the Tiamat method did not have much sedimentation during the monitoring weeks. On the other hand, for the cohesive sediments, with a medium depth and high current velocities circumstances using the WID method showed sediment returning after just 2 weeks. This is because, during the Tiamat dredging process, the sediments are more diluted and higher in the water column where they can be transported farther away. As for the WID, the sediments are transported as a highly concentrated density current. Another reason can be due to seasonality and sedimentation from upstream. The Tiamat pilot was conducted in October and the WID pilot was conducted in December. The amount of sedimentation in October is lower compared to November, with a potential difference of up to 250000 m^3 throughout the whole Port of Rotterdam, with the highest amount occurring at the Maasvlakte. (Kirichek, 2018)

It was observed in figure 41, that the tracks made by the Barney for SH did not fall within the pilot area made for dredging due to miscommunication. This is confirmed from the track data of the Barney and the difference map created using the data from the Multibeam Echosounder taken

before and after dredging. Additionally, there are noticeable irregularities in certain lines within the pilot area that do not align with the width of the Tiamat. These irregularities are caused by the Tiamat being skewed as a result of sediment buildup within it. This skewness causes the Tiamat to pass over the bed at an angle, resulting in lines with greater depth on the lower part of the Tiamat.

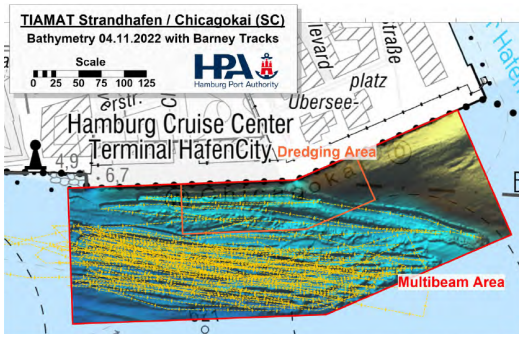

(a) The tracks of the Barney (with the Tiamat) made in the area.

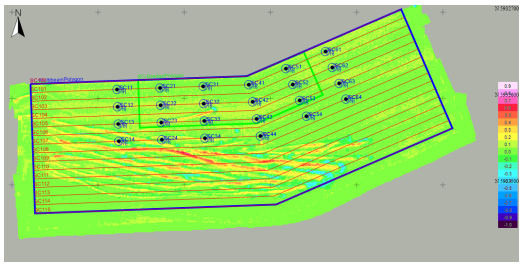

(b) Difference map made with the Multibeam Echosounder data before and after dredging with the Tiamat. The yellow and red parts represents where the depth after dredging has increased and the green and blue parts represents where the depth become shallower.

Figure 41: Dredging area Strandhafen.

The depth to which the Tiamat can perform dredging operations depends on the length of its discharge pipe, which is determined by the distance between the bed and the section of the water column with the strongest currents. If the length of the discharge pipe exceeds a certain threshold, the stability of the Tiamat is compromised, resulting in a maximum reach of 14 meters above the bed. The depth at which the WID can perform depends on the length of the water injector on the WID, this can reach a depth up to 25 meters. (Laboyrie et al., 2018) The depth at which the UWP can perform depends on the length of the lifting wire and the towing wires and when the plough is still stable. This can reach a depth of 30 meters, this is the deepest point tested in the Port of Rotterdam. (van den Bosch, 2023)

3.5 Production rate

To calculate the production rate, two pieces of information are required: the dredging time and the volume of material dredged. The volume dredged is measured using the Multibeam Echosounder before and after dredging. Additionally, the dredging time is recorded and log data is used to confirm.

For calculating the production rate equations 1 and 2 of appendix II can be used. For the different circumstances and different dredging methods, the production rates are calculated and can be found in table 4, the production rate is given in m^3/OH where OH is short for Operational Hours:

Area	**Tiamat (Barney)** out of the box	**Tiamat (Barney)** in or out of the box	**WID (Mersey)**	**UWP (Husky**
EH left	52.37 m^3/OH	x	x	x
EH right	Day 1: 45.83 m^3/OH Day 2: 21.05 m^3/OH Mean: 31.71 m^3/OH	x	82.03 m^3/OH	x
KK	187.49 m^3/OH	219.31 m^3/OH	881.3 m^3/OH	x
PH	Day 1: 7.07 m^3/OH Day 2: 230.63 m^3/OH Mean: 114.8 m^3/OH	Day 1: 105.01 m^3/OH Day 2: 321.09 m^3/OH Mean: 213.05 m^3/OH	2673 m^3/OH	765.54 m^3/OH
SH	569.67 m^3/OH			

Table 4: Production rates for the Tiamat, the WID and the UWP.

The production rate for day 2 of the Tiamat in the non-cohesive sediments, with a great depth and low current velocities circumstances, is significantly lower than day 1. This is because the Tiamat left the coarser sediments behind. The Tiamat does not work optimally in coarser sediments because coarser sediments settle too quickly with not enough currents. (Winterwerp & van Kesteren, 2004) The production rate for the cohesive sediments, with a medium depth and high current velocities circumstances, is significantly higher for the second day. This is because on the first day, the sediments shifted to the deeper parts of the soil and these were the pits in the pilot area, therefore the volume of sediments shifted out of the area is lower. By the second day, the pits were filled, resulting in much higher production. Another factor that affected the production rate is the human factor, over the days the crew of the Barney with the Tiamat gained more experience.

By analyzing the production rates across various depths, it has been determined that the Tiamat can perform dredging at different depths, as long as the Tiamat remains stationary. This means that during dredging, the Tiamat remains at the same position and not swining from front to back creating bites in the seabed with the knife plate as a result of currents coming against the Tiamat. However, its subsequent depth limitation is dependent on the length of the discharge pipe. The length of the discharge pipe is determined by the height in the water column where currents are strongest and the maximum length of the discharge pipe is 12 meters, which will allow sediments to be brought up to 14 meters from the bed. Additionally, the type and grain size of sediment plays a more significant role in the production of the Tiamat, rather than the depth, as long as the Tiamat remains stable.

The production rate for dredging with the WID in the cohesive sediments, with a medium depth and high current velocities circumstances, is significantly higher than the other production rates. At this location, the WID method with an agitation function is used. Primarily looking at production, this seems like a good location for this feature; high currents and cohesive sediments. For the normal WID methods, it can be concluded that the WID works better for higher currents and finer sediments.

The WID exhibits the highest production rate for all three locations, the UWP falling in the middle range of production rates and the Tiamat showing the lowest production rate. The relatively lower production rate of the Tiamat compared to the other dredging methods can be due to the longer dredging time it requires to achieve the same depth. Specifically, the Tiamat needs at least twice the amount of time compared to the WID and the UWP to reach the same depth. Because the production rate also depends on the experience of the crew on the dredging vessel, this is discussed in the discussion section.

With the data for the KK and the PH after dredging with the Tiamat, figure 42, the conclusion could be done with the PSD and the depth profiles that the sediments shifted within the area to the deeper parts.

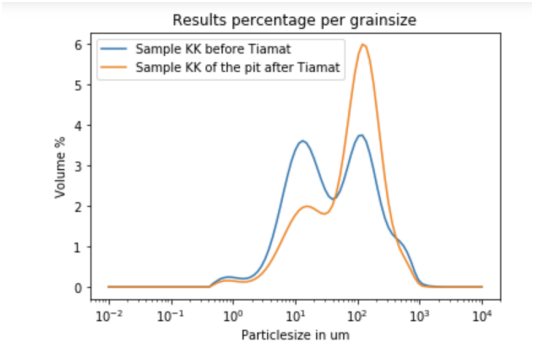

Figure 42: PSD of the deeper pit in the estuary of the Koolekade.

Figure 42 reveals that the peak is shifted to a coarser grain size and the peak is also higher. This means that the sediments are shifted within the pilot area. Therefore, the production rate for the shifted sediments in or out of the pilot area is also calculated with equation 2. For the locations, KK and PH, and can be found in table 4.

The production rate for the second dredging day with the Tiamat is still higher. This is because the bottom is less stiff using the Tiamat on the second day. The soil stiffness affects the effectiveness of water injection dredging. With softer soil, a higher rate of sediment removal will be achieved. (Zhang et al., 2016) The expertise of the crew operating the Tiamat is another important factor in determining the production rate. As the crew gains more experience with the Tiamat over an extended period, the production rate is likely to increase. But for determining how the production

rate will increase in the next couple of days the production rate from Harwich Haven Authority is used, this port has dredged more often with the Tiamat and has therefore more data available, figure 43. The production rate has been calculated using the same method, equation 1, as the production rate calculation for the Port of Rotterdam, based on more available data.

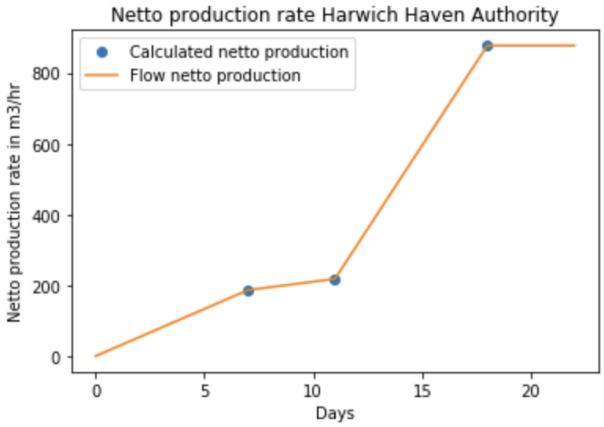

Figure 43: Production rate Harwich Haven Authority

For calculating the maximum production rate over days for the Port of Rotterdam, the slope of figure 43 of the production rate of Harwich Haven Authority is used in combination with the calculated data from the pilot with the Tiamat in the Port of Rotterdam. The calculations are based on the production rate of the cohesive sediments, with medium depth and high current velocities circumstances, because this is most similar to Harwich Haven. The calculations can be found in appendix VIII.

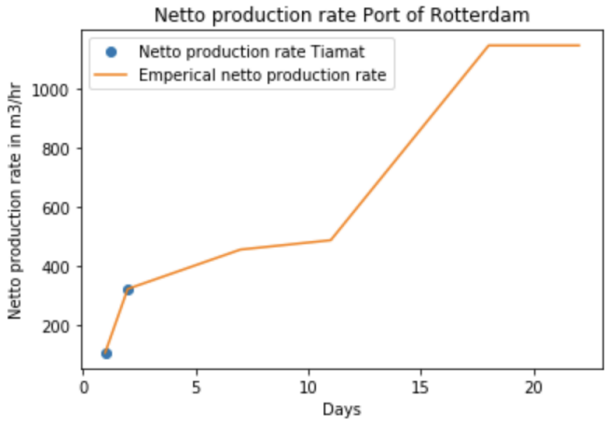

Figure 44: Production rate Port of Rotterdam

This means that after using the Tiamat for 15 days the maximum production of 1145 m^3/OH is reached, observed in figure 44. This production rate is used to calculate the fuel consumption of dredging with the Tiamat for the long term. The dredging schedule of the Tiamat is determined by the tides. Based on the tidal pattern of the upper water column, the Tiamat can dredge for an average of 15 hours per day in the Port of Rotterdam.

It is possible that the long-term use of a water injection dredger could cause changes to the structure and composition of the seabed, which may in turn affect the stiffness of the sediment. This could potentially impact the production rate over a period of 10 years or more. However, since the water injection dredger has already been in use in the Port of Rotterdam for several years, it is reasonable to assume that the production rate will remain relatively stable over the next years, assuming that the conditions at the dredging site do not undergo significant changes.

Due to the track problem with the Tiamat in SH as mentioned before a new area is created to calculate the production rate, this area is shown in figure 45.

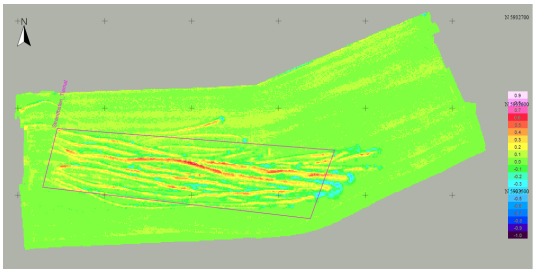

Figure 45: New dredging area created for the calculation of the production rate of SH.

The dredging time was 7.5 hours and the volume dredged was 4272.52 m^3, calculating with equation 1, the production rate for the SH in Hamburg is 569.67 m^3/OH. This the production rate after dredging for 2 days. This is higher than the production for the Port of Rotterdam. This can be due to the sediment characteristics, depth and currents.

3.6 Fuel consumption

The fuel consumption for the Barney with the Tiamat during dredging was 86.67 L/hr. Taking the mean production of shifted sediments out of the area in the Port of Rotterdam to calculate the fuel per cubic meters of removed sediment: 0.58 L/m^3. Using the mean production of the shifted sediments within or out of the area the fuel consumption will be: 0.56 L/m^3. Also, the fuel use in different sediments is interesting; per m^3 shifted non-cohesive sediments in or out of the area 2.06 L is necessary, and per m^3 shifted cohesive sediments in or out of the area 0.32 L is necessary. For calculating the fuel consumption when using the Tiamat for 10 years, this is for the long term, the dredging time per day of 15 hours is taken, as it can only be used when there is an outgoing tide in the top layer.
Cubic meter shifted = 10 years * 365 days * 15 hours * 1145 = 62688750 m^3

Fuel consumption = 62688750 * 0.56 = 35105700 L
The fuel consumption per cubic meter shifted sediment for the use of the Tiamat for 10 years is 0.076 L/m^3.

The fuel consumption for the Mersey with the WID during dredging was 230 L/hr. Taking the mean production of the shifted sediments within or out of the area the fuel consumption will be 0.19 L/m^3. Also, the fuel use in different sediments for the normal WID method is interesting; per m^3 shifted non-cohesive sediments out of the area 2.80 L is necessary, and per m^3 shifted cohesive sediments in or out of the area 0.26 L is necessary. The fuel consumption for the WID with agitation function is 0.086 L/m^3. For calculating the fuel consumption when using the WID for 10 years, the dredging time per day for the normal WID of 10 hours is taken, as it can only be used when there is an outgoing tide near the bottom. This is influenced by the sweet and salt water distribution. And the dredging time per day for the WID with the agitation method of 15 hours is used, as it uses the outgoing tide of the top layer. To compare fuel consumption with the other methods, the production rate for the KK, normal WID, and the production rate for PH, agitation function, is used.
Cubic meter shifted for the KK = 10 years * 365 days * 10 hours * 881.3 = 3216745 m^3
Fuel consumption normal WID = 3216745 * 0.086 = 276640.07 L
Cubic meter shifted for PH = 10 years * 365 days * 15 hours * 2673 = 146346750 m^3
Fuel consumption normal WID = 46346750 * 0.086 = 12585820,5 L

The fuel consumption for the Husky with the UWP during dredging was 24.8 L/hr. Taking the mean production of the shifted sediments out of the area the fuel consumption will be 0.032 L/m^3. This pilot is only done at the location where a mud layer, cohesive sediments, was located. When using the UWP for 10 years the production rate and so fuel consumption will be the same, as the crew already have a lot of experience in the Port of Rotterdam and distribution of the sediments will not be changed due to the UWP.

The fuel consumption for the different dredging vessels in different sediments is displayed in table 5.

Fuel consumption	**Tiamat (Barney)** Martens en van Oord	**WID (Mersey)** Van Oord	**UWP (Husky)**
Hourly	86.67 L/hr	230 L/hr	24.8 L/hr
Per m^3 shifted sediments out of the pilot area	0.58 L/m^3	0.19 L/m^3	0.032 L/m^3
Per m^3 shifted sediments in or out of the pilot area	0.56 L/m^3	0.19 L/m^3	0.032 L/m^3
Per m^3 shifted non-cohesive sediments in or out of the pilot area	2.06 L/m^3	2.80 L/m^3	x
Per m^3 shifted cohesive sediments in or out of the pilot area	0.32 L/m^3	0.26 L/m^3 0.086 L/m^3 (with agitation function)	0.032 L/m^3

Table 5: Fuel consumption for dredging with the Tiamat, WID and UWP.

The fuel consumption of a dredging vessel depends on the dredging depth, the soil type, the vessel size, the engine, and the operating conditions. Although the depth and soil type is the same for all three dredging methods, the vessel size varies significantly. The vessel of the UWP, the Husky, is notably smaller than the Mersey (WID) or Barney (Tiamat), resulting in differences in engine size and power. It can be assumed that the operating conditions remained the same during the three pilot weeks. The fuel consumption also depends on the time needed for dredging. Because the production rate of the Tiamat is the lowest, the fuel needed for shifting 1 cubic meter of sediment is higher compared to WID and UWP. With the type of vessel and the lower production rate the Tiamat has now, the CO_2 footprint of the Port of Rotterdam can not significantly be reduced by using the Tiamat system. To lower the CO_2 footprint significantly in the short term, it is necessary to use an electric vessel with green electricity with the Tiamat. However, Martens and Van Oord are currently lacking a suitable electric vessel for the Tiamat system. Once an electric vessel is available for Tiamat, the electric winch can be used during dredging to reduce the CO_2 footprint even more, there can be electric winning with lowering the winch during dredging. This method works by utilizing a dynamo, but it is expensive to implement. Nonetheless, it can effectively lower the CO_2 footprint. The electric vessel can also use hydropower, which is a renewable energy form that uses the power of moving water to generate electricity.

The prediction of the fuel consumption over the long term can be found in table 6:

Fuel consumption	**Tiamat (Barney)** Martens en van Oord	**WID (Mersey)** Van Oord	**UWP (Husky)**
Per m^3 shifted cohesive sediments in or out of the pilot area	0.076 L/m^3	0.26 L/m^3 0.086 L/m^3 (with agitation function)	0.032 L/m^3

Table 6: Fuel consumption for dredging with the Tiamat, WID and UWP over the long term.

However, analyzing the production rate for the Tiamat for the long term, the fuel consumption for the Tiamat will be lower than for the WID. The WID vessel is a more comparable vessel for the Tiamat than the UWP vessel, this will be an advantage for the Tiamat when using it for the long term. But not that the production rate is calculated with the data of the Harwich Haven Authority, this indicates that this is a prediction of how the production rate will increase when using the Tiamat for the long term.

3.7 Costs

The cost of the dredgers to be hired is confidential information, therefore it can not be published within this report. To facilitate a cost comparison of various dredging methods, a custom currency has been established. The currency is called the DredgeCoin (DC). Renting the Barney with the Tiamat costs 459712.5 DC for (de)mobilization and the trip from and to Rotterdam (Asperen & van Hassent, 2023). The rent price weekly is 963975 DC. This means that the hourly rent is 16948.65 DC. When using the Tiamat more often the (de)mobilization and trip from and to Rotterdam can be neglected. This will give a hourly rent of 11475.9 DC. This means that the price per m^3 shifted sediment without (de)mobilization and the trip from and to Rotterdam is 73.5 DC/m^3.

Renting the Mersey with the WID costs 68310 DC for 9.2 hours (Asperen & van Hassent, 2023). This means that the hourly rent is 7425 DC. This means that the price per m^3 shifted sediment is 6.15 DC/m^3. The price of the Mersey is the price when using the Mersey 24/7 when renting the Mersey for a shorter time the costs will be higher.

Renting the Husky with the UWP costs 3277.5 DC for 2.3 hours (van den Bosch, 2023). This means that the hourly rent is 1425 DC. This means that the price per m^3 shifted sediment is 1.88 DC/m^3. The price of the Husky is the price when using the Husky 24/7 when renting the Husky for a shorter time the costs will be higher.

	Tiamat (Barney) Martens en van Oord	**WID (Mersey)** Van Oord	**UWP (Husky)**
(De)mobilization and trip to and from Rotterdam	459712.5 DC		
Rent weekly (12/7)	963975 DC		
Rent for 9.2 hours		68310 DC	
Rent for 2.3 hours			327.5 DC
Rent hourly	16948.65 DC	7425 DC	1425 DC
Rent hourly without (de)mobilization	11475.9 DC		
Price per m^3 (without (de)mobilization)	73.5 DC/m^3	6.15 DC/m^3	1.88 DC/m^3

Table 7: Costs in DC for dredging with the Tiamat, WID and UWP.

When comparing costs, table 7, the most accurate way is to analyze the costs per cubic meter of sediment shifted. But because the production rate of the Tiamat is the lowest, the cost of shifting 1 cubic meter of sediment is high compared to WID and UWP.

3.8 Summery

The summery is given in an overview in table 8 with details for the Tiamat, WID and UWP under different circumstances.

		EH left	**EH right**	**KK**	**PH**
	Sediment characteristics	Non-cohesive sediments	Non-cohesive sediments	Cohesive sediments with a mud layer	Cohesive sediments with the thickest mud layer
	Depth	Around 19 meters with bed level differences	Around 19 meters	Around 16 meters	Around 16 meters
	Salinity [PSU]	25-30	25-32	5-25	3-22

Table 8: An overview with all the boundary conditions for dredging with the Tiamat (blue), WID (green) and UWP (red).

		EH left	**EH right**	**KK**	**PH**
Tiamat	Sediments plume transport	681 m 68 m width	931 m 72 m width	2207 m 198 m width	3923 m 227 m width
	Return time	35 minutes	20 minutes	47 minutes	38 minutes
	Production rate [m^3/OH] out of the area	52.37	45.83, 21.05	187.49	104.01
	Production rate [m^3/OH] in/out of the area	x	x	219.31	105.01, 321.09
	Fuel consumption per m^3 shifted sediments		2.06 L/m^3		0.32 L/m^3
	Fuel consumption per m^3 shifted sediments over 10 years				0.076 L/m^3
	Cost [DC/m^3] for the average production	73.5			
WID	Sediment plume transport	x x	487 m 35 m width	401 m 27 m width	912 m 33 m width agitation method
	Return time	x	45 minutes	38 minutes	25 minutes with agitation method
	Production rate [m^3/OH]	x	82.03	881.3	2673 with agitation method

Table 8: An overview with all the boundary conditions for dredging with the Tiamat (blue), WID (green) and UWP (red).

		EH left	**EH right**	**KK**	**PH**
	Fuel consumption per m^3 shifted sediments		2.80 L/m^3	0.26 L/m^3	0.086 L/m^3 with agitation method
	Fuel consumption per m^3 shifted sediments over 10 years			0.26 L/m^3	0.086 L/m^3 with the agitation method
	Cost [DC/m^3] for the average production	6.15			
UWP	Sediment plume transport	x	x	x	x
	Return time	x	x	x	55 minutes
	Production rate [m^3/OH]	x	x	x	765.54
	Fuel consumption per m^3 shifted sediments				0.032 L/m^3
	Fuel consumption per m^3 shifted sediments over 10 years				0.032 L/m^3
	Cost [DC/m^3] for the average production	1.88			

Table 8: An overview with all the boundary conditions for dredging with the Tiamat (blue), WID (green) and UWP (red).

4 Discussion

To properly understand the conclusion and results, it is important to take into account the following assumptions, limitations and weaknesses. Therefore, this chapter reflects on the research. First, in section 4.1, the results of the monitoring tools are discussed. Second, in section 4.2, the results of the sediment transport. Third, in section 4.3, the calculations and assumptions of the production rate are discussed. Subsequently, section 4.4, there is described how the locations affected the outcome of the boundary conditions. At the end of this chapter, section 4.5, the technical improvements for increasing the production rate for the three different maintenance dredging equipment are discussed.

4.1 Monitoring tools

According to Ossian, all monitoring tools have a degree of measuring error, which can be lessened through calibration. It is important when interpreting the results to consider the margin of error, especially when comparing data from the same location at different times, as current conditions may vary. While comparing data before and after dredging may not pose an issue, it is important to factor in the margin of error when using the data for calculations like production rates. Multibeam Echosounder data is typically employed for calculating production rates, but when flow rates are low, slight data variations can occur and must be taken into account. To reduce the measuring error of monitoring tools, a correction factor or more frequent calibration may be utilized (Ossian, 2021).

The Rheotune data is affected by both measurement error and winch usage, therefore a solution for more accurate data can be using the Slib sampler, but it is a more time-consuming process. The Rheotune was lowered into the water using a winch. However, the winch was broken just before the Tiamat pilot. There was an attempt to make the winch temporarily, but this proved ineffective. As a result, the Rheotune data was affected. The Rheotune data was also influenced by sediments in the device. At the end of the Rheotune measuring, it was discovered that the Rheotune was not completely clean even though we had attempted to clean it using water from the port. It is unsure where the contamination originated from. Additionally, the bottom in the area may have been influenced by other dredging activities. Although there were no dredging activities in the pilot area during the Tiamat monitor weeks, there were some dredging activities near the area which may have impacted the Rheotune results. To decrease the uncertainties of the Rheotune the Slib Sampler can be used, this method is more time-consuming than using the Rheotune. The Slibsampler utilizes a cylindrical tube with lateral openings to extract sediment core samples. These openings can also be used to gather fluid mud samples from the core, which can be analyzed immediately on board using an Anton Paar density meter. On the other hand, the Frahmlot method involves a cylinder connected to the Frahmlot, allowing for the collection of soft sediment core samples up to 1 meter in length and 0.1 meter in diameter. After collection the sample, it can be placed into buckets and transported to a laboratory for further characterization analysis. In the laboratory, the density and yield stresses of the collected samples can be measured as well (Kirichek & Rutgers, 2020).

ABP Marine Environmental and Sassi et al. have solutions to reduce the measurement error of the ADCP Backscatter and a solution for tracking the sediment plume with less of a blind spot

compared to the ADCP Backscatter. As mentioned, the ADCP backscatter data has a blind spot 1 meter above the bed (Dunn & Zedel, 2022). Consequently, the accuracy of the WID data may be lower compared to the Tiamat data, which follows the sediment plume at the height of 12 to 14 meters instead of close to the bed. For the UWP, the ADCP Backscatter did not work. Because the ADCP Backscatter did not work for the UWP the sediment transport is assumed with the Multibeam Echosounder data and the Swift turbidity profiles. One solution is to utilize ABPmer support to measure sediment flow, which has already been tried and tested in conjunction with WID, making it a valuable tool for monitoring. ABPmer utilizes a predefined set of analysis techniques for its monitoring activities. This involves comparing the before, after, and dredge conditions within the water column at several fixed locations on the seabed. The results obtained, in conjunction with continuous fixed station monitoring and dual-frequency echo sounder tracking of sediment plumes, provide insights into the movement of dredged material within and around the harbor (ABP Marine Environmental, 2011). Also, regarding the travel distance of sediments after being tracked by the ADCP Backscatter, it is assumed to be carried away further to the North Sea due to stronger currents. A solution to decrease the uncertainty is to use the bathymetry of the whole area so there can be determined where the settlements are settled down, and the sediments can be spread out over the area. Another solution to make the ADCP Backscatter more accurate is to use the calibration method of Sassi et al. This approach involves estimating specific attenuation and mass concentration in order to calculate the reference attenuation caused by sediment. To achieve this, the method utilizes an explicit approach for estimating mass concentration through calibration, coupled with an empirical derivation of specific attenuation.

To reduce the uncertainty of the location of the Valeport Swift Turbidity the ADCP Backscatter data with OBS measurement can be used. The Valeport Swift Turbidity is influenced by the location where the turbidity is measured. Because it only measures one point for the returning time to the reference situation and this is influenced by currents if the turbidity is going further than that point or not. A solution can be using the estimation of SSC (Suspended Solid Concentration) of the ADCP Backscatter data with the calibration of the OBS measurement (Kim & Voulgaris, 2017). This can determine the concentrated solids in the water and therefore the turbidity over a greater area. At the locations where the SSC is high, the Valeport Swift turbidity can be used.

4.2 Sediment transport

Taking measurements of both the density of the particles and the shapes of the sediments could potentially lead to improved outcomes when using Stoke's law. This is because Stoke's law relies on certain assumptions, such as the spherical shape of soil particles, a dilute suspension that prevents particle interaction and laminar fluid flow, which means no turbulence. Also, an assumption is done that the sediments have a uniform density (Cartwright, 2020). In reality, sediments in rivers come in various shapes and sizes, and there can be turbulence present. Additionally, the assumption of uniform sediment density was made for the boundary condition. The outcome can be improved by measuring the density of the particles and the shapes. With a flocculation camera and the PSD, the settling velocity can be derived as a function of equivalent spherical diameter (Ali et al., 2022).

4.3 Production rate

The production rate formula of Ma for WID can be used to reduce the uncertainty of the production rate. This is because equation 2, for the production rate, relies on the zero line to determine the number of sediments that have been shifted. The zero line can be determined when the net volumetric cubic meters are nearly 0. However, the depth is calculated as an average and does not take into account the bed elevation within the area. One way to reduce the uncertainty is to apply the formula used by Ma for WID, which utilizes parameters such as intrusion depth, sediment concentration, jet bar width, and transverse velocity to determine the production rate. Although not all of this information is currently available for the Tiamat and the formula needs to use the discharge pipe in the equation as well, conducting further research to obtain this data can help provide a more accurate estimate using this equation.

Using Harwich Haven production rates and the fall cone method to determine the stiffness of sediments can reduce uncertainty when calculating the maximum production rate with frequent use of Tiamat. This is because Harwich Haven Authority has different sediments, depths and currents, therefore using their data to determine the maximum production rate of the Port of Rotterdam has some uncertainties. Using the fall cone method the stiffness of the bottom sediments can be determined before and after dredging and this can be used in the production rate over time for the Tiamat at the Port of Rotterdam and at Harwich Haven. This will decrease the uncertainty (Wang et al., 2022).

4.4 Locations

Measurements for determining the boundary conditions of the Tiamat are done by testing the Tiamat in the Port of Rotterdam, modelling these data can be a solution for even more accurate boundary conditions. Thus for determining the boundary conditions of the Tiamat the results for the Port of Rotterdam were used, however, this can be different when other parameters, like sedimentation, are taken into account. Or this can already be different when using the Tiamat another time at the same location. Additionally, it can also be different when using the Tiamat more often at the same location, as proven at PH location. Given that this port is a tide-dominated port, the results obtained can be extrapolated to other tide-dominated ports. Nonetheless, it is crucial to acknowledge that other factors, such as currents, organic matter, and seasonal variations, can also significantly affect the outcome. Therefore, to validate these findings, further testing of Tiamat is required in different seasonal conditions. Additionally, parameters like sediment composition, bed elevation, and operational experience should also be considered to provide a comprehensive evaluation of the performance of the Tiamat. A solution can be to use and test the Tiamat in the same areas more times to determine the influence of such parameters.

KK has the area next to the berth, during the Tiamat pilot and the WID pilot, vessels were entering and leaving the berth. For the Tiamat pilot the area was more within the berth than for the WID pilot area. Which affected the transport of the sediment plume. The movement of vessels resulted in the plume being carried out of the port by these vessels.

The dredging activities at EH faced challenges due to the presence of rocks in the area. This ge-

ological condition was not previously known, which could have an impact on the outcome of the production rate. Both Tiamat and WID systems are not designed to handle rocky substrates, and for Tiamat, this proved particularly problematic as the presence of rocks was near the pilot area, this was a problem for the sediment flow near the seabed, thereby could affect the production results.

A solution to decrease these uncertainties that can have influenced the data is to use the measurements of the different locations connected to the boundary conditions to model the measurement data with the boundary conditions (Tuinhof, 2014).

4.5 Maintenance equipment

When comparing the three dredging methods, it is essential to consider the various factors that can impact the outcome. The production rate can be influenced by several variables, including the experience of the crew and the operating conditions during dredging. Additionally, external factors such as the velocity of the currents, weather conditions, and sedimentation from upstream can also affect the outcome. Therefore, a comprehensive analysis of these factors is necessary to provide an accurate comparison of the three dredging methods.

As the dredging methods are still being refined, the following subsections will focus on the technical improvements that have been identified to enhance the productivity of the dredging equipment. These improvements are based on the experiences gained during the pilot weeks. However, it is important to note that these enhancements have not been fully tested yet.

4.5.1 Technical improvements of the Tiamat

In appendix X, a technical drawing of the Tiamat can be found. This drawing is used for determining the technical improvements for the Tiamat.

The width of the Tiamat application can be increased to increase the production rate. Upon initial observation, the Tiamat appears to have relatively small dredging equipment, only 8 meters in length. This means that the Tiamat may require multiple passes over the same area to reach the desired depth in the whole area. To increase the rate of production and efficiency, widening the width of the Tiamat could lead to a larger ground coverage per pass and a reduction in operational time. This can be concluded out of the track data of the Mersey and the Barney in appendix IX, as the density of the dots for the Mersey is lower than for the Barney and the width of the dredging equipment for the WID is larger than for the Tiamat.

Additionally, tow wires on the sides and incline sensors on the Tiamat can be the solution for the frequently angled Tiamat application during dredging operations due to the high concentration of sediment present on one side of its application. The tow wires should then be able to be controlled separately from each other. This was also seen when the Tiamat was lifted out of the water. A solution for this problem can be tow wires on both sides of the Tiamat, the wires would ensure that the Tiamat always hangs straight by pulling harder on one tow than the other. Also, this would enhance the productivity of the Tiamat during dredging operations in areas with different

bed elevations.

In addition to that, an adjustable discharge pipe can be the solution for the depth challenges in the Port of Rotterdam. Each depth required a different length of the discharge pipe of the Tiamat, which had to be customized and then installed during the pilot week. This process was time-consuming and required the use of a crane, making it a complex task. An option to provide a solution for this problem is to make an adjustable discharge pipe. Making the discharge pipe adjustable can be done with a telescopic section. This can be done by making a pipe with multiple sections so that the discharge pipe can slide in and out of each other (Kim, 2000). This can be done more easily and faster than changing the whole discharge pipe. The adjustable discharge pipe can only be changed for a couple of meters, this is why all the ports using the Tiamat more often need their adjustable discharge pipe. Another way to improve the discharge pipe is by reducing its diameter, which will result in a higher production rate because the flow velocity in the discharge pipe is higher and the pressure in the discharge pipe will increase (Kaji & Azzopardi, 2010). But this is only possible if the capacity of the suction pump also increases. More sediments will go through the discharge pipe in a shorter amount of time. An extra improvement on the discharge pipe can be a rotating head. The design of Hamburg demonstrates the significance of the direction in which sediments are jetted out, as this may vary across different ports and locations within each port. This is because the sediments in the sediment plume that need to be transported by the natural current already have the correct flow direction, making it easier for them to be carried away further by the currents (MacDiarmid, 2006). This can be done with a rotary union, this is a mechanical device that can transfer water, air, coolant, and steam within 360 degrees from a stationary pipe to a rotating shaft. This device consists of a rotating element and seals to prevent leaking between the pipe and the rotating head (MOFLON, 2020).

Another improvement can be done to the angle of the knife plate of the Tiamat. By giving the hoist wire in the middle of the Tiamat more space, the Tiamat works easier and more productively, this was tested during the pilot week. This was due to the knife plate, which was currently positioned to cut through the sediment directly in front of the Tiamat, as opposed to scraping the sediments on the bed surface. Therefore, another solution can be a better angle of the knife plate, because this also depends on the grain size of the bed sediments an rotational knife plate can also be an option.

Another logical improvement is that the pump could improve the vessel speed and the production rate of the Tiamat. At present, the vessel carrying Tiamat must navigate through the area at low speeds to avoid that the Tiamat is getting stuck in the sediments. Wilson concluded that the capacity of the pumps have influence on the velocity of the injected water. Therefore, there can be concluded that the pumps will also influence the suction capacity. By using a stronger suction pump, the vessel can move over the dredging area at a greater speed, which can reduce the dredging time and increase the production rate. Also, an increase in the suction pump can result in more sediments into the discharge pipe and less water.

One potential enhancement concerns the use of the Tiamat, a density meter that can be calibrated within the discharge pipe, to increase production rates. During dredging operations in the pilot

week, it was difficult for the crew to determine whether the Tiamat was cutting into the seabed or just the water. To address this issue, a surveyor boat equipped with an ADCP backscatter was used to track the sediment plume and could determine if the Tiamat needed to be lowered again. But the Tiamat has not been cutting into bottom sediments for several minutes when detected with the ADCP Backscatter, the Tiamat was above the bed and already needed to be lowered again. For this reason, a density meter can be adjusted in the discharge pipe. This allows for immediate detection of either newly accumulated sediment within the pipeline or a situation where the knife plat is no longer cutting into the seabed.

4.5.2 Technical improvements of the WID

The sediments for the WID technique with an agitation function can be transported further by the currents as a result of the angle in the jetting nozzle. The WID technique with an agitation function demonstrated good productivity during testing. As observed from the bathymetry data and the ADCP Backscatter some sediments are settled down in the nearby area. In order to enhance production rates even further, it might be advantageous to not only jet the fluidized sediments upwards but also provide an impulse in the direction of the currents. This can be accomplished by employing a nozzle angle. With an angled nozzle, the fluidized sediments are propelled in the direction of the currents, enabling them to be carried more easily. This approach may also be valuable in confined areas such as KK and berths. MacDiarmid already investigated the streamwise flow velocity of a single grain has an impact on the flow distance and flow velocity of the single grain when carried with the currents compared to when this start from zero velocity.

During the WID pilot with the agitation method, it was discovered that adjusting the pressure at which the sediment plume is jetted upwards impacts the height of the sediment plume. IADC already proven that changing the pressure can increase the depth where the WID can work. This means that the increasing the pressure has an influence on the height also for jetting upwards. Initially, the plume did not reach the required height, so the pressure was increased until the desired height was achieved. This change in plume height was observed using the ADCP Backscatter onboard the Survey boat. Additional monitoring devices, such as ADCP Backscatter, could be employed on board the WID vessel to determine if the pressure is sufficient to attain the required height. Another solution to reach the required height with less pressure on the nozzle is to use more nozzles. This is already proven by Swart for the water injection nozzles and can be used to determine how many nozzels are needed for jetting up the fluidized sediments.

4.5.3 Technical improvements of the UWP

During the UWP pilot, the ability to generate a density current with the plough was tested by dividing the sediment into layers of 10 centimeters. This was the chosen thickness of the layers for the UWP, based on the experiences of both Tiamat, which had cut the sediment into layers, and the experience gained in Hamburg (Barney crew, 2023). To increase the production rate, it may be necessary to investigate the effectiveness of other layer thicknesses and the flow velocities needed.

5 Conclusion

This chapter elaborates on the key findings of this research. The key findings of this study are summarised by answering the research questions. Section 5.1, described the answer to research question 1 about the boundary conditions of the Tiamat. Section 5.2, is a comparison between the Tiamat, WID and UWP and this answers research question 2. Subsequently, section 5.3, is about the future of the Tiamat. This is about the long-term use of the three dredging equipments and technical improvements for the Tiamat, and this will answer research question 3.

5.1 Boundary conditions of the Tiamat

RQ1: What boundary conditions are most suitable for the Tiamat application for tide-dominated ports taking into account factors such as sediment characteristics, sediment transport, turbidity, top sediment layer, different depths, production rate and fuel consumption?

The production of the Tiamat and therefore the boundary conditions are mainly influenced by the depth, the currents and the sediment characteristics. The boundary conditions for the currents are given by the minimal current velocity needed, this is for the particles of 195 μm, 0.0030·traveldistance. Furthermore, a minimal current velocity for the particles of 210 μm is 0.0034·traveldistance.

Additionally, the sediment boundary condition requires that the sediments must be finer than 195 μm, resulting in a lower production rate for non-cohesive sediments. As already confirmed by other water injection dredgers, the production rate will be the highest in cohesive sediments.

The depth boundary condition for the Tiamat is limited by the length of the discharge pipe, with a maximum length of 12 meters. As a result, the maximum allowable depth is such that the sediment plume can be lifted no more than 14 meters above the seabed.

Next to the previously mentioned boundary conditions for operating the Tiamat, there are other important factors to consider as well. One such factor is minimizing hindrance to marine traffic, as well as minimizing any negative effects on water quality. The turbidity is used as a measure of water quality. Turbidity dissipates more quickly for non-cohesive sediments, which gives a return time of 20 (for non-cohesive sediment) to 47 minutes (for cohesive sediments) for the turbidity to return to the reference situation, not including turbidity at 1 meter above the bottom.

The use of the Tiamat has minimal impact on the yield strength but influences the depth of the nautical density.

In order to minimize hindrance to marine traffic, it is necessary to reduce the dredging time. To achieve this, improvements to the Tiamat vessel are required to simultaneously minimize CO_2 emissions and turbidity while increasing production. At present, the application of the Tiamat is not sufficient to reduce the CO_2 footprint significantly of the Port of Rotterdam. However, by making predictions of the production rate for long-term use, it may be possible to reduce CO_2 emissions.

5.2 Comparing the Tiamat, WID and UWP

RQ2: How does the Tiamat perform compared to the Water Injection Dredging (WID) and the Underwater Plough (UWP) taking into account factors such as sediment characteristics, sediment transport, turbidity, different depths, production rate, fuel consumption and costs?

The Tiamat and WID are more effective, and thus have a higher production rate, in cohesive sediments, as non-cohesive sediments settle easily and are difficult to move out of the port because higher currents are necessary. The UWP pushes aside all sediment, including coarser ones, making it less of an issue.

The next difference in the dredging methods is the turbidity generated during dredging. When dredging with the Tiamat, more staggered turbidity is caused within the whole water column due to its technology of bringing sediments higher. In comparison, the WID and UWP only generate turbidity near the bed.

For the performance at different depths, the Tiamat has a depth restriction based on discharge pipe length, while the UWP has a depth limitation based on the length of the tow and lifting wires and the WID has a depth limitation based on the length of the water injector.

Finally, the Tiamat has a lower production rate compared to the WID and the UWP, resulting in higher fuel consumption per cubic meter of sediment shifted. But the sediments can be carried away further than for the WID and the UWP. Additionally, the Tiamat is more expensive to operate, leading to higher costs per cubic meter shifted.

5.3 Future

RQ3: How is the fuel consumption from the dredging vessels for the long term using the Tiamat compared to using the WID and UWP and how can the production of the Tiamat be improved?

With a prediction about the production rate for the Tiamat when using it for a long term the fuel consumption per cubic meter shifted sediment can be calculated. This increase in production rate is due to the stiffness of the bottom sediments and the experience of the crew. The fuel consumption can be reduced and can be lower compared to the WID and the UWP.

In the future, the production rate of the Tiamat can be increased through technical improvements, including upgrades to the discharge pipe and suction pump, optimization of the tow wires, adjustments to the angle of the knife plate, and the use of density meters.

6 Recommendation

This chapter contains recommendations for further research that follows from this study.

First, more research can be done in improving the technique of the Tiamat. Some improvements are already given in the discussion of this report but the feasibility of these improvements needs to be determined. For more research, a scale model can be used to test the improvements.

Second, a better understanding of sedimentation from upstream, both natural sedimentation and seasonal sedimentation, is required. This can be done with a sediment return flow model for the Tiamat. The model that can be used is developed by PRISMA and Deltares, with this model and the measurements the new sediment and return of the sediments can be determined. With a better understanding of the sedimentation also the final destination of the dredged sediments can be determined or better tracked with the ADCP Backscatter. This is not only useful for the Tiamat but also for other Water Injection Dredgers.

Next, there is potential for further research to increase the depth of nautical density and yield stress using the Tiamat. One potential approach is to utilize clean water and inject water into the bottom sediments. This is an area of interest for muddy ports and could lead to significant improvements in dredging efficiency.

Another point of consideration is that this study primarily focused on Tiamat and compared it with WID and UWP. However, during the pilot, two new functions of the methods were tested and found to be effective. Further research can be conducted on these functions specifically for the Port of Rotterdam. The WID with agitation function proved to have the highest production rate, leading to lower fuel consumption and costs than the Tiamat. This method can use some improvements and the technique should be further investigated to gain a better understanding.

Additionally, during the pilot weeks, the UWP method was used to create a density current, which had the lowest costs and fuel consumption. However, further research and improvements are required, particularly in regard to the plough. As discussed in the previous section, two key areas for improvement are the thickness of the sediment layer cut by the plough and the technical enhancements required to create a more effective density current. As result, the UWP method may offer a more nature-based dredging solution, as the vessels are readily available and fuel consumption is minimal.

Finally, for future research, there can be looked into other energy transition methods of all three dredging methods (Penny, 2021). This will be easier for the WID and the UWP since the Tiamat requires more energy due to having an additional suction pump in addition to the water injection pumps. For the UWP, this will be easiest since the dredging method does not require a pump but only a hydraulic system to use for the plough. This may be a more environmentally friendly solution to dredging methods for the long term.

References

ABP Marine Environmental. (2011). *Water injection dredging – monitoring leads to effective planning.*

Alamy Stock Photo. (2021). Hybrid powered water-injection dredger mersey working around the king george v lock in london [Accessed April 2, 2023].

Ali, W., Enthoven, D., Kirichek, A., Chassagne, C., & Helmons, R. (2022). *Effect of flocculation on turbidity currents.*

Asperen, J., & van Hassent, A. (2023). Interview.

Barney crew. (2023). Face to face.

Bergs, & Bossinade. (2000). *Baggeren met water: ervaringen en meetresultaten.*

Bhonsle, J. (2022). *Evolution and Upsizing of Container Vessels.*

Borst, W., Vellinga, T., & van Tongeren, O. (2013). *THE MONITORING PROGRAMME FOR THE MAASVLAKTE 2 CONSTRUCTION AT THE PORT OF ROTTERDAM – PART II.*

BV, W. S. (2022). *Getijden Rotterdam 2022.*

Cartwright, J. (2020). *Stokes' law, viscometry, and the Stokes falling sphere clock.*

Cox, J., Huismans, Y., Knaake, S., Leuven, J., Vellinga, N., van der Vegt, M., Hoitink, A., & Kleinhans, M. (2020). *Anthropogenic Effects on the Contemporary Sediment Budget of the Lower Rhine-Meuse Delta Channel Network.*

Damen. (2022). *Dredging pumps.* https://products.damen.com 2023

de Boer, P. J., & Werner, C. J. (2016). *Provide end users with the most accurate nautical depth measurement by using the combination of echo sounders and density measurement equipment.*

de Haas, R. (2022). Tiamat 2022 discharge port of rotterdam.

Deltares. (2015). *Evaluatie van het OSR-model voor zoutindringing in de Rijn-Maasmonding II.*

Dredgepoint. (2021). *Maas2.0.* https://www.dredgepoint.org/dredging-database/equipment/wid-20-maas 2023

Dunn, M., & Zedel, L. (2022). *Evaluation of discrete target detection with an acoustic Doppler current profiler.*

EL-Hattab, A. I. (2014). *Single beam bathymetric data modelling techniques for accurate maintenance dredging.*

Engineering Toolbox. (2020a). *Solids - densities.* https://www.engineeringtoolbox.com/density-solids-d_1265.html 2023

Engineering Toolbox. (2020b). *Water - dynamic (absolute) and kinematic viscosity vs. temperature and pressure.* https://www.engineeringtoolbox.com/water-dynamic-kinematic-viscosity-d_596.html 2023

European Patent Office. (1998). *Improvements in underwater ploughing.*

Gandrass, J., & Salomons, W. (2001). *Dredged Material in the Port of Rotterdam – Interface between Rhine Catchment Area and North Sea -.*

Ganic, E. (2022). *Port of rotterdam accelerates reduction of carbon emissions.* https://www.dredgingtoday.com/2022/06/06/port-of-rotterdam-accelerates-reduction-of-carbon-emissions/ 2023

Guarnieri, A., Saremi, S., Pedroncini, A., & Vincenzi, C. (2021). *Effects of marine traffic on sediment erosion and accumulation in ports: a new model-based methodology.*

Hales, L. (1995). Accomplishments of the corps of engineers dredging research program. *Journal of Coastal Research*, *11*, 68–88.

HHA, H. H. A. (2021). *The Tiamat, Dredging with nature.*
Holdaway, G. P., Thorne, P. D., Flatt, D., Jones, S. E., & Prandle, D. (2000). *Comparison between ADCP and transmissometer measurements of suspended sediment concentrationn.*
IADC. (2013). *Facts about water injection dredging.*
IADC. (2014). *Facts about Trailing Hopper Suction Dredger.*
IADC. (2015). *An Information Update from the IADC; Turbidity and Dredging.*
IADC. (2020). *Ra water injection dredger injects large volumes of water into the waterbed, fluidising the sediment so that it can flow naturally to other deeper areas.* https://www-iadc-dredging-com.tudelft.idm.oclc.org/subject/equipment/water-injection-dredgers/ 2023
Institute for Water Education. (2023). *Nature-based solutions.* https://www.un-ihe.org/collection/nature-based-solutions 2023
Kaji, R., & Azzopardi, B. (2010). *The effect of pipe diameter on the structure of gas/liquid flow in vertical pipes.*
Kim. (2000). *Method of making bent adjustable pipe by shape measurement.*
Kim, & Voulgaris, G. (2017). *Estimation of suspended sediment concentration in estuarine environments using acoustic backscatter from an ADCP.*
Kiriche k, A., Chassagne, C., Winterwerp, H., Noordijk, A., Rutgers, R., Schot, C., Nipius, K., & Vellinga, T. (2018a). *How navigable are fluid mud layers?*
Kirichek. (2018). *M3- 2017-2018 xlsx.* Port of Rotterdam.
Kirichek, Cronin, K., de Wit, L., & van Kessel, T. (2021). *Advances in Maintenance of Ports and Waterways: Water Injection Dredging.*
Kirichek, Rutgers, R., Wensveen, M., & van Hassent, A. (2018b). *Sediment management in the Port of Rotterdam.*
Kirichek, & Rutgers, R. (2020). *Monitoring of settling and consolidation of mud after water injection dredging in the Calandkanaal.*
Koop, L. (2022). *Using Multibeam Echosounders for Multiscale and Interdisciplinary Habitat Mapping on the Dutch Continental Shelf.*
Kortmann. (1994a). *Water Injection Dredging.*
Kortmann. (1994b). *Waterinjectie baggeren, een vernieuwde modellering.*
Laboyrie, P., van Koningsveld, M., Arrninkhof, S., van Parys, M., Lee, M., Jensen, A., Csiti, A., & Kolman, R. (2018). *Dredging for sustainable infrastructure.*
Lagaillarde, J. (2022). *Internal navigation solutions for navies.* https://www.ixblue.com/defense/naval-navigation/inertial-navigation-solutions-for-navies// 2022
Ma, S. (2022). *Laboratory study on the efficiency of water injection dredging. An analysis on the influence of different dredge settings on the density current and production rate.*
MacDiarmid, H. (2006). *Sediment grains in fluids: settling, transport and feedback.*
Malvern Instrument. (2005). *Mastersizer 2000 Integrated systems for particle sizing.*
Manik, H. M., Gultom, D. A., Firdaus, & Elson, L. (2020). *Evaluation of ADCP backscatter computation for quantifying suspended sediment concentration.*
MarineTraffic. (2021). *Search for marine.* https://marinetraffic.com/en/ais/details/ships/ 2023
MOFLON. (2020). *Rotary joint and rotary unions.* https://www.moflon.com/rotary-unions/?utm_source=googleads&vt_keyword=rotary%20union&gclid=Cj0KCQiAx6ugBhCcARIsAGNmMbjRXeU-jKM2krBAmtm4Jy4iA9XDQhueLnysLKLnWNq3lu1qtBU4qMMaAtfpEALw_wcB 2023
My agriculture information bank. (2017). *Density of soil: Bulk density and particle density.* https://agriinfo.in/density-of-soil-bulk-density-and-particle-density-260/ 2023
Omar, A. F., & Jafri, M. Z. M. (2010). *The Swift Turbidity Marker.*

Organization, E. S. P., & the Ecoports Foundation. (2020). *Port Environmental Review System (PERS)*.
Ossian. (2021). *How to Reduce Measurement Error*.
Penny, T. (2021). *Hydrogen-fuelled dredgers to maintain Netherlands' coastline*.
PIANC. (1997). *Approach channels- A guide for design*.
PIANC. (2014). *Harbour Approach Channels Design Guidelines*.
Port of Rotterdam. (2022). *Wheather and tide hydro meteo dashboard*. https://weather-tide.portofrotterdam.com/desktop/ 2022
PortMaps. (2022). *Portmaps of the port of rotterdam*. https://portmaps.ad.portofrotterdam.com/PortMaps/Index.html?viewer=PortMaps.Portmaps_UH2&LayerTheme=9 2022
Redactie Scheepsbouw. (2021). *'hybride water injection dredgers zijn state of the art'*. https://www.maritiemnederland.com/nieuws/van-oord-doopt-hybride-waterinjectievaartuigen 2023
Royal Haskoning DHV. (2022). *Verspreiden in zoet water*.
Safety4Sea. (2022). *Port of rotterdam aims to cut carbon emissions by 23 million tonnes*. https://products.damen.com 2023
Sánchez, Perrotti, R., Paz, D. G., & Alejandra, M. (2020). Ongoing challenges to ports: The increasing size of container ships. *16*, 1–15.
Sassi, M., Holtink, A., & Vermeulen, B. (2012). *Impact of sound attenuation by suspended sediment on ADCP backscatter calibrations*.
Science facts. (2020). *Stokes' law*. https://www.sciencefacts.net/stokes-law.html#:~:text=Stokes'%20law%20can%20explain%20the,in%20the%20form%20of%20rain. 2023
Septentrio. (2019). *AsteRx-U MARINE*.
Sigwald, R., Ledoux, S., & Spencer, K. (2015). *WATER INJECTION DREDGING GUIDANCE*.
Simpson, M., & Vural, M. (2022). *Proposed use of agitation techniques for maintenance dredging in Harwich Harbour*.
Spearman, J., & Benson, T. (2022). *EVOLUTION OF NATURE-BASED DREDGING SOLUTIONS AT HARWICH, UK*.
StemaSystems. (1990). *SILAS: Seismic acquisition and processing software suite*.
StemaSystems. (2020). *Demonstration video Rheotune*.
Svasek. (2007). *Het operationele stromingsmodel rotterdam osr*. https://www.svasek.nl/project/het-operationele-stromingsmodel-rotterdam-osr/ 2023
Swart, R. (2015). *Autonomous dredging of mud*.
Tiessen, M., Kranenburg, W., ter Maat, J., Huismans, Y., Kuijper, K., Mens, M., & van der Wijk, R. (2016). *Systeemanalyse van de RijnMaasmonding voor verzilting*.
Tuinhof, T. (2014). *Modelling far-field dredge plume dispersion*.
Valeport. (2022). *Swift turbidity device*. Retrieved September 20, 2022, from https://www.valeport.co.uk/products/swift-svpplus-turbidity/
van den Bosch, A. (2023). Call.
Van Oord. (2020). *Water Injection Dredging; The natural way of dredging*.
Verhagen, H. J. (2000). *Water injection dredger*.
Wang, Wu, S., Jing, X., Liu, K., & Ren, L. (2022). *Strength and Stiffness Degradation Mechanisms of Stabilized/Solidified Sediments by Freeze–Thaw Cycles*.
Wasserman, J., Wasserman, M., Barrocas, P., & Almeida, A. (2016). *Predicting pollutant concentrations in the water column during dredging operations: Implications for sediment quality criteria*.
Wells, J. T. (1995). *Geomorphology and Sedimentology of Estuaries*.

Welp, T. L., Tubman, M. W., Wilson, D. A., & Pollock, C. E. (2017). *Water Injection Dredging.*
Wilcock, P. R. (1994). *Critical Shear Stress of Natural Sediments.*
Wilson, D. (2012). *Water injection dredging in U.S. waterways, history and expectations.*
Winterwerp, & van Kesteren, W. (2004). *Introduction to the Physics of Cohesive Sediment Dynamics in the Marine Environment.*
Winterwerp, Wang, Z., van Kesteren, J., & Verweij, J. (2002). *Far-field impact of water injection dredging in the Crouch River.*
Zhang, S., Zhao, M., Ge, T., & Wang, C. (2016). Experimental research on trenching in stiff clay by submerged vertical traveling jets. *Coastal Research*, *32*.

Appendix I: Schedule Tiamat and WID pilot

Tiamat pilot

The tide is very important for planning the locations because you don't want the sediments to get back into the channel. This is the reason why we are not very flexible with the hours of scheduling. The time when using the Tiamat is estimated using the OSR models and the 'getijde boekje 2022'. (BV, 2022) On the day, we may choose to have the Tiamat go over the areas for longer than the estimated four hours. Another problem is the different depths of the discharge pipe of the Tiamat. Replacing the pipe costs money and time, which is why we have to do the sections in one port for the first few days and the other days in the other port. In addition, the locations are about an hour by boat from each other, making sailing between them in one day an expensive alternative.

Since the Tiamat is in the port of Rotterdam for the first time, Saturday and Sunday will be used to get the Tiamat settings as optimal as possible. Saturday the Tiamat will arrive and the pipe will be installed. Then the end of Saturday and Sunday the Tiamat will do maintenance dredging in the Port of Rotterdam to get used to the depth and the sediments. The optimal speed will also be determined these days. The optimal speed in Harwich Haven Authority was 3 knots, sailing too slow will lead to clogging of the Tiamat.

On Monday the Tiamat will start with the pilot. Areas have dimensions of 200 meters by 25 meters. With a generous time estimate, we would use the Tianat for 4 hours per area. For the calculation, the vessel speed used is 2 to 3 knots and the Tiamat will go 5 to 6 times over the area. The following schedule is set.

Maandag 17-10-2022	**Tiamat**	**Monitoren Surveyor 1**	**Monitoren Tender**
8:00 - 12:00	Europa haven vak 1	Europa haven vak 1 sediment pluim volgen: ADCP backscatter	Boot voor Swift turbidity
12:00-16:00	Europa haven vak 2	Europa haven vak 2 sediment pluim volgen: ADCP Backscatter	Boot voor Swift turbidity
16:00-20:00		Europa haven vak 1 en 2: Rheotune and Multibeam	
Dinsdag 18-10-2022	**Tiamat**	**Monitoren Surveyor 1**	**Monitoren Tender**
9:00-13:00	Europa haven vak 1	Europa haven vak 1 sediment pluim volgen; ADCP backscatter	Boot voor Swift turbidity
13:00-17:00		Europa haven vak 1; Rheotune and Multibeam	Sailing to the Koolekade
17:00-21:00	Tiamat changing the pipe and sailing to the Koolekade	Sailing to the Koolekade	
Woensdag 19-10-2022	**Tiamat**	**Monitoren Surveyor 1**	**Monitoren Tender**
6:00-12:00	Koole haven vak 1	Koole haven vak 1 sediment pluim volgen; ADCP backscatter	Boot voor Swift turbidity
12:00 -16:00		Koole haven vak 1; Rheotune and Multibeam	
Donderdag 20-10-2022	**Tiamat**	**Monitoren Surveyor 1**	**Monitoren Tender**
7:00-13:00	Koole haven vak 1	Koole haven vak 1 sediment pluim volgen; ADCP backscatter	Boot voor Swift turbidity
13:00-16:00		Koole haven vak 1; Rheotune and Multibeam	
Vrijdag 21-10-2022	**Tiamat**	**Monitoren Surveyor 1**	**Monitoren Tender**
7:00-12:00	Koole haven vak 2	Koole haven vak 2 sediment pluim volgen; ADCP backscatter	Boot voor Swift turbidity
12:00- 16:00		Kool haven vak 2; Rheotune and Multibeam	

Figure 46: Schedule Tiamat pilot.

WID pilot

For the WID pilot, the tide was again important for the dredging schedule. But the Mersey has already dredged several times in the Port of Rotterdam, so I didn't need to schedule a time to get used to the conditions of the Port of Rotterdam. I also knew better how many hours it would take the Mersey to dredge and how long it would take the survey boats. The following schedule for the WID pilot is set.

On Wednesday we start with normal WID in the Europahaven. After this, the Mersey will sail to the Koolekade so that the Mersey can start at this location on Thursday. On Thursday the Mersey start with the agitation technique of the WID, which is at the estuary of the Koolekade and the 2e Petroleumhaven, this is the reason for 'WID+jetten' in the schedule. When this is done the Mersey starts with the last area at the Koolekade, here the dredging technique is just normal WID again. Eventually, I did not use the Mersey on Friday.

Woensdag 30-11-2022	**Mersey**	**Monitoren Surveyor 1**	**Monitoren Tender**
8:00-10:00	WID Europahaven	Europa haven sediment pluim volgen: ADCP backscatter	Boot voor Swift turbidity
10:00-13:00		Europahaven : Rheotune, Silas, Siltprofiler and Multibeam	Boot voor Swift turbidity
13:00-15:00		Varen richting Koolekade	Varen richting Koolekade
Donderdag 1-12-2022	**Mersey**	**Monitoren Surveyor 1**	**Monitoren Tender**
10:30-12:30	WID+jetten Koolekade/2e Petroleumhaven	Koolekade/2e PH sediment pluim volgen: ADCP backscatter	Boot voor Swift turbidity
12:30-14:30	WID Koolekade	Koolekade sediment pluim volgen: ADCP backscatter	Boot voor Swift turbidity
14:30-16:30		Both areas: Rheotune, Silas, Siltprofiler and Multibeam	Boot voor Swift turbidity
Vrijdag 2-12-2022	**Mersey**	**Monitoren Surveyor 1**	**Monitoren Tender**
9:00-17:00	Voor eventuele uitloop	Voor eventuele uitloop	Voor eventuele uitloop

Figure 47: Schedule WID pilot.

Appendix II: Equations

Production rate

The production rate for the Tiamat, WID and UWP can be calculated with equation 1 or 2:

$$Productionrate[m^3/OH] = \frac{Volume_1[m^3]}{Dredgingtime[Operationalhours]} \tag{1}$$

$Volume_1$ is the volume shifted out of the box and is calculated with the netto volumetric difference between the data of the multibeam before dredging and after dredging.

The other equation is:

$$Productionrate[m^3/OH] = \frac{Volume_2[m^3]}{Dredgingtime[Operationalhours]} \tag{2}$$

$Volume_2$ is the volume of sediments shifted in or out of the box and is determined by the first search for the 'zero-line' in the after-dredging data. This is the depth where the netto-volumetric difference is close to 0 m^3. Next, the area above the zero line for the reference data is calculated. These are the sediments shifted within the area. The accuracy of the assumptions made in using equation 2 should be discussed in the discussion section. This will provide insights into the reliability of the results obtained from the calculations based on these assumptions.

The choice of which formula to use depends on the condition of the bed in the reference situation and the dredging technique used. If the bed has significant variations in elevation or pits, sediments may accumulate in deeper areas during dredging using the Tiamat or WID, making equation 2 more applicable. Before using equation 2, it is necessary to verify whether the sediments have been shifted to deeper areas.

Settling velocity

For determining the settling velocity of the particles Stoke's law is used. After calculating the settling velocity the minimal current velocity can be determined. Using Stoke's law a couple of assumptions are made, see the discussion session. Stoke's law is based on two forces on a grain, the drag force and the gravity force. (Science facts, 2020)

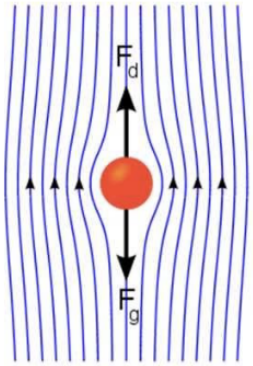

Figure 48: The currents and forces for Stoke's Law (Science facts, 2020).

The equations for the forces are equations 3 and 4:

$$Fd = 6 \cdot \pi \cdot \eta \cdot r \cdot u \tag{3}$$

$$Fg = \frac{4}{3} \cdot \pi \cdot r^3 \cdot (\rho_s - \rho_w) \cdot g \tag{4}$$

$$Fd = Fg \tag{5}$$

Solving these equations leads to the settling velocity of:

$$u = \frac{d^2 \cdot g \cdot (\rho_s - \rho_w)}{18 \cdot \eta} \tag{6}$$

Solving equation 5 leads to equation 6. In equation 6 the d represents the diameter of the particle in meters, the g is the gravitational force of 9.81 m/s^2 and the ρ_s and ρ_w the density of the particle in g/L and the density of the medium which is water in g/L respectively. The η is the viscosity of the water in Pa·s, this is determined using figure 49, and the water temperature is determined with the data from the Swift Turbidity measurement.

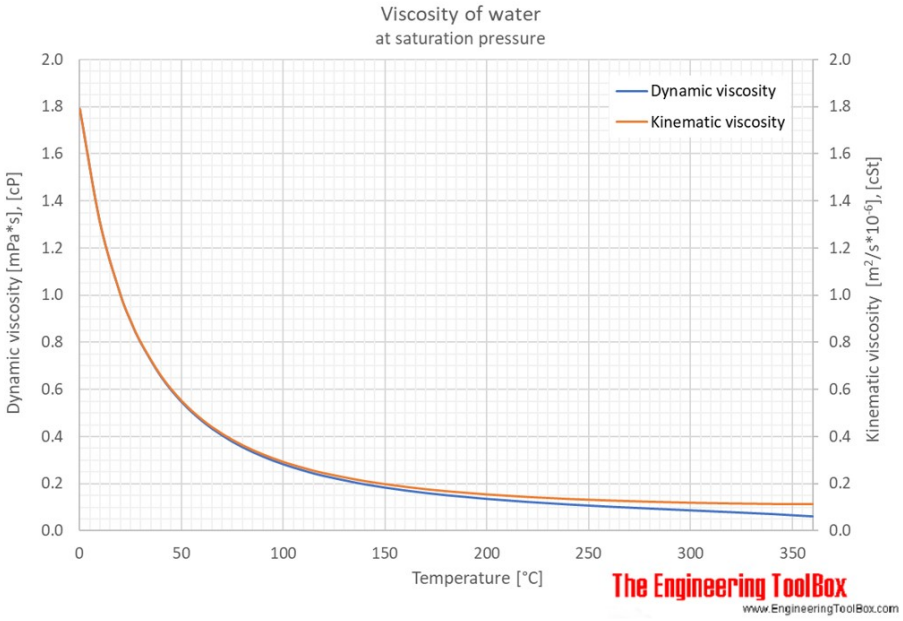

Figure 49: Graph for determining the viscosity of the water (Engineering Toolbox, 2020b).

When the settling velocity is calculated the time it takes for the sediment to reach a certain depth can be calculated with equation 7.

$$Time_{forparticletosettle} = \frac{depth}{settlingvelocity} \tag{7}$$

In equation 7 the depth in meters and the settling velocity in m/s give the time in seconds. With the time and distance, the minimal current velocity can be calculated with equation 8.

$$Minimalvelocitycurrent = \frac{distance}{time} \tag{8}$$

The distance is in meters and the time is in seconds, this gives a result of the minimal velocity current in m/s.

Appendix III: ADCP Backscatter data

From the following figures, the overview of the path of the sediment plume is determined.

Tiamat

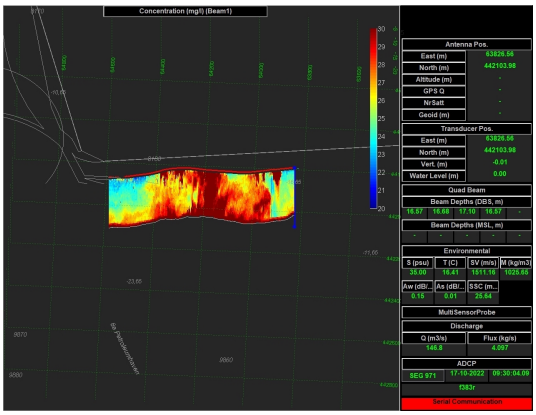

Figure 50: ADCP Backscatter figure on 17-10-2022 from the center row.

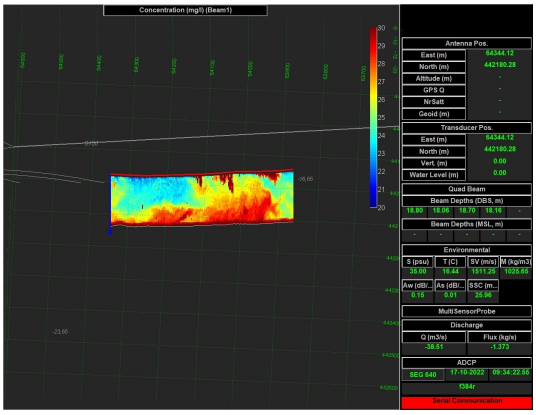

Figure 51: ADCP Backscatter figure on 17-10-2022 from the row on the North of the pilot area.

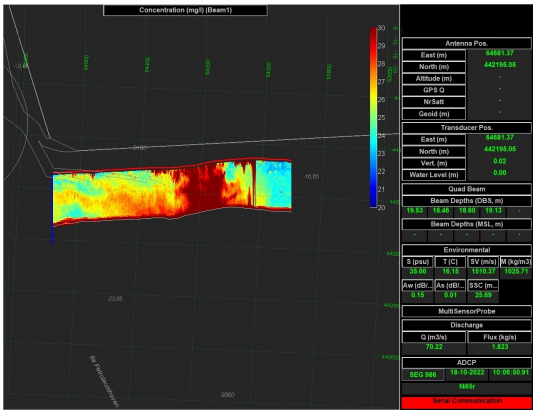

Figure 52: ADCP Backscatter figure on 18-10-2022 from the center row.

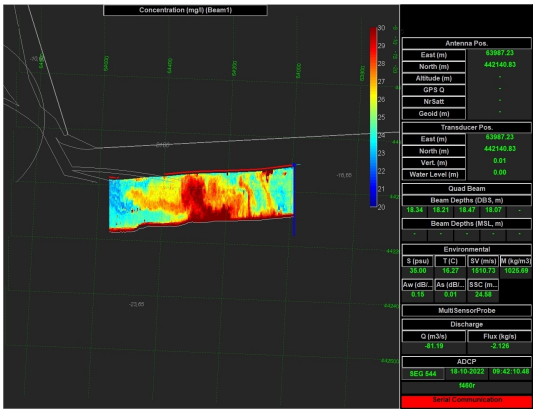

Figure 53: ADCP Backscatter figure on 18-10-2022 from the row on the North of the pilot area.

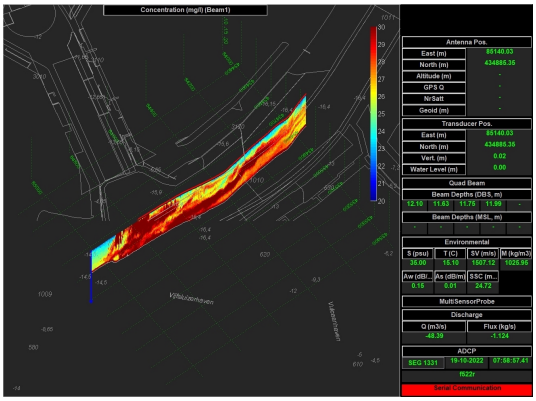

Figure 54: ADCP Backscatter figure on 19-10-2022 from the center row.

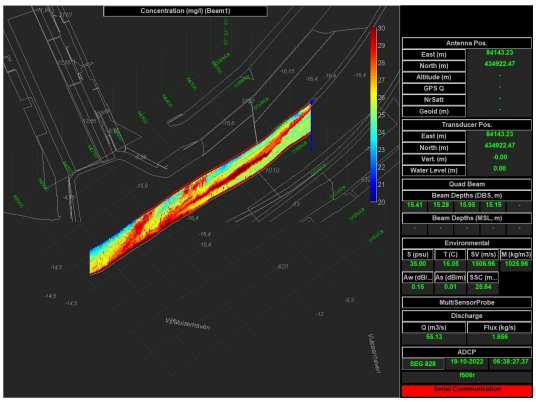

Figure 55: ADCP Backscatter figure on 19-10-2022 from the row on the North of the pilot area.

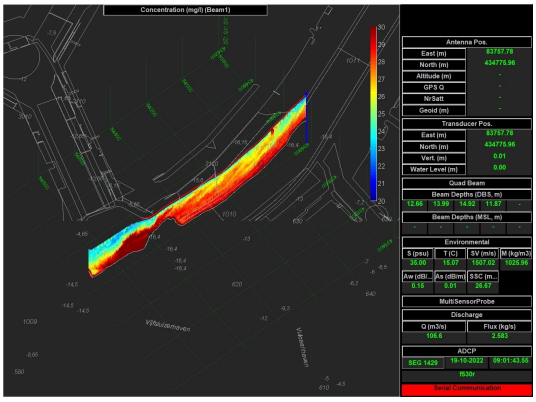

Figure 56: ADCP Backscatter figure on 19-10-2022 from the row on the South of the pilot area.

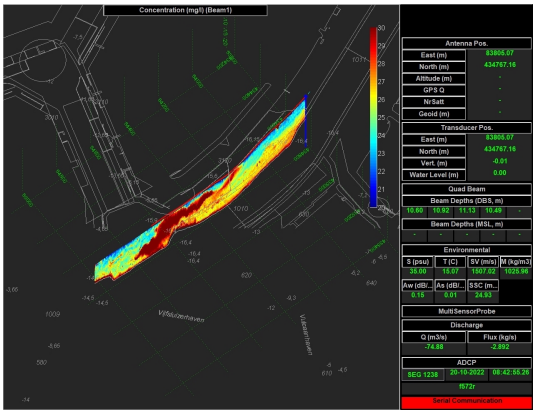

Figure 57: ADCP Backscatter figure on 20-10-2022 from the center row.

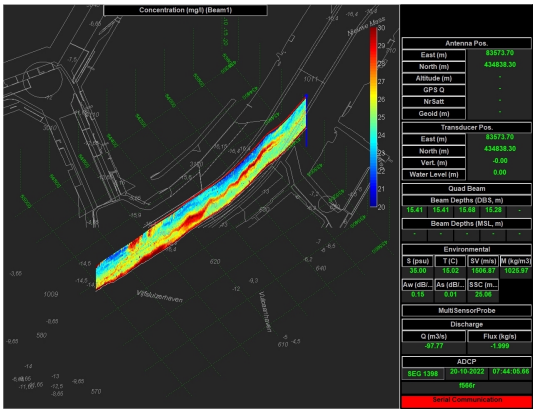

Figure 58: ADCP Backscatter figure on 20-10-2022 from the row on the North of the pilot area..

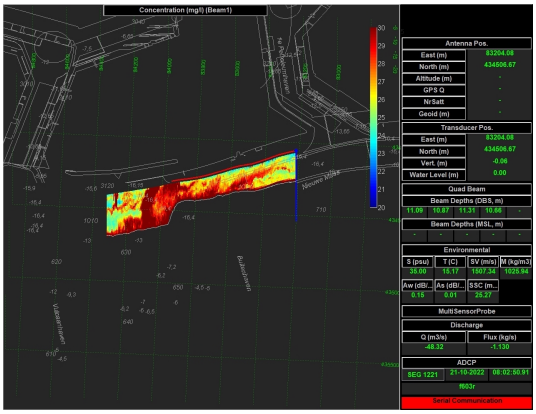

Figure 59: ADCP Backscatter figure on 21-10-2022 from the center row.

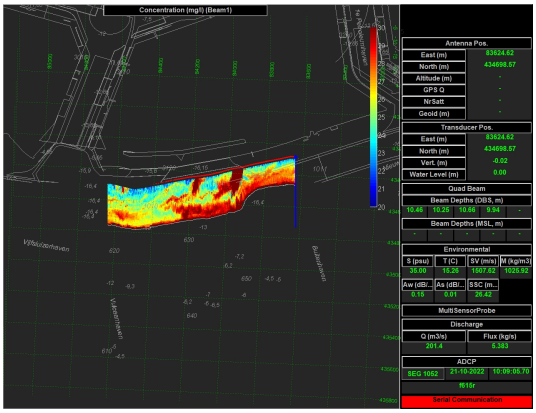

Figure 60: ADCP Backscatter figure on 21-10-2022 from the row on the North of the pilot area.

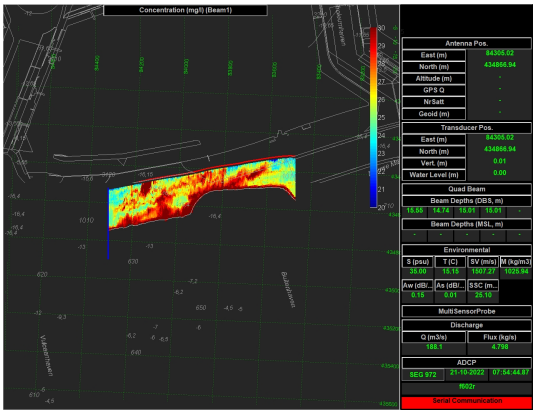

Figure 61: ADCP Backscatter figure on 21-10-2022 from the row on the South of the pilot area.

WID

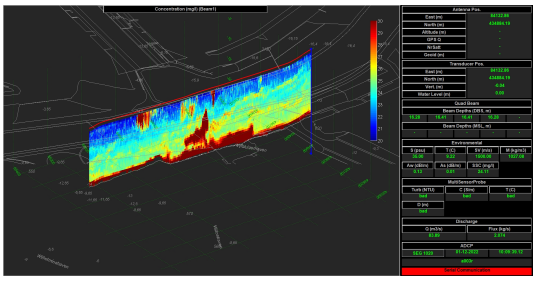

Figure 62: ADCP Backscatter figure on 01-12-2022 from the row on the North of the pilot area.

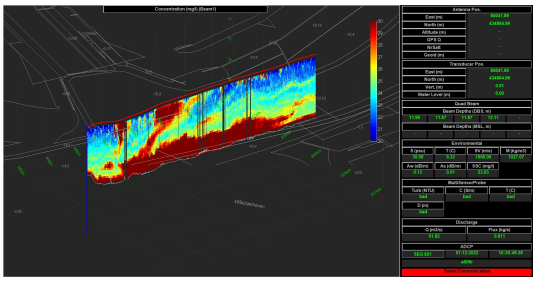

Figure 63: ADCP Backscatter figure on 01-12-2022 from the row on the North of the pilot area with the jetting function of the WID.

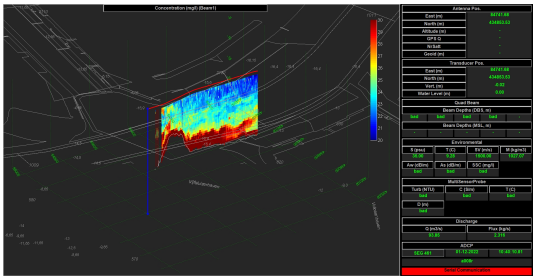

Figure 64: ADCP Backscatter figure on 01-12-2022 from the row on the South of the pilot area with the jetting function of the WID.

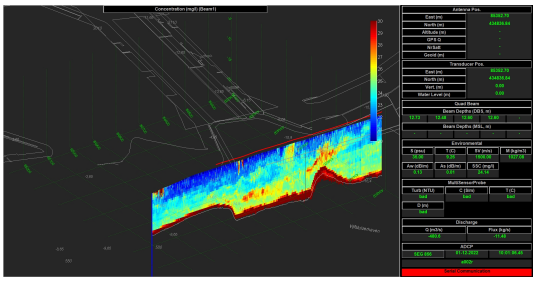

Figure 65: ADCP Backscatter figure on 01-12-2022 from the row on the South of the pilot area.

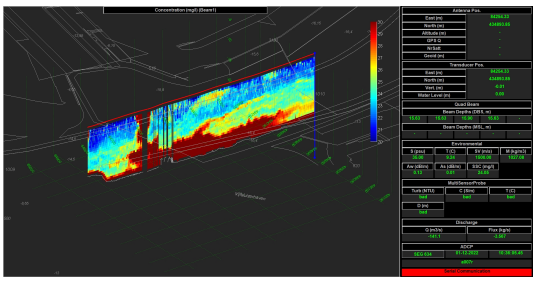

Figure 66: ADCP Backscatter figure on 01-12-2022 a row from the center of the pilot area with the jetting function of the WID.

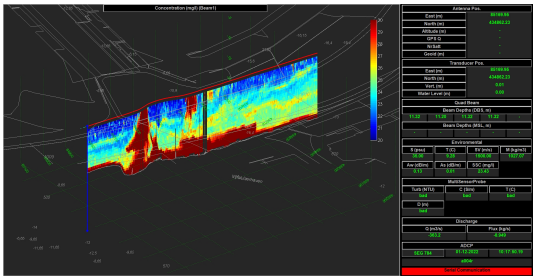

Figure 67: ADCP Backscatter figure on 01-12-2022 a row from the center of the pilot area.

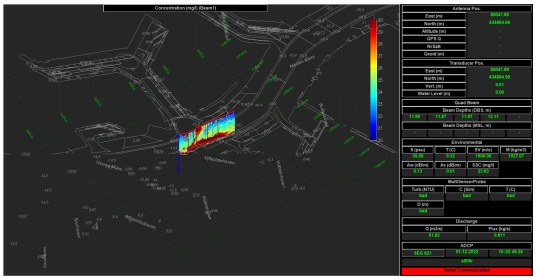

Figure 68: ADCP Backscatter figure on 01-12-2022 overview of the location.

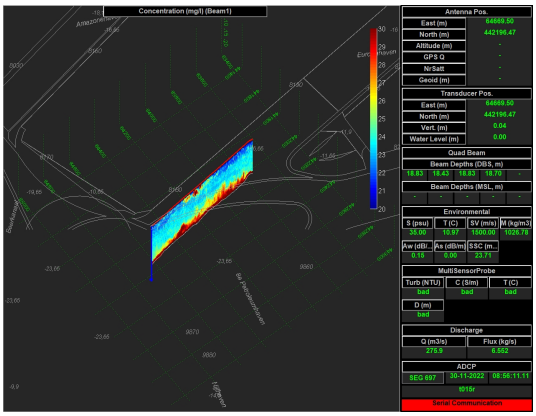

Figure 69: ADCP Backscatter figure on 30-11-2022 a row from the center of the pilot area.

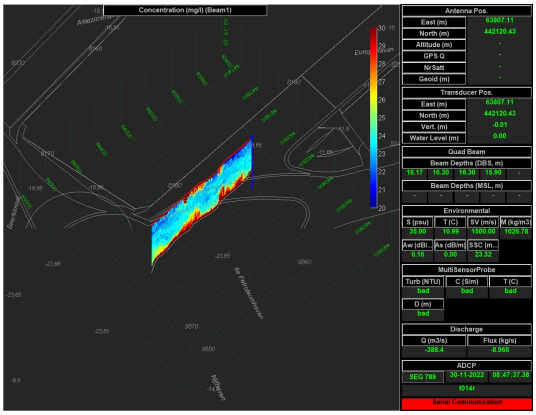

Figure 70: ADCP Backscatter figure on 30-11-2022 from the row on the North of the pilot area.

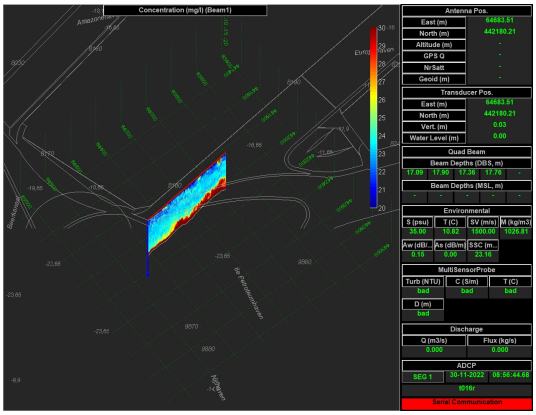

Figure 71: ADCP Backscatter figure on 30-11-2022 from the row on the South of the pilot area.

Appendix IV: Stream profiles

In this appendix, the streaming profiles overtime on the date of the pilot can be found. The profiles were created for the elevation where the Tiamat, the WID and the UWP deposited the sediments.

Tiamat

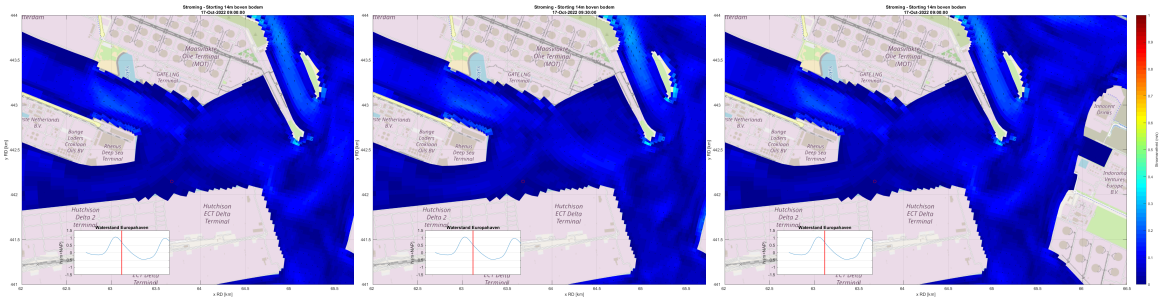

(a) Current profile on 17-10-2022 of the Europahaven and surrounding area.

(b) Current profile on 17-10-2022 of the Europahaven and surrounding area.

(c) Current profile on 17-10-2022 of the Europahaven and surrounding area.

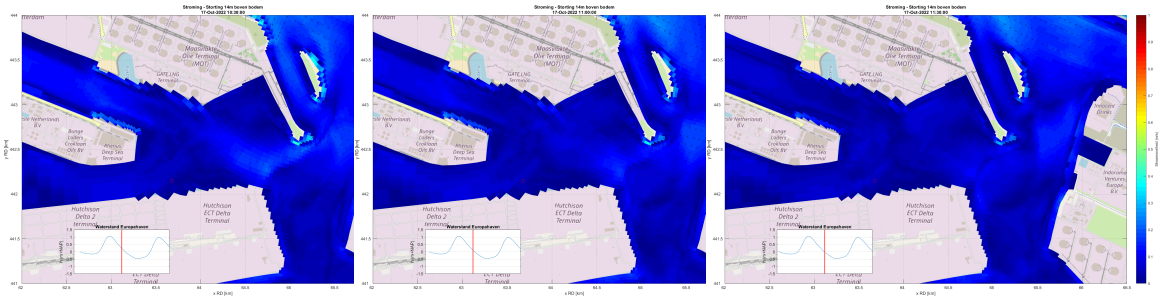

(d) Current profile on 17-10-2022 of the Europahaven and surrounding area.

(e) Current profile on 17-10-2022 of the Europahaven and surrounding area.

(f) Current profile on 17-10-2022 of the Europahaven and surrounding area.

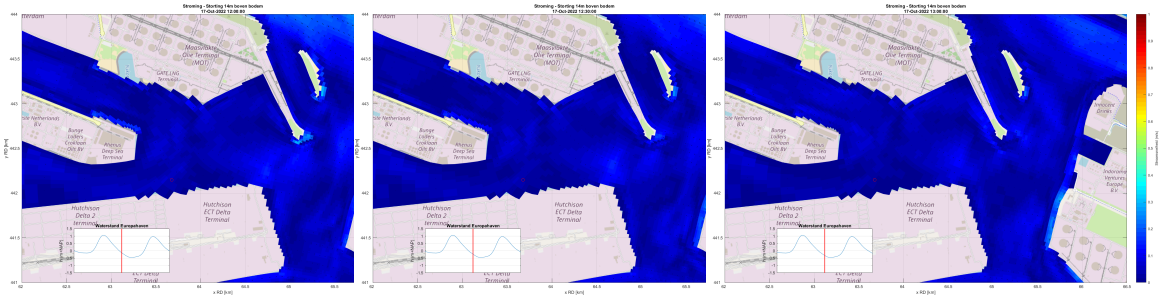

(g) Current profile on 17-10-2022 of the Europahaven and surrounding area.

(h) Current profile on 17-10-2022 of the Europahaven and surrounding area.

(i) Current profile on 17-10-2022 of the Europahaven and surrounding area.

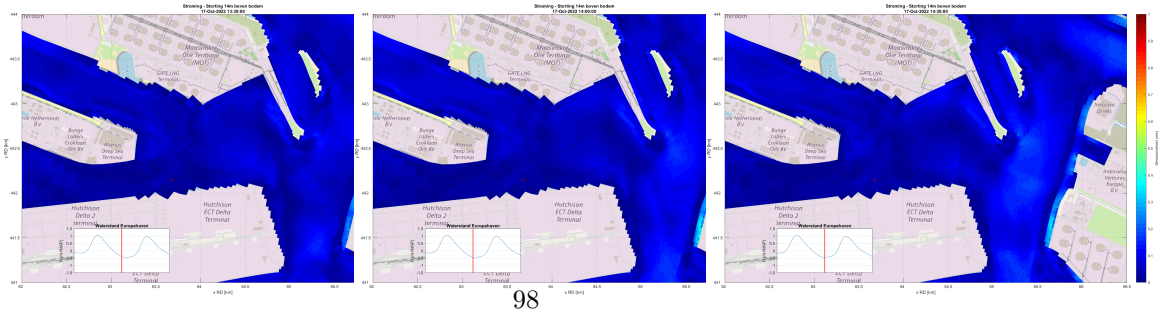

(j) Current profile on 17-10-2022 of the Europahaven and surrounding area.

(k) Current profile on 17-10-2022 of the Europahaven and surrounding area.

(l) Current profile on 17-10-2022 of the Europahaven and surrounding area.

Figure 72: Current profiles on 17-10-2022 overtime started from 9:00 until 14:30 on a height of 14 meters above the bottom, part 1.

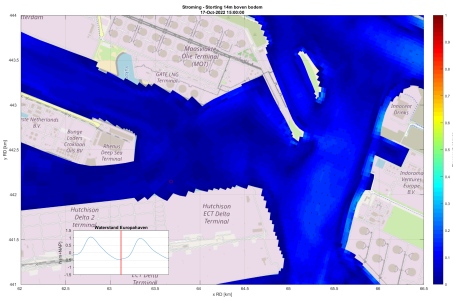

(a) Current profile on 17-10-2022 of the Europahaven and surrounding area.

Figure 73: Current profiles on 17-10-2022 over time started from 9:00 until 14:30 on a height of 14 meters above the bottom, part 2.

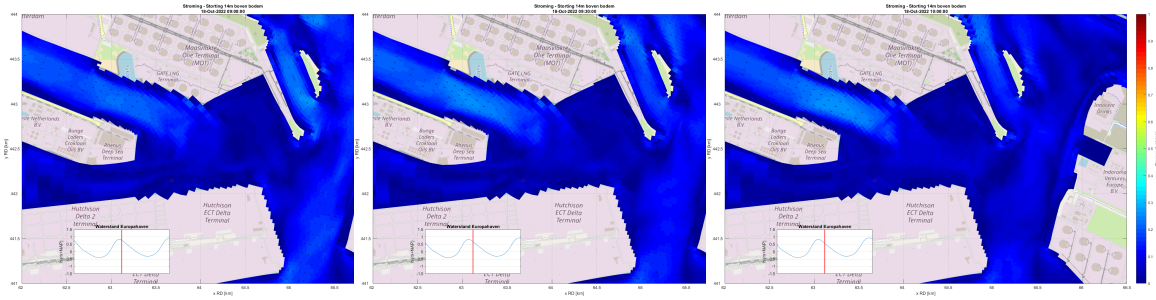

(a) Current profile on 18-10-2022 of the Europahaven and surrounding area.

(b) Current profile on 18-10-2022 of the Europahaven and surrounding area.

(c) Current profile on 18-10-2022 of the Europahaven and surrounding area.

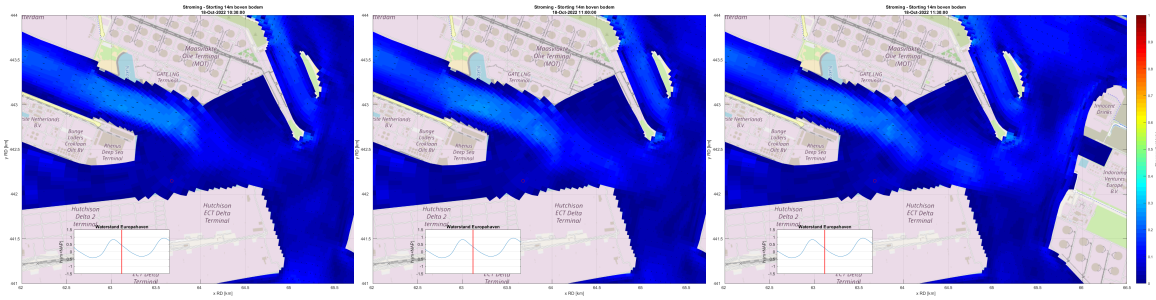

(d) Current profile on 18-10-2022 of the Europahaven and surrounding area.

(e) Current profile on 18-10-2022 of the Europahaven and surrounding area.

(f) Current profile on 18-10-2022 of the Europahaven and surrounding area.

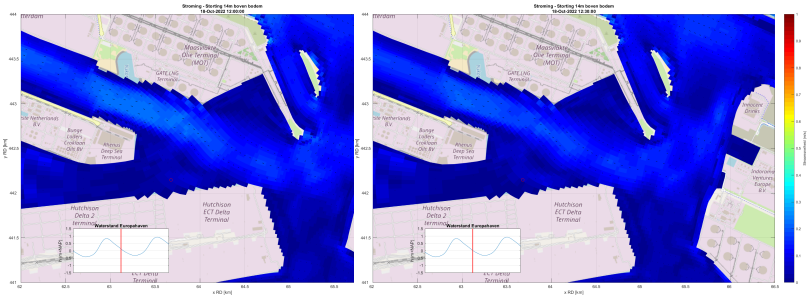

(g) Current profile on 18-10-2022 of the Europahaven and surrounding area.

(h) Current profile on 18-10-2022 of the Europahaven and surrounding area.

Figure 74: Current profiles on 18-10-2022 overtime started 9:00 until 12:30 on a height of 14 meters above the bottom.

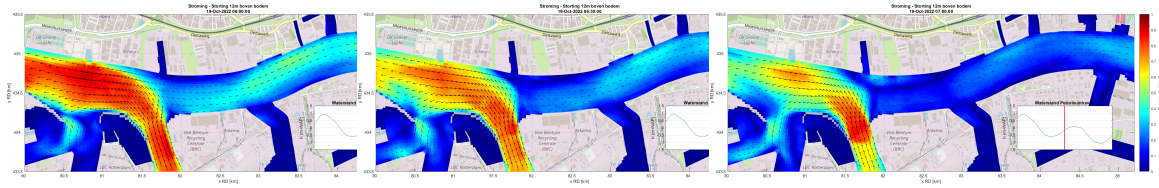

(a) Current profile on 19-10-2022 of the 2nd Petroleumhaven, Koolekade and surrounding area.

(b) Current profile on 19-10-2022 of the 2nd Petroleumhaven, Koolekade and surrounding area.

(c) Current profile on 19-10-2022 of the 2nd Petroleumhaven, Koolekade and surrounding area.

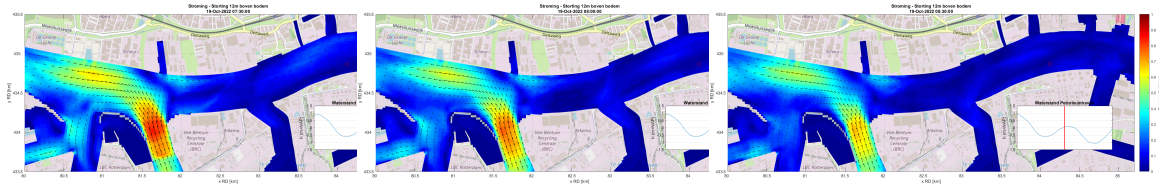

(d) Current profile on 19-10-2022 of the 2nd Petroleumhaven, Koolekade and surrounding area.

(e) Current profile on 19-10-2022 of the 2nd Petroleumhaven, Koolekade and surrounding area.

(f) Current profile on 19-10-2022 of the 2nd Petroleumhaven, Koolekade and surrounding area.

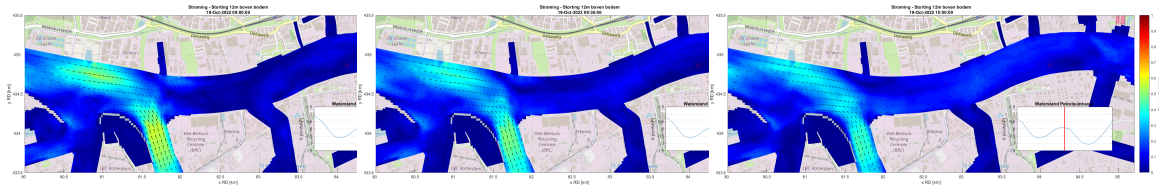

(g) Current profile on 19-10-2022 of the 2nd Petroleumhaven, Koolekade and surrounding area.

(h) Current profile on 19-10-2022 of the 2nd Petroleumhaven, Koolekade and surrounding area.

(i) Current profile on 19-10-2022 of the 2nd Petroleumhaven, Koolekade and surrounding area.

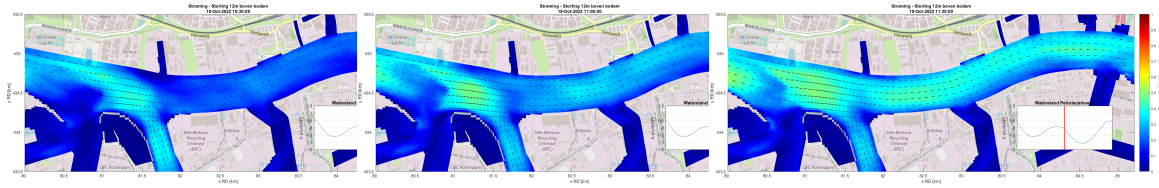

(j) Current profile on 19-10-2022 of the 2nd Petroleumhaven, Koolekade and surrounding area.

(k) Current profile on 19-10-2022 of the 2nd Petroleumhaven, Koolekade and surrounding area.

(l) Current profile on 19-10-2022 of the 2nd Petroleumhaven, Koolekade and surrounding area.

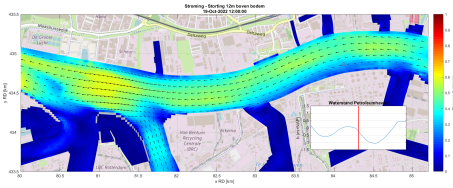

(m) Current profile on 19-10-2022 of the 2nd Petroleumhaven, Koolekade and surrounding area.

Figure 75: Current profiles on 19-10-2022 overtime started from 6:00 until 12:00 on a height of 12 meters above the bottom.

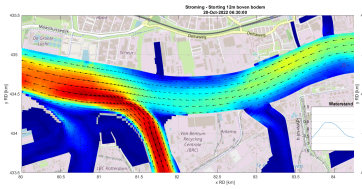

(a) Current profile on 20-10-2022 of the 2nd Petroleumhaven, Koolekade and surrounding area.

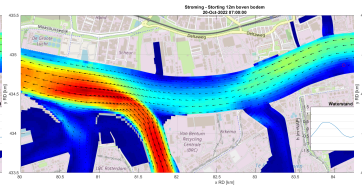

(b) Current profile on 20-10-2022 of the 2nd Petroleumhaven, Koolekade and surrounding area.

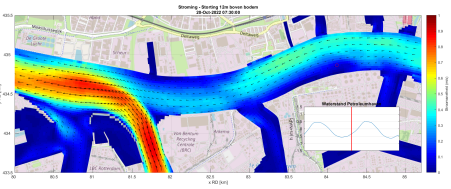

(c) Current profile on 20-10-2022 of the 2nd Petroleumhaven, Koolekade and surrounding area.

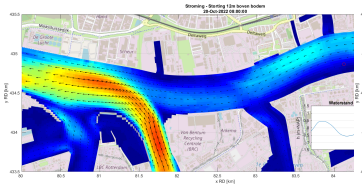

(d) Current profile on 20-10-2022 of the 2nd Petroleumhaven, Koolekade and surrounding area.

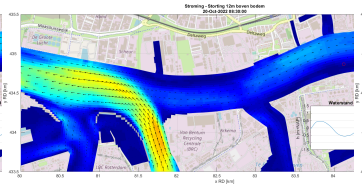

(e) Current profile on 20-10-2022 of the 2nd Petroleumhaven, Koolekade and surrounding area.

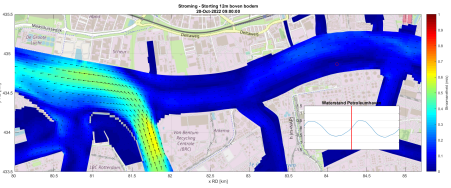

(f) Current profile on 20-10-2022 of the 2nd Petroleumhaven, Koolekade and surrounding area.

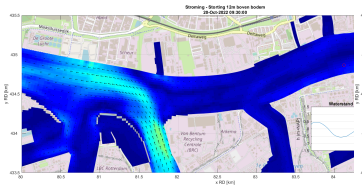

(g) Current profile on 20-10-2022 of the 2nd Petroleumhaven, Koolekade and surrounding area.

(h) Current profile on 20-10-2022 of the 2nd Petroleumhaven, Koolekade and surrounding area.

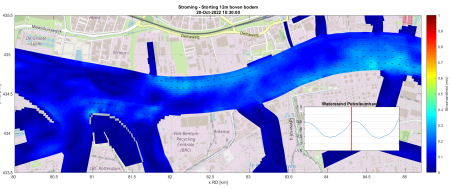

(i) Current profile on 20-10-2022 of the 2nd Petroleumhaven, Koolekade and surrounding area.

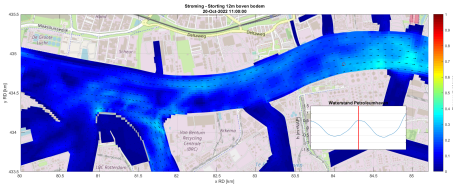

(j) Current profile on 20-10-2022 of the 2nd Petroleumhaven, Koolekade and surrounding area.

Figure 76: Current profiles on 20-10-2022 overtime started from 6:30 until 11:00 on a height of 12 meters above the bottom.

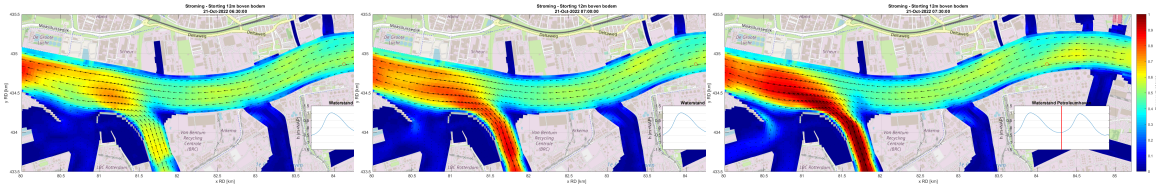

(a) Current profile on 21-10-2022 of the 2nd Petroleumhaven, Koolekade and surrounding area.

(b) Current profile on 21-10-2022 of the 2nd Petroleumhaven, Koolekade and surrounding area.

(c) Current profile on 21-10-2022 of the 2nd Petroleumhaven, Koolekade and surrounding area.

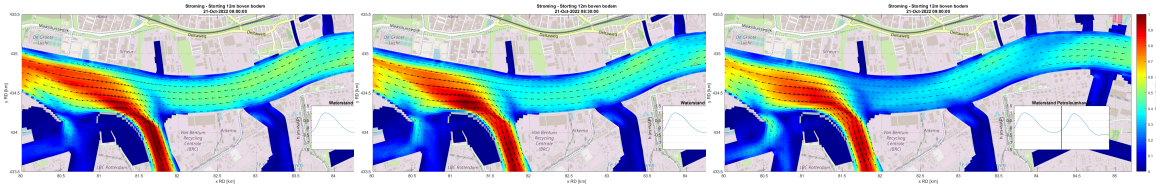

(d) Current profile on 21-10-2022 of the 2nd Petroleumhaven, Koolekade and surrounding area.

(e) Current profile on 21-10-2022 of the 2nd Petroleumhaven, Koolekade and surrounding area.

(f) Current profile on 21-10-2022 of the 2nd Petroleumhaven, Koolekade and surrounding area.

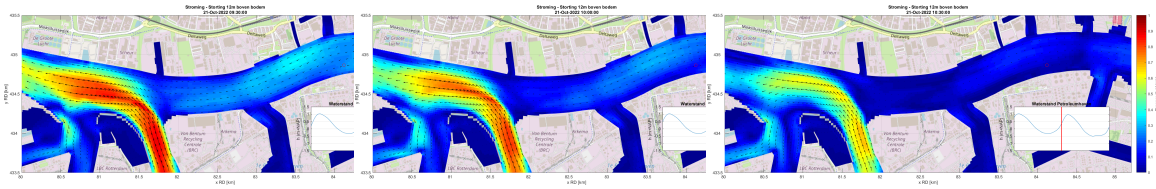

(g) Current profile on 21-10-2022 of the 2nd Petroleumhaven, Koolekade and surrounding area.

(h) Current profile on 21-10-2022 of the 2nd Petroleumhaven, Koolekade and surrounding area.

(i) Current profile on 21-10-2022 of the 2nd Petroleumhaven, Koolekade and surrounding area.

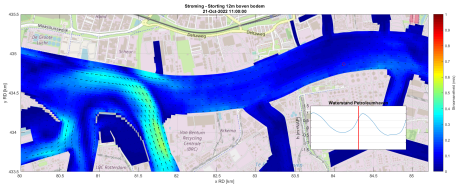

(j) Current profile on 21-10-2022 of the 2nd Petroleumhaven, Koolekade and surrounding area.

Figure 77: Current profiles on 21-10-2022 overtime started from 6:30 until 11:00 on a height of 12 meters above the bottom.

WID

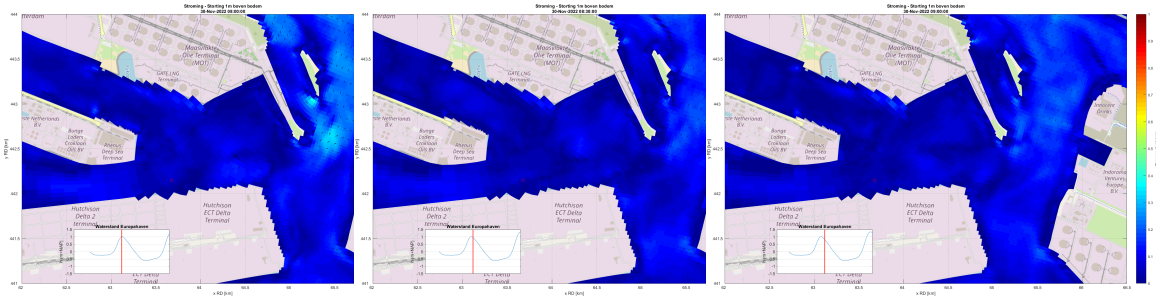

(a) Current profile on 30-11-2022 of the Europahaven and surrounding area.

(b) Current profile on 30-11-2022 of the Europahaven and surrounding area.

(c) Current profile on 30-11-2022 of the Europahaven and surrounding area.

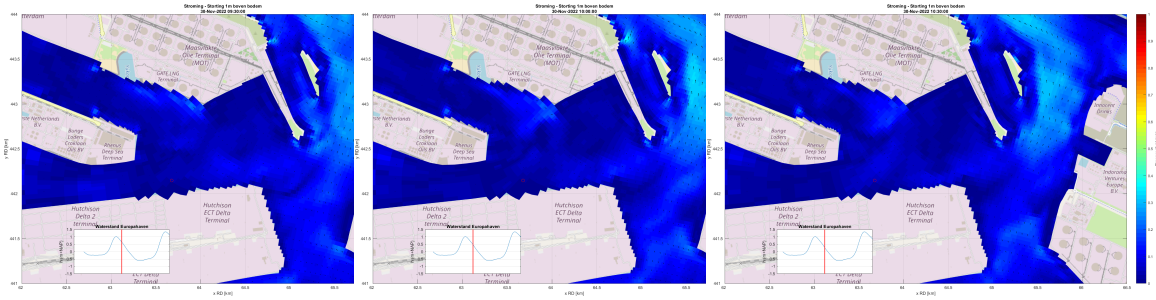

(d) Current profile on 30-11-2022 of the Europahaven and surrounding area.

(e) Current profile on 30-11-2022 of the Europahaven and surrounding area.

(f) Current profile on 30-11-2022 of the Europahaven and surrounding area.

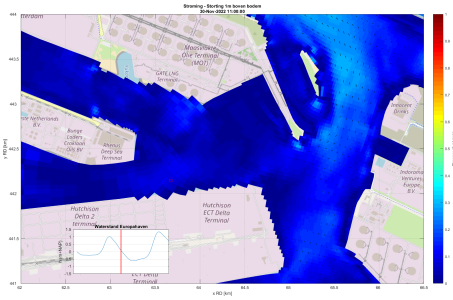

(g) Current profile on 30-11-2022 of the Europahaven and surrounding area.

Figure 78: Current profiles on 30-11-2022 overtime started from 8:00 until 11:00 on a height of 1 meter above the bottom.

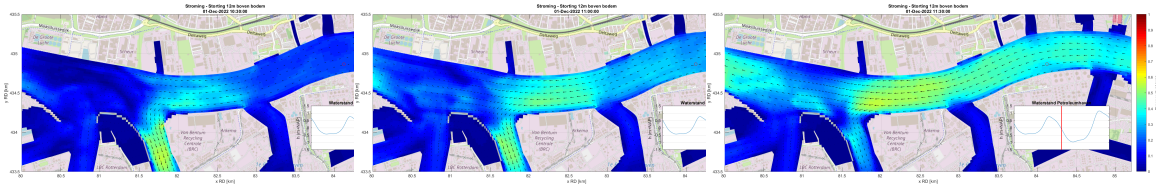

(a) Current profile on 01-12-2022 of the 2nd Petroleumhaven, Koolekade and surrounding area.

(b) Current profile on 01-12-2022 of the 2nd Petroleumhaven, Koolekade and surrounding area.

(c) Current profile on 01-12-2022 of the 2nd Petroleumhaven, Koolekade and surrounding area.

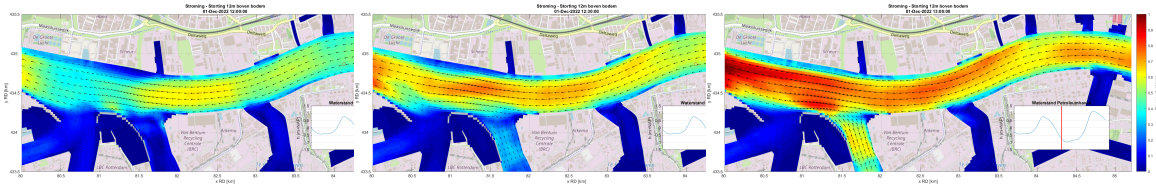

(d) Current profile on 01-12-2022 of the 2nd Petroleumhaven, Koolekade and surrounding area.

(e) Current profile on 01-12-2022 of the 2nd Petroleumhaven, Koolekade and surrounding area.

(f) Current profile on 01-12-2022 of the 2nd Petroleumhaven, Koolekade and surrounding area.

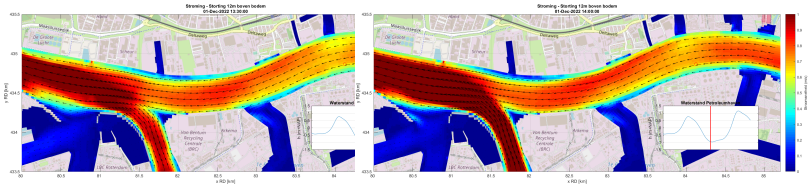

(g) Current profile on 01-12-2022 of the 2nd Petroleumhaven, Koolekade and surrounding area.

(h) Current profile on 01-12-2022 of the 2nd Petroleumhaven, Koolekade and surrounding area.

Figure 79: Current profiles on 01-12-2022 overtime started from 10:30 until 14:00 on a height of 12 meters above the bottom.

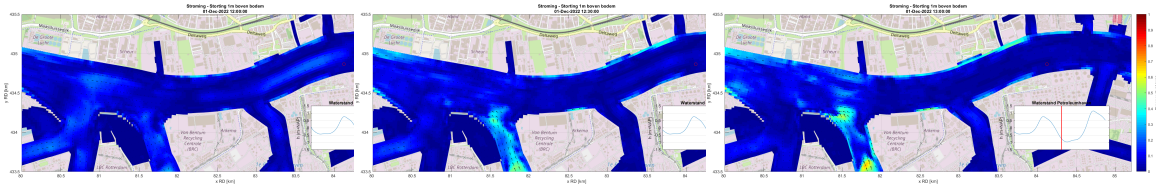

(a) Current profile on 01-12-2022 of the 2nd Petroleumhaven, Koolekade and surrounding area.

(b) Current profile on 01-12-2022 of the 2nd Petroleumhaven, Koolekade and surrounding area.

(c) Current profile on 01-12-2022 of the 2nd Petroleumhaven, Koolekade and surrounding area.

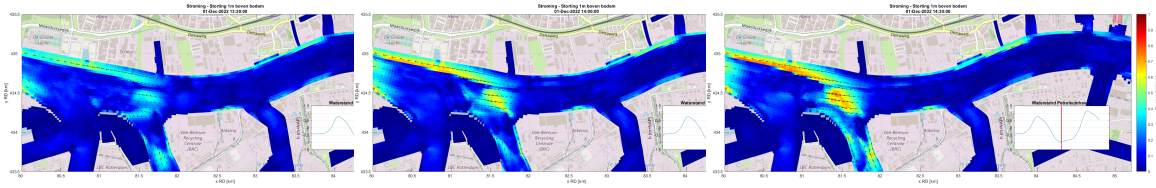

(d) Current profile on 01-12-2022 of the 2nd Petroleumhaven, Koolekade and surrounding area.

(e) Current profile on 01-12-2022 of the 2nd Petroleumhaven, Koolekade and surrounding area.

(f) Current profile on 01-12-2022 of the 2nd Petroleumhaven, Koolekade and surrounding area.

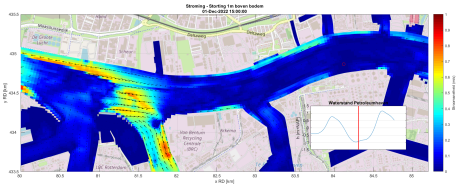

(g) Current profile on 01-12-2022 of the 2nd Petroleumhaven, Koolekade and surrounding area.

Figure 80: Current profiles on 01-12-2022 overtime started from 12:00 until 15:00 on a height of 1 meter above the bottom.

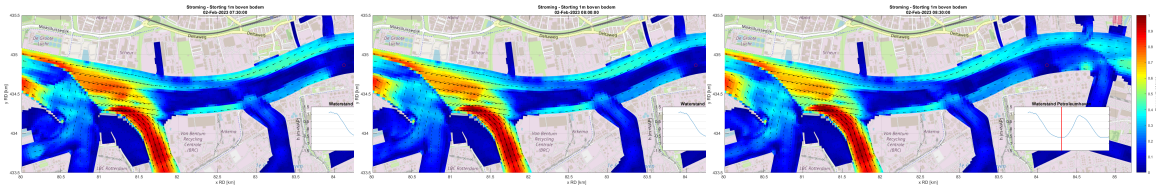

(a) Current profile on 02-02-2023 of the estuary of the 2nd Petroleumhaven and the Koolekade with the surrounding area.

(b) Current profile on 02-02-2023 of the estuary of the 2nd Petroleumhaven and the Koolekade with the surrounding area.

(c) Current profile on 02-02-2023 of the estuary of the 2nd Petroleumhaven and the Koolekade with the surrounding area.

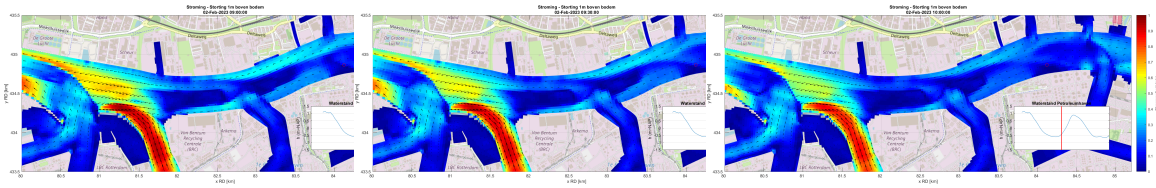

(d) Current profile on 02-02-2023 of the estuary of the 2nd Petroleumhaven and the Koolekade with the surrounding area.

(e) Current profile on 02-02-2023 of the estuary of the 2nd Petroleumhaven and the Koolekade with the surrounding area.

(f) Current profile on 02-02-2023 of the estuary of the 2nd Petroleumhaven and the Koolekade with the surrounding area..

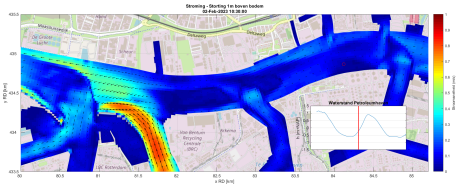

(g) Current profile on 02-02-2023 of the estuary of the 2nd Petroleumhaven and the Koolekade with the surrounding area.

Figure 81: Current profiles on 02-02-2023 overtime started from 07:30 until 10:30 on a height of 1 meter above the bottom.

Appendix V: Turbidity profiles over depth during the pilot week

During the pilot week, the Valenport Swift Turbidity collected data for the turbidity over depth. With these data, depth profiles are made. In this appendix, the figures can be found.

Tiamat

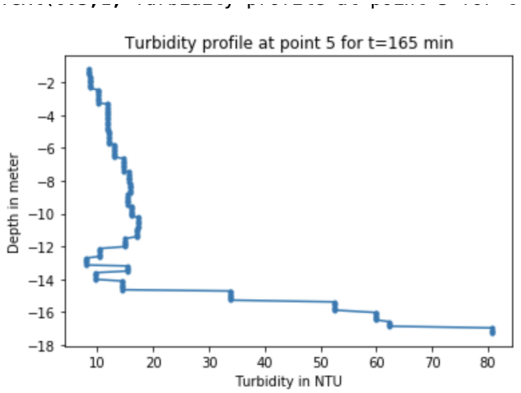

Figure 82: Location 5 at 165 minutes after the start of dredging with the Tiamat. This is the turbidity depth profile of 17-10-2022.

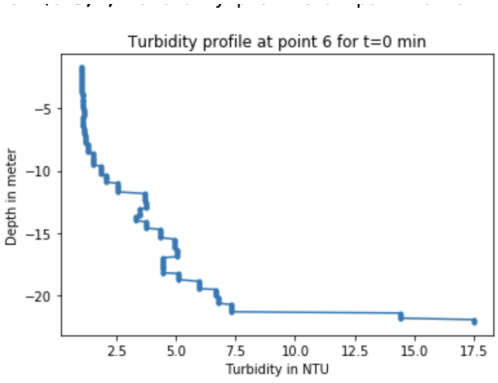

Figure 83: Location 6 at 0 minutes after the start of dredging with the Tiamat. This is the turbidity depth profile of 17-10-2022.

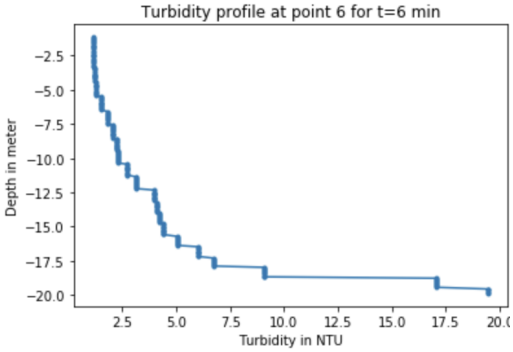

Figure 84: Location 6 at 6 minutes after the start of dredging with the Tiamat. This is the turbidity depth profile of 17-10-2022.

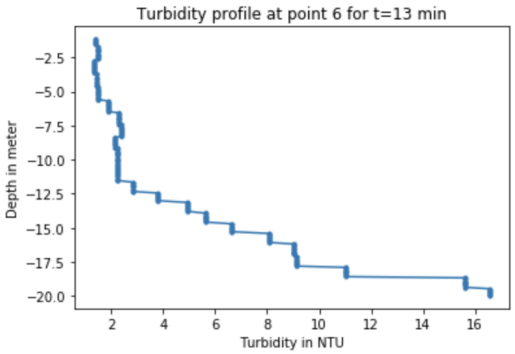

Figure 85: Location 6 at 13 minutes after the start of dredging with the Tiamat. This is the turbidity depth profile of 17-10-2022.

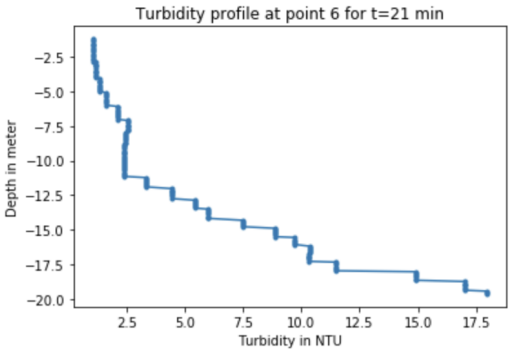

Figure 86: Location 6 at 21 minutes after the start of dredging with the Tiamat. This is the turbidity depth profile of 17-10-2022.

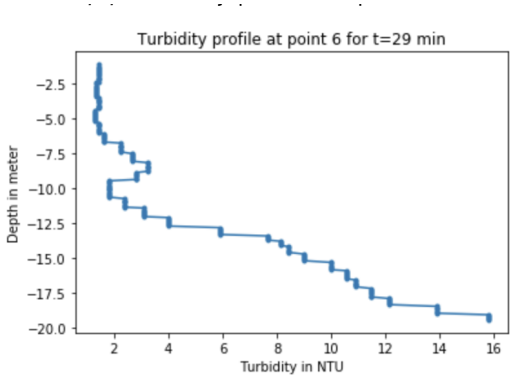

Figure 87: Location 6 at 29 minutes after the start of dredging with the Tiamat. This is the turbidity depth profile of 17-10-2022.

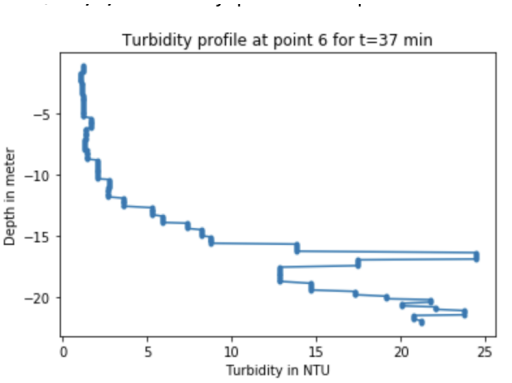

Figure 88: Location 6 at 37 minutes after the start of dredging with the Tiamat. This is the turbidity depth profile of 17-10-2022.

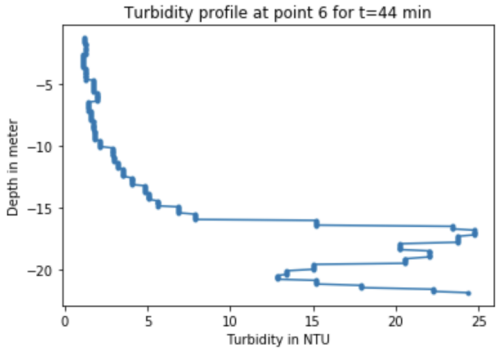

Figure 89: Location 6 at 44 minutes after the start of dredging with the Tiamat. This is the turbidity depth profile of 17-10-2022.

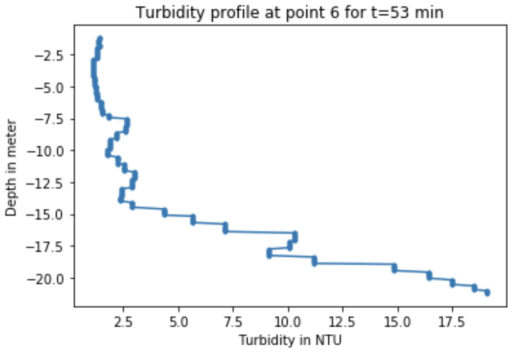

Figure 90: Location 6 at 53 minutes after the start of dredging with the Tiamat. This is the turbidity depth profile of 17-10-2022.

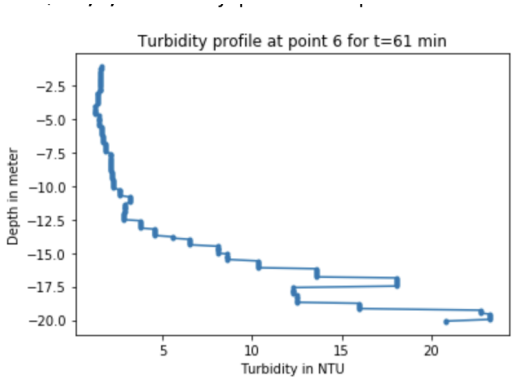

Figure 91: Location 6 at 61 minutes after the start of dredging with the Tiamat. This is the turbidity depth profile of 17-10-2022.

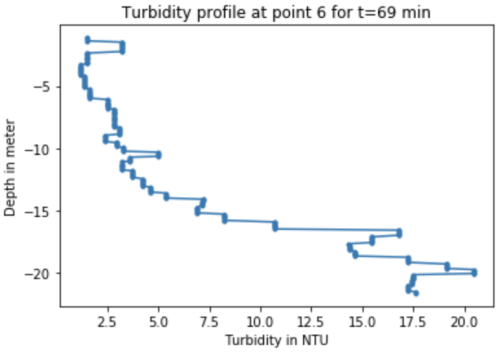

Figure 92: Location 6 at 69 minutes after the start of dredging with the Tiamat. This is the turbidity depth profile of 17-10-2022.

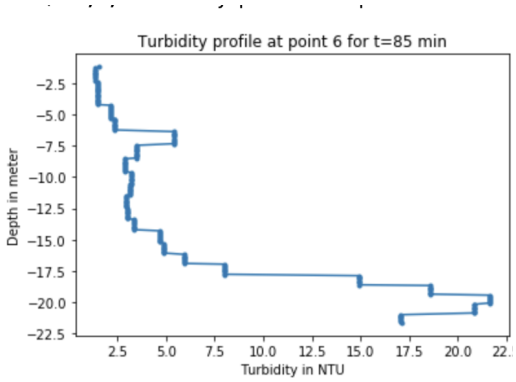

Figure 93: Location 6 at 85 minutes after the start of dredging with the Tiamat. This is the turbidity depth profile of 17-10-2022.

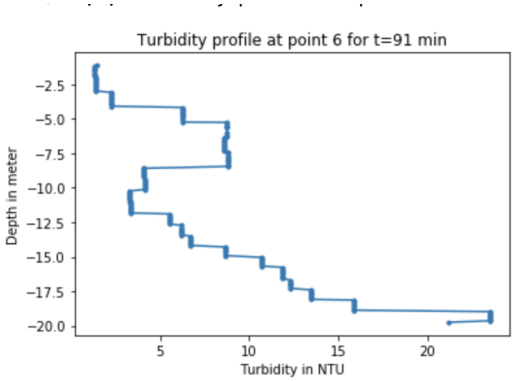

Figure 94: Location 6 at 91 minutes after the start of dredging with the Tiamat. This is the turbidity depth profile of 17-10-2022.

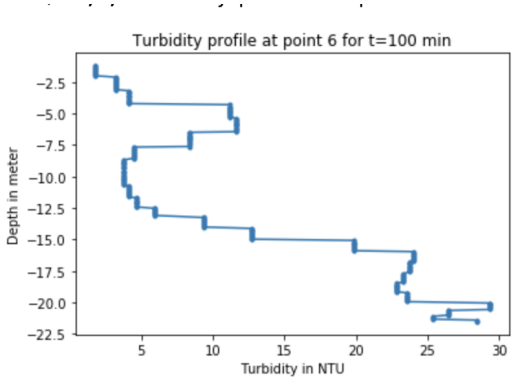

Figure 95: Location 6 at 100 minutes after the start of dredging with the Tiamat. This is the turbidity depth profile of 17-10-2022.

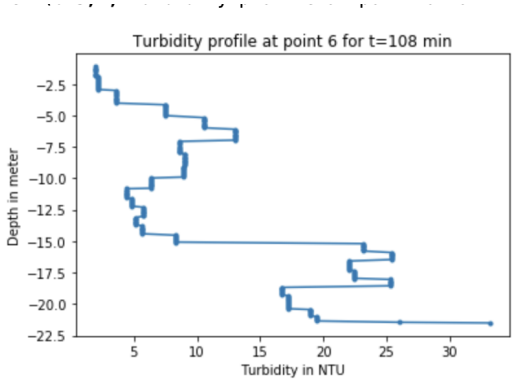

Figure 96: Location 6 at 108 minutes after the start of dredging with the Tiamat. This is the turbidity depth profile of 17-10-2022.

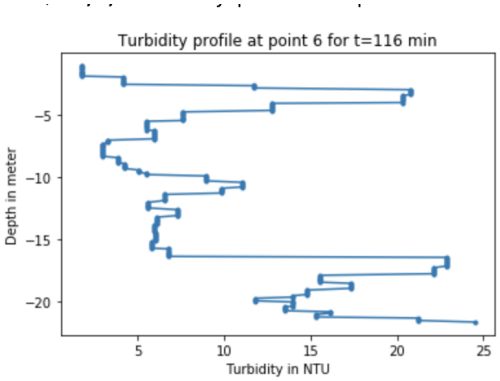

Figure 97: Location 6 at 116 minutes after the start of dredging with the Tiamat. This is the turbidity depth profile of 17-10-2022.

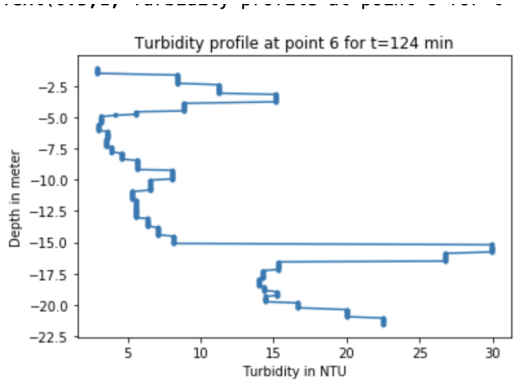

Figure 98: Location 6 at 124 minutes after the start of dredging with the Tiamat. This is the turbidity depth profile of 17-10-2022.

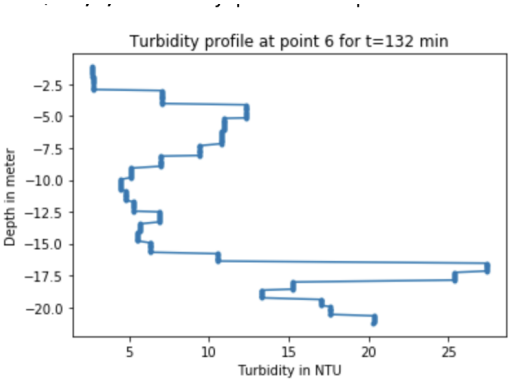

Figure 99: Location 6 at 132 minutes after the start of dredging with the Tiamat. This is the turbidity depth profile of 17-10-2022.

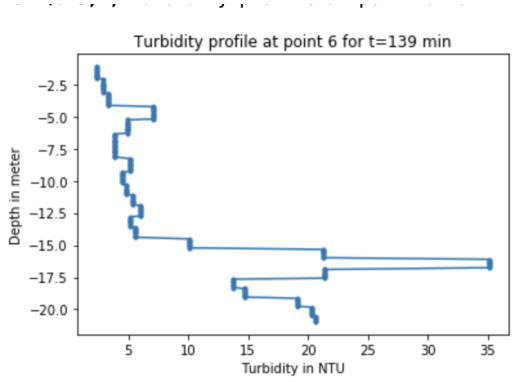

Figure 100: Location 6 at 139 minutes after the start of dredging with the Tiamat. This is the turbidity depth profile of 17-10-2022.

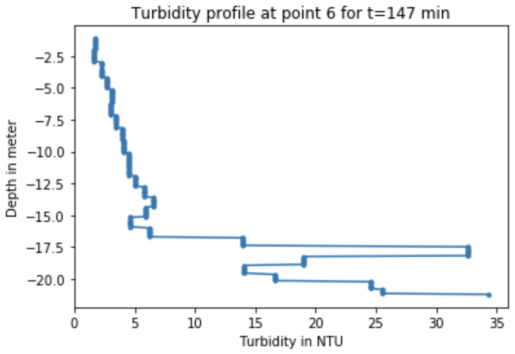

Figure 101: Location 6 at 147 minutes after the start of dredging with the Tiamat. This is the turbidity depth profile of 17-10-2022.

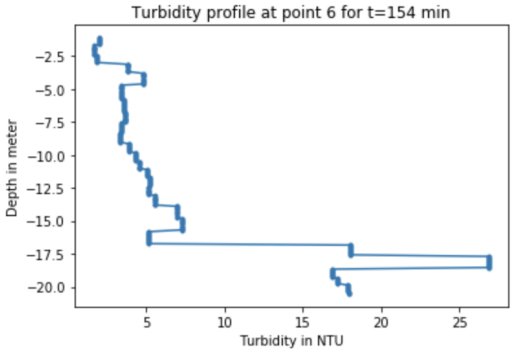

Figure 102: Location 6 at 154 minutes after the start of dredging with the Tiamat. This is the turbidity depth profile of 17-10-2022.

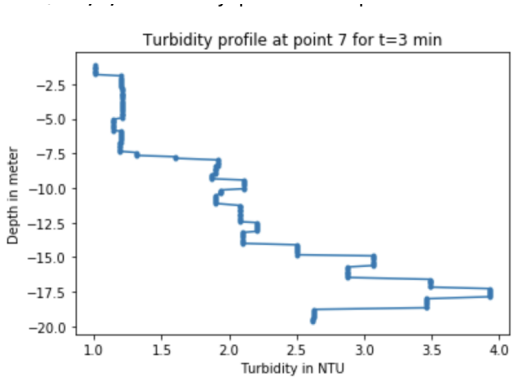

Figure 103: Location 7 at 3 minutes after the start of dredging with the Tiamat. This is the turbidity depth profile of 17-10-2022.

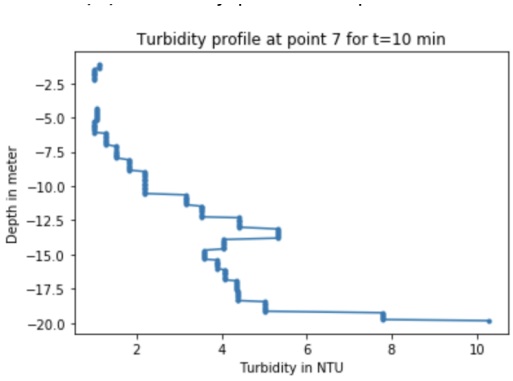

Figure 104: Location 7 at 10 minutes after the start of dredging with the Tiamat. This is the turbidity depth profile of 17-10-2022.

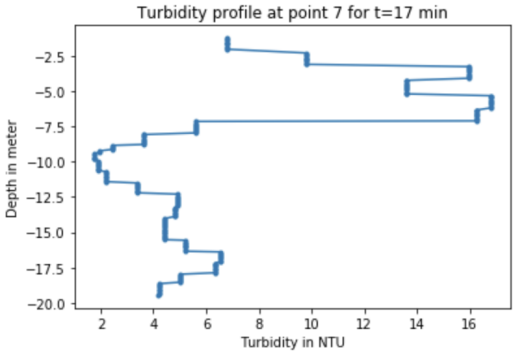

Figure 105: Location 7 at 17 minutes after the start of dredging with the Tiamat. This is the turbidity depth profile of 17-10-2022.

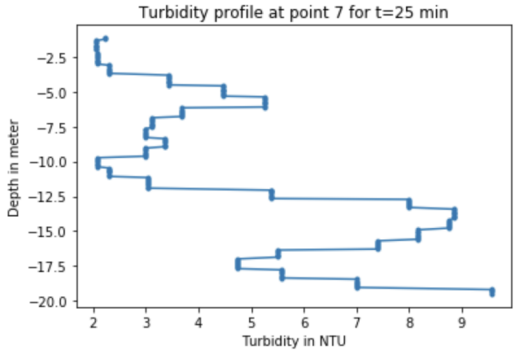

Figure 106: Location 7 at 25 minutes after the start of dredging with the Tiamat. This is the turbidity depth profile of 17-10-2022.

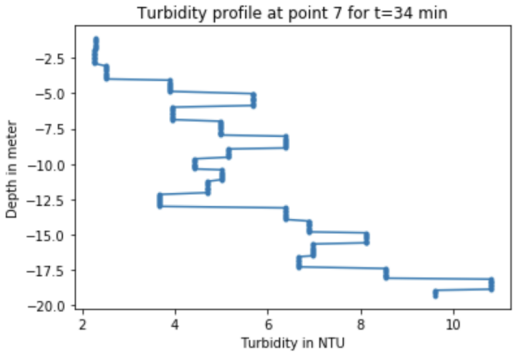

Figure 107: Location 7 at 34 minutes after the start of dredging with the Tiamat. This is the turbidity depth profile of 17-10-2022.

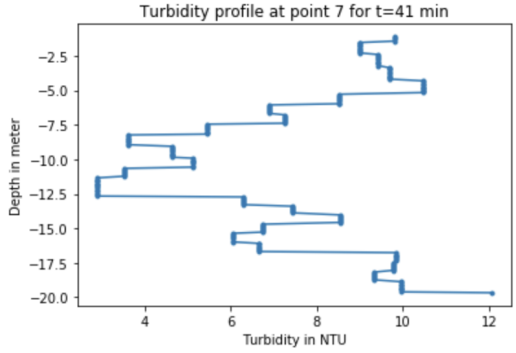

Figure 108: Location 7 at 41 minutes after the start of dredging with the Tiamat. This is the turbidity depth profile of 17-10-2022.

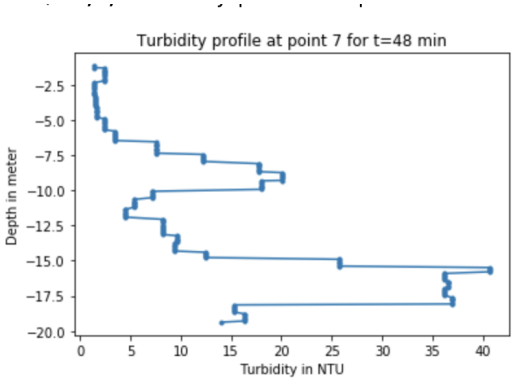

Figure 109: Location 7 at 48 minutes after the start of dredging with the Tiamat. This is the turbidity depth profile of 17-10-2022.

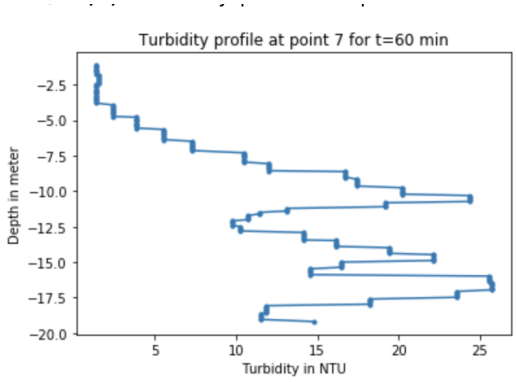

Figure 110: Location 7 at 60 minutes after the start of dredging with the Tiamat. This is the turbidity depth profile of 17-10-2022.

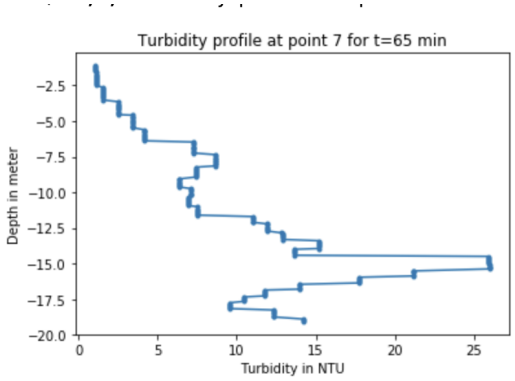

Figure 111: Location 7 at 65 minutes after the start of dredging with the Tiamat. This is the turbidity depth profile of 17-10-2022.

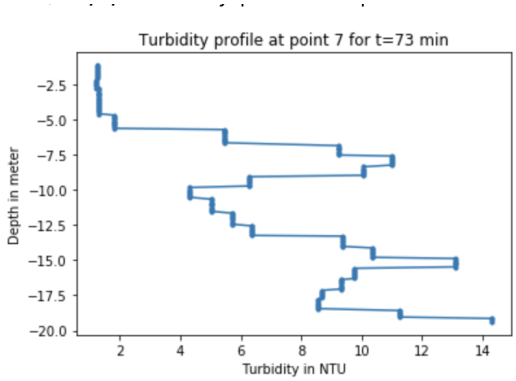

Figure 112: Location 7 at 73 minutes after the start of dredging with the Tiamat. This is the turbidity depth profile of 17-10-2022.

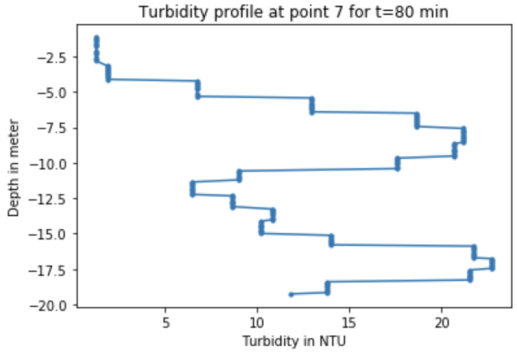

Figure 113: Location 7 at 80 minutes after the start of dredging with the Tiamat. This is the turbidity depth profile of 17-10-2022.

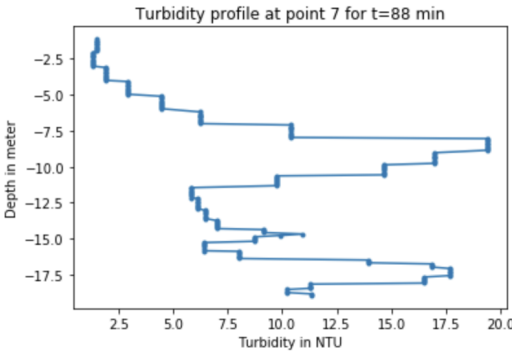

Figure 114: Location 7 at 88 minutes after the start of dredging with the Tiamat. This is the turbidity depth profile of 17-10-2022.

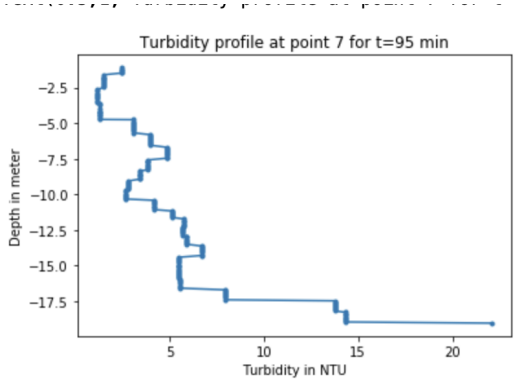

Figure 115: Location 7 at 95 minutes after the start of dredging with the Tiamat. This is the turbidity depth profile of 17-10-2022.

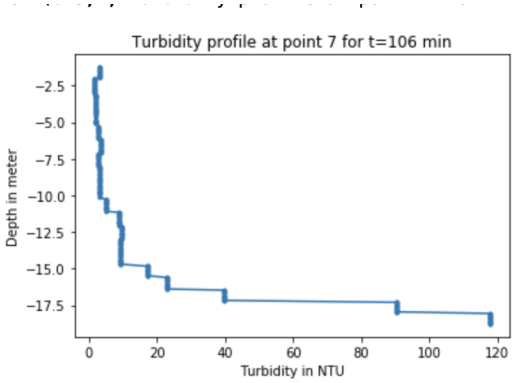

Figure 116: Location 7 at 106 minutes after the start of dredging with the Tiamat. This is the turbidity depth profile of 17-10-2022.

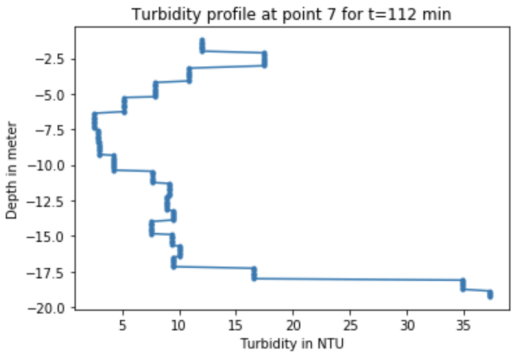

Figure 117: Location 7 at 112 minutes after the start of dredging with the Tiamat. This is the turbidity depth profile of 17-10-2022.

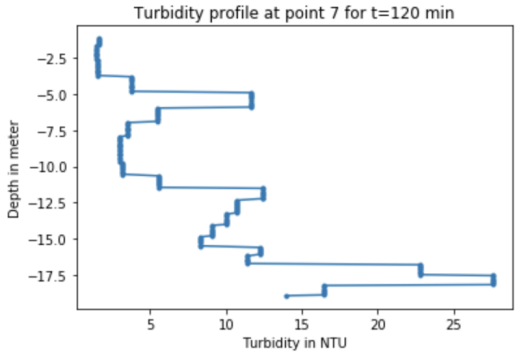

Figure 118: Location 7 at 120 minutes after the start of dredging with the Tiamat. This is the turbidity depth profile of 17-10-2022.

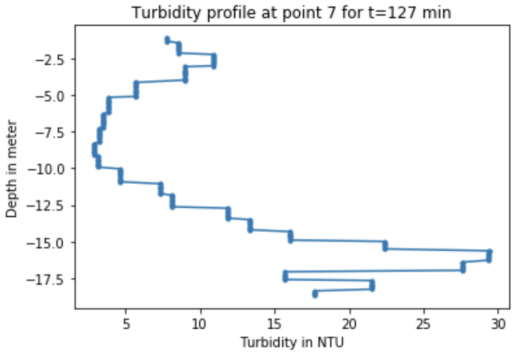

Figure 119: Location 7 at 127 minutes after the start of dredging with the Tiamat. This is the turbidity depth profile of 17-10-2022.

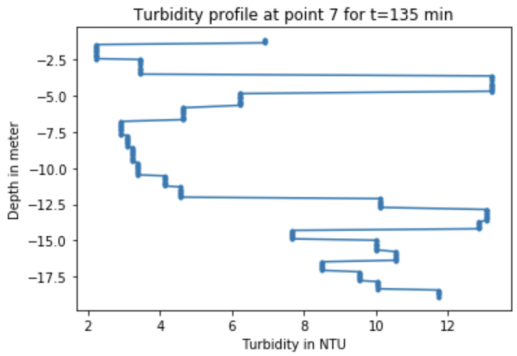

Figure 120: Location 7 at 135 minutes after the start of dredging with the Tiamat. This is the turbidity depth profile of 17-10-2022.

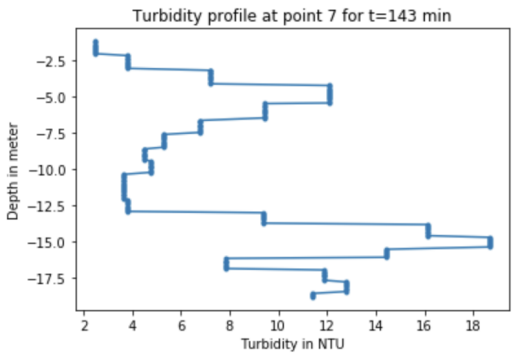

Figure 121: Location 7 at 143 minutes after the start of dredging with the Tiamat. This is the turbidity depth profile of 17-10-2022.

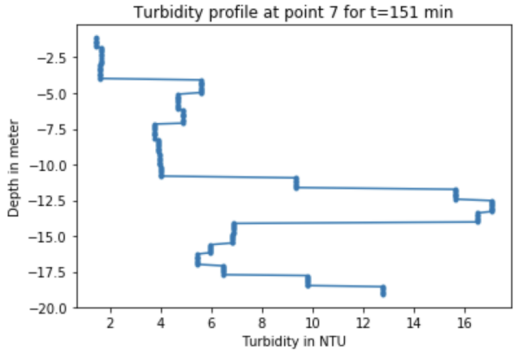

Figure 122: Location 7 at 151 minutes after the start of dredging with the Tiamat. This is the turbidity depth profile of 17-10-2022.

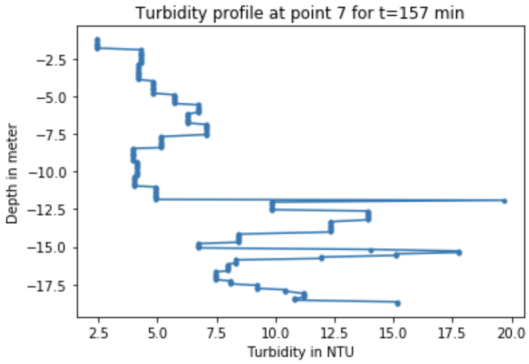

Figure 123: Location 7 at 157 minutes after the start of dredging with the Tiamat. This is the turbidity depth profile of 17-10-2022.

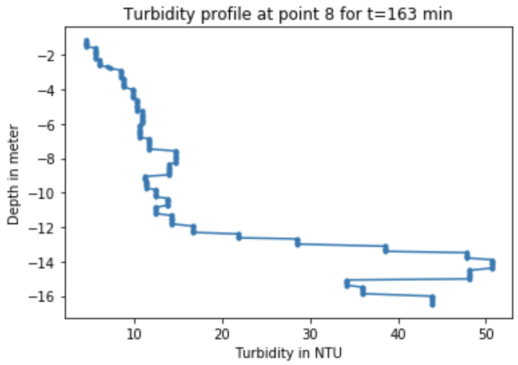

Figure 124: Location 8 at 163 minutes after the start of dredging with the Tiamat. This is the turbidity depth profile of 17-10-2022.

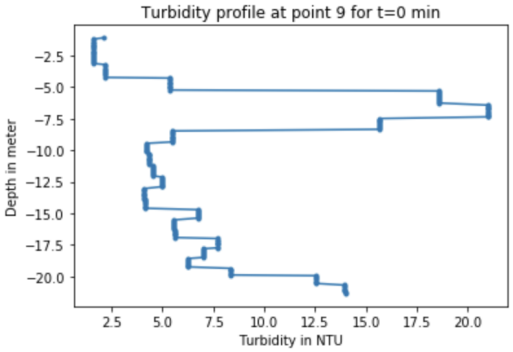

Figure 125: Location 9 at 0 minutes after the start of dredging with the Tiamat. This is the turbidity depth profile of 17-10-2022.

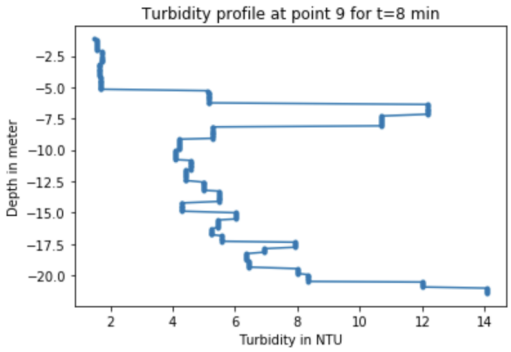

Figure 126: Location 9 at 8 minutes after the start of dredging with the Tiamat. This is the turbidity depth profile of 17-10-2022.

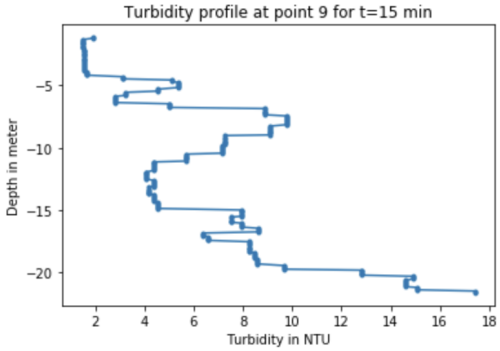

Figure 127: Location 9 at 15 minutes after the start of dredging with the Tiamat. This is the turbidity depth profile of 17-10-2022.

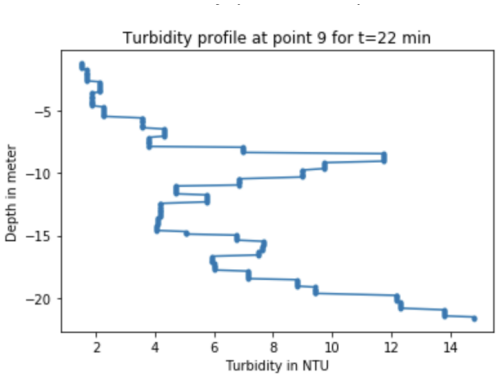

Figure 128: Location 9 at 22 minutes after the start of dredging with the Tiamat. This is the turbidity depth profile of 17-10-2022.

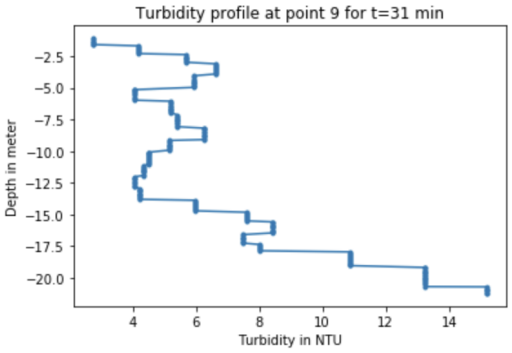

Figure 129: Location 9 at 31 minutes after the start of dredging with the Tiamat. This is the turbidity depth profile of 17-10-2022.

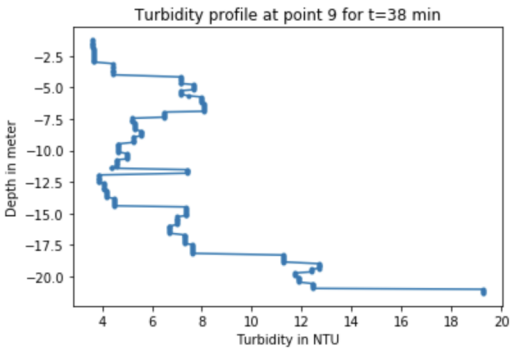

Figure 130: Location 9 at 38 minutes after the start of dredging with the Tiamat. This is the turbidity depth profile of 17-10-2022.

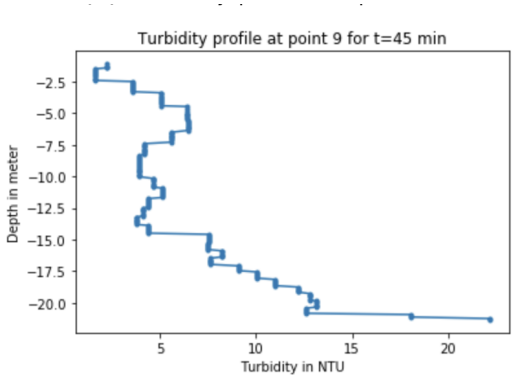

Figure 131: Location 9 at 45 minutes after the start of dredging with the Tiamat. This is the turbidity depth profile of 17-10-2022.

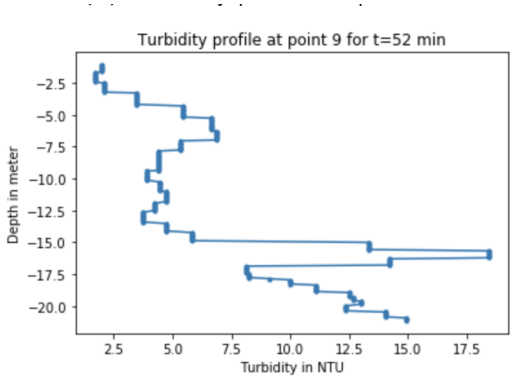

Figure 132: Location 9 at 52 minutes after the start of dredging with the Tiamat. This is the turbidity depth profile of 17-10-2022.

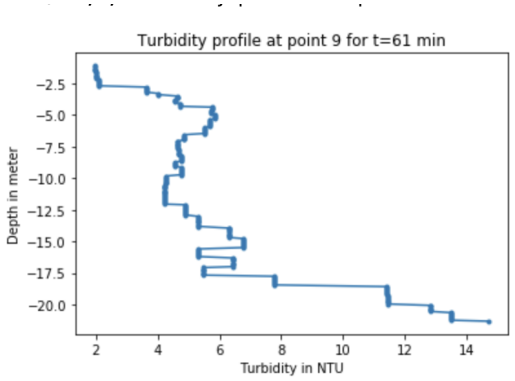

Figure 133: Location 9 at 61 minutes after the start of dredging with the Tiamat. This is the turbidity depth profile of 17-10-2022.

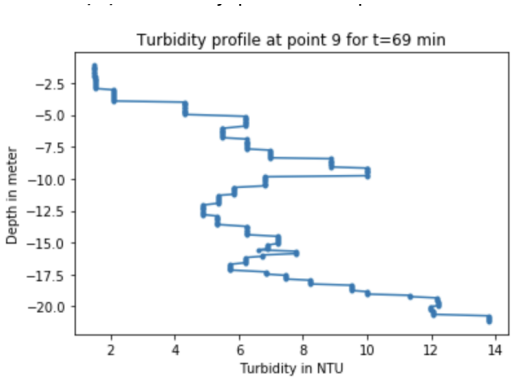

Figure 134: Location 9 at 69 minutes after the start of dredging with the Tiamat. This is the turbidity depth profile of 17-10-2022.

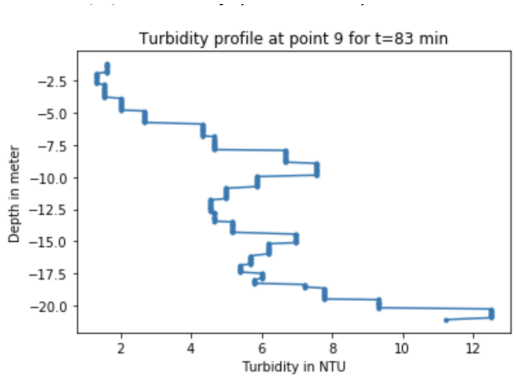

Figure 135: Location 9 at 83 minutes after the start of dredging with the Tiamat. This is the turbidity depth profile of 17-10-2022.

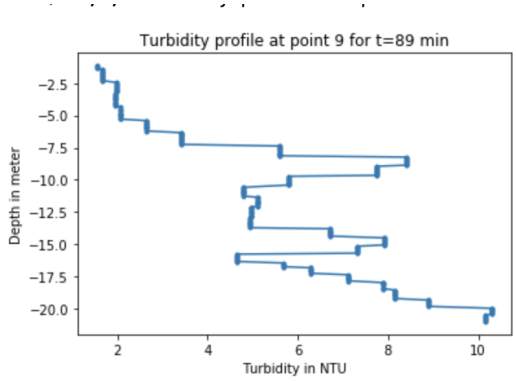

Figure 136: Location 9 at 89 minutes after the start of dredging with the Tiamat. This is the turbidity depth profile of 17-10-2022.

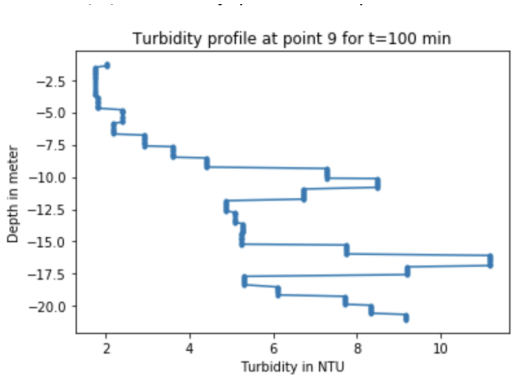

Figure 137: Location 9 at 100 minutes after the start of dredging with the Tiamat. This is the turbidity depth profile of 17-10-2022.

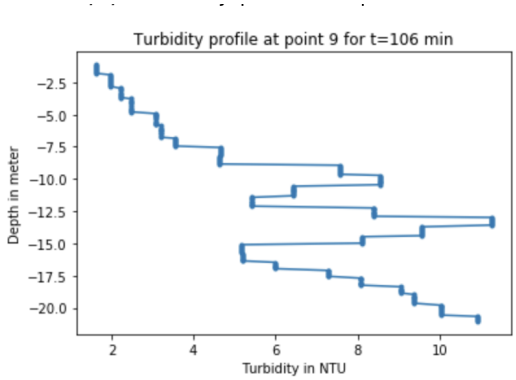

Figure 138: Location 9 at 106 minutes after the start of dredging with the Tiamat. This is the turbidity depth profile of 17-10-2022.

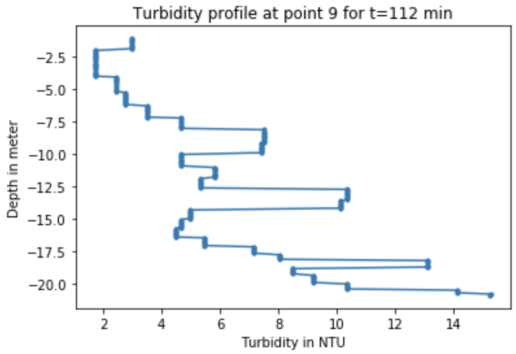

Figure 139: Location 9 at 112 minutes after the start of dredging with the Tiamat. This is the turbidity depth profile of 17-10-2022.

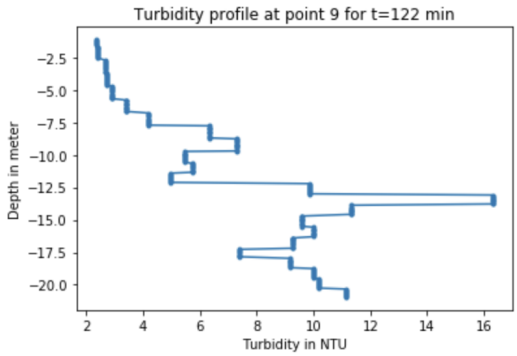

Figure 140: Location 9 at 122 minutes after the start of dredging with the Tiamat. This is the turbidity depth profile of 17-10-2022.

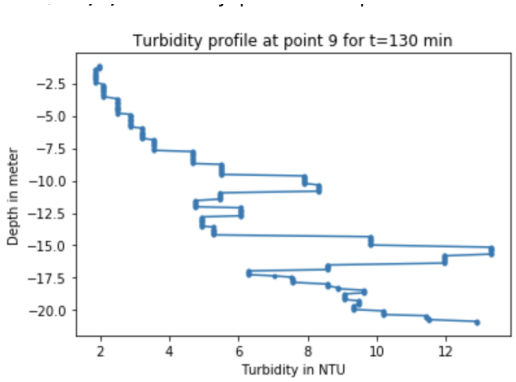

Figure 141: Location 9 at 130 minutes after the start of dredging with the Tiamat. This is the turbidity depth profile of 17-10-2022.

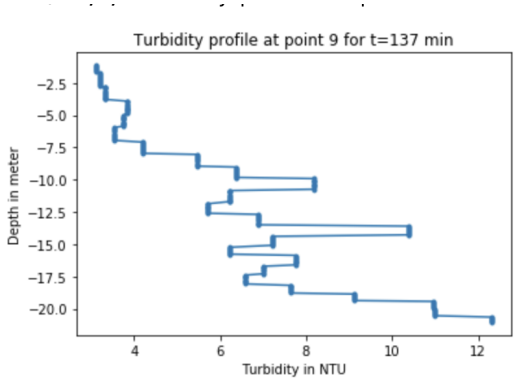

Figure 142: Location 9 at 137 minutes after the start of dredging with the Tiamat. This is the turbidity depth profile of 17-10-2022.

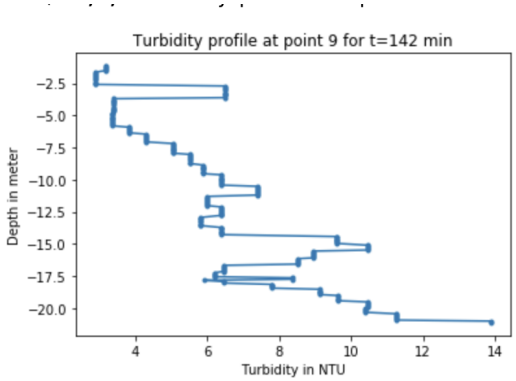

Figure 143: Location 9 at 142 minutes after the start of dredging with the Tiamat. This is the turbidity depth profile of 17-10-2022.

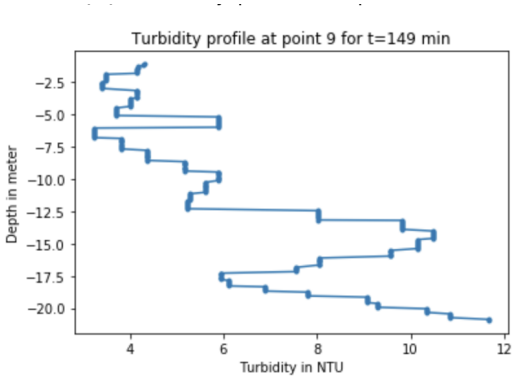

Figure 144: Location 9 at 149 minutes after the start of dredging with the Tiamat. This is the turbidity depth profile of 17-10-2022.

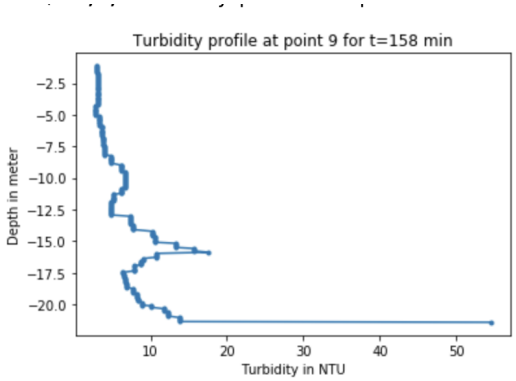

Figure 145: Location 9 at 158 minutes after the start of dredging with the Tiamat. This is the turbidity depth profile of 17-10-2022.

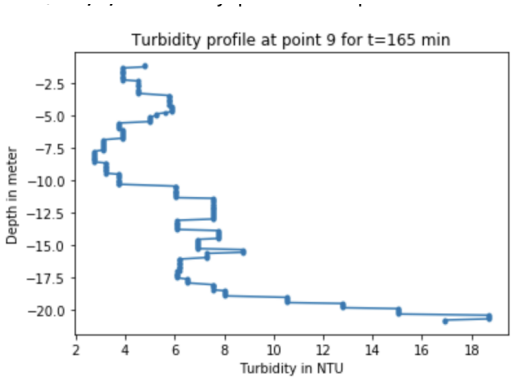

Figure 146: Location 9 at 165 minutes after the start of dredging with the Tiamat. This is the turbidity depth profile of 17-10-2022.

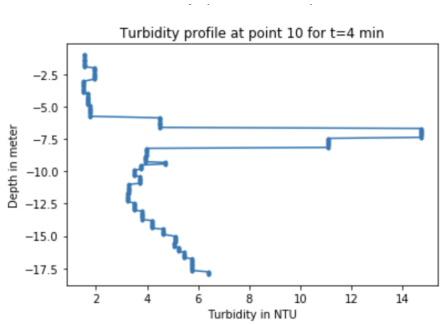

Figure 147: Location 10 at 4 minutes after the start of dredging with the Tiamat. This is the turbidity depth profile of 17-10-2022.

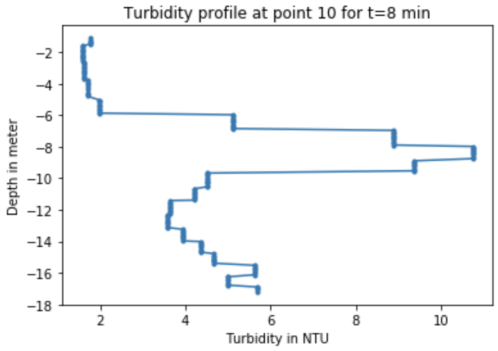

Figure 148: Location 10 at 8 minutes after the start of dredging with the Tiamat. This is the turbidity depth profile of 17-10-2022.

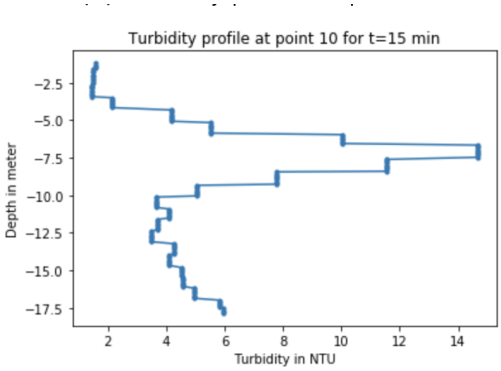

Figure 149: Location 10 at 15 minutes after the start of dredging with the Tiamat. This is the turbidity depth profile of 17-10-2022.

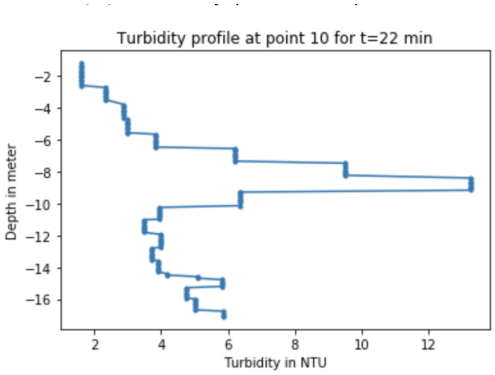

Figure 150: Location 10 at 22 minutes after the start of dredging with the Tiamat. This is the turbidity depth profile of 17-10-2022.

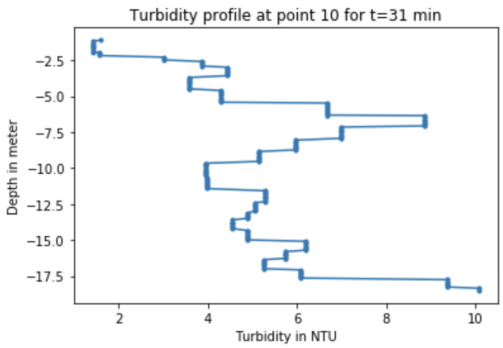

Figure 151: Location 10 at 31 minutes after the start of dredging with the Tiamat. This is the turbidity depth profile of 17-10-2022.

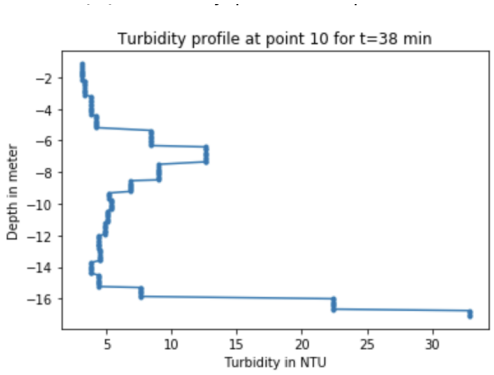

Figure 152: Location 10 at 38 minutes after the start of dredging with the Tiamat. This is the turbidity depth profile of 17-10-2022.

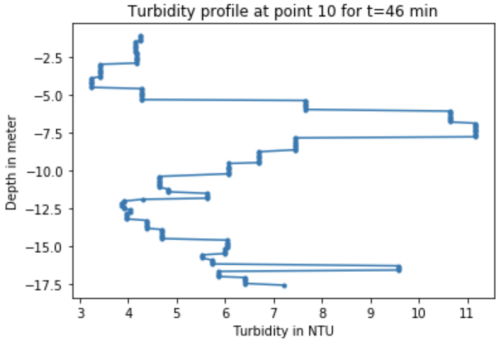

Figure 153: Location 10 at 46 minutes after the start of dredging with the Tiamat. This is the turbidity depth profile of 17-10-2022.

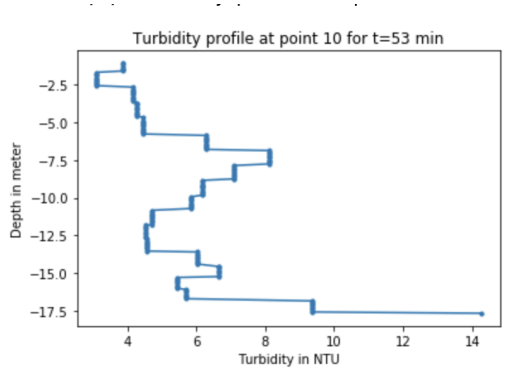

Figure 154: Location 10 at 53 minutes after the start of dredging with the Tiamat. This is the turbidity depth profile of 17-10-2022.

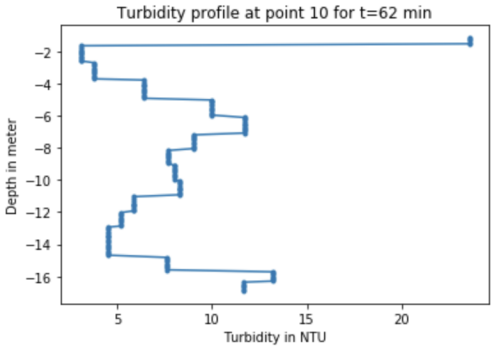

Figure 155: Location 10 at 62 minutes after the start of dredging with the Tiamat. This is the turbidity depth profile of 17-10-2022.

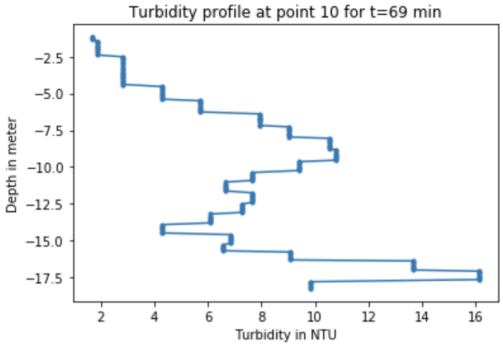

Figure 156: Location 10 at 69 minutes after the start of dredging with the Tiamat. This is the turbidity depth profile of 17-10-2022.

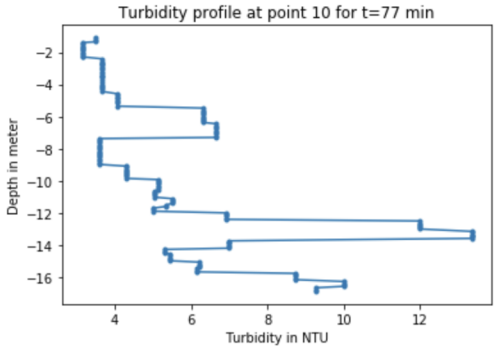

Figure 157: Location 10 at 77 minutes after the start of dredging with the Tiamat. This is the turbidity depth profile of 17-10-2022.

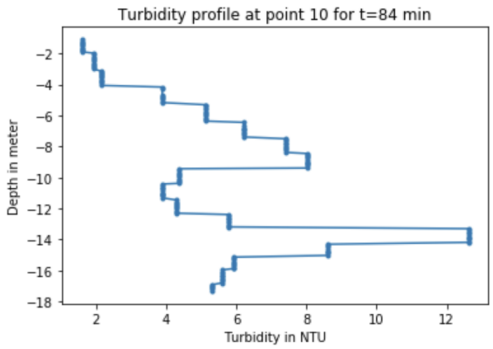

Figure 158: Location 10 at 84 minutes after the start of dredging with the Tiamat. This is the turbidity depth profile of 17-10-2022.

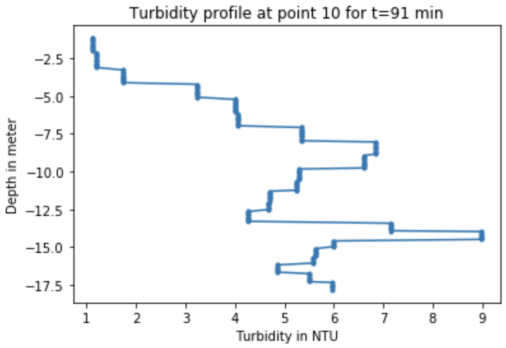

Figure 159: Location 10 at 91 minutes after the start of dredging with the Tiamat. This is the turbidity depth profile of 17-10-2022.

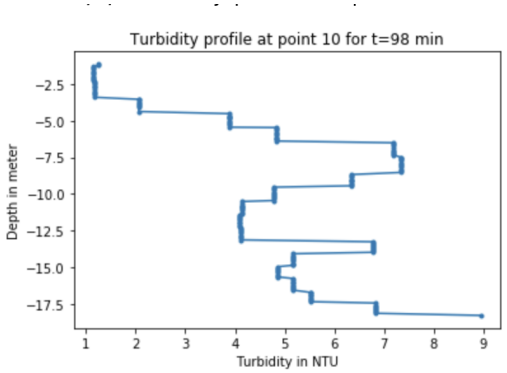

Figure 160: Location 10 at 98 minutes after the start of dredging with the Tiamat. This is the turbidity depth profile of 17-10-2022.

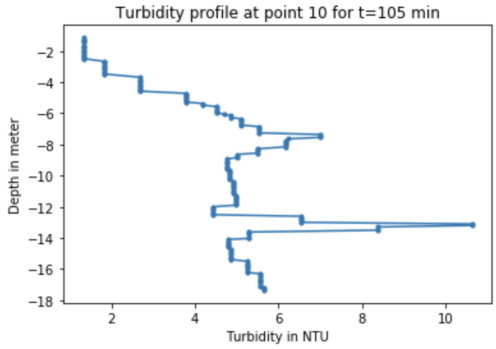

Figure 161: Location 10 at 105 minutes after the start of dredging with the Tiamat. This is the turbidity depth profile of 17-10-2022.

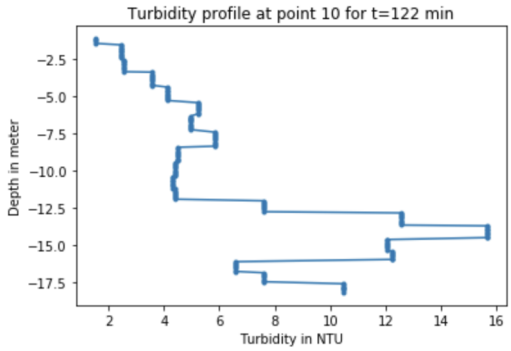

Figure 162: Location 10 at 122 minutes after the start of dredging with the Tiamat. This is the turbidity depth profile of 17-10-2022.

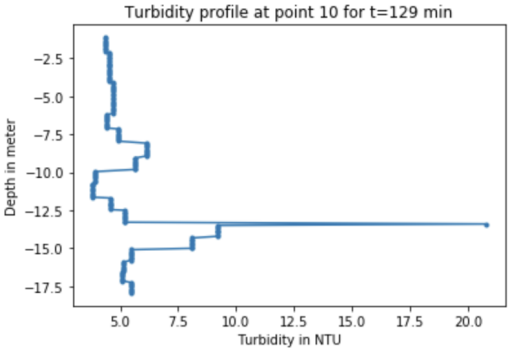

Figure 163: Location 10 at 129 minutes after the start of dredging with the Tiamat. This is the turbidity depth profile of 17-10-2022.

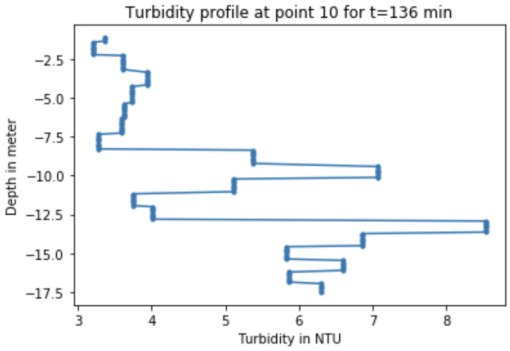

Figure 164: Location 10 at 136 minutes after the start of dredging with the Tiamat. This is the turbidity depth profile of 17-10-2022.

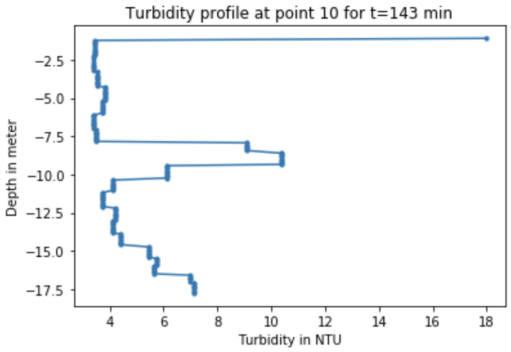

Figure 165: Location 10 at 143 minutes after the start of dredging with the Tiamat. This is the turbidity depth profile of 17-10-2022.

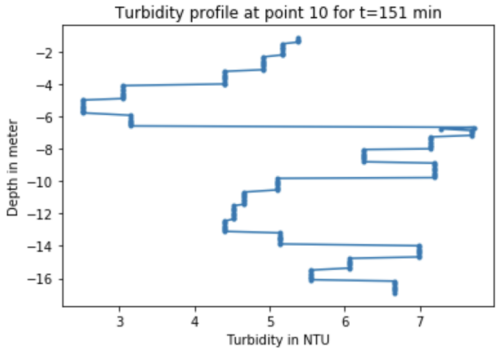

Figure 166: Location 10 at 151 minutes after the start of dredging with the Tiamat. This is the turbidity depth profile of 17-10-2022.

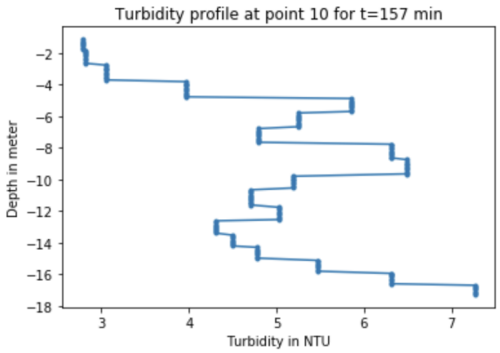

Figure 167: Location 10 at 157 minutes after the start of dredging with the Tiamat. This is the turbidity depth profile of 17-10-2022.

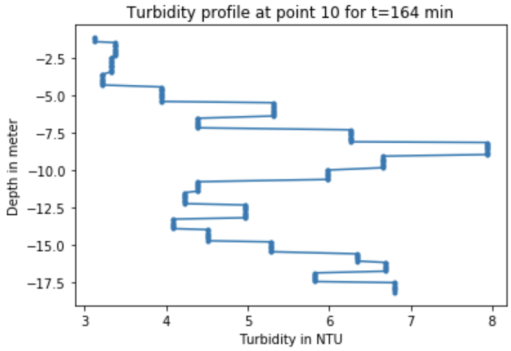

Figure 168: Location 10 at 164 minutes after the start of dredging with the Tiamat. This is the turbidity depth profile of 17-10-2022.

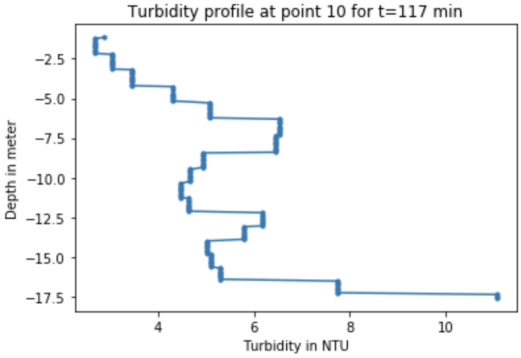

Figure 169: Location 10 at 177 minutes after the start of dredging with the Tiamat. This is the turbidity depth profile of 17-10-2022.

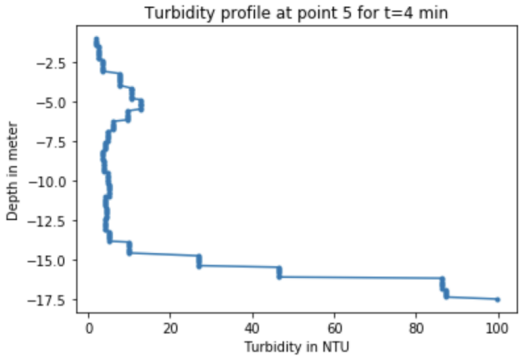

Figure 170: Location 5 at 4 minutes after the start of dredging with the Tiamat. This is the turbidity depth profile of 18-10-2022.

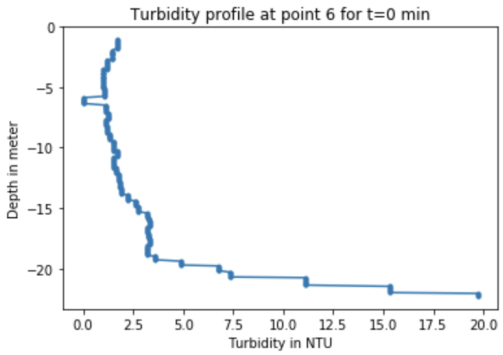

Figure 171: Location 6 at 0 minutes after the start of dredging with the Tiamat. This is the turbidity depth profile of 18-10-2022.

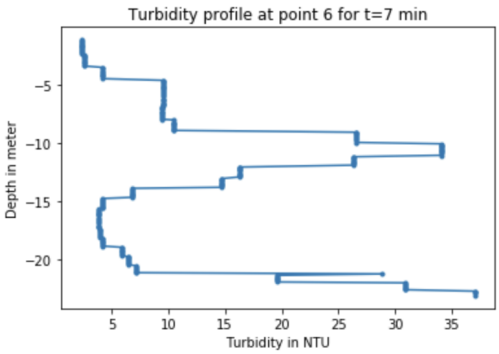

Figure 172: Location 6 at 7 minutes after the start of dredging with the Tiamat. This is the turbidity depth profile of 18-10-2022.

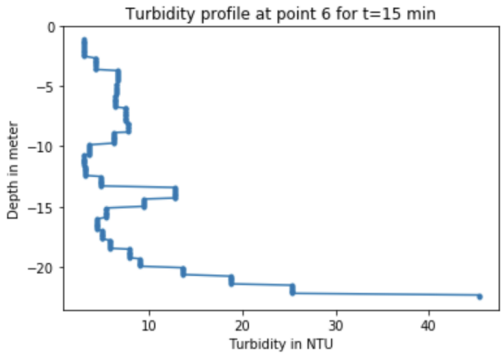

Figure 173: Location 6 at 15 minutes after the start of dredging with the Tiamat. This is the turbidity depth profile of 18-10-2022.

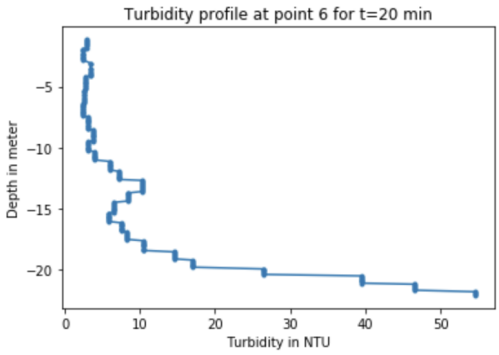

Figure 174: Location 6 at 20 minutes after the start of dredging with the Tiamat. This is the turbidity depth profile of 18-10-2022.

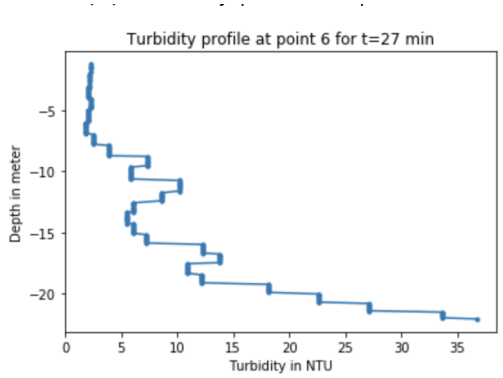

Figure 175: Location 6 at 27 minutes after the start of dredging with the Tiamat. This is the turbidity depth profile of 18-10-2022.

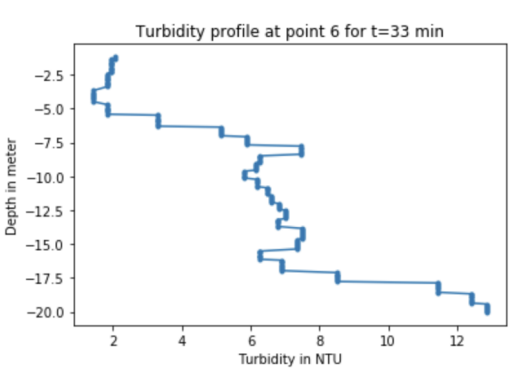

Figure 176: Location 6 at 33 minutes after the start of dredging with the Tiamat. This is the turbidity depth profile of 18-10-2022.

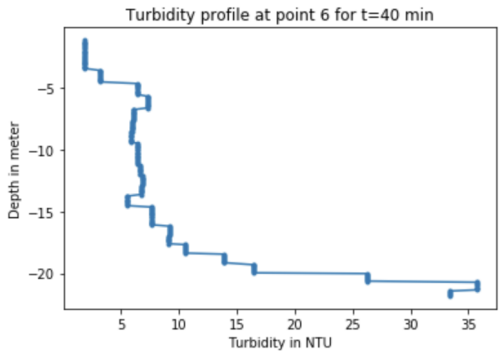

Figure 177: Location 6 at 40 minutes after the start of dredging with the Tiamat. This is the turbidity depth profile of 18-10-2022.

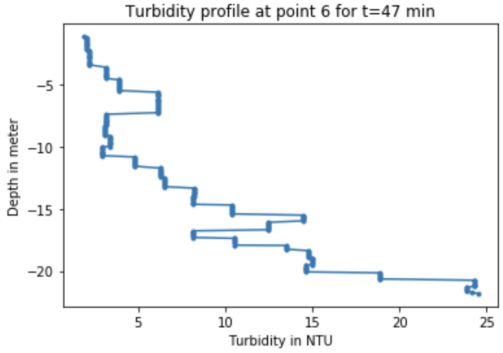

Figure 178: Location 6 at 47 minutes after the start of dredging with the Tiamat. This is the turbidity depth profile of 18-10-2022.

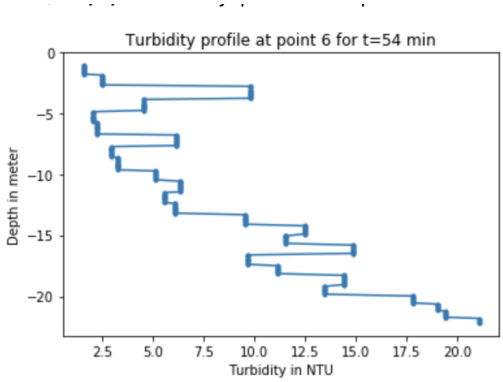

Figure 179: Location 6 at 54 minutes after the start of dredging with the Tiamat. This is the turbidity depth profile of 18-10-2022.

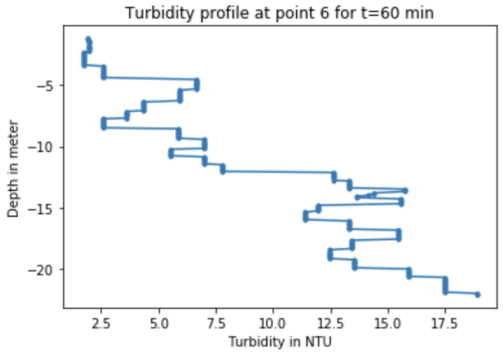

Figure 180: Location 6 at 60 minutes after the start of dredging with the Tiamat. This is the turbidity depth profile of 18-10-2022.

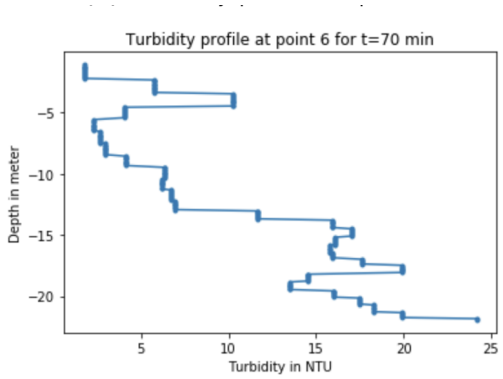

Figure 181: Location 6 at 70 minutes after the start of dredging with the Tiamat. This is the turbidity depth profile of 18-10-2022.

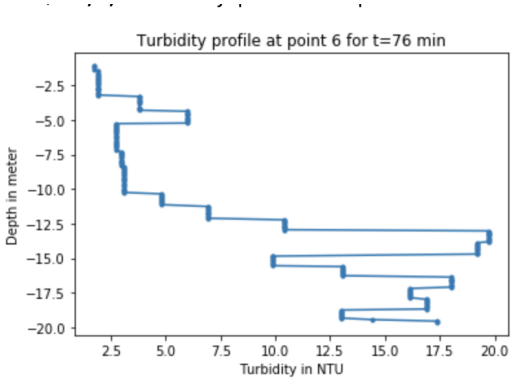

Figure 182: Location 6 at 76 minutes after the start of dredging with the Tiamat. This is the turbidity depth profile of 18-10-2022.

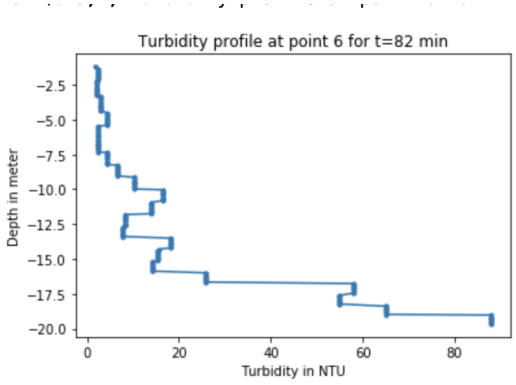

Figure 183: Location 6 at 82 minutes after the start of dredging with the Tiamat. This is the turbidity depth profile of 18-10-2022.

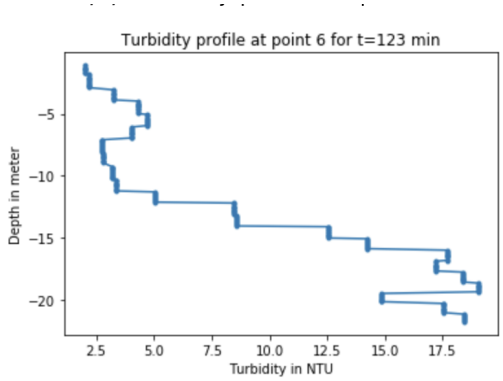

Figure 184: Location 6 at 123 minutes after the start of dredging with the Tiamat. This is the turbidity depth profile of 18-10-2022.

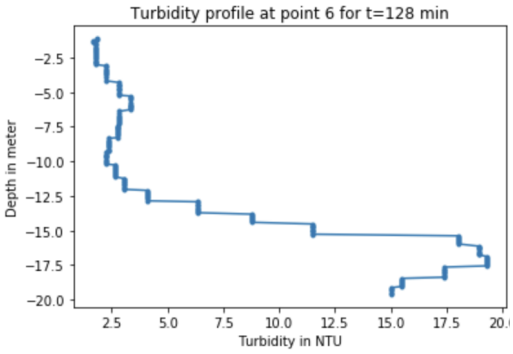

Figure 185: Location 6 at 128 minutes after the start of dredging with the Tiamat. This is the turbidity depth profile of 18-10-2022.

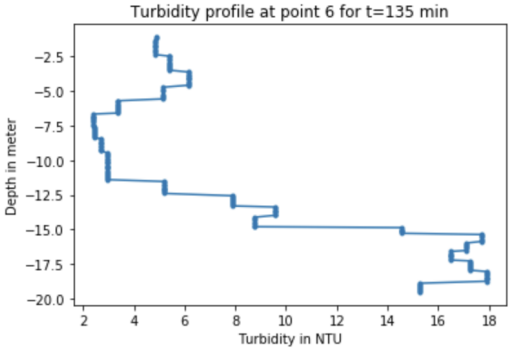

Figure 186: Location 6 at 135 minutes after the start of dredging with the Tiamat. This is the turbidity depth profile of 18-10-2022.

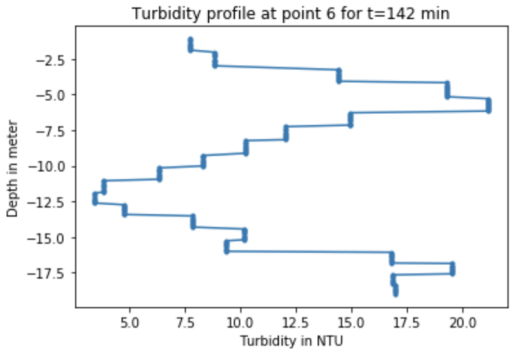

Figure 187: Location 6 at 142 minutes after the start of dredging with the Tiamat. This is the turbidity depth profile of 18-10-2022.

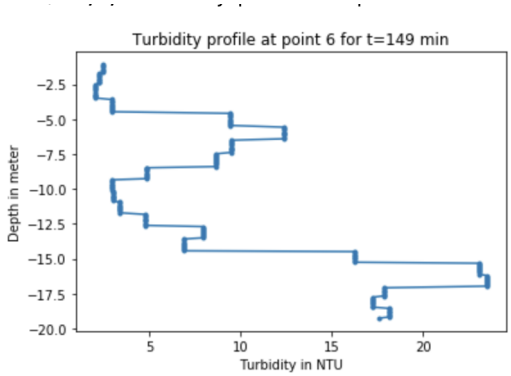

Figure 188: Location 6 at 149 minutes after the start of dredging with the Tiamat. This is the turbidity depth profile of 18-10-2022.

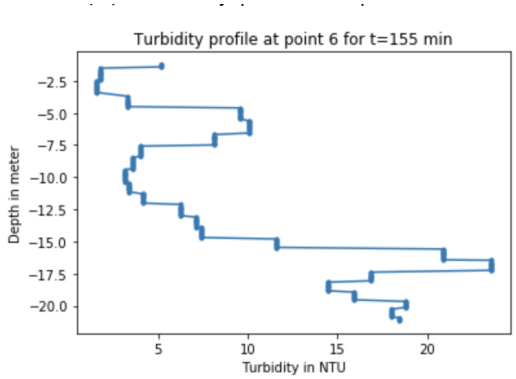

Figure 189: Location 6 at 155 minutes after the start of dredging with the Tiamat. This is the turbidity depth profile of 18-10-2022.

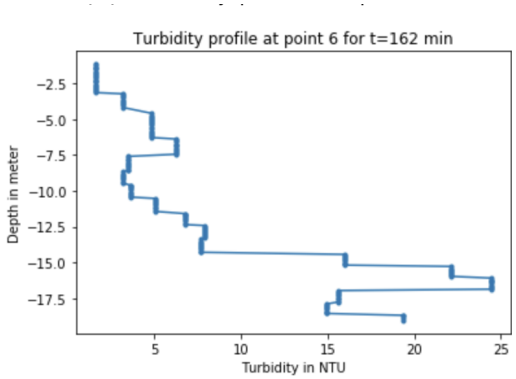

Figure 190: Location 6 at 162 minutes after the start of dredging with the Tiamat. This is the turbidity depth profile of 18-10-2022.

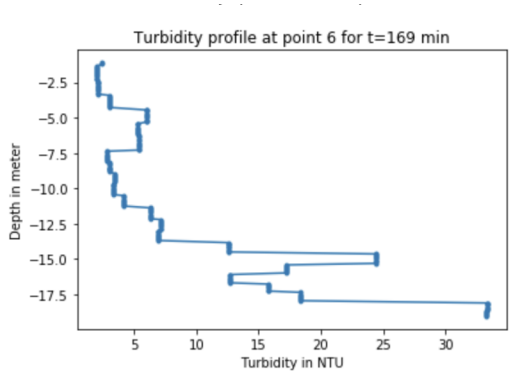

Figure 191: Location 6 at 169 minutes after the start of dredging with the Tiamat. This is the turbidity depth profile of 18-10-2022.

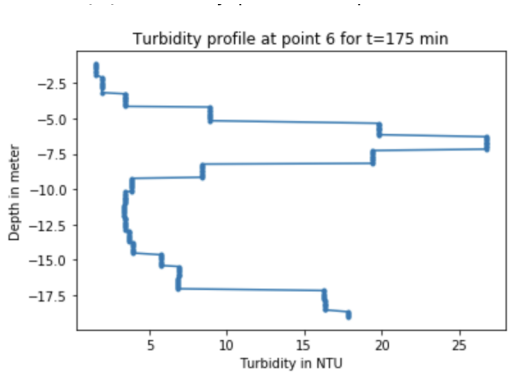

Figure 192: Location 6 at 175 minutes after the start of dredging with the Tiamat. This is the turbidity depth profile of 18-10-2022.

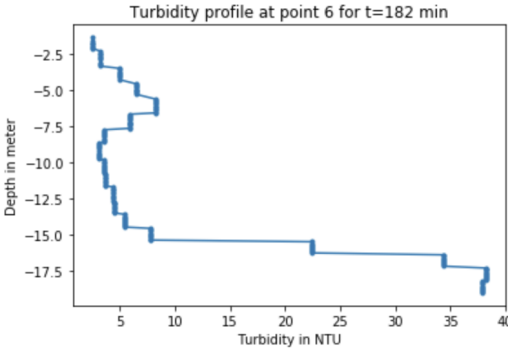

Figure 193: Location 6 at 182 minutes after the start of dredging with the Tiamat. This is the turbidity depth profile of 18-10-2022.

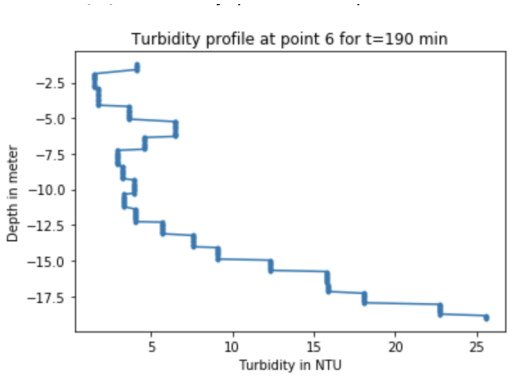

Figure 194: Location 6 at 190 minutes after the start of dredging with the Tiamat. This is the turbidity depth profile of 18-10-2022.

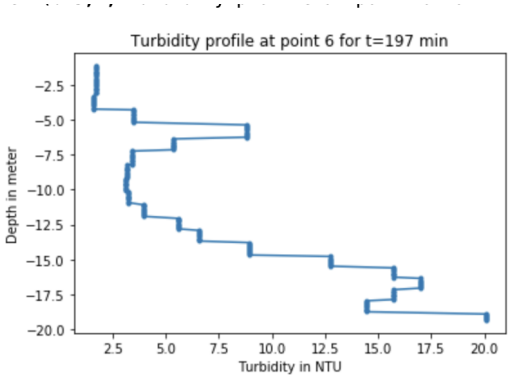

Figure 195: Location 6 at 197 minutes after the start of dredging with the Tiamat. This is the turbidity depth profile of 18-10-2022.

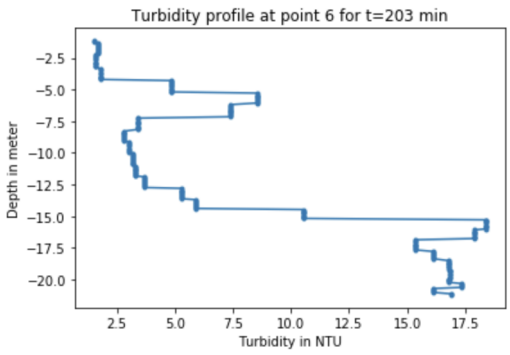

Figure 196: Location 6 at 203 minutes after the start of dredging with the Tiamat. This is the turbidity depth profile of 18-10-2022.

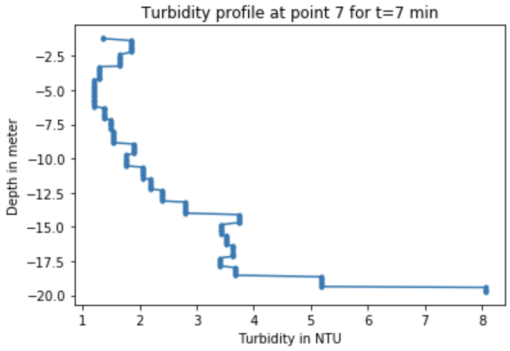

Figure 197: Location 7 at 7 minutes after the start of dredging with the Tiamat. This is the turbidity depth profile of 18-10-2022.

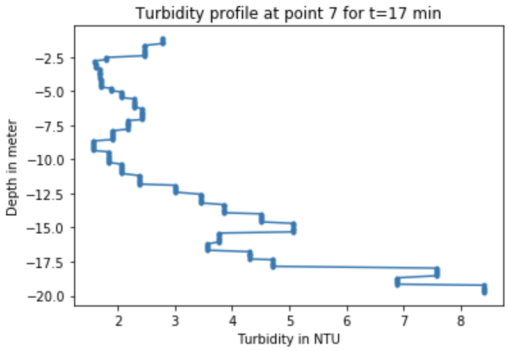

Figure 198: Location 7 at 17 minutes after the start of dredging with the Tiamat. This is the turbidity depth profile of 18-10-2022.

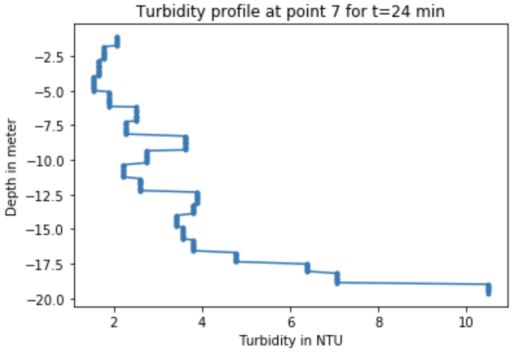

Figure 199: Location 7 at 24 minutes after the start of dredging with the Tiamat. This is the turbidity depth profile of 18-10-2022.

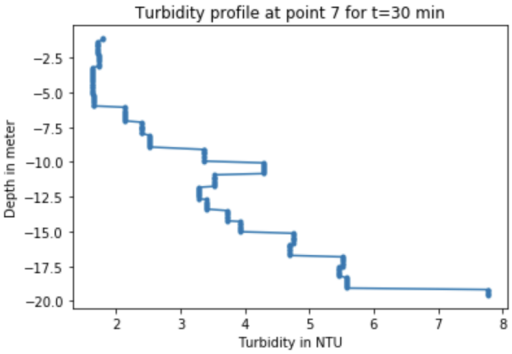

Figure 200: Location 7 at 30 minutes after the start of dredging with the Tiamat. This is the turbidity depth profile of 18-10-2022.

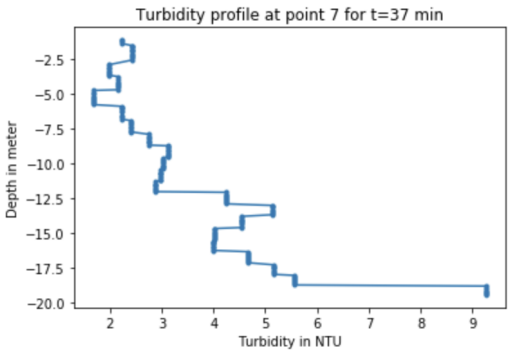

Figure 201: Location 7 at 37 minutes after the start of dredging with the Tiamat. This is the turbidity depth profile of 18-10-2022.

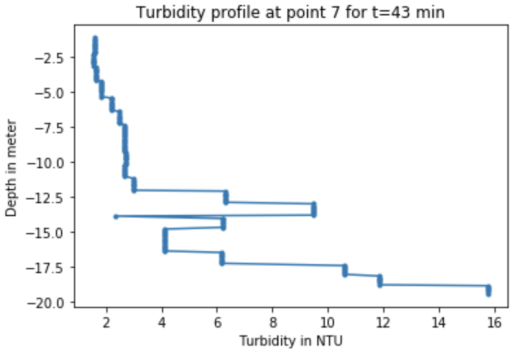

Figure 202: Location 7 at 43 minutes after the start of dredging with the Tiamat. This is the turbidity depth profile of 18-10-2022.

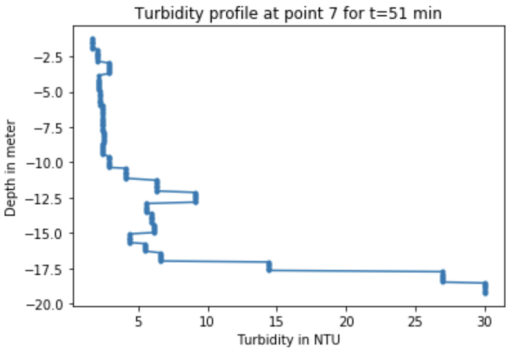

Figure 203: Location 7 at 51 minutes after the start of dredging with the Tiamat. This is the turbidity depth profile of 18-10-2022.

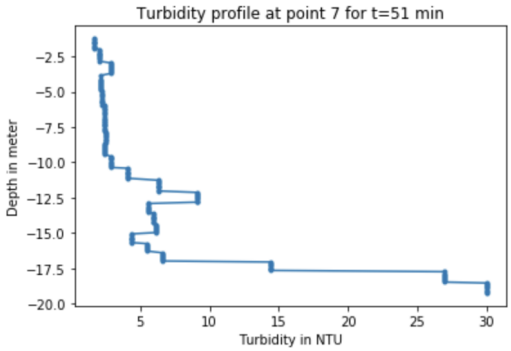

Figure 204: Location 7 at 51 minutes after the start of dredging with the Tiamat. This is the turbidity depth profile of 18-10-2022.

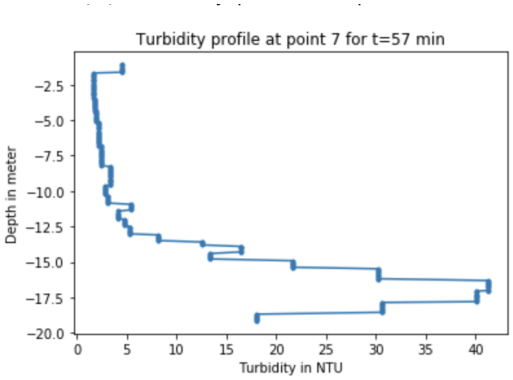

Figure 205: Location 7 at 57 minutes after the start of dredging with the Tiamat. This is the turbidity depth profile of 18-10-2022.

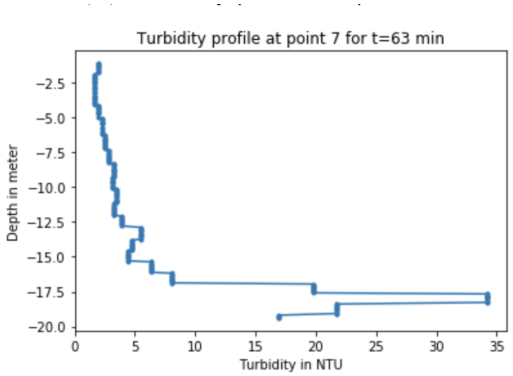

Figure 206: Location 7 at 63 minutes after the start of dredging with the Tiamat. This is the turbidity depth profile of 18-10-2022.

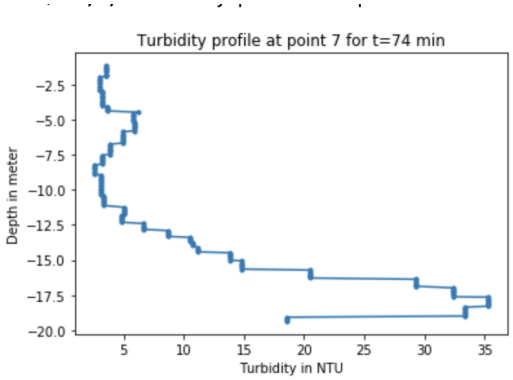

Figure 207: Location 7 at 74 minutes after the start of dredging with the Tiamat. This is the turbidity depth profile of 18-10-2022.

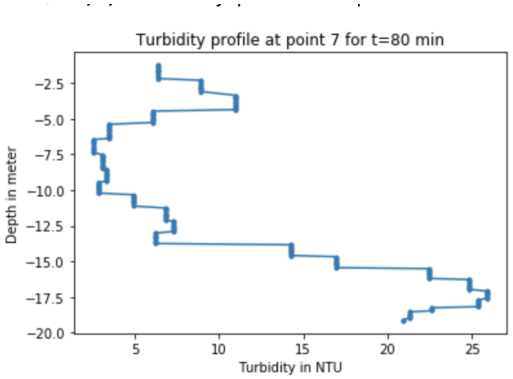

Figure 208: Location 7 at 80 minutes after the start of dredging with the Tiamat. This is the turbidity depth profile of 18-10-2022.

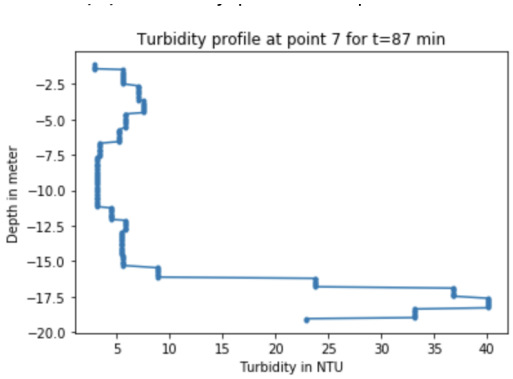

Figure 209: Location 7 at 87 minutes after the start of dredging with the Tiamat. This is the turbidity depth profile of 18-10-2022.

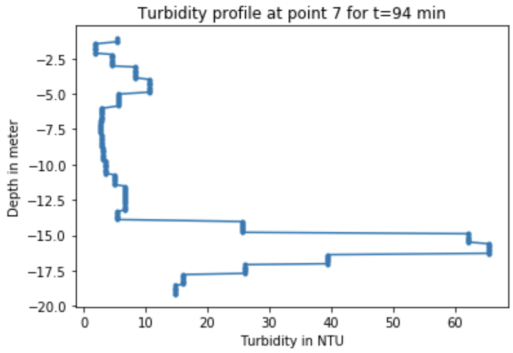

Figure 210: Location 7 at 94 minutes after the start of dredging with the Tiamat. This is the turbidity depth profile of 18-10-2022.

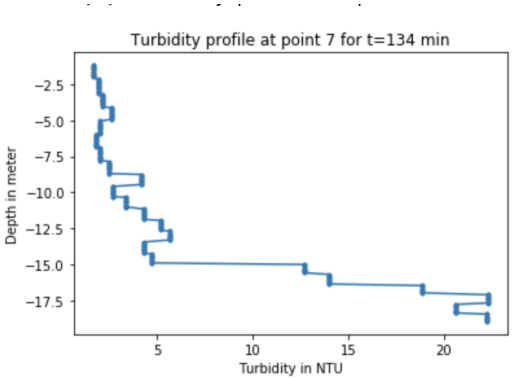

Figure 211: Location 7 at 134 minutes after the start of dredging with the Tiamat. This is the turbidity depth profile of 18-10-2022.

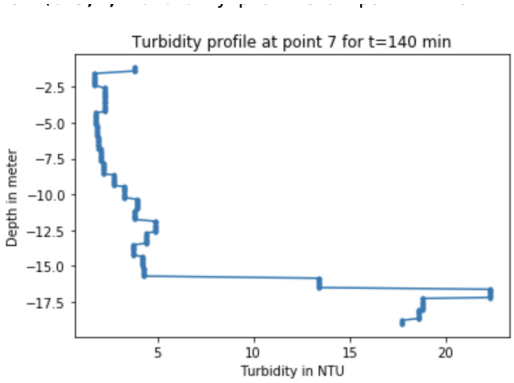

Figure 212: Location 7 at 140 minutes after the start of dredging with the Tiamat. This is the turbidity depth profile of 18-10-2022.

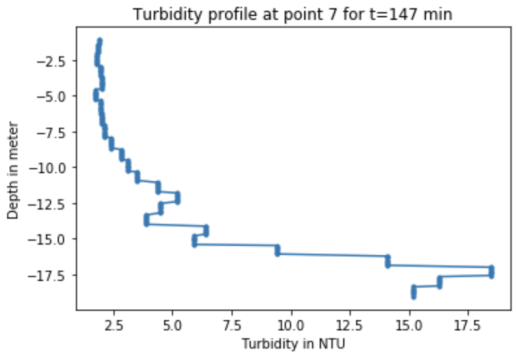

Figure 213: Location 7 at 147 minutes after the start of dredging with the Tiamat. This is the turbidity depth profile of 18-10-2022.

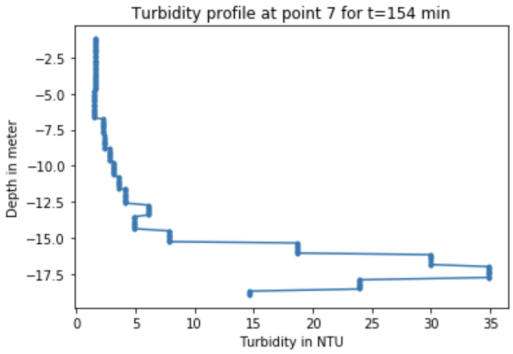

Figure 214: Location 7 at 154 minutes after the start of dredging with the Tiamat. This is the turbidity depth profile of 18-10-2022.

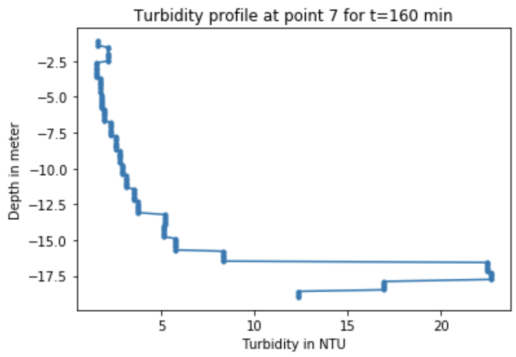

Figure 215: Location 7 at 160 minutes after the start of dredging with the Tiamat. This is the turbidity depth profile of 18-10-2022.

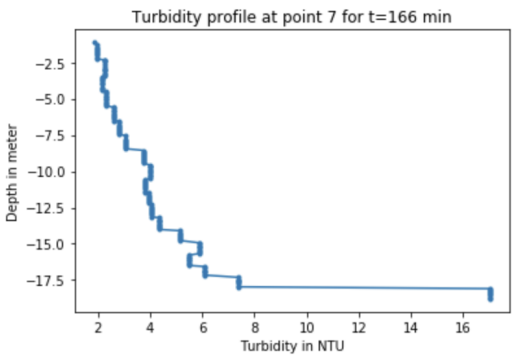

Figure 216: Location 7 at 166 minutes after the start of dredging with the Tiamat. This is the turbidity depth profile of 18-10-2022.

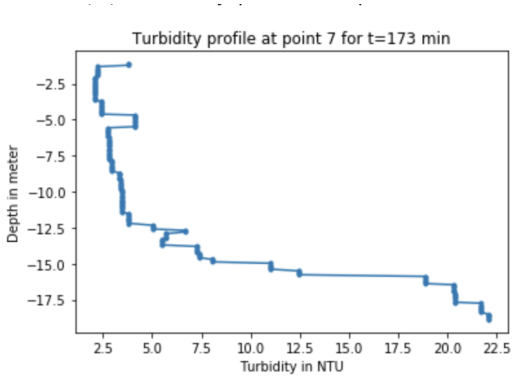

Figure 217: Location 7 at 173 minutes after the start of dredging with the Tiamat. This is the turbidity depth profile of 18-10-2022.

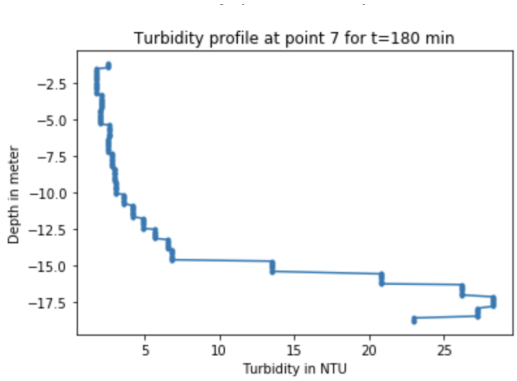

Figure 218: Location 7 at 180 minutes after the start of dredging with the Tiamat. This is the turbidity depth profile of 18-10-2022.

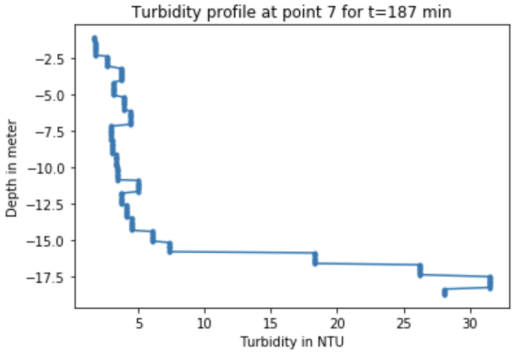

Figure 219: Location 7 at 187 minutes after the start of dredging with the Tiamat. This is the turbidity depth profile of 18-10-2022.

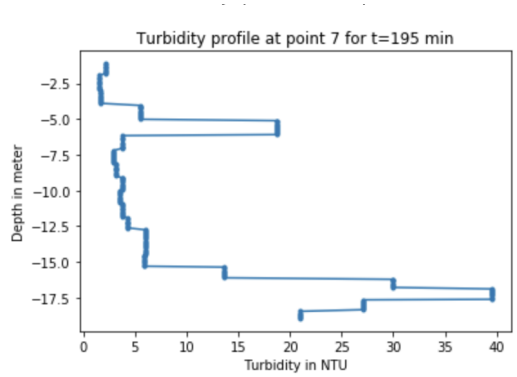

Figure 220: Location 7 at 195 minutes after the start of dredging with the Tiamat. This is the turbidity depth profile of 18-10-2022.

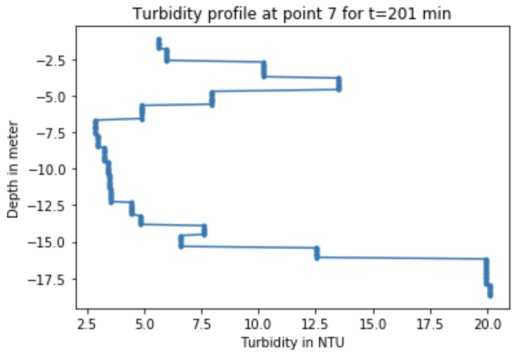

Figure 221: Location 7 at 201 minutes after the start of dredging with the Tiamat. This is the turbidity depth profile of 18-10-2022.

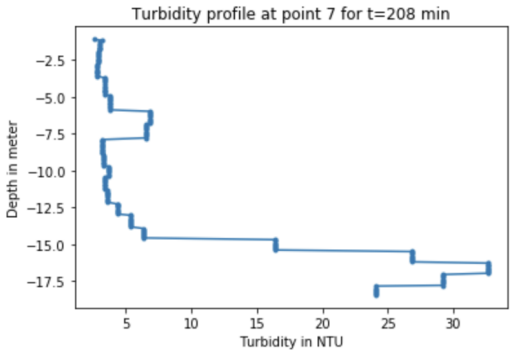

Figure 222: Location 7 at 208 minutes after the start of dredging with the Tiamat. This is the turbidity depth profile of 18-10-2022.

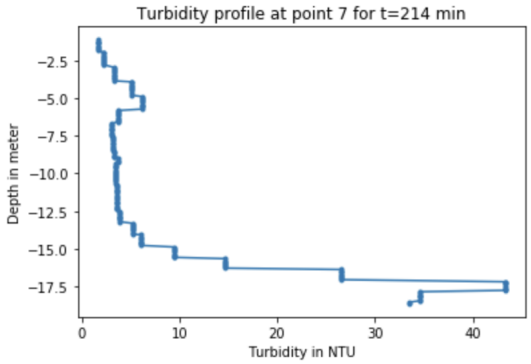

Figure 223: Location 7 at 214 minutes after the start of dredging with the Tiamat. This is the turbidity depth profile of 18-10-2022.

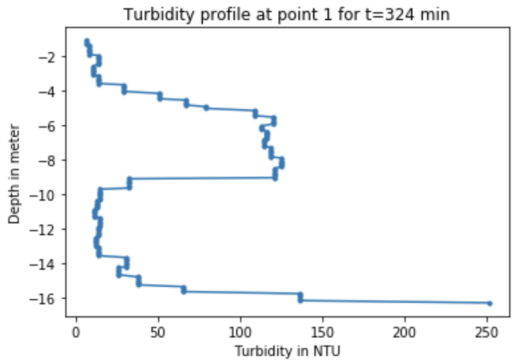

Figure 224: Location 1 at 324 minutes after the start of dredging with the Tiamat. This is the turbidity depth profile of 19-10-2022.

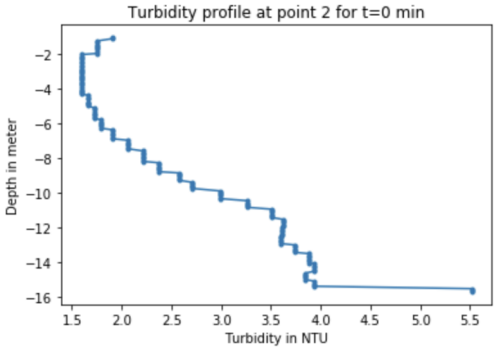

Figure 225: Location 2 at 0 minutes after the start of dredging with the Tiamat. This is the turbidity depth profile of 19-10-2022.

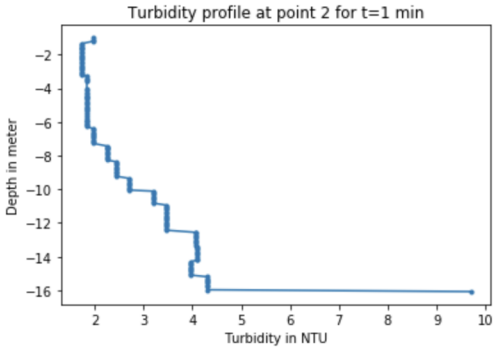

Figure 226: Location 2 at 1 minutes after the start of dredging with the Tiamat. This is the turbidity depth profile of 19-10-2022.

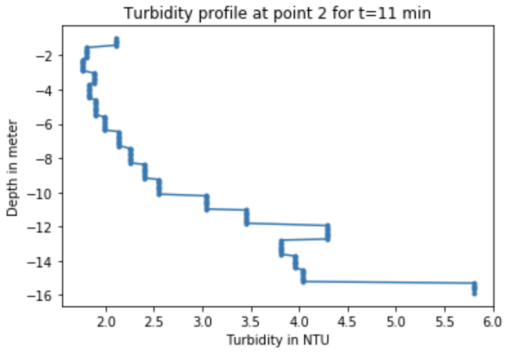

Figure 227: Location 2 at 11 minutes after the start of dredging with the Tiamat. This is the turbidity depth profile of 19-10-2022.

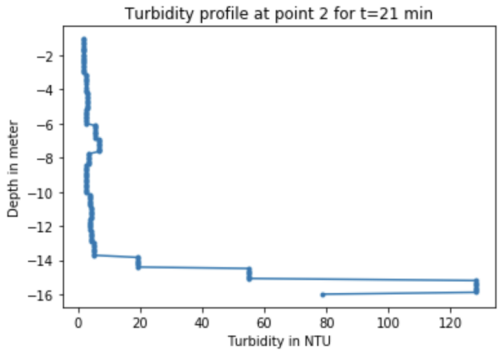

Figure 228: Location 2 at 21 minutes after the start of dredging with the Tiamat. This is the turbidity depth profile of 19-10-2022.

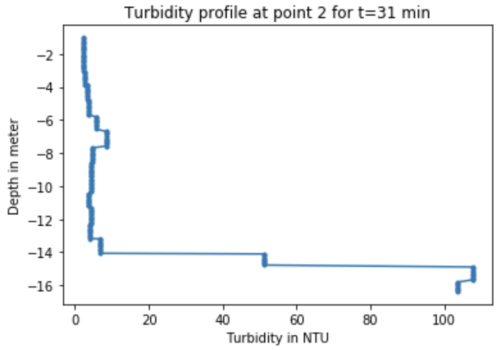

Figure 229: Location 2 at 31 minutes after the start of dredging with the Tiamat. This is the turbidity depth profile of 19-10-2022.

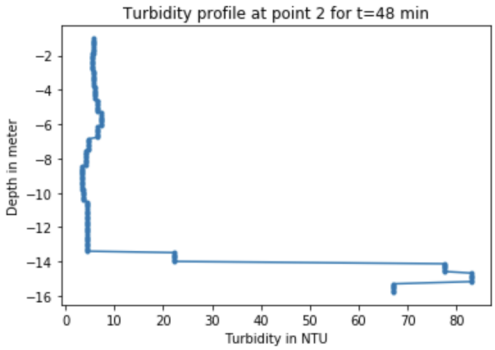

Figure 230: Location 2 at 48 minutes after the start of dredging with the Tiamat. This is the turbidity depth profile of 19-10-2022.

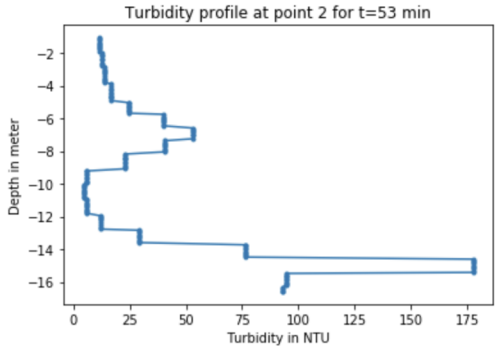

Figure 231: Location 2 at 53 minutes after the start of dredging with the Tiamat. This is the turbidity depth profile of 19-10-2022.

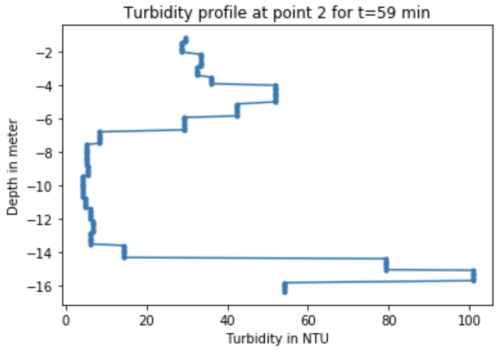

Figure 232: Location 2 at 59 minutes after the start of dredging with the Tiamat. This is the turbidity depth profile of 19-10-2022.

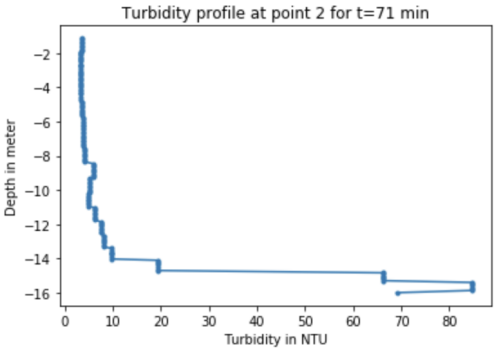

Figure 233: Location 2 at 71 minutes after the start of dredging with the Tiamat. This is the turbidity depth profile of 19-10-2022.

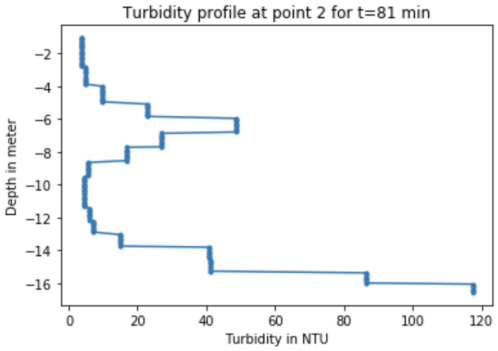

Figure 234: Location 2 at 81 minutes after the start of dredging with the Tiamat. This is the turbidity depth profile of 19-10-2022.

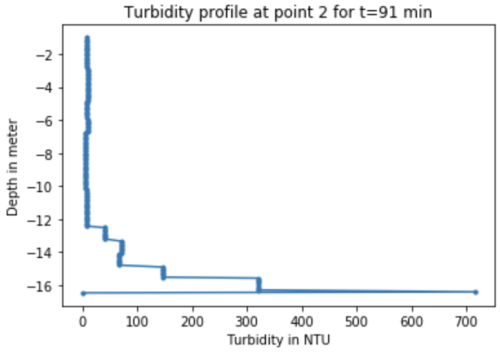

Figure 235: Location 2 at 91 minutes after the start of dredging with the Tiamat. This is the turbidity depth profile of 19-10-2022.

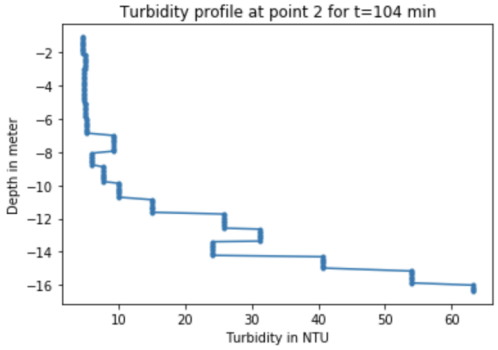

Figure 236: Location 2 at 104 minutes after the start of dredging with the Tiamat. This is the turbidity depth profile of 19-10-2022.

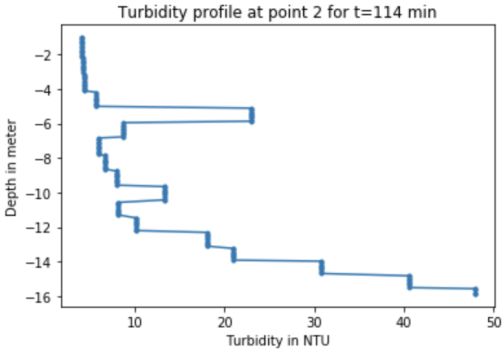

Figure 237: Location 2 at 114 minutes after the start of dredging with the Tiamat. This is the turbidity depth profile of 19-10-2022.

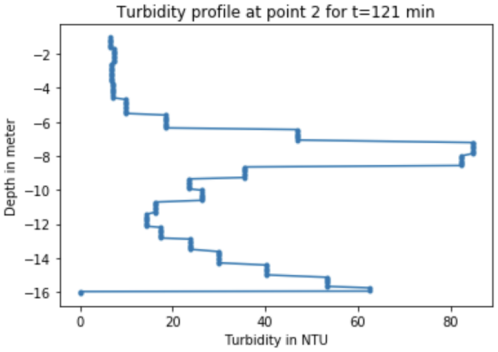

Figure 238: Location 2 at 121 minutes after the start of dredging with the Tiamat. This is the turbidity depth profile of 19-10-2022.

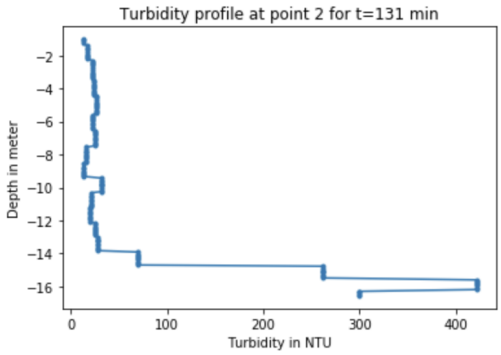

Figure 239: Location 2 at 131 minutes after the start of dredging with the Tiamat. This is the turbidity depth profile of 19-10-2022.

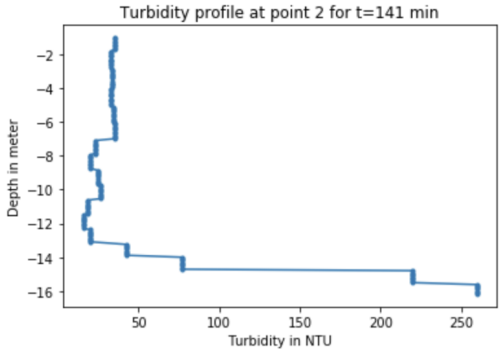

Figure 240: Location 2 at 141 minutes after the start of dredging with the Tiamat. This is the turbidity depth profile of 19-10-2022.

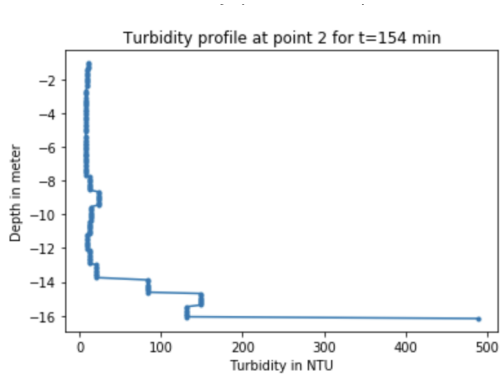

Figure 241: Location 2 at 154 minutes after the start of dredging with the Tiamat. This is the turbidity depth profile of 19-10-2022.

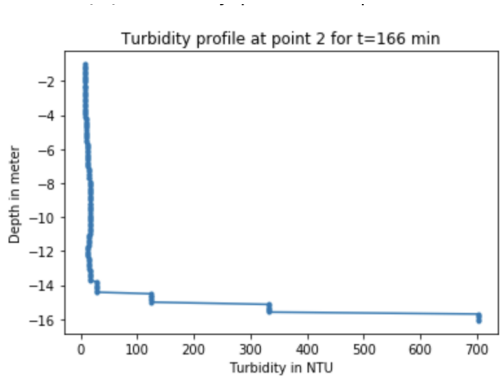

Figure 242: Location 2 at 166 minutes after the start of dredging with the Tiamat. This is the turbidity depth profile of 19-10-2022.

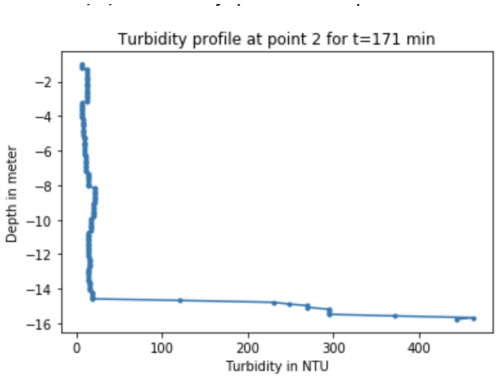

Figure 243: Location 2 at 171 minutes after the start of dredging with the Tiamat. This is the turbidity depth profile of 19-10-2022.

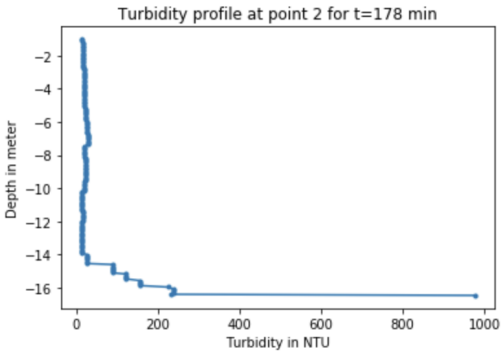

Figure 244: Location 2 at 178 minutes after the start of dredging with the Tiamat. This is the turbidity depth profile of 19-10-2022.

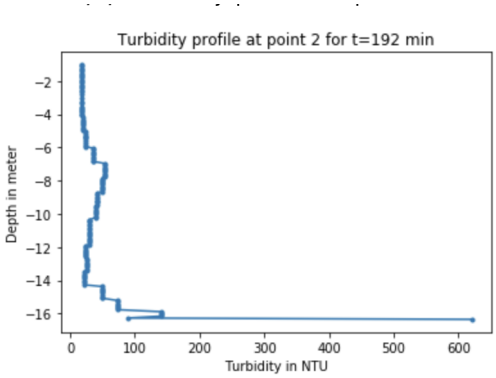

Figure 245: Location 2 at 191 minutes after the start of dredging with the Tiamat. This is the turbidity depth profile of 19-10-2022.

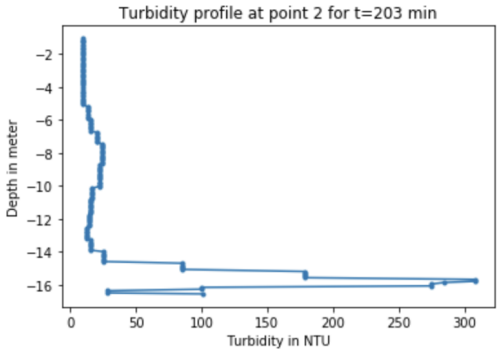

Figure 246: Location 2 at 203 minutes after the start of dredging with the Tiamat. This is the turbidity depth profile of 19-10-2022.

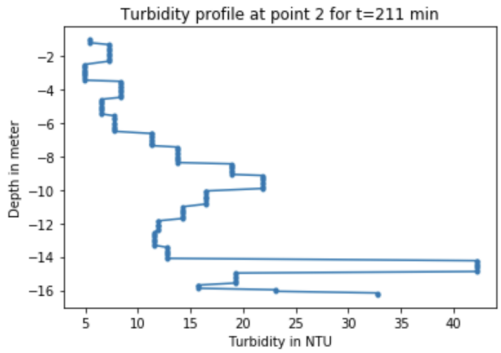

Figure 247: Location 2 at 211 minutes after the start of dredging with the Tiamat. This is the turbidity depth profile of 19-10-2022.

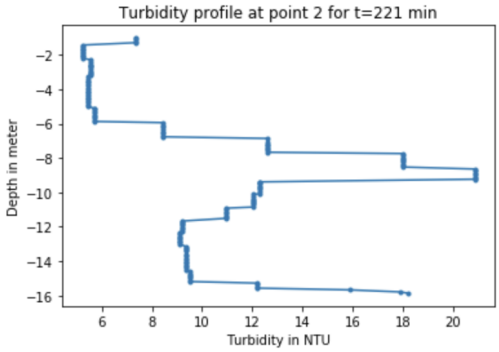

Figure 248: Location 2 at 221 minutes after the start of dredging with the Tiamat. This is the turbidity depth profile of 19-10-2022.

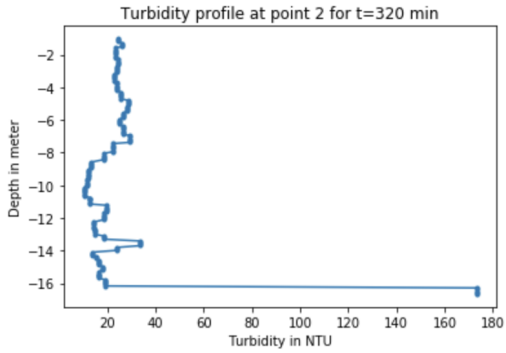

Figure 249: Location 2 at 230 minutes after the start of dredging with the Tiamat. This is the turbidity depth profile of 19-10-2022.

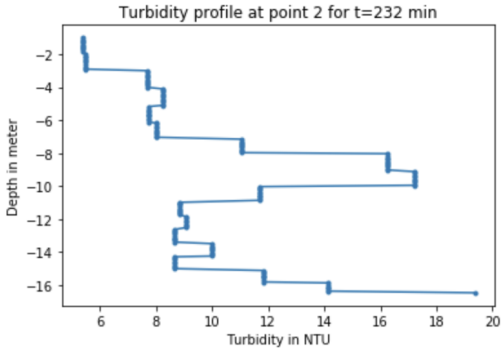

Figure 250: Location 2 at 232 minutes after the start of dredging with the Tiamat. This is the turbidity depth profile of 19-10-2022.

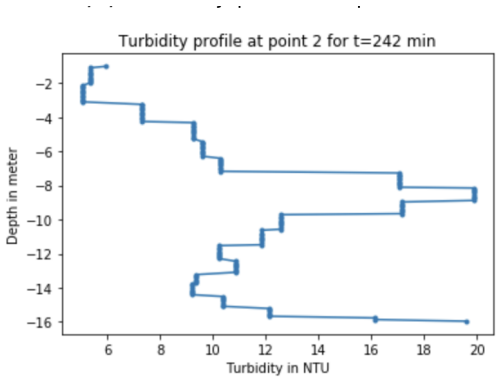

Figure 251: Location 2 at 242 minutes after the start of dredging with the Tiamat. This is the turbidity depth profile of 19-10-2022.

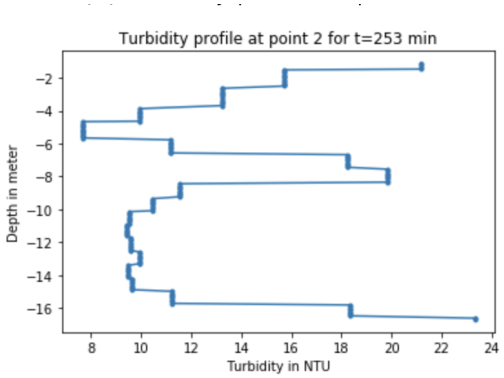

Figure 252: Location 2 at 253 minutes after the start of dredging with the Tiamat. This is the turbidity depth profile of 19-10-2022.

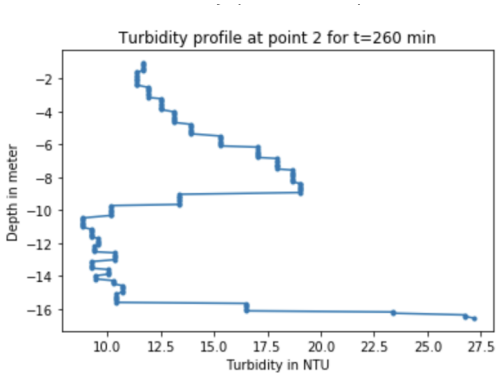

Figure 253: Location 2 at 260 minutes after the start of dredging with the Tiamat. This is the turbidity depth profile of 19-10-2022.

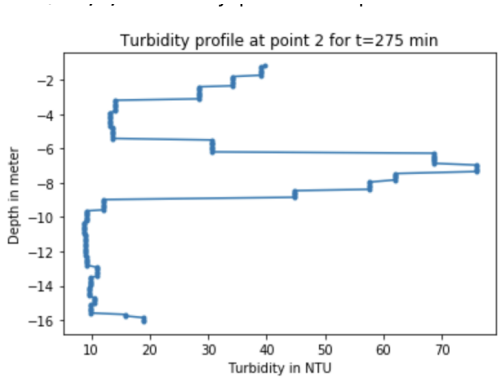

Figure 254: Location 2 at 275 minutes after the start of dredging with the Tiamat. This is the turbidity depth profile of 19-10-2022.

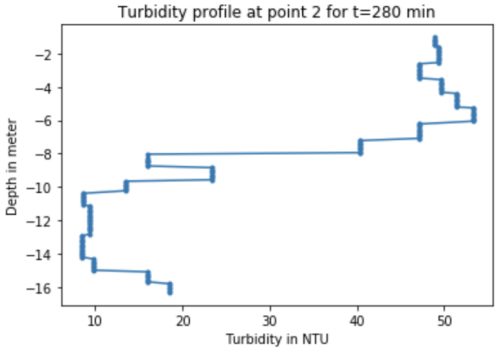

Figure 255: Location 2 at 280 minutes after the start of dredging with the Tiamat. This is the turbidity depth profile of 19-10-2022.

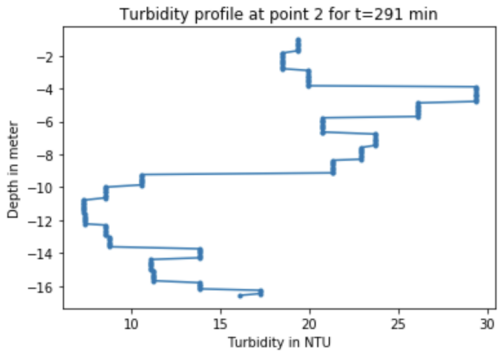

Figure 256: Location 2 at 291 minutes after the start of dredging with the Tiamat. This is the turbidity depth profile of 19-10-2022.

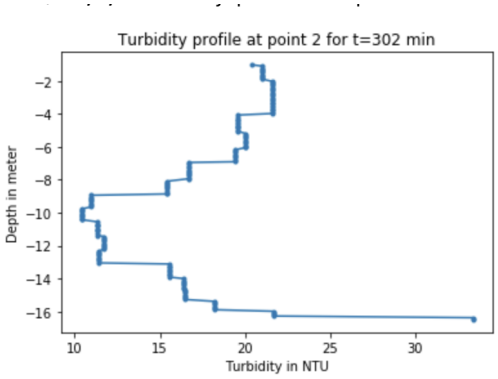

Figure 257: Location 2 at 302 minutes after the start of dredging with the Tiamat. This is the turbidity depth profile of 19-10-2022.

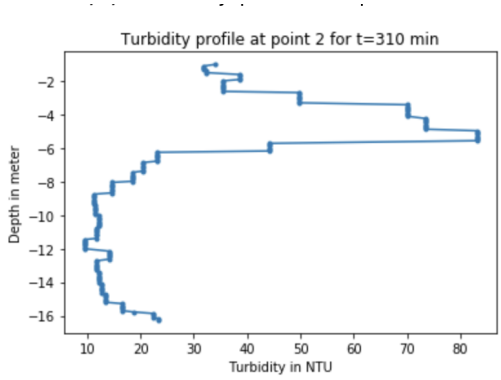

Figure 258: Location 2 at 310 minutes after the start of dredging with the Tiamat. This is the turbidity depth profile of 19-10-2022.

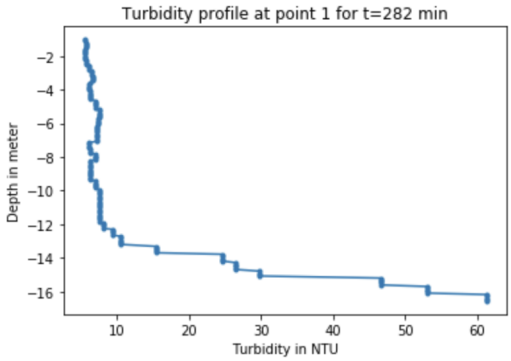

Figure 259: Location 1 at 282 minutes after the start of dredging with the Tiamat. This is the turbidity depth profile of 20-10-2022.

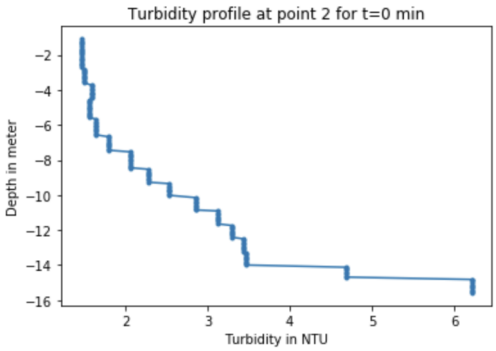

Figure 260: Location 2 at 0 minutes after the start of dredging with the Tiamat. This is the turbidity depth profile of 20-10-2022.

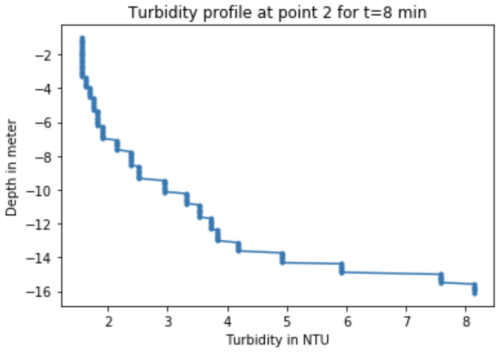

Figure 261: Location 2 at 8 minutes after the start of dredging with the Tiamat. This is the turbidity depth profile of 20-10-2022.

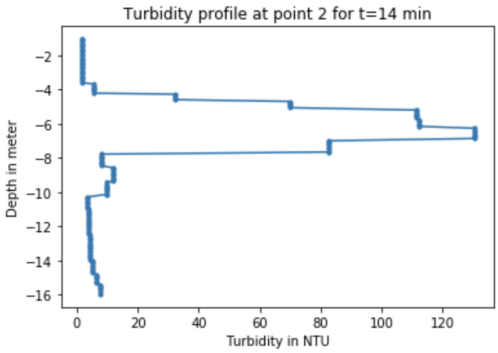

Figure 262: Location 2 at 14 minutes after the start of dredging with the Tiamat. This is the turbidity depth profile of 20-10-2022.

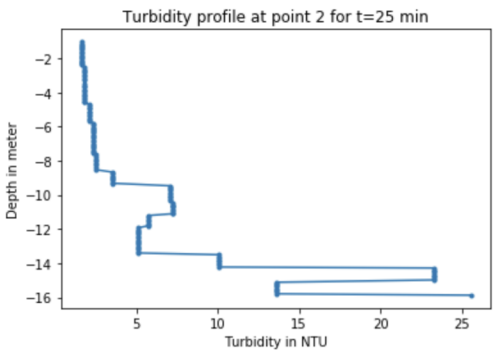

Figure 263: Location 2 at 25 minutes after the start of dredging with the Tiamat. This is the turbidity depth profile of 20-10-2022.

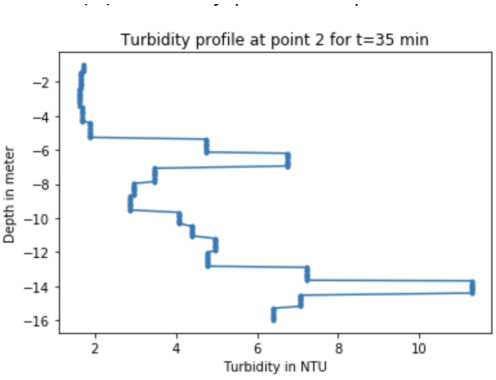

Figure 264: Location 2 at 35 minutes after the start of dredging with the Tiamat. This is the turbidity depth profile of 20-10-2022.

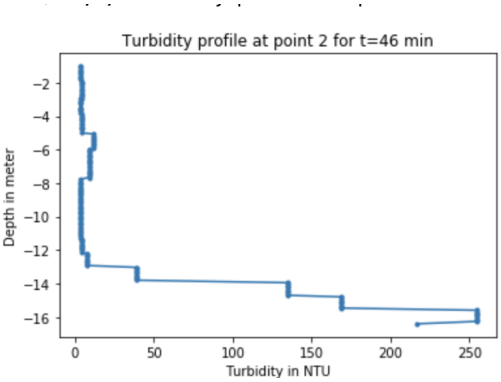

Figure 265: Location 2 at 46 minutes after the start of dredging with the Tiamat. This is the turbidity depth profile of 20-10-2022.

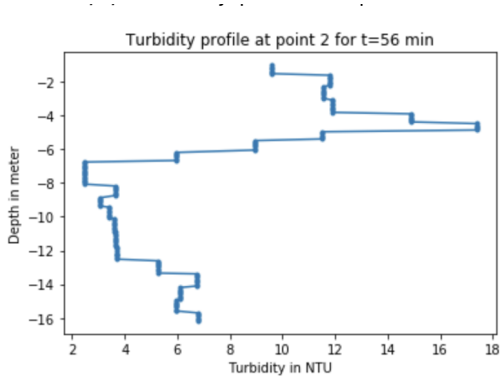

Figure 266: Location 2 at 56 minutes after the start of dredging with the Tiamat. This is the turbidity depth profile of 20-10-2022.

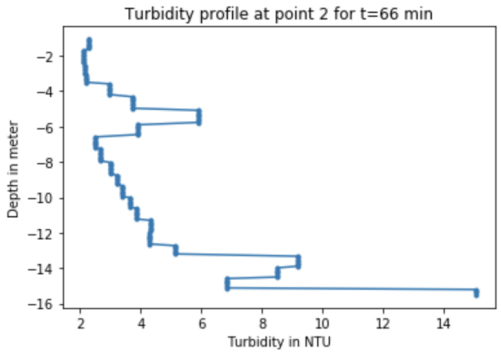

Figure 267: Location 2 at 66 minutes after the start of dredging with the Tiamat. This is the turbidity depth profile of 20-10-2022.

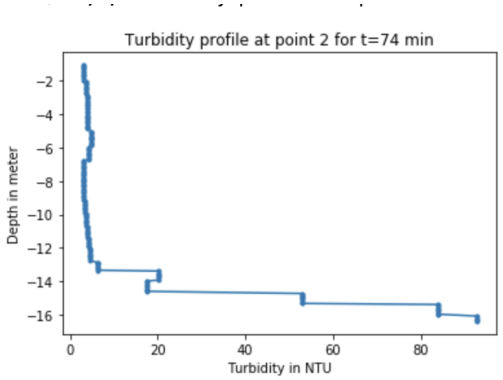

Figure 268: Location 2 at 74 minutes after the start of dredging with the Tiamat. This is the turbidity depth profile of 20-10-2022.

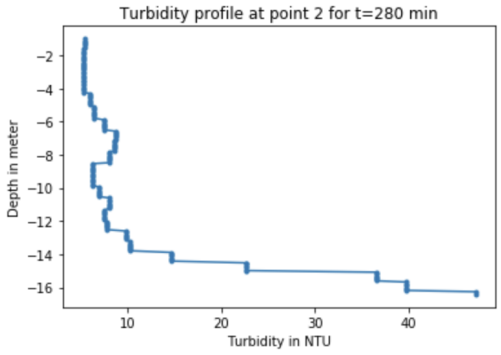

Figure 269: Location 2 at 80 minutes after the start of dredging with the Tiamat. This is the turbidity depth profile of 20-10-2022.

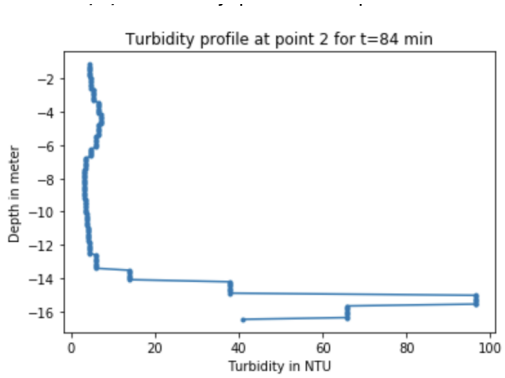

Figure 270: Location 2 at 84 minutes after the start of dredging with the Tiamat. This is the turbidity depth profile of 20-10-2022.

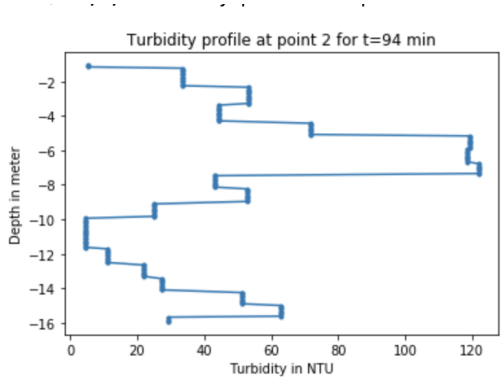

Figure 271: Location 2 at 94 minutes after the start of dredging with the Tiamat. This is the turbidity depth profile of 20-10-2022.

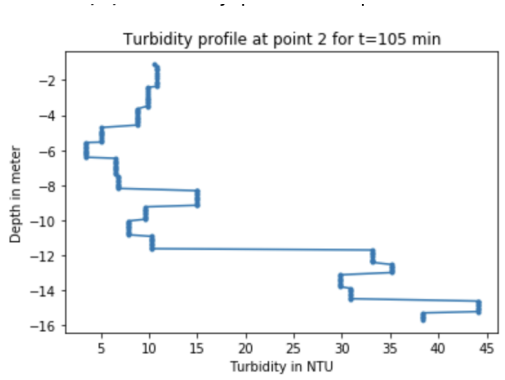

Figure 272: Location 2 at 105 minutes after the start of dredging with the Tiamat. This is the turbidity depth profile of 20-10-2022.

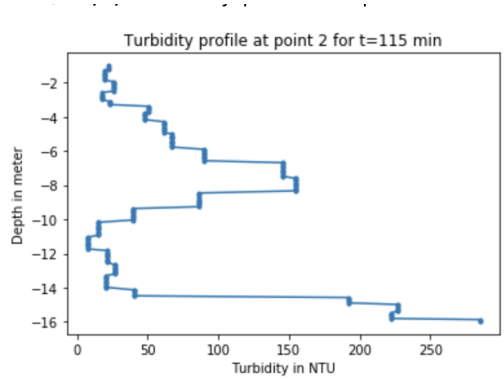

Figure 273: Location 2 at 115 minutes after the start of dredging with the Tiamat. This is the turbidity depth profile of 20-10-2022.

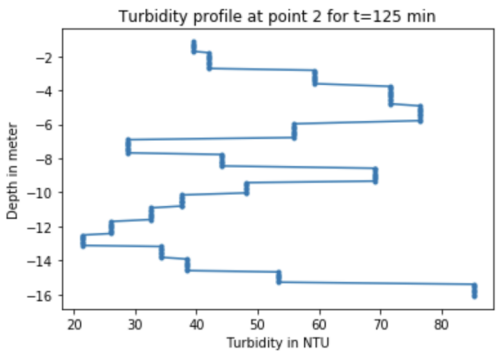

Figure 274: Location 2 at 125 minutes after the start of dredging with the Tiamat. This is the turbidity depth profile of 20-10-2022.

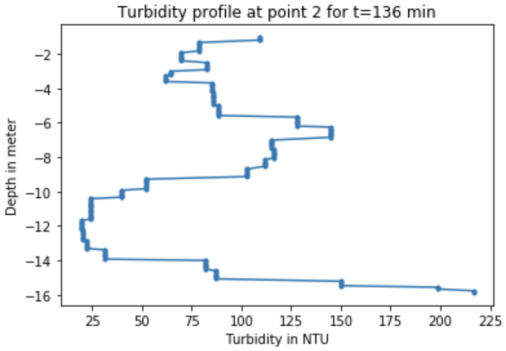

Figure 275: Location 2 at 136 minutes after the start of dredging with the Tiamat. This is the turbidity depth profile of 20-10-2022.

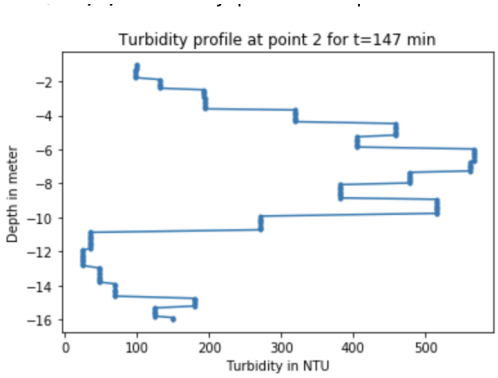

Figure 276: Location 2 at 147 minutes after the start of dredging with the Tiamat. This is the turbidity depth profile of 20-10-2022.

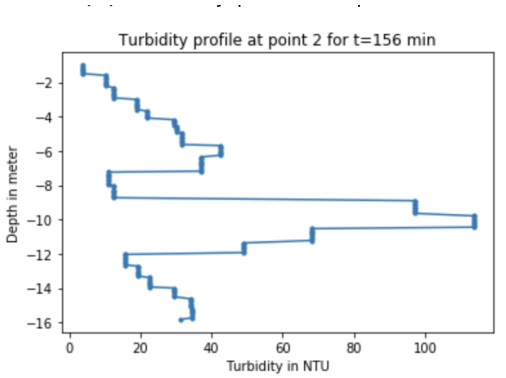

Figure 277: Location 2 at 156 minutes after the start of dredging with the Tiamat. This is the turbidity depth profile of 20-10-2022.

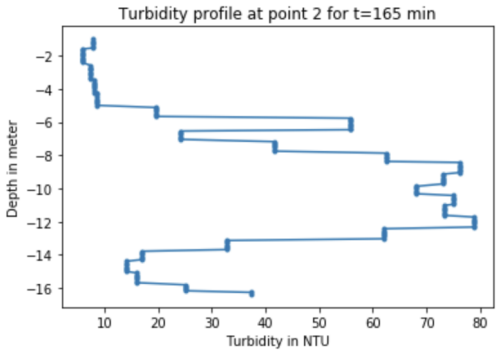

Figure 278: Location 2 at 165 minutes after the start of dredging with the Tiamat. This is the turbidity depth profile of 20-10-2022.

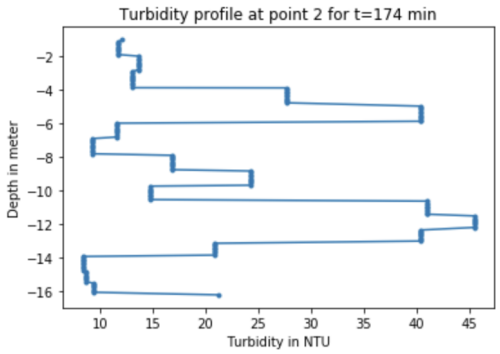

Figure 279: Location 2 at 174 minutes after the start of dredging with the Tiamat. This is the turbidity depth profile of 20-10-2022.

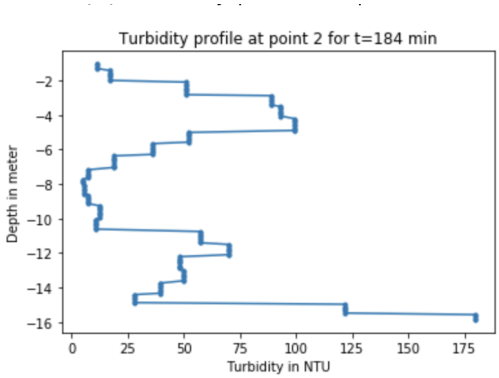

Figure 280: Location 2 at 184 minutes after the start of dredging with the Tiamat. This is the turbidity depth profile of 20-10-2022.

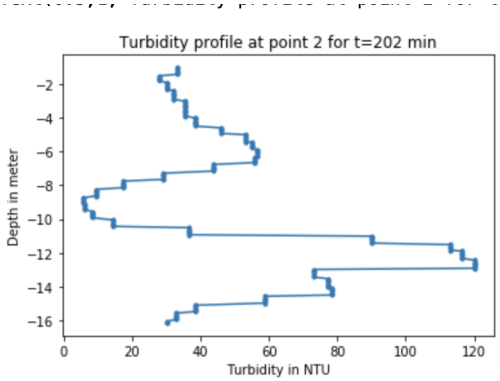

Figure 281: Location 2 at 202 minutes after the start of dredging with the Tiamat. This is the turbidity depth profile of 20-10-2022.

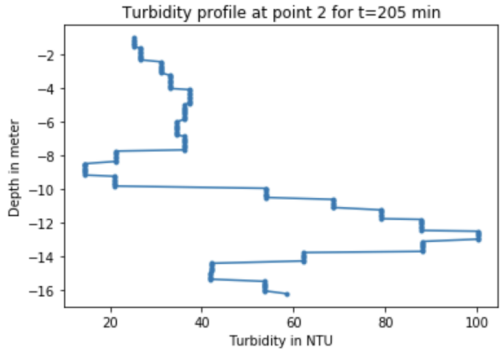

Figure 282: Location 2 at 205 minutes after the start of dredging with the Tiamat. This is the turbidity depth profile of 20-10-2022.

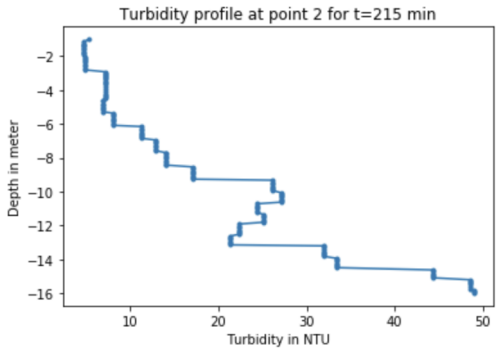

Figure 283: Location 2 at 215 minutes after the start of dredging with the Tiamat. This is the turbidity depth profile of 20-10-2022.

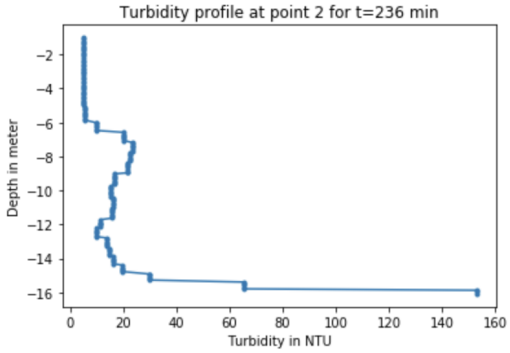

Figure 284: Location 2 at 236 minutes after the start of dredging with the Tiamat. This is the turbidity depth profile of 20-10-2022.

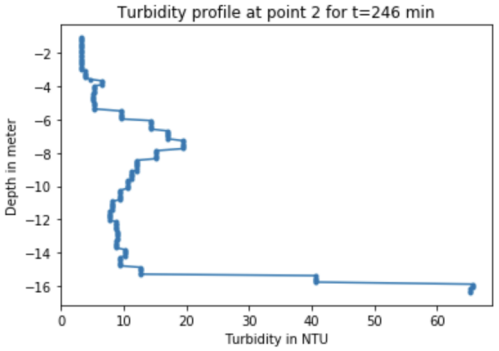

Figure 285: Location 2 at 246 minutes after the start of dredging with the Tiamat. This is the turbidity depth profile of 20-10-2022.

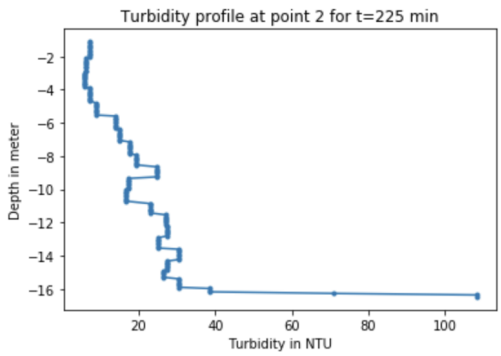

Figure 286: Location 2 at 255 minutes after the start of dredging with the Tiamat. This is the turbidity depth profile of 20-10-2022.

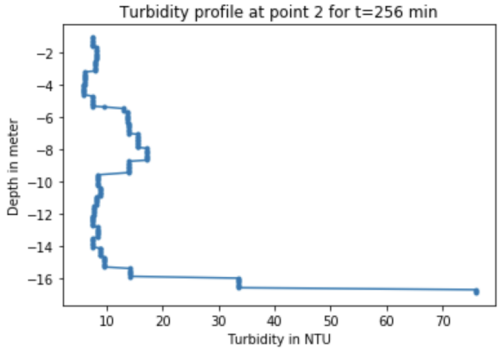

Figure 287: Location 2 at 256 minutes after the start of dredging with the Tiamat. This is the turbidity depth profile of 20-10-2022.

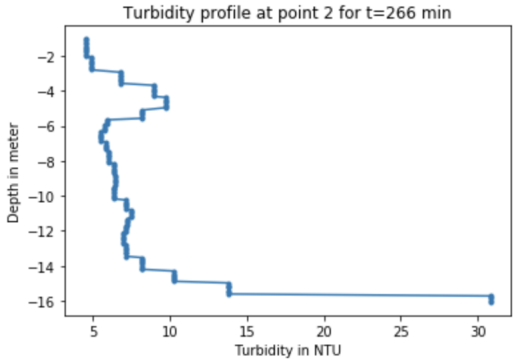

Figure 288: Location 2 at 266 minutes after the start of dredging with the Tiamat. This is the turbidity depth profile of 20-10-2022.

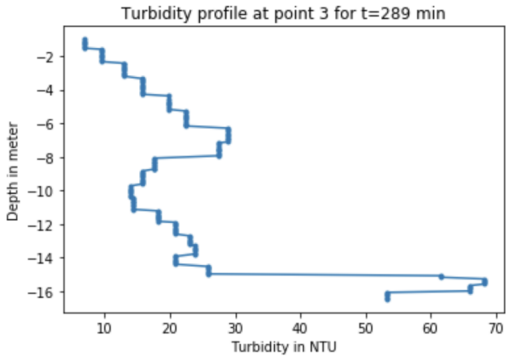

Figure 289: Location 3 at 289 minutes after the start of dredging with the Tiamat. This is the turbidity depth profile of 21-10-2022.

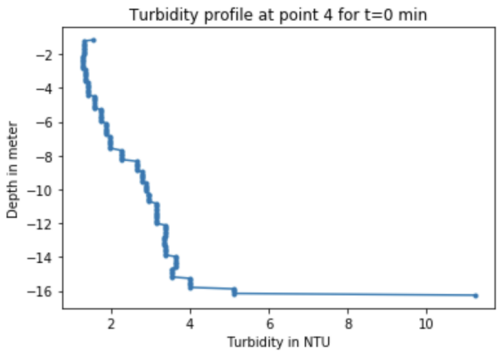

Figure 290: Location 4 at 0 minutes after the start of dredging with the Tiamat. This is the turbidity depth profile of 21-10-2022.

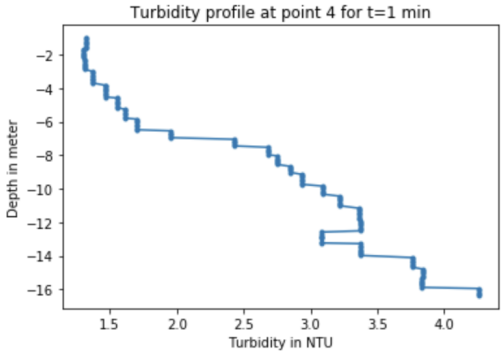

Figure 291: Location 4 at 1 minutes after the start of dredging with the Tiamat. This is the turbidity depth profile of 21-10-2022.

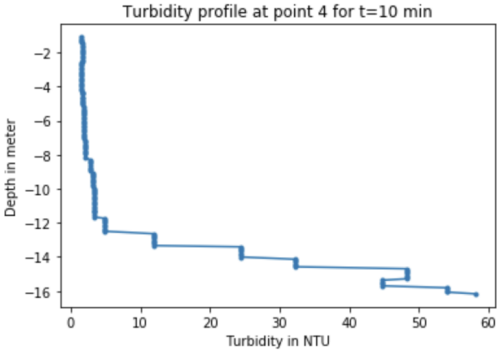

Figure 292: Location 4 at 10 minutes after the start of dredging with the Tiamat. This is the turbidity depth profile of 21-10-2022.

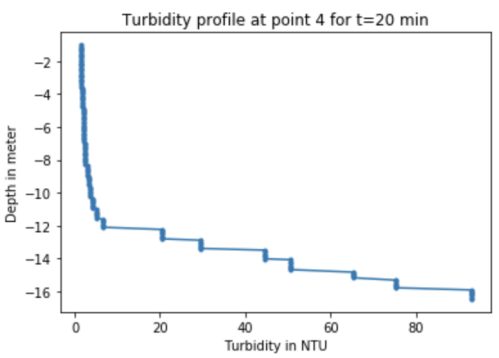

Figure 293: Location 4 at 20 minutes after the start of dredging with the Tiamat. This is the turbidity depth profile of 21-10-2022.

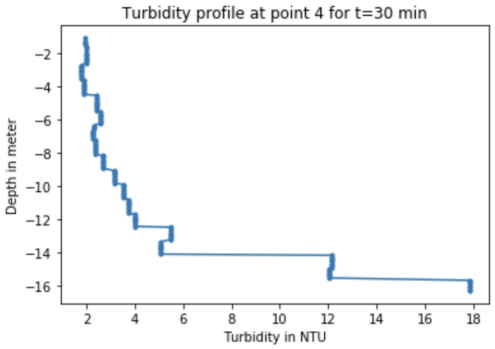

Figure 294: Location 4 at 30 minutes after the start of dredging with the Tiamat. This is the turbidity depth profile of 21-10-2022.

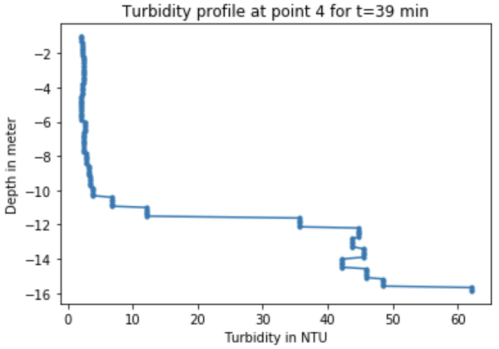

Figure 295: Location 4 at 39 minutes after the start of dredging with the Tiamat. This is the turbidity depth profile of 21-10-2022.

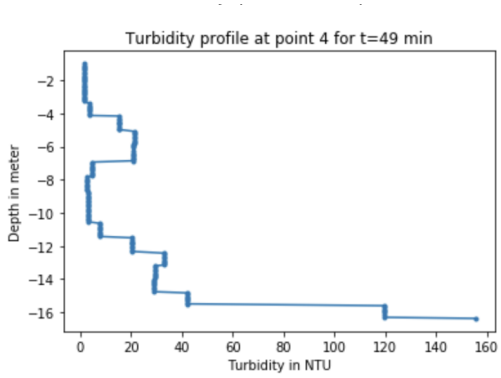

Figure 296: Location 4 at 49 minutes after the start of dredging with the Tiamat. This is the turbidity depth profile of 21-10-2022.

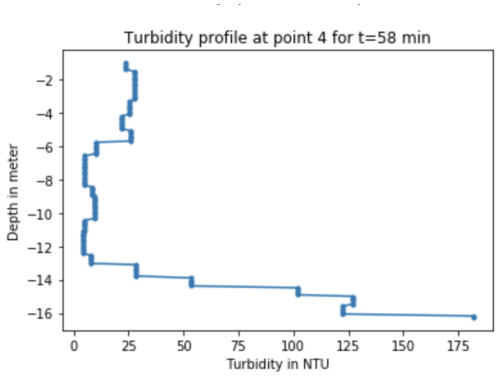

Figure 297: Location 4 at 58 minutes after the start of dredging with the Tiamat. This is the turbidity depth profile of 21-10-2022.

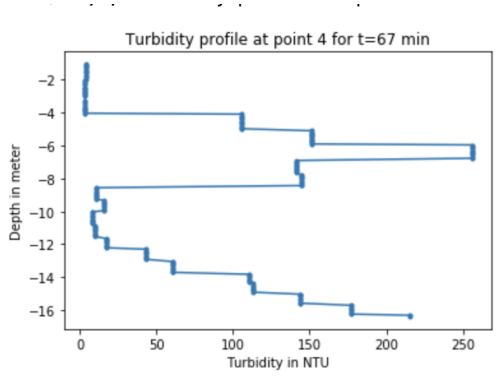

Figure 298: Location 4 at 67 minutes after the start of dredging with the Tiamat. This is the turbidity depth profile of 21-10-2022.

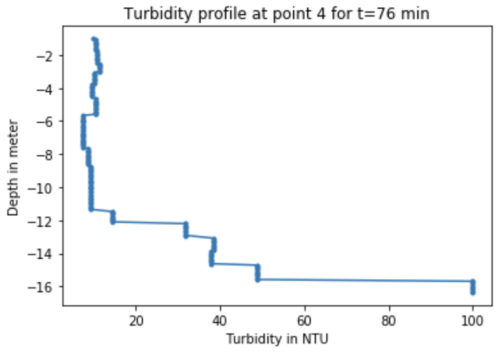

Figure 299: Location 4 at 76 minutes after the start of dredging with the Tiamat. This is the turbidity depth profile of 21-10-2022.

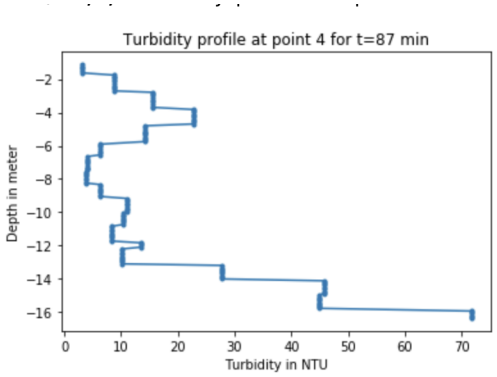

Figure 300: Location 4 at 87 minutes after the start of dredging with the Tiamat. This is the turbidity depth profile of 21-10-2022.

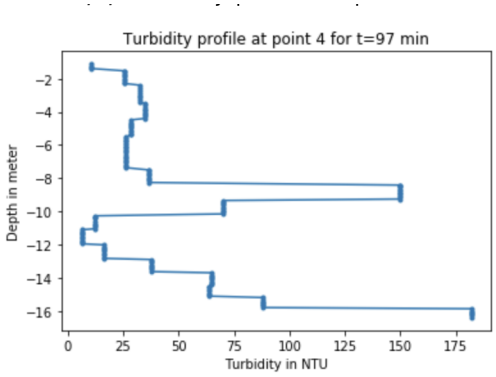

Figure 301: Location 4 at 97 minutes after the start of dredging with the Tiamat. This is the turbidity depth profile of 21-10-2022.

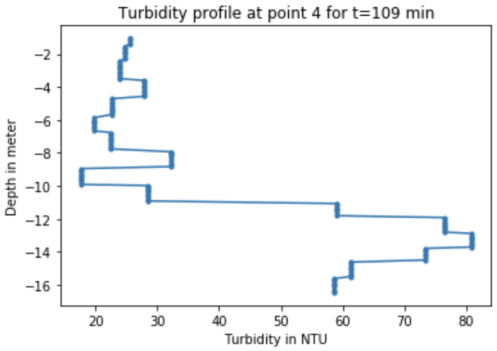

Figure 302: Location 4 at 109 minutes after the start of dredging with the Tiamat. This is the turbidity depth profile of 21-10-2022.

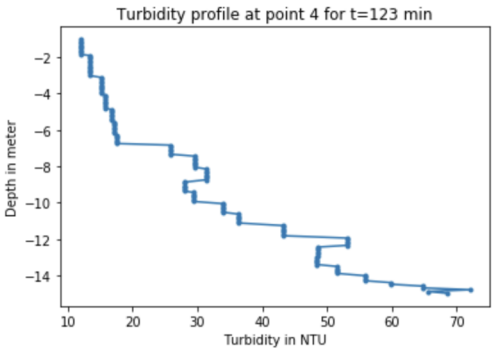

Figure 303: Location 4 at 123 minutes after the start of dredging with the Tiamat. This is the turbidity depth profile of 21-10-2022.

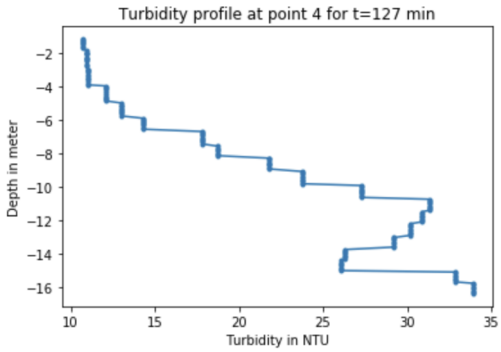

Figure 304: Location 4 at 127 minutes after the start of dredging with the Tiamat. This is the turbidity depth profile of 21-10-2022.

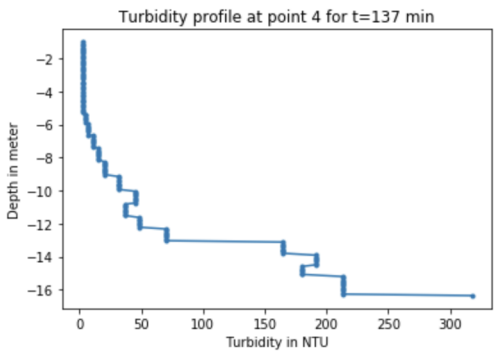

Figure 305: Location 4 at 137 minutes after the start of dredging with the Tiamat. This is the turbidity depth profile of 21-10-2022.

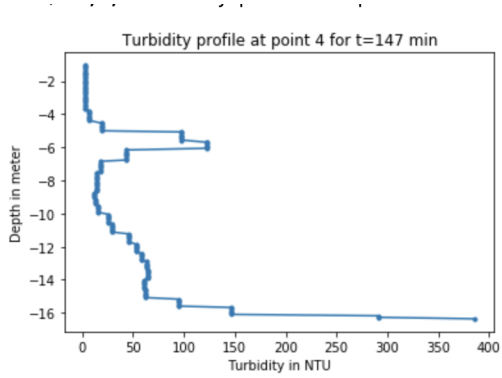

Figure 306: Location 4 at 147 minutes after the start of dredging with the Tiamat. This is the turbidity depth profile of 21-10-2022.

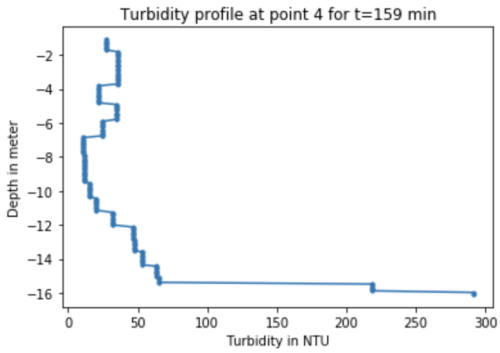

Figure 307: Location 4 at 159 minutes after the start of dredging with the Tiamat. This is the turbidity depth profile of 21-10-2022.

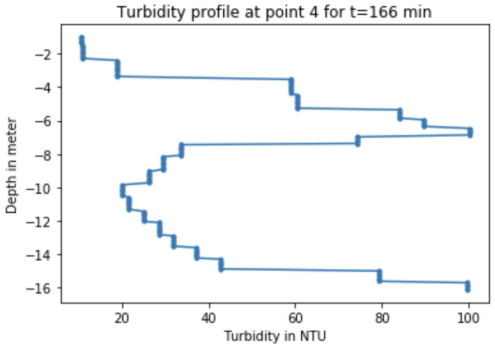

Figure 308: Location 4 at 166 minutes after the start of dredging with the Tiamat. This is the turbidity depth profile of 21-10-2022.

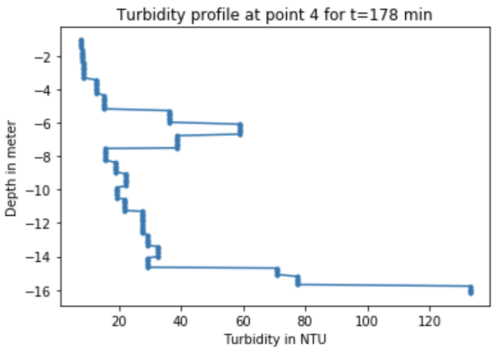

Figure 309: Location 4 at 178 minutes after the start of dredging with the Tiamat. This is the turbidity depth profile of 21-10-2022.

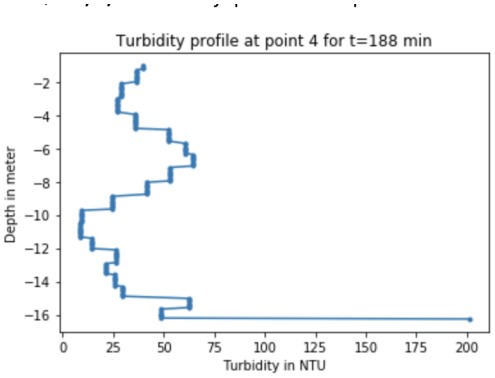

Figure 310: Location 4 at 188 minutes after the start of dredging with the Tiamat. This is the turbidity depth profile of 21-10-2022.

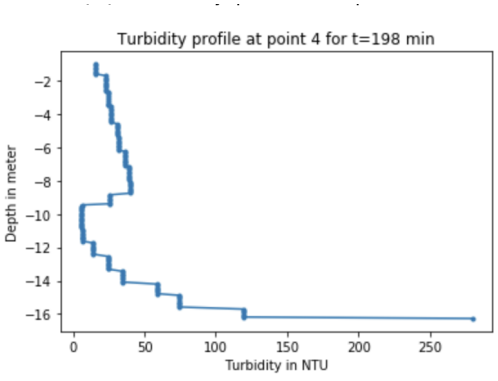

Figure 311: Location 4 at 198 minutes after the start of dredging with the Tiamat. This is the turbidity depth profile of 21-10-2022.

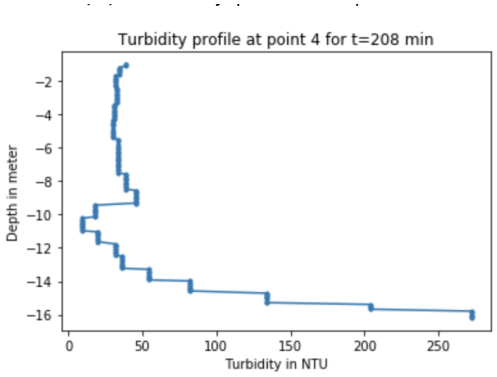

Figure 312: Location 4 at 208 minutes after the start of dredging with the Tiamat. This is the turbidity depth profile of 21-10-2022.

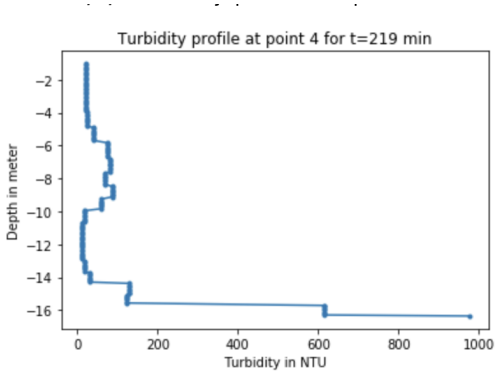

Figure 313: Location 4 at 219 minutes after the start of dredging with the Tiamat. This is the turbidity depth profile of 21-10-2022.

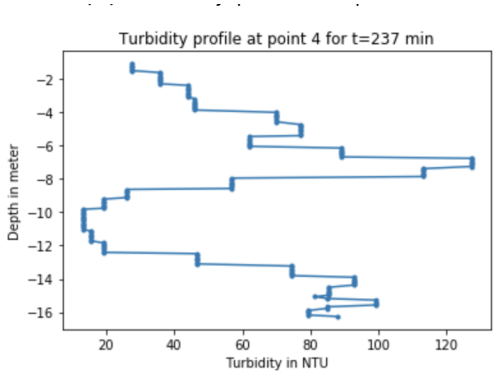

Figure 314: Location 4 at 237 minutes after the start of dredging with the Tiamat. This is the turbidity depth profile of 21-10-2022.

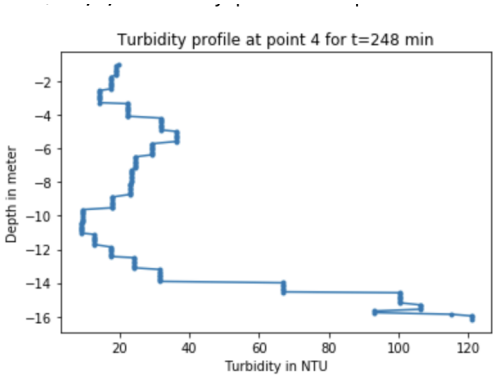

Figure 315: Location 4 at 248 minutes after the start of dredging with the Tiamat. This is the turbidity depth profile of 21-10-2022.

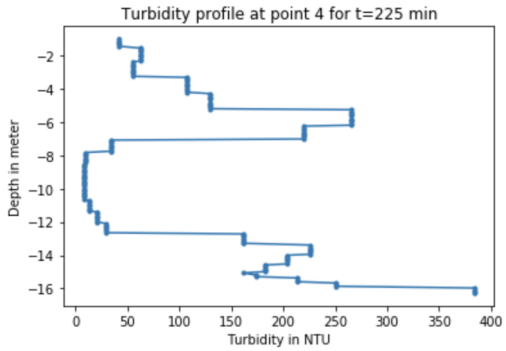

Figure 316: Location 4 at 255 minutes after the start of dredging with the Tiamat. This is the turbidity depth profile of 21-10-2022.

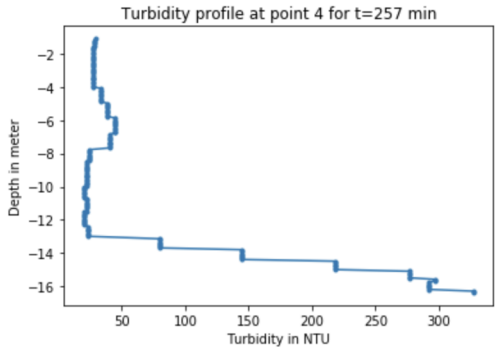

Figure 317: Location 4 at 257 minutes after the start of dredging with the Tiamat. This is the turbidity depth profile of 21-10-2022.

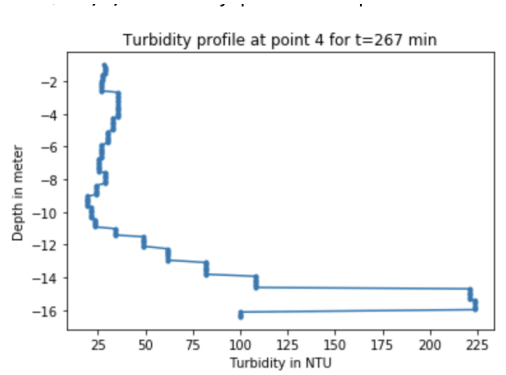

Figure 318: Location 4 at 267 minutes after the start of dredging with the Tiamat. This is the turbidity depth profile of 21-10-2022.

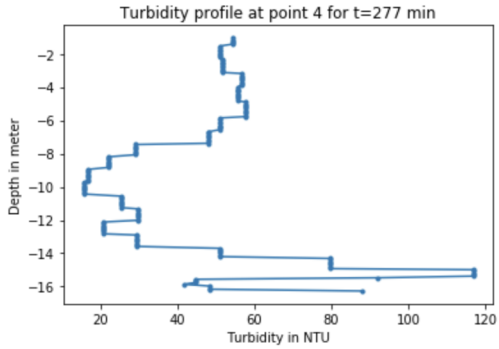

Figure 319: Location 4 at 277 minutes after the start of dredging with the Tiamat. This is the turbidity depth profile of 21-10-2022.

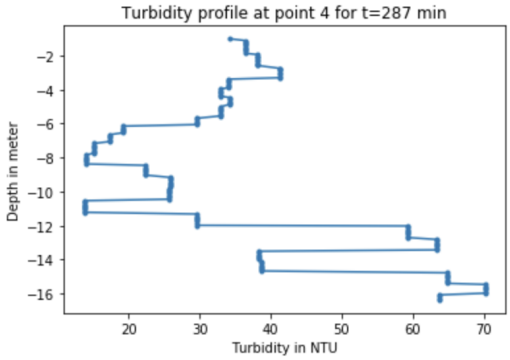

Figure 320: Location 4 at 287 minutes after the start of dredging with the Tiamat. This is the turbidity depth profile of 21-10-2022.

WID

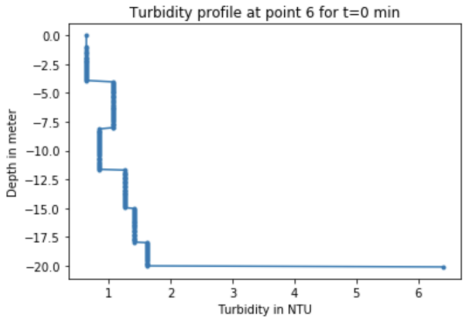

Figure 321: Location 6 at 0 minutes after the start of dredging with the WID. This is the turbidity depth profile of 30-11-2022.

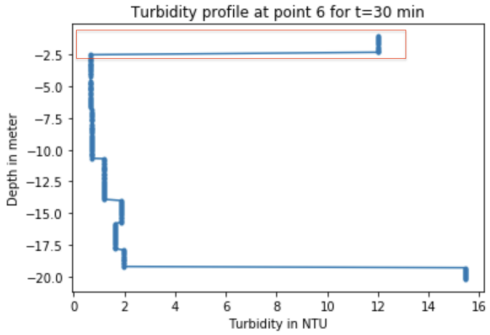

Figure 322: Location 6 at 30 minutes after the start of dredging with the WID. This is the turbidity depth profile of 30-11-2022.

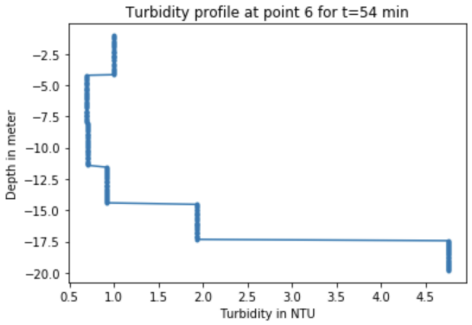

Figure 323: Location 6 at 54 minutes after the start of dredging with the WID. This is the turbidity depth profile of 30-11-2022.

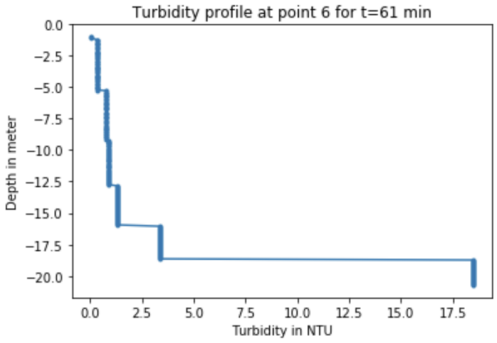

Figure 324: Location 6 at 61 minutes after the start of dredging with the WID. This is the turbidity depth profile of 30-11-2022.

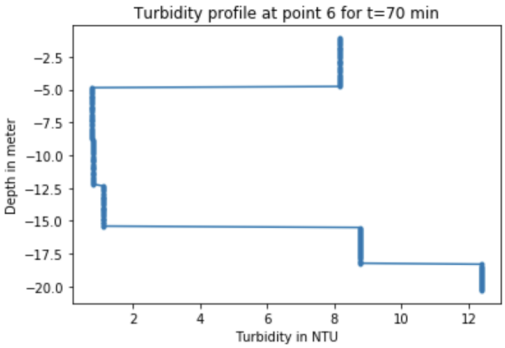

Figure 325: Location 6 at 70 minutes after the start of dredging with the WID. This is the turbidity depth profile of 30-11-2022.

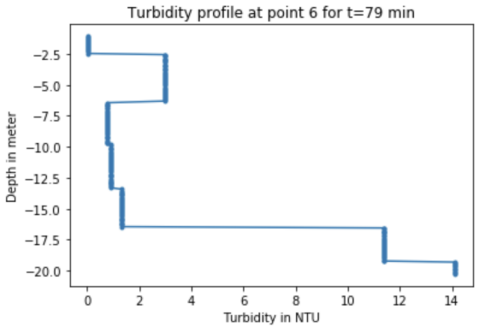

Figure 326: Location 6 at 79 minutes after the start of dredging with the WID. This is the turbidity depth profile of 30-11-2022.

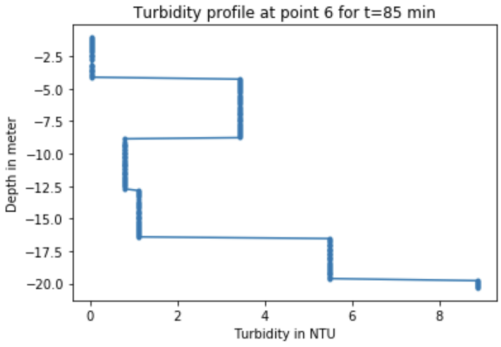

Figure 327: Location 6 at 85 minutes after the start of dredging with the WID. This is the turbidity depth profile of 30-11-2022.

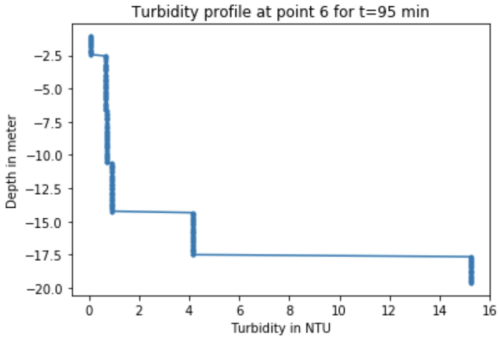

Figure 328: Location 6 at 95 minutes after the start of dredging with the WID. This is the turbidity depth profile of 30-11-2022.

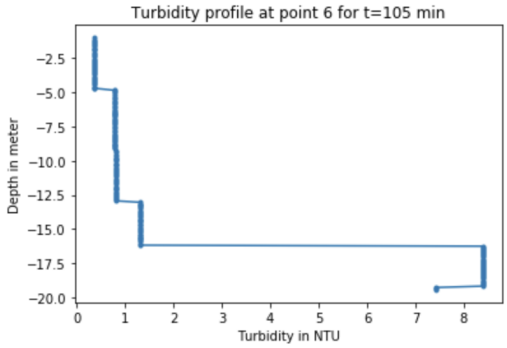

Figure 329: Location 6 at 105 minutes after the start of dredging with the WID. This is the turbidity depth profile of 30-11-2022.

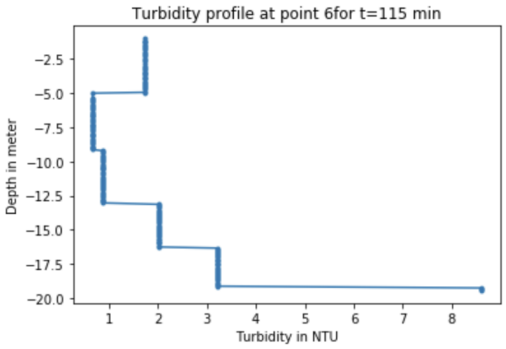

Figure 330: Location 6 at 115 minutes after the start of dredging with the WID. This is the turbidity depth profile of 30-11-2022.

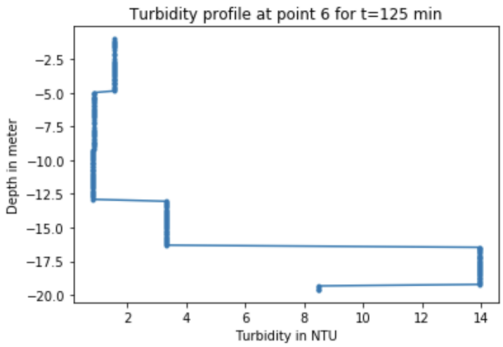

Figure 331: Location 6 at 125 minutes after the start of dredging with the WID. This is the turbidity depth profile of 30-11-2022.

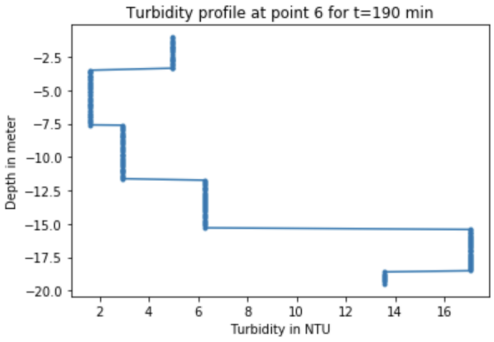

Figure 332: Location 6 at 190 minutes after the start of dredging with the WID. This is the turbidity depth profile of 30-11-2022.

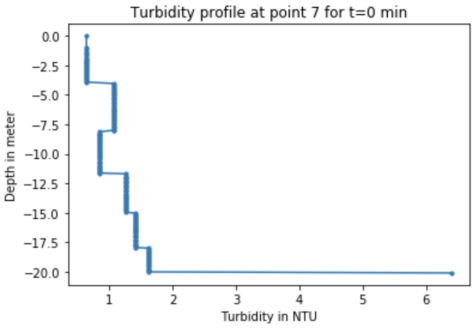

Figure 333: Location 7 at 0 minutes after the start of dredging with the WID. This is the turbidity depth profile of 30-11-2022.

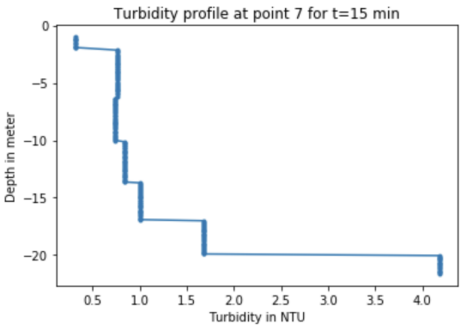

Figure 334: Location 7 at 15 minutes after the start of dredging with the WID. This is the turbidity depth profile of 30-11-2022.

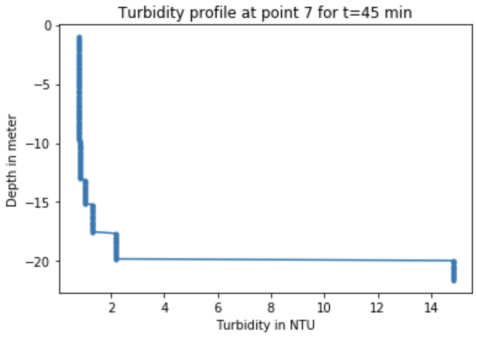

Figure 335: Location 7 at 45 minutes after the start of dredging with the WID. This is the turbidity depth profile of 30-11-2022.

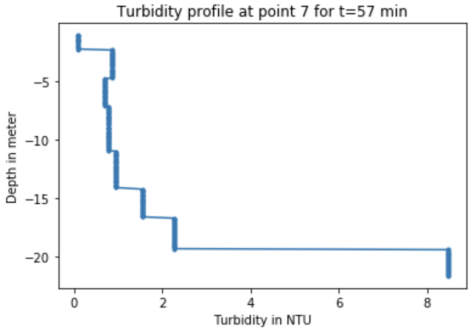

Figure 336: Location 7 at 57 minutes after the start of dredging with the WID. This is the turbidity depth profile of 30-11-2022.

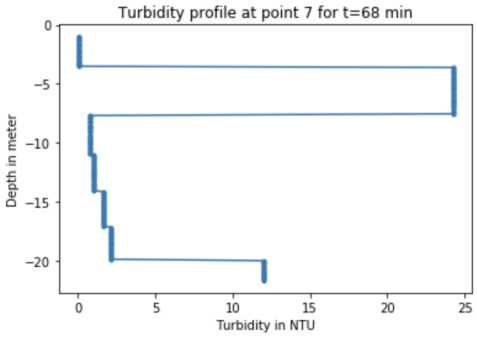

Figure 337: Location 7 at 68 minutes after the start of dredging with the WID. This is the turbidity depth profile of 30-11-2022.

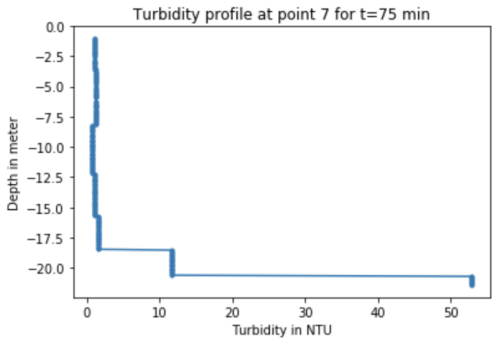

Figure 338: Location 7 at 75 minutes after the start of dredging with the WID. This is the turbidity depth profile of 30-11-2022.

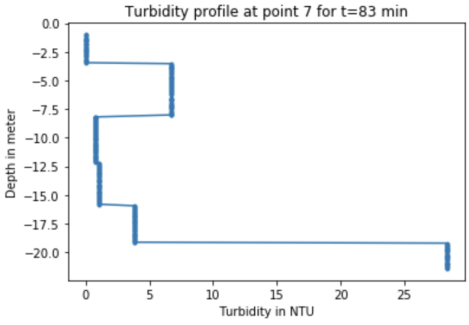

Figure 339: Location 7 at 83 minutes after the start of dredging with the WID. This is the turbidity depth profile of 30-11-2022.

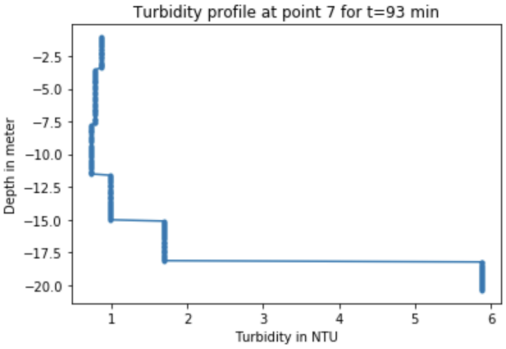

Figure 340: Location 7 at 93 minutes after the start of dredging with the WID. This is the turbidity depth profile of 30-11-2022.

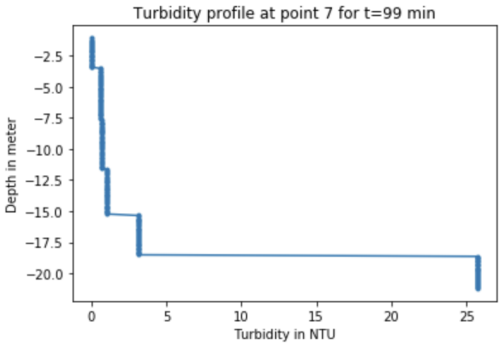

Figure 341: Location 7 at 99 minutes after the start of dredging with the WID. This is the turbidity depth profile of 30-11-2022.

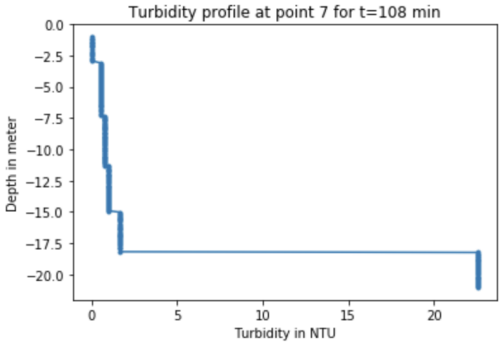

Figure 342: Location 7 at 108 minutes after the start of dredging with the WID. This is the turbidity depth profile of 30-11-2022.

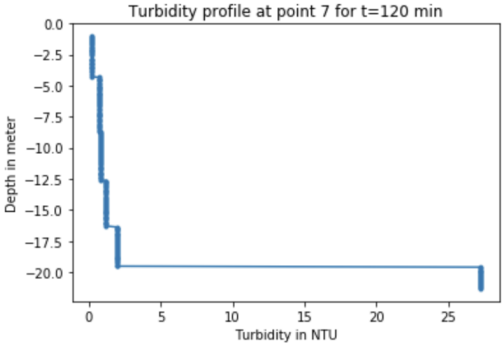

Figure 343: Location 7 at 120 minutes after the start of dredging with the WID. This is the turbidity depth profile of 30-11-2022.

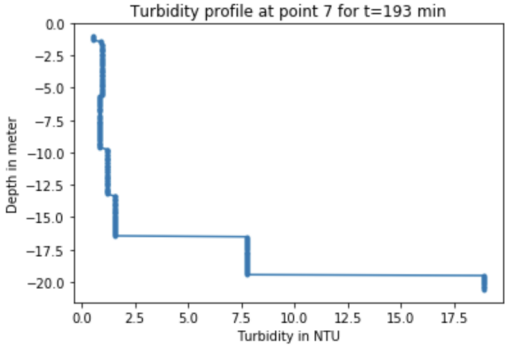

Figure 344: Location 7 at 193 minutes after the start of dredging with the WID. This is the turbidity depth profile of 30-11-2022.

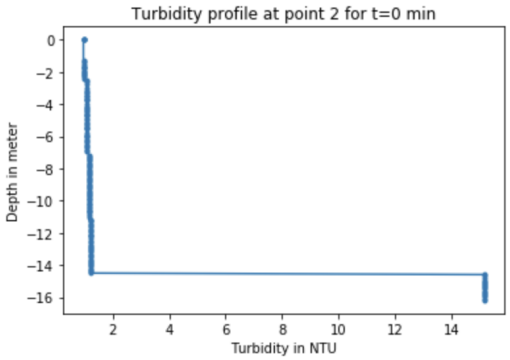

Figure 345: Location 2 at 0 minutes after the start of dredging with the WID. This is the turbidity depth profile of 01-12-2022.

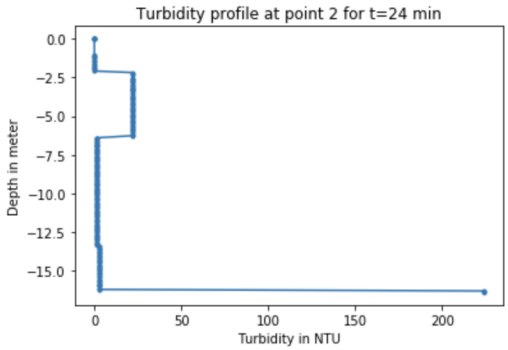

Figure 346: Location 2 at 24 minutes after the start of dredging with the WID. This is the turbidity depth profile of 01-12-2022.

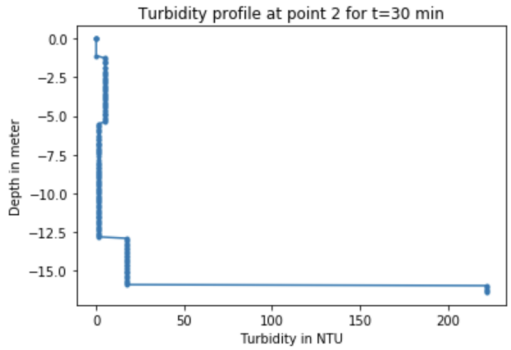

Figure 347: Location 2 at 30 minutes after the start of dredging with the WID. This is the turbidity depth profile of 01-12-2022.

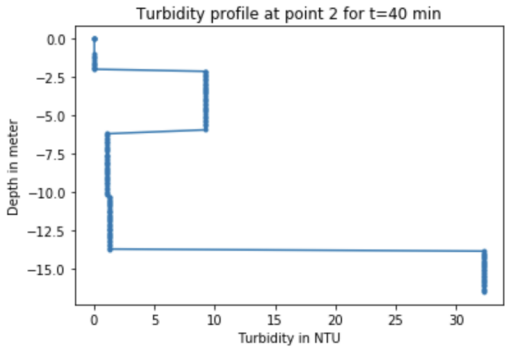

Figure 348: Location 2 at 40 minutes after the start of dredging with the WID. This is the turbidity depth profile of 01-12-2022.

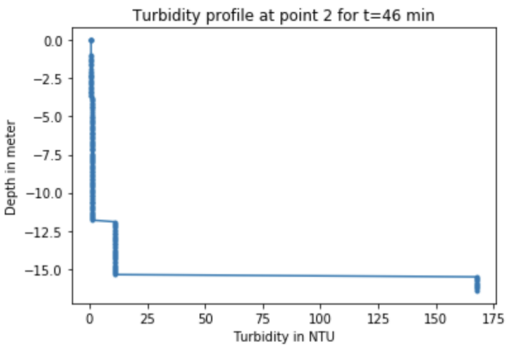

Figure 349: Location 2 at 46 minutes after the start of dredging with the WID. This is the turbidity depth profile of 01-12-2022.

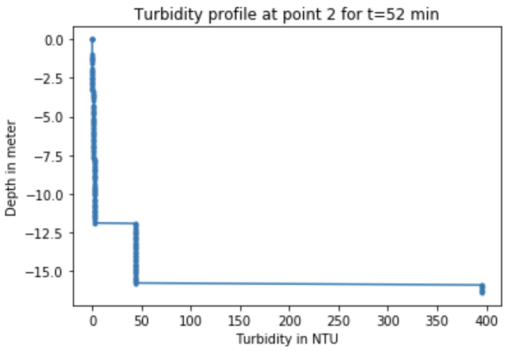

Figure 350: Location 2 at 52 minutes after the start of dredging with the WID. This is the turbidity depth profile of 01-12-2022.

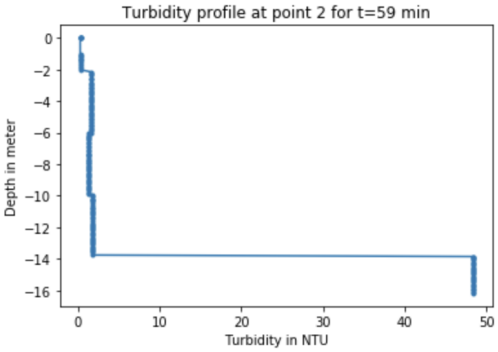

Figure 351: Location 2 at 59 minutes after the start of dredging with the WID. This is the turbidity depth profile of 01-12-2022.

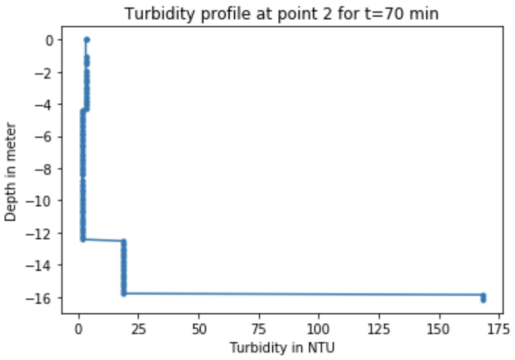

Figure 352: Location 2 at 70 minutes after the start of dredging with the WID. This is the turbidity depth profile of 01-12-2022.

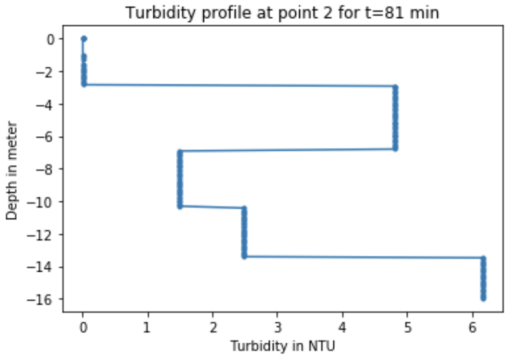

Figure 353: Location 2 at 81 minutes after the start of dredging with the WID. This is the turbidity depth profile of 01-12-2022.

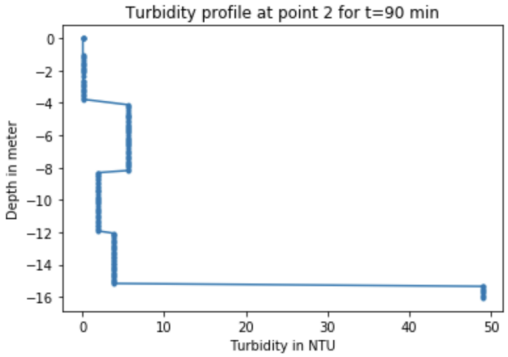

Figure 354: Location 2 at 90 minutes after the start of dredging with the WID. This is the turbidity depth profile of 01-12-2022.

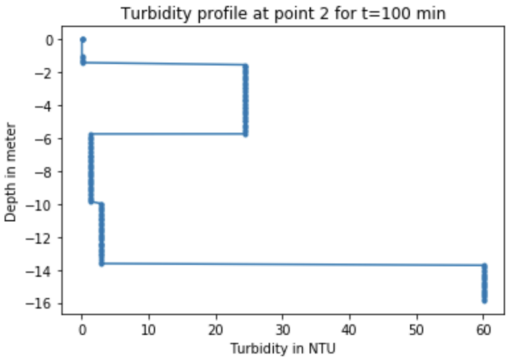

Figure 355: Location 2 at 100 minutes after the start of dredging with the WID. This is the turbidity depth profile of 01-12-2022.

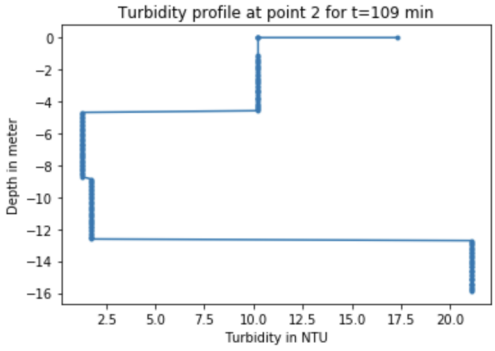

Figure 356: Location 2 at 109 minutes after the start of dredging with the WID. This is the turbidity depth profile of 01-12-2022.

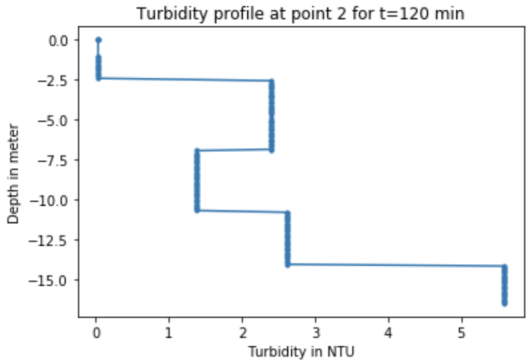

Figure 357: Location 2 at 120 minutes after the start of dredging with the WID. This is the turbidity depth profile of 01-12-2022.

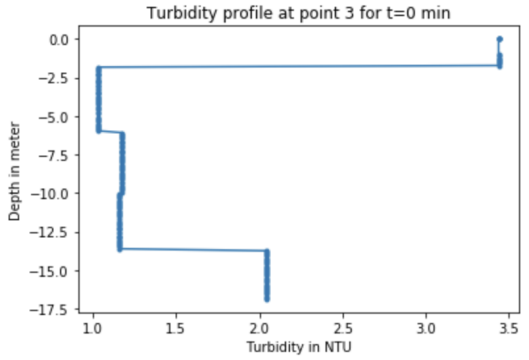

Figure 358: Location 3 at 0 minutes after the start of dredging with the WID. This is the turbidity depth profile of 01-12-2022.

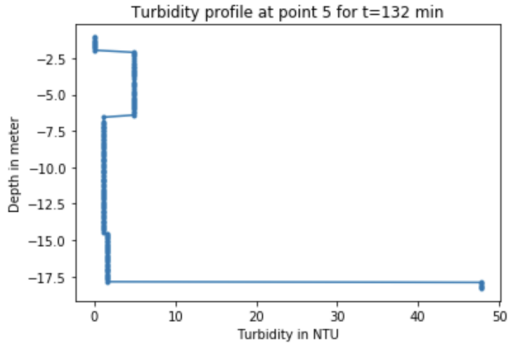

Figure 373: Location 5 at 132 minutes after the start of dredging with the WID. This is the turbidity depth profile of 01-12-2022.

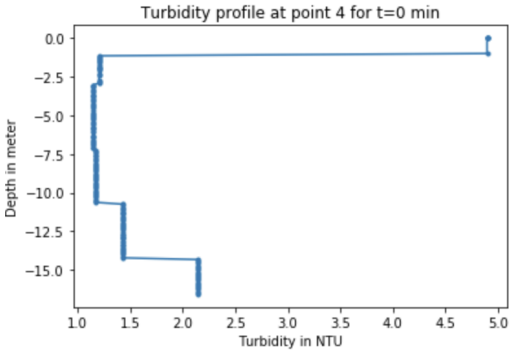

Figure 359: Location 4 at 0 minutes after the start of dredging with the WID. This is the turbidity depth profile of 01-12-2022.

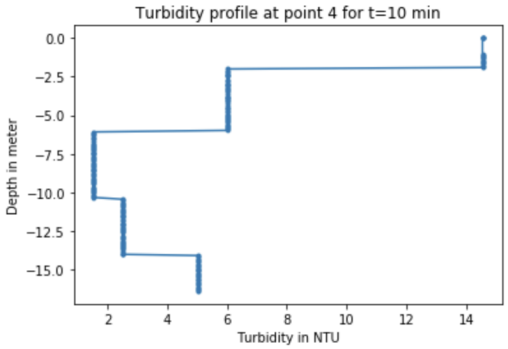

Figure 360: Location 4 at 10 minutes after the start of dredging with the WID. This is the turbidity depth profile of 01-12-2022.

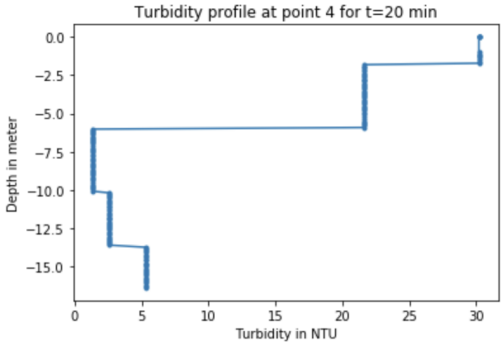

Figure 361: Location 4 at 20 minutes after the start of dredging with the WID. This is the turbidity depth profile of 01-12-2022.

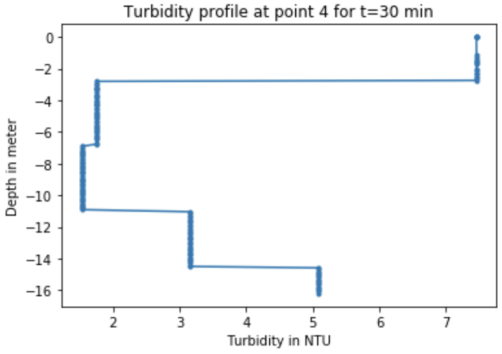

Figure 362: Location 4 at 30 minutes after the start of dredging with the WID. This is the turbidity depth profile of 01-12-2022.

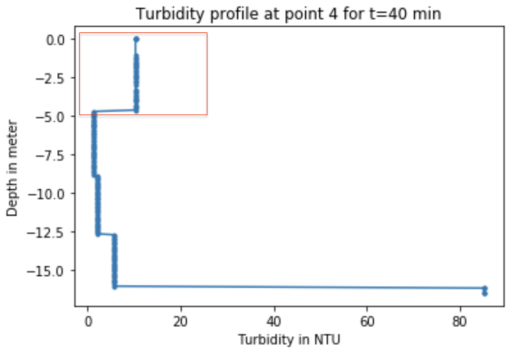

Figure 363: Location 4 at 40 minutes after the start of dredging with the WID. This is the turbidity depth profile of 01-12-2022.

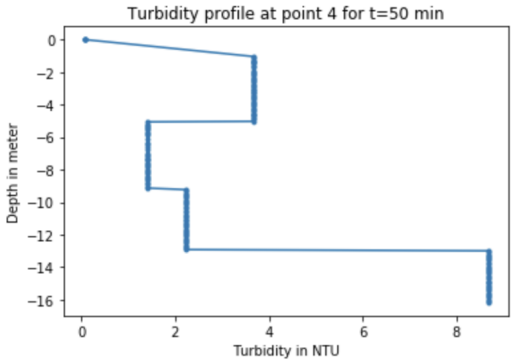

Figure 364: Location 4 at 50 minutes after the start of dredging with the WID. This is the turbidity depth profile of 01-12-2022.

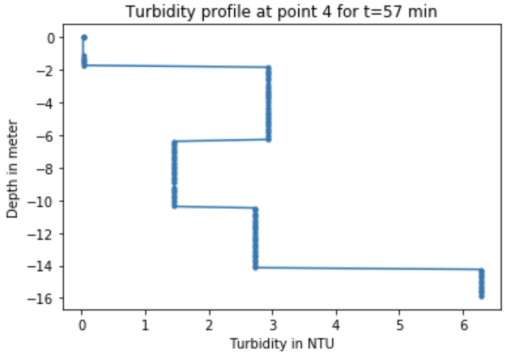

Figure 365: Location 4 at 57 minutes after the start of dredging with the WID. This is the turbidity depth profile of 01-12-2022.

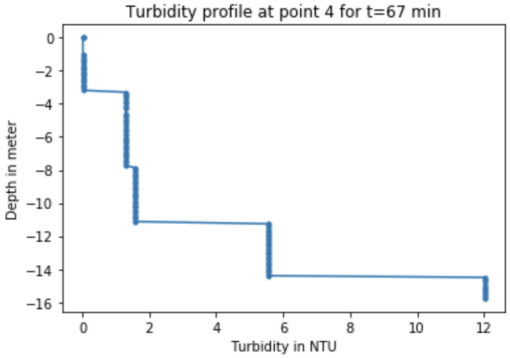

Figure 366: Location 4 at 67 minutes after the start of dredging with the WID. This is the turbidity depth profile of 01-12-2022.

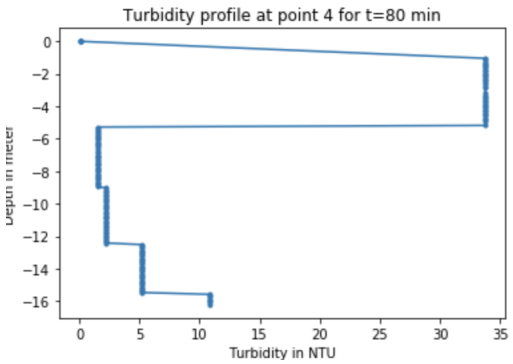

Figure 367: Location 4 at 80 minutes after the start of dredging with the WID. This is the turbidity depth profile of 01-12-2022.

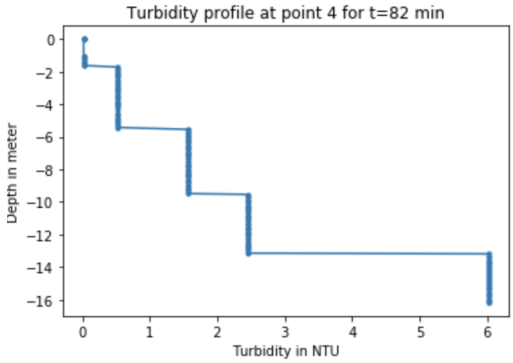

Figure 368: Location 4 at 82 minutes after the start of dredging with the WID. This is the turbidity depth profile of 01-12-2022.

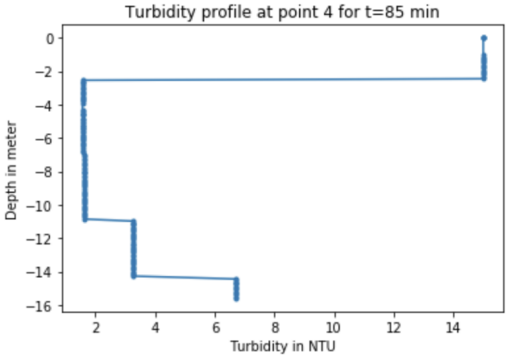

Figure 369: Location 4 at 85 minutes after the start of dredging with the WID. This is the turbidity depth profile of 01-12-2022.

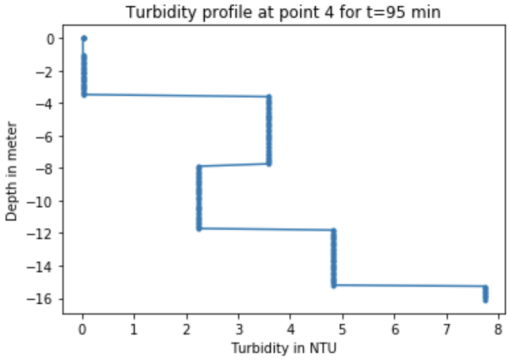

Figure 370: Location 4 at 95 minutes after the start of dredging with the WID. This is the turbidity depth profile of 01-12-2022.

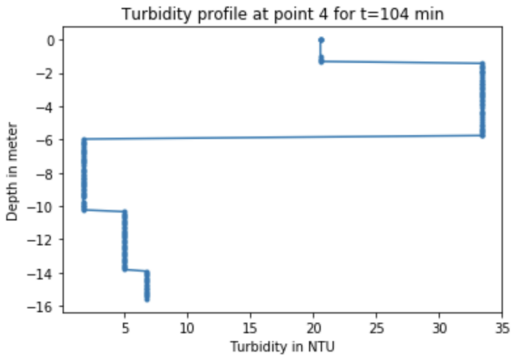

Figure 371: Location 4 at 104 minutes after the start of dredging with the WID. This is the turbidity depth profile of 01-12-2022.

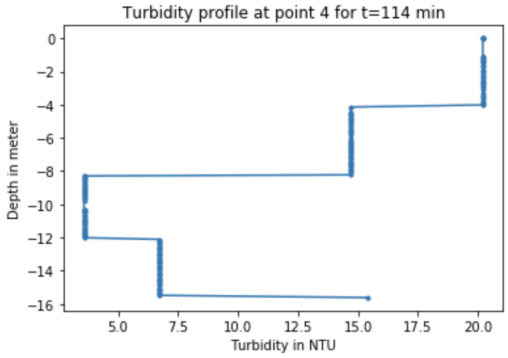

Figure 372: Location 4 at 114 minutes after the start of dredging with the WID. This is the turbidity depth profile of 01-12-2022.

Husky

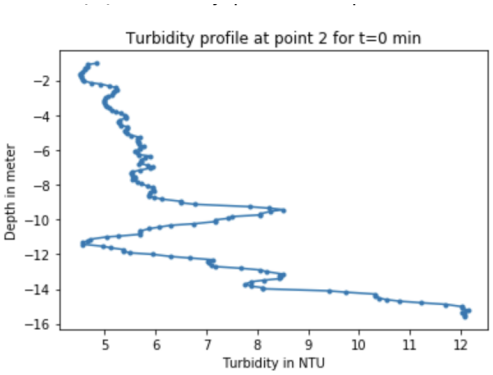

Figure 374: Location 2 at 0 minutes after the start of dredging with the UWP. This is the turbidity depth profile of 02-02-2023.

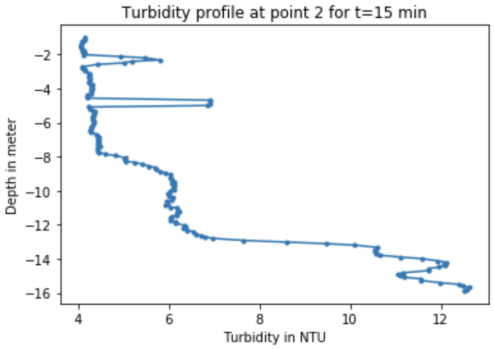

Figure 375: Location 2 at 15 minutes after the start of dredging with the UWP. This is the turbidity depth profile of 02-02-2023.

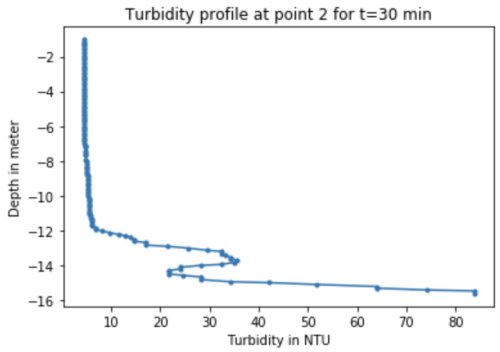

Figure 376: Location 2 at 30 minutes after the start of dredging with the UWP. This is the turbidity depth profile of 02-02-2023.

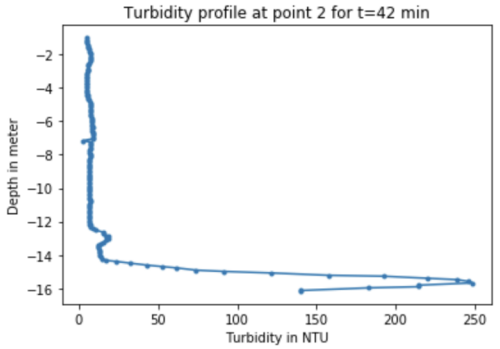

Figure 377: Location 2 at 42 minutes after the start of dredging with the UWP. This is the turbidity depth profile of 02-02-2023.

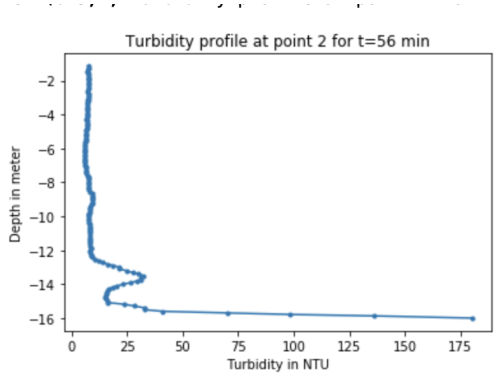

Figure 378: Location 2 at 56 minutes after the start of dredging with the UWP. This is the turbidity depth profile of 02-02-2023.

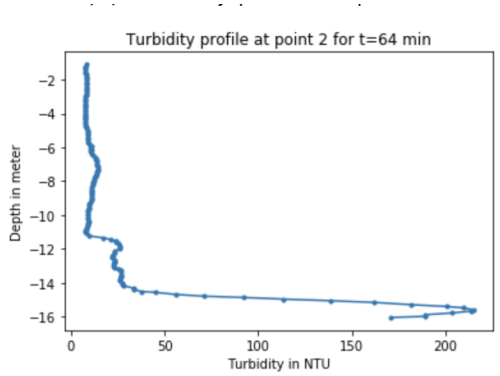

Figure 379: Location 2 at 64 minutes after the start of dredging with the UWP. This is the turbidity depth profile of 02-02-2023.

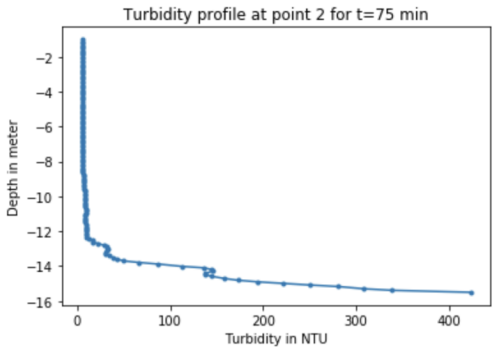

Figure 380: Location 2 at 75 minutes after the start of dredging with the UWP. This is the turbidity depth profile of 02-02-2023.

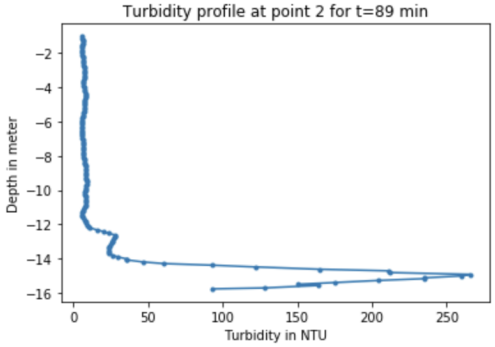

Figure 381: Location 2 at 89 minutes after the start of dredging with the UWP. This is the turbidity depth profile of 02-02-2023.

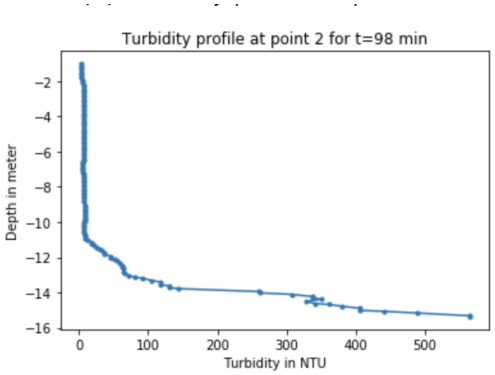

Figure 382: Location 2 at 98 minutes after the start of dredging with the UWP. This is the turbidity depth profile of 02-02-2023.

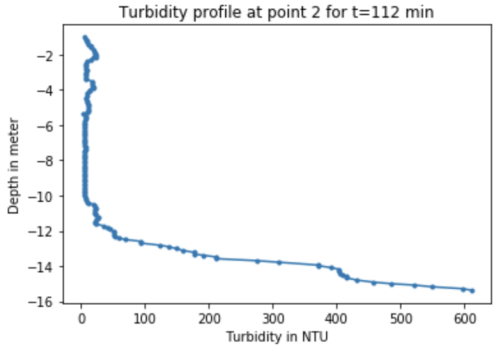

Figure 383: Location 2 at 112 minutes after the start of dredging with the UWP. This is the turbidity depth profile of 02-02-2023.

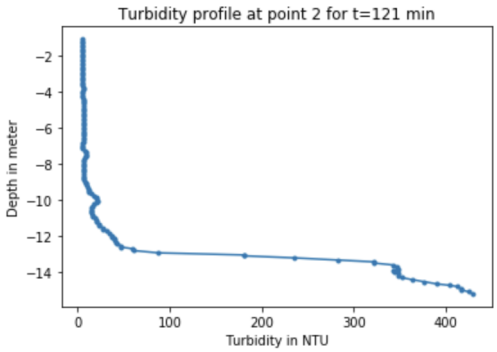

Figure 384: Location 2 at 121 minutes after the start of dredging with the UWP. This is the turbidity depth profile of 02-02-2023.

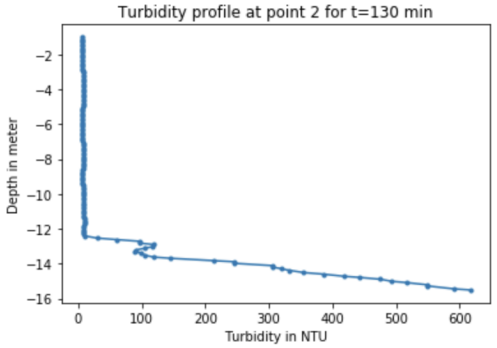

Figure 385: Location 2 at 130 minutes after the start of dredging with the UWP. This is the turbidity depth profile of 02-02-2023.

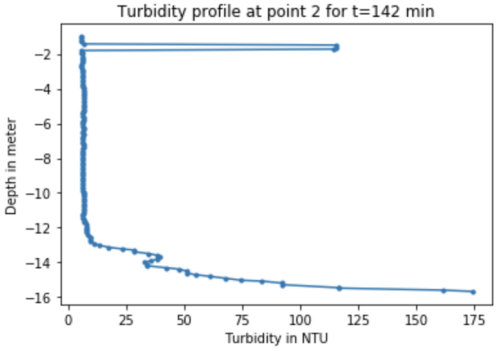

Figure 386: Location 2 at 142 minutes after the start of dredging with the UWP. This is the turbidity depth profile of 02-02-2023.

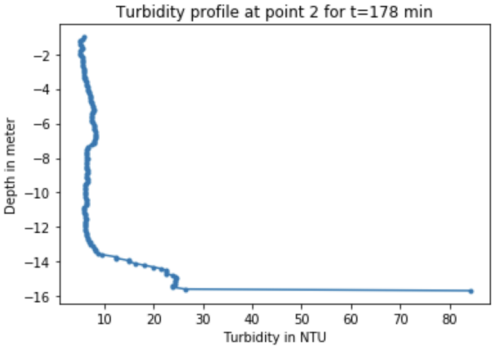

Figure 387: Location 2 at 178 minutes after the start of dredging with the UWP. This is the turbidity depth profile of 02-02-2023.

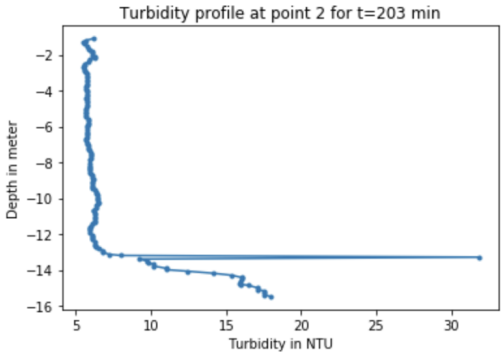

Figure 388: Location 2 at 203 minutes after the start of dredging with the UWP. This is the turbidity depth profile of 02-02-2023.

Appendix VI: Rheotune graphs per point over time

This appendix contains information about various Rheotune points over time. The graphs included in this appendix show the development of the mud layer by indicating the depth of the 1030 g/L line and the depth of the 1200 g/L line. Also the Rheotune profiles over depth are given in this appendix.

Rheotune: Tiamat

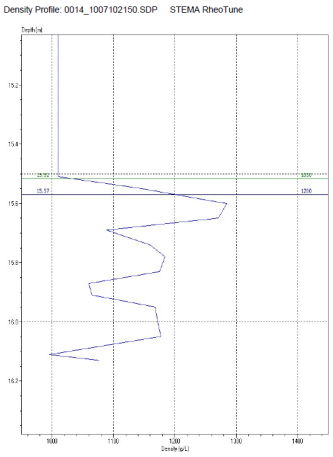

(a) Week 41: Reference measurement

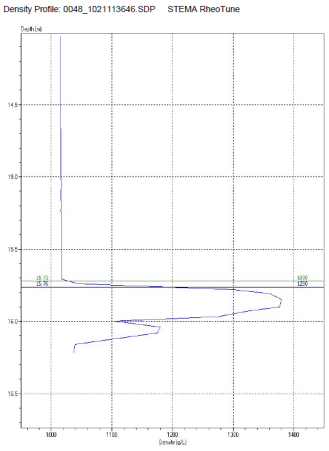

(b) Week 42: Pilot week

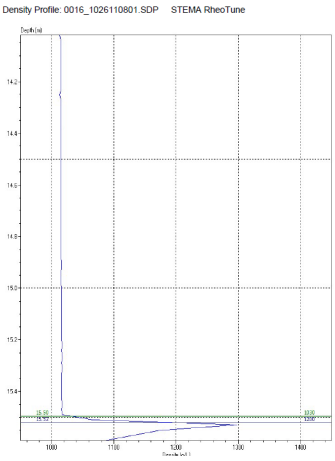

(c) Week 43: Monitorweek 1

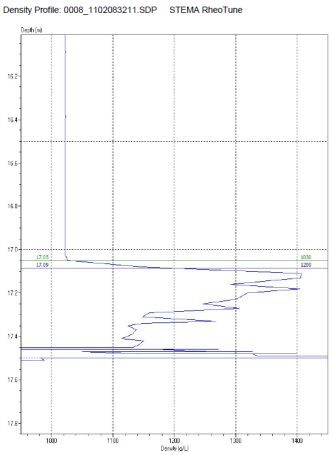

(d) Week 44: Monitorweek 2

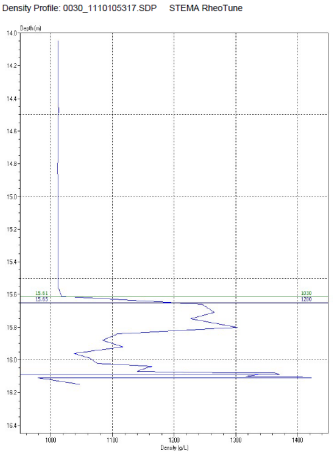

(e) Week 45: Monitorweek 3

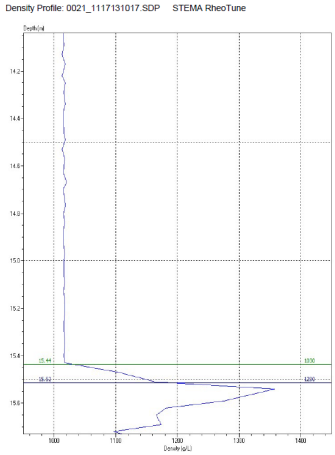

(f) Week 46: Monitorweek 4

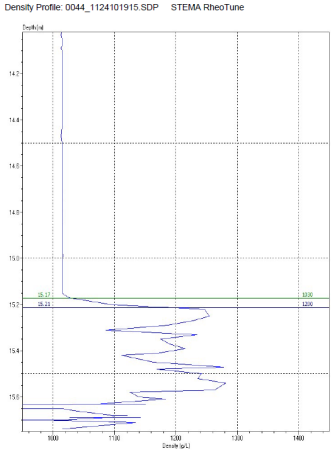

(g) Week 47: Monitorweek 5

Figure 389: Rheotune data of the Koolekade.

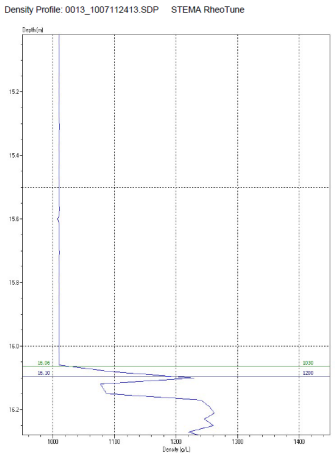

(a) Week 41: Reference measurement

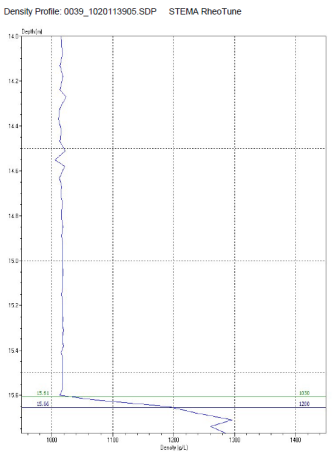

(b) Week 42: Pilot week

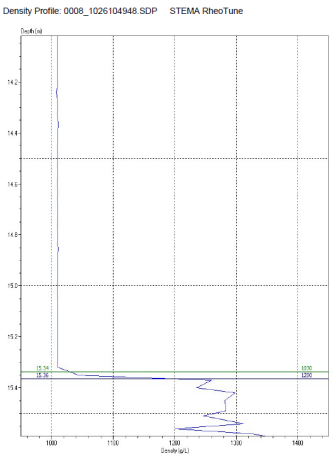

(c) Week 43: Monitorweek 1

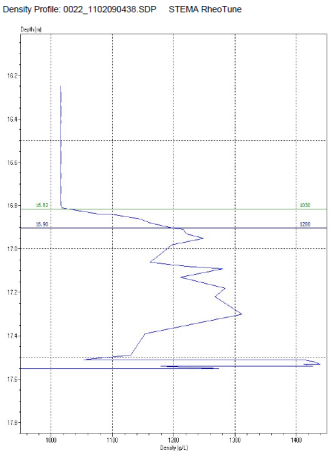

(d) Week 44: Monitorweek 2

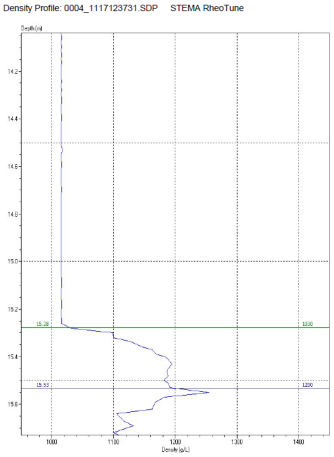

(e) Week 46: Monitorweek 4

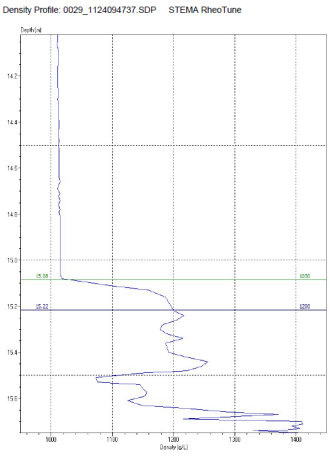

(f) Week 47: Monitorweek 5

Figure 390: Rheotune data of the estuary of the 2nd Petroleumhaven.

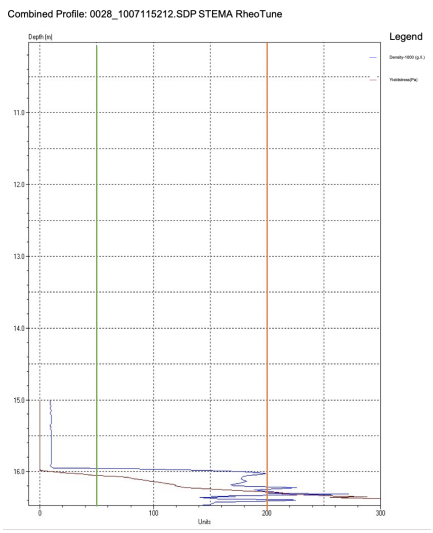

(a) Before dredging with the Tiamat.

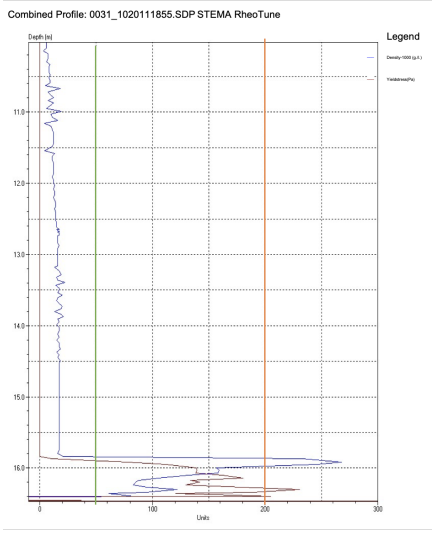

(b) 20-10-2022 after dredging with the Tiamat.

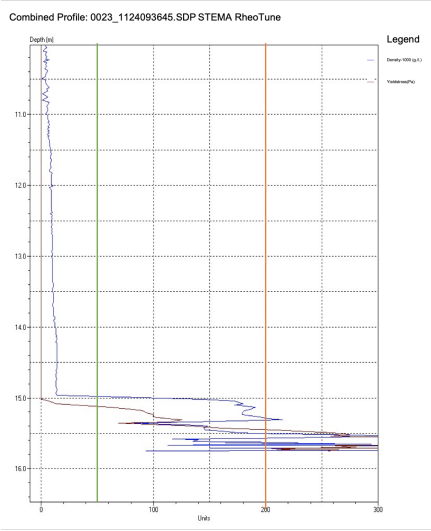

(c) Monitor week 5.

Figure 391: Limits for the density and yield strength for the estuary of the 2nd Petroleumhaven.

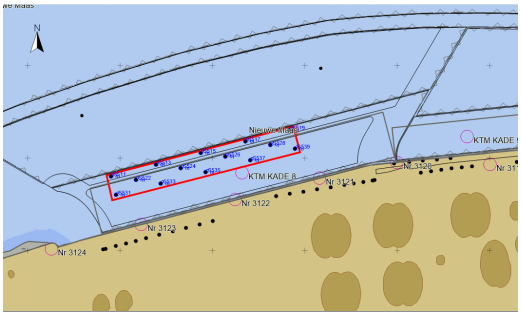

Figure 392: Location of the Rheotune for the Koolekade.

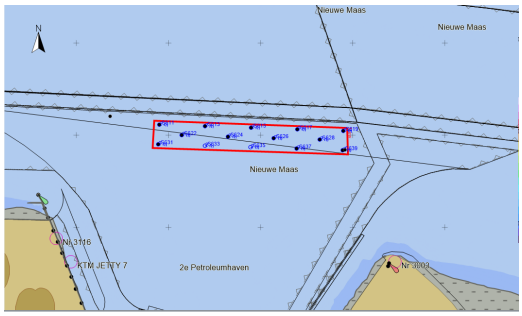

Figure 393: Location of the Rheotune for the estuary of the 2nd Petroleumhaven and the Koolekade.

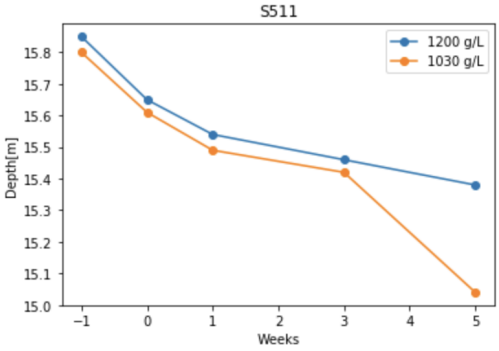

Figure 394: Rheotune data for point S511.

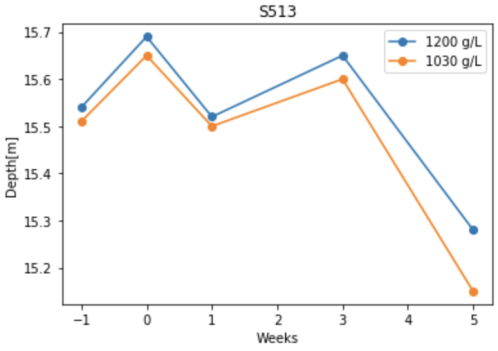

Figure 395: Rheotune data for point S513.

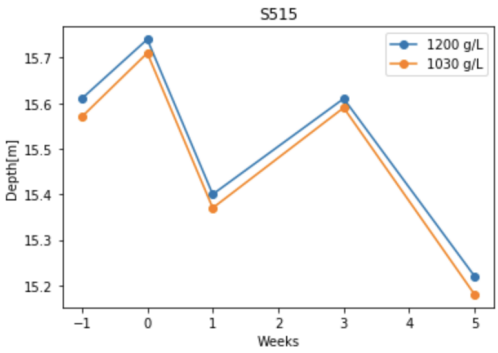

Figure 396: Rheotune data for point S515.

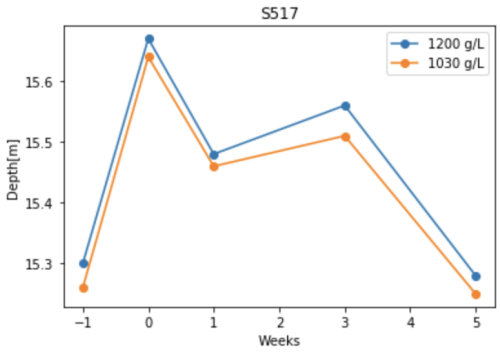

Figure 397: Rheotune data for point S517.

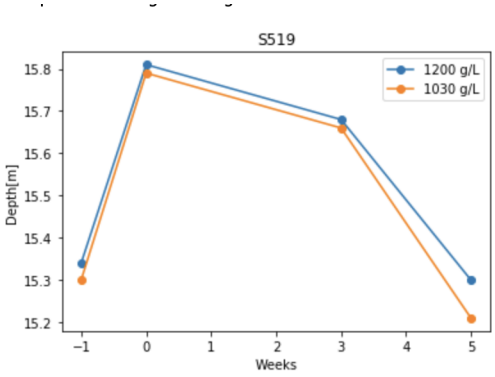

Figure 398: Rheotune data for point S519.

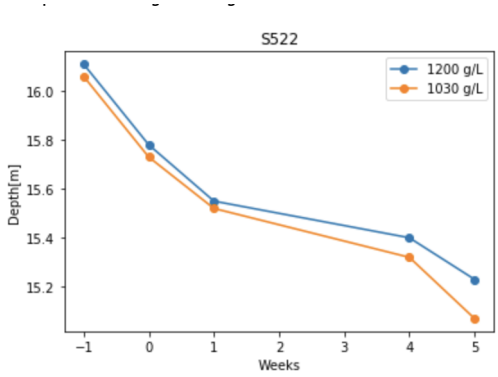

Figure 399: Rheotune data for point S522.

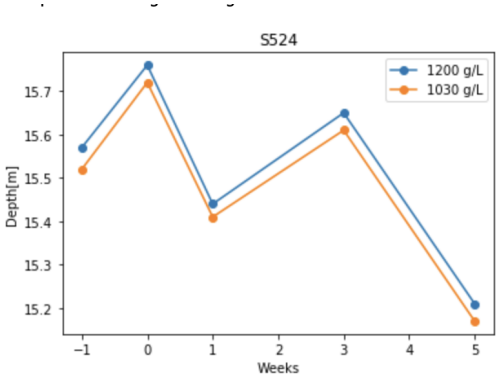

Figure 400: Rheotune data for point S524.

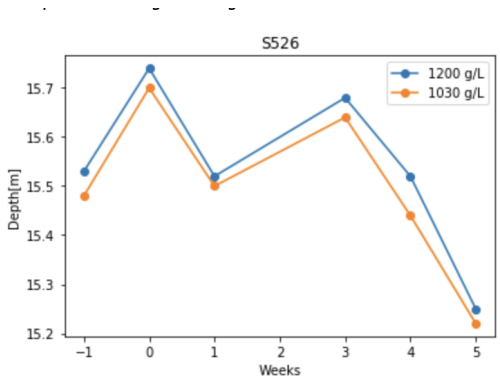

Figure 401: Rheotune data for point S526.

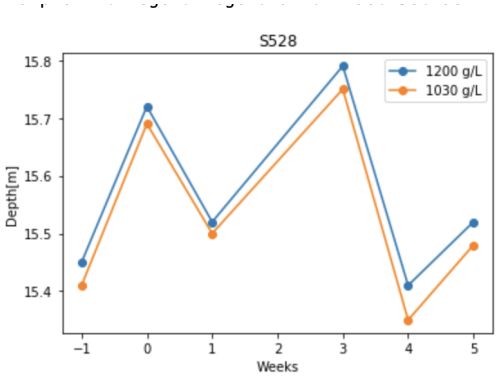

Figure 402: Rheotune data for point S528.

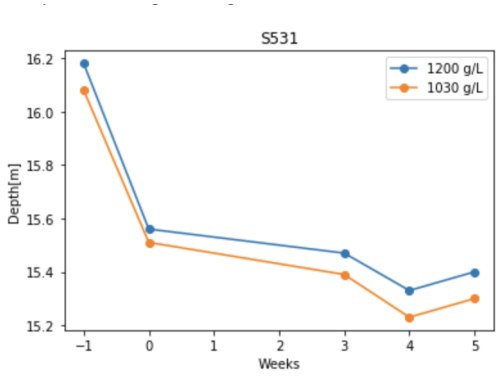

Figure 403: Rheotune data for point S531.

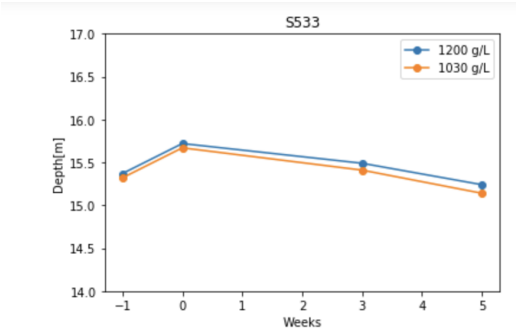

Figure 404: Rheotune data for point S533.

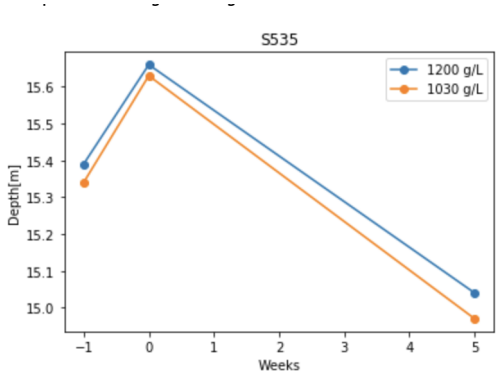

Figure 405: Rheotune data for point S535.

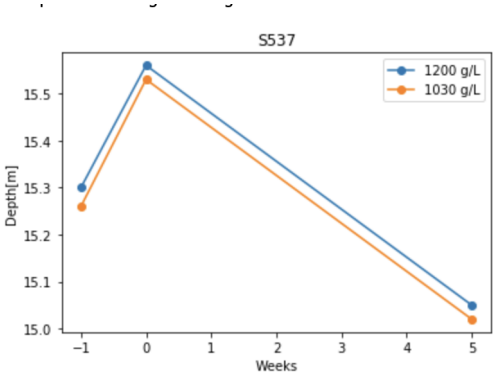

Figure 406: Rheotune data for point S537.

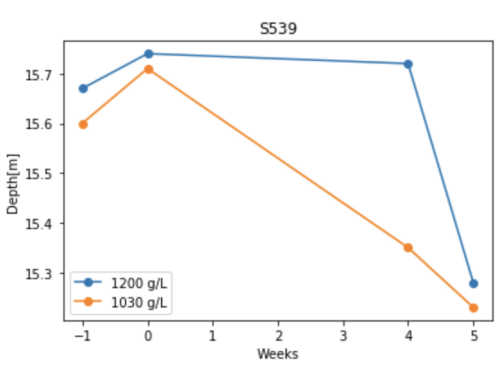

Figure 407: Rheotune data for point S539.

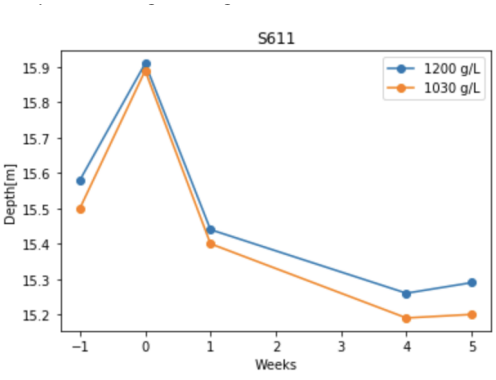

Figure 408: Rheotune data for point S611.

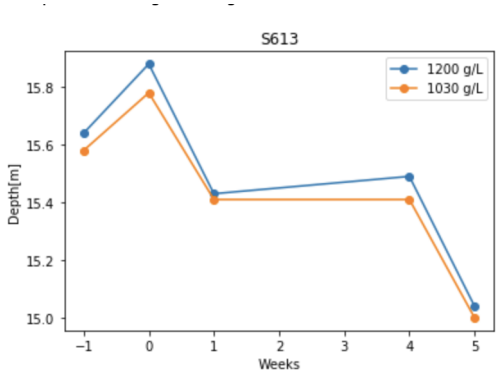

Figure 409: Rheotune data for point S613.

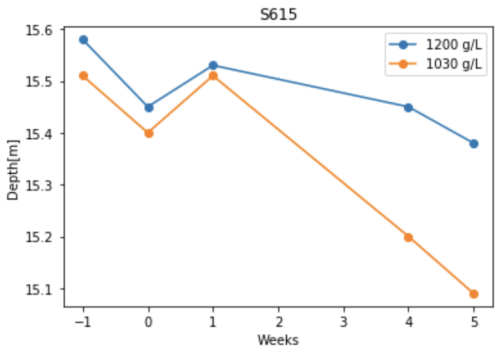

Figure 410: Rheotune data for point S615.

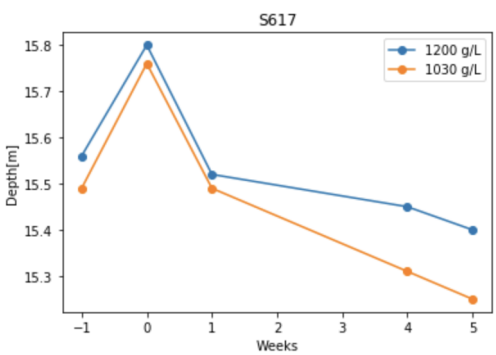

Figure 411: Rheotune data for point S617.

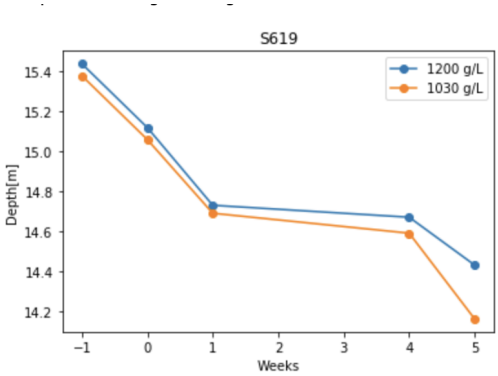

Figure 412: Rheotune data for point S619.

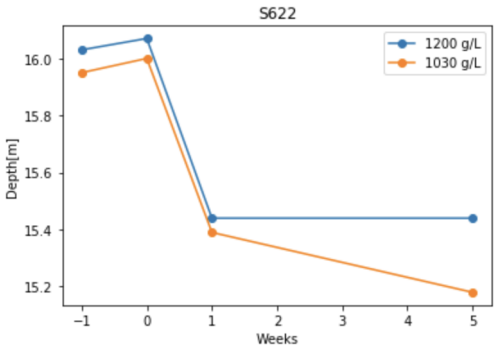

Figure 413: Rheotune data for point S622.

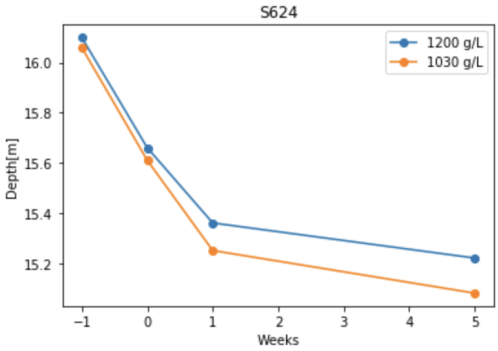

Figure 414: Rheotune data for point S624.

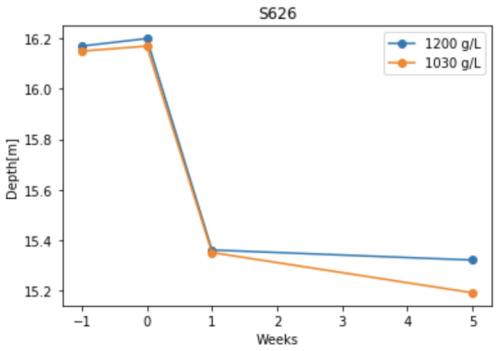

Figure 415: Rheotune data for point S626.

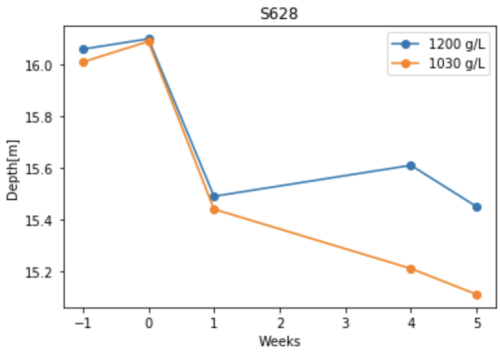

Figure 416: Rheotune data for point S628.

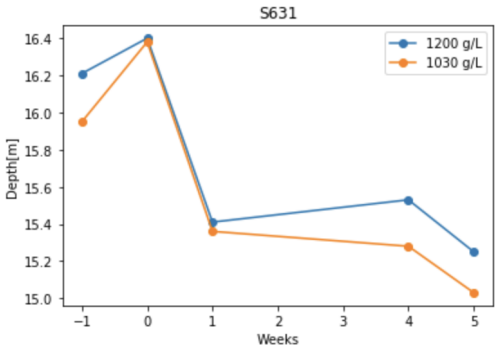

Figure 417: Rheotune data for point S631.

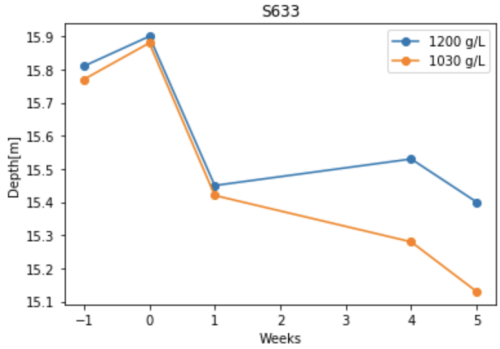

Figure 418: Rheotune data for point S633.

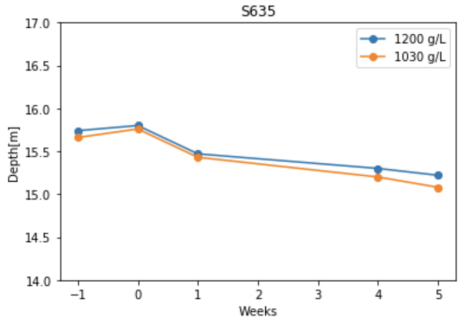

Figure 419: Rheotune data for point S635.

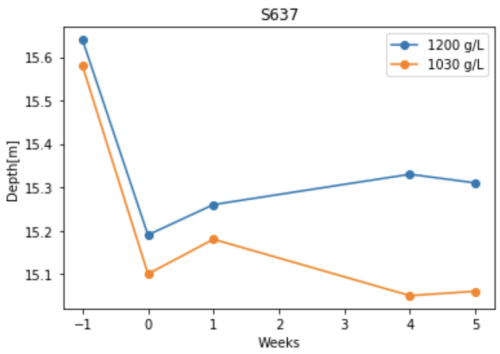

Figure 420: Rheotune data for point S637.

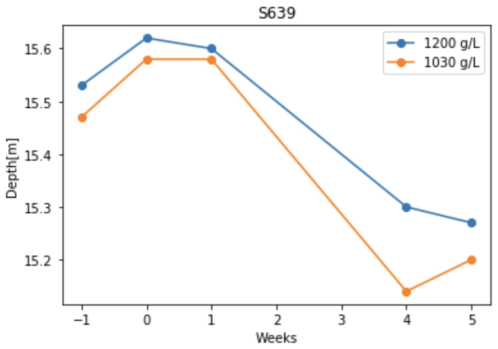

Figure 421: Rheotune data for point S639.

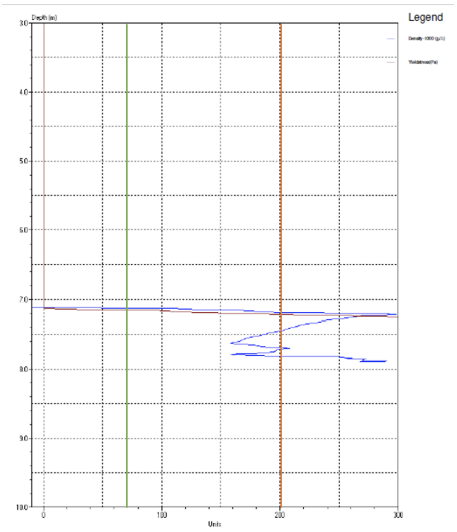

(a) Before dredging

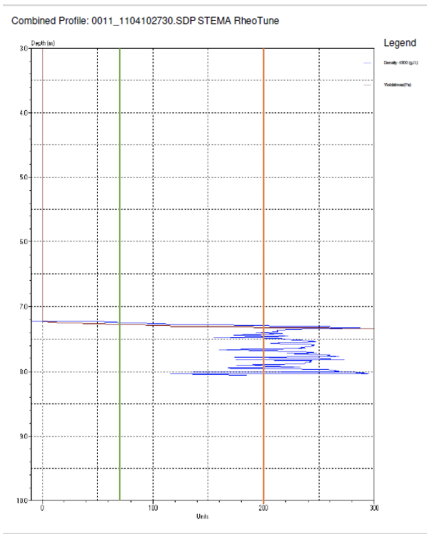

(b) Two days after dredging

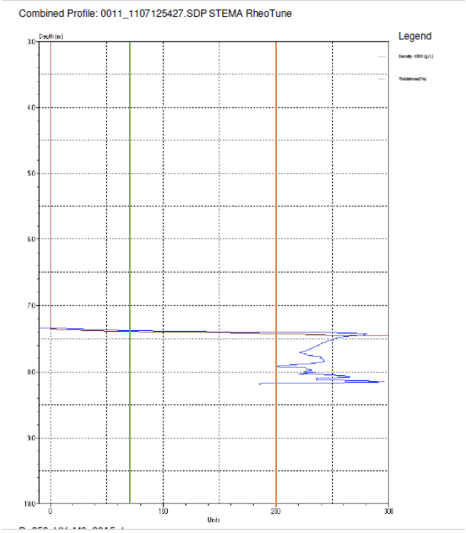

(c) Monitor week 1

Figure 422: Rheotune data Strandhafen.

Silas: Tiamat

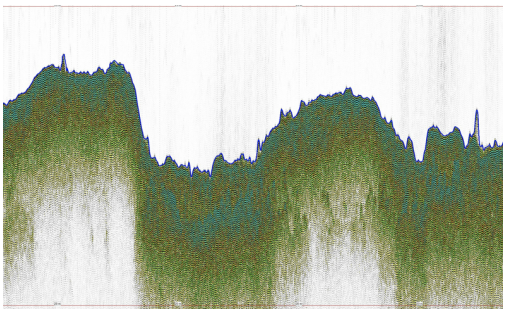

(a) Week 43: Monitorweek 1.

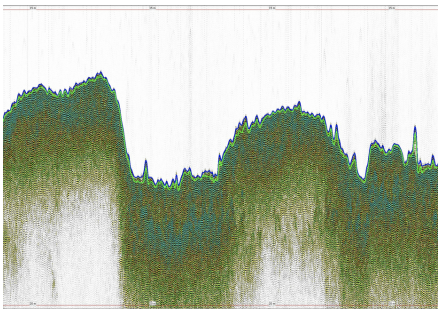

(b) Week 44: Monitorweek 2.

Figure 423: Silas data for the fine sand sediments, with great depth and bed elevation differences and the lowest current velocities circumstances. The blue line represents the 1030 g/L layer and the green line the 1200 g/L layer.

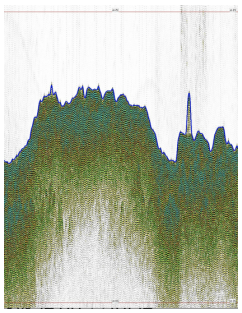

(a) Week 43: Monitorweek 1.

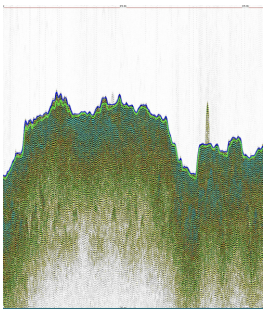

(b) Week 44: Monitorweek 2.

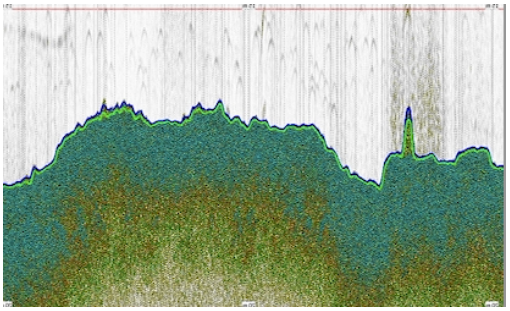

(c) Week 45: Monitorweek 3.

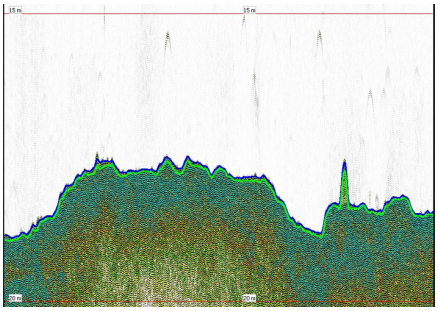

(d) Week 46: Monitorweek 4.

Figure 424: Silas data for the fine sand sediments, with a great depth and low current velocities circumstances. The blue line represents the 1030 g/L layer and the green line the 1200 g/L layer.

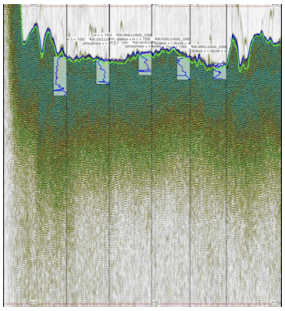

(a) Week 43: Monitorweek 1.

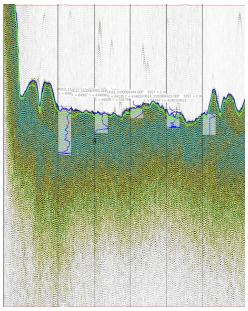

(b) Week 44: Monitorweek 2.

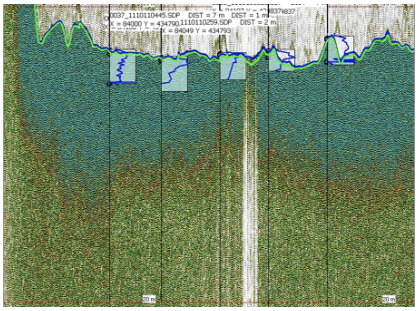

(c) Week 45: Monitorweek 3.

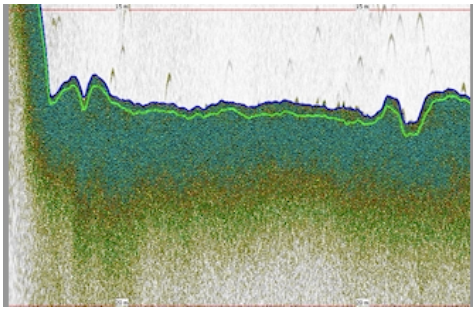

(d) Week 46: Monitorweek 4.

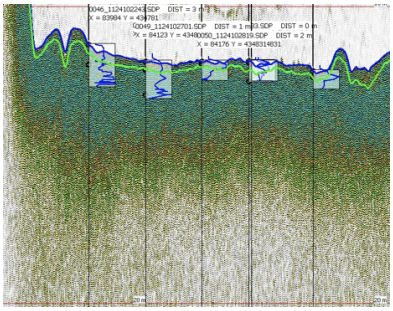

(e) Week 47: Monitorweek 5.

Figure 425: Silas data for the medium silt sediments, with a medium depth in the pocket area and high current velocities circumstances. The blue line represents the 1030 g/L layer and the green line the 1200 g/L layer.

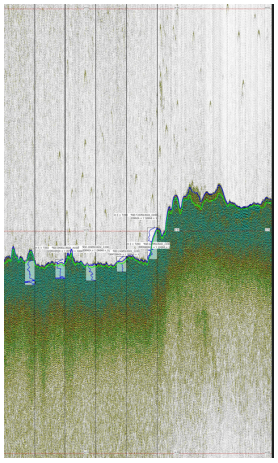

(a) Week 43: Monitorweek 1.

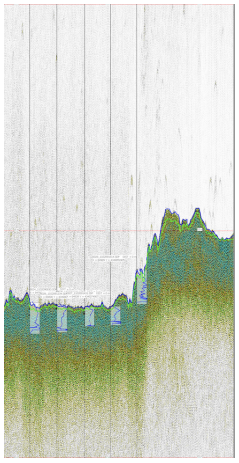

(b) Week 44: Monitorweek 2.

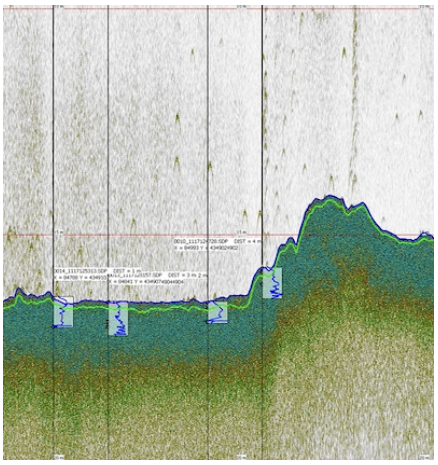

(c) Week 46: Monitorweek 4.

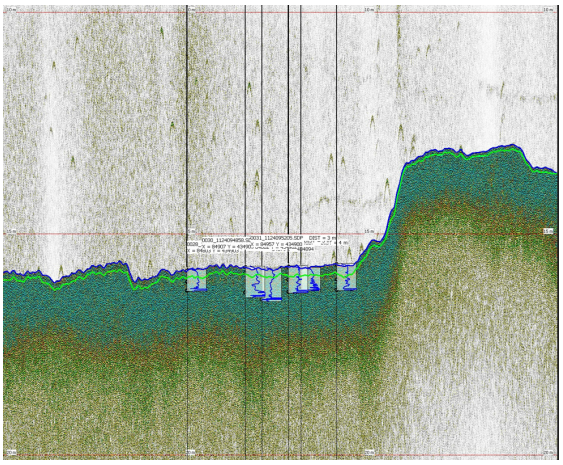

(d) Week 47: Monitorweek 5.

Figure 426: Silas data for the medium silt sediments, with a medium depth and high current velocities circumstances. The blue line represents the 1030 g/L layer and the green line the 1200 g/L layer.

Rheotune: Water Injection Dredging

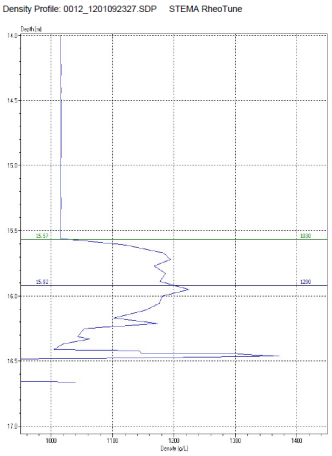

(a) Week 47: Reference measurement

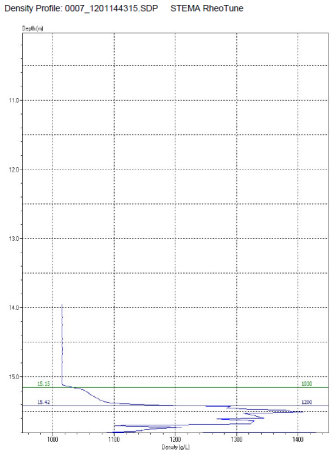

(b) Week 48: Pilot week

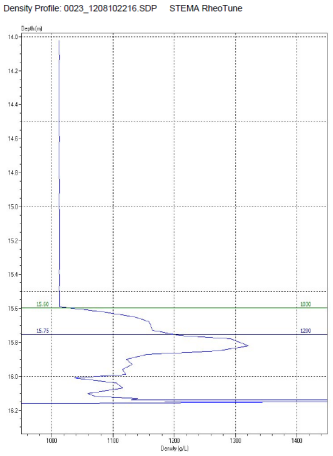

(c) Week 49: Monitorweek 1

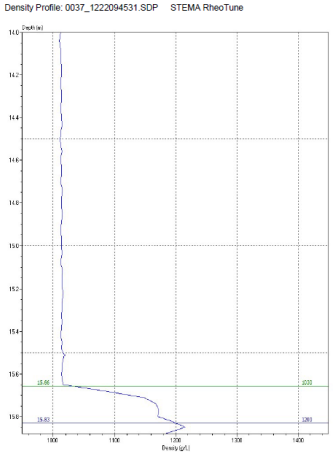

(d) Week 51: Monitorweek 3

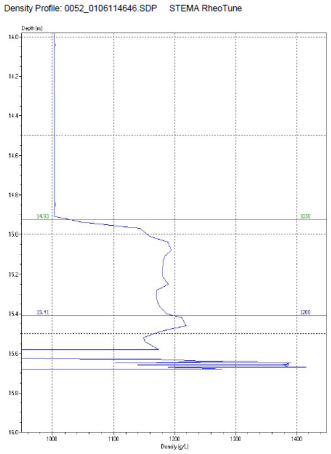

(e) Week 1: Monitorweek 5

Figure 427: Rheotune data of the estuary of the 2nd Petroleumhaven.

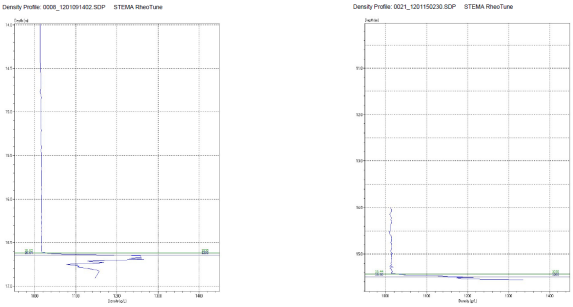

(a) Week47: Reference situation (b) Week 48: Pilot week

Figure 428: Rheotune data of the Koolekade.

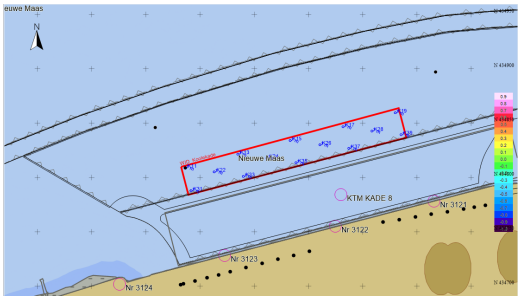

Figure 429: Location of the Rheotune for the Koolekade.

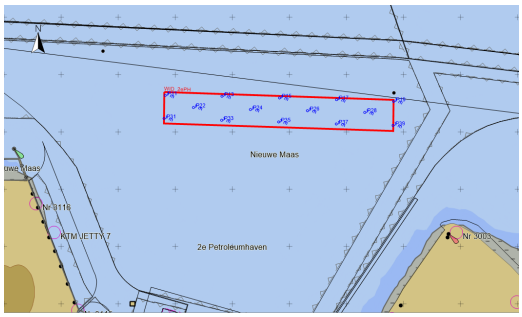

Figure 430: Location of the Rheotune for the estuary of the 2nd Petroleumhaven and the Koolekade.

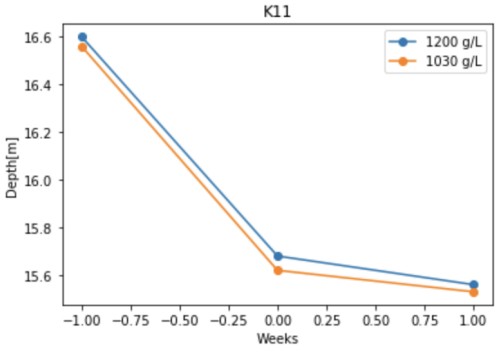

Figure 431: Rheotune data for point K11.

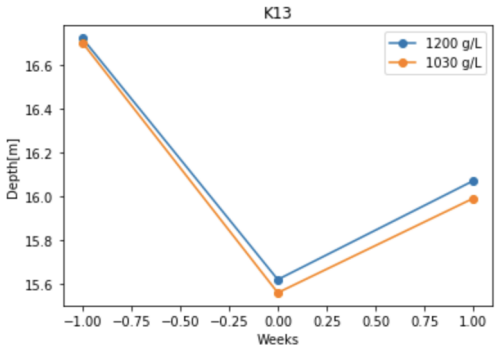

Figure 432: Rheotune data for point K13.

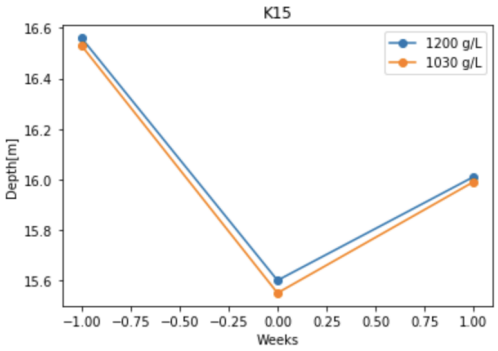

Figure 433: Rheotune data for point K15.

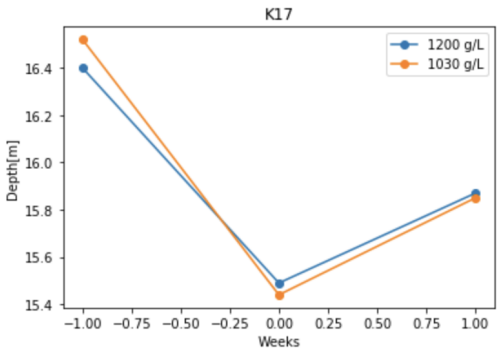

Figure 434: Rheotune data for point K17.

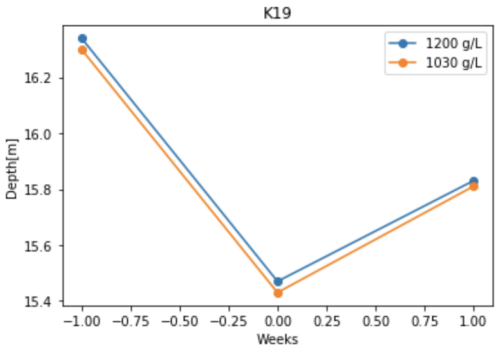

Figure 435: Rheotune data for point K19.

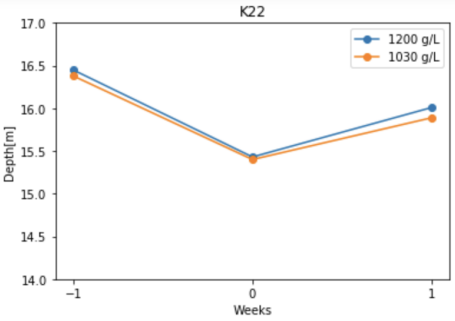

Figure 436: Rheotune data for point K22.

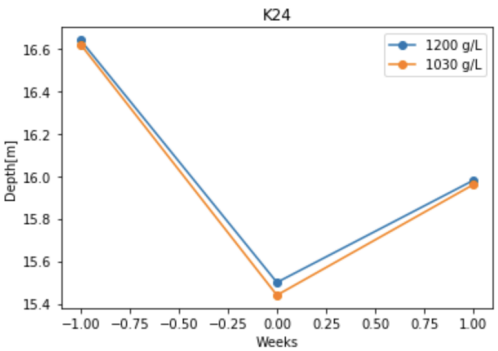

Figure 437: Rheotune data for point K24.

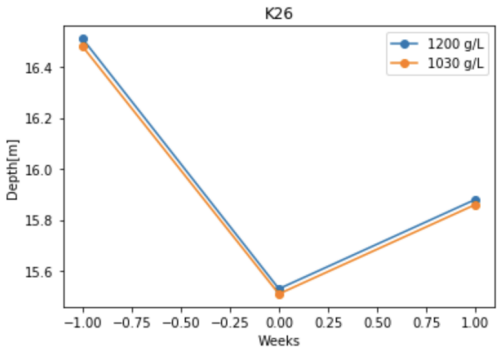

Figure 438: Rheotune data for point K26.

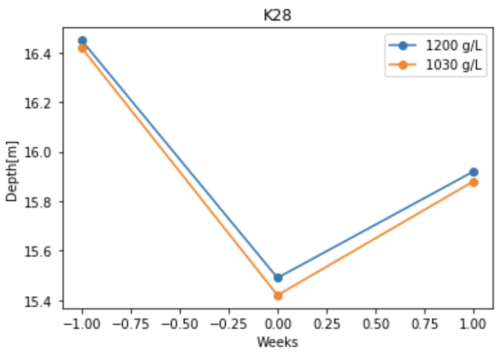

Figure 439: Rheotune data for point K28.

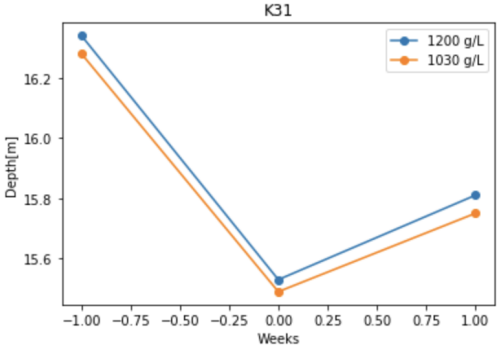

Figure 440: Rheotune data for point K31.

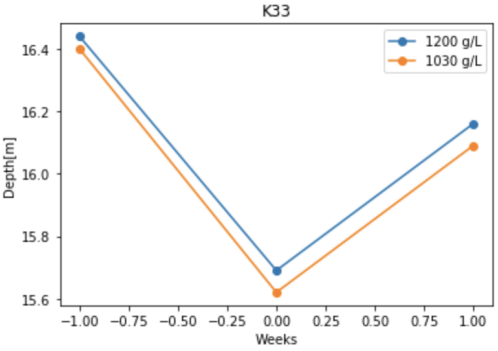

Figure 441: Rheotune data for point K33.

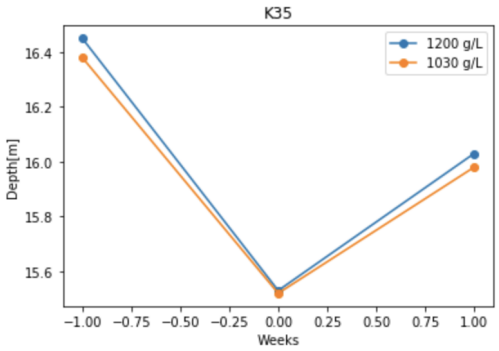

Figure 442: Rheotune data for point K35.

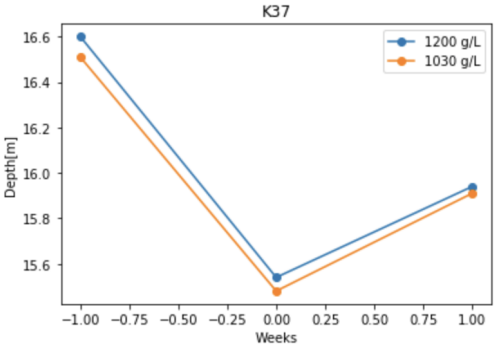

Figure 443: Rheotune data for point K37.

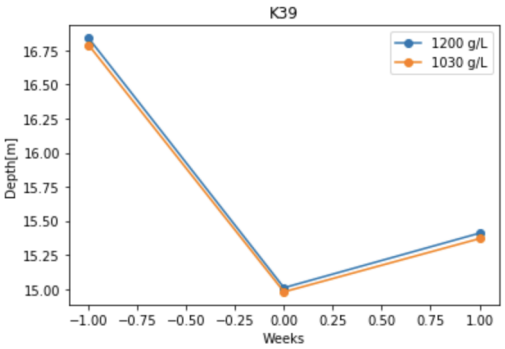

Figure 444: Rheotune data for point K39.

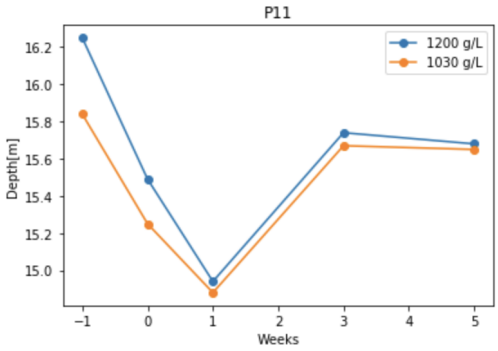

Figure 445: Rheotune data for point P11.

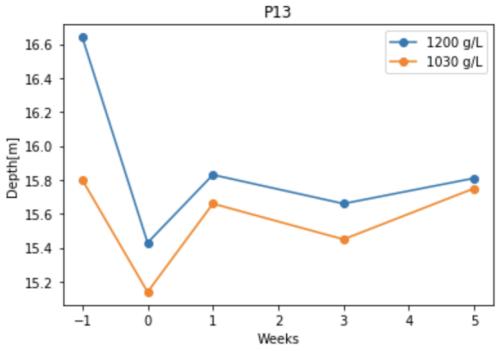

Figure 446: Rheotune data for point P13.

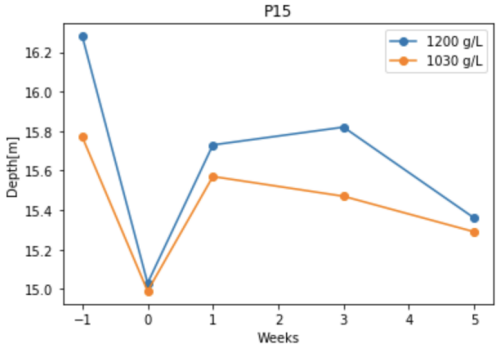

Figure 447: Rheotune data for point P15.

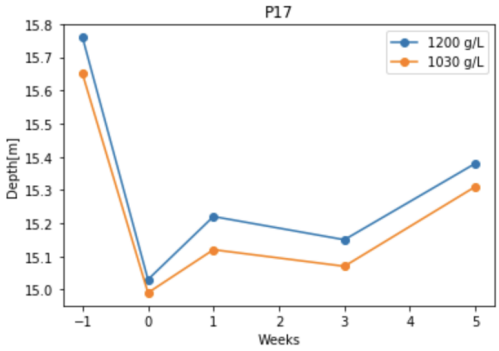

Figure 448: Rheotune data for point P17.

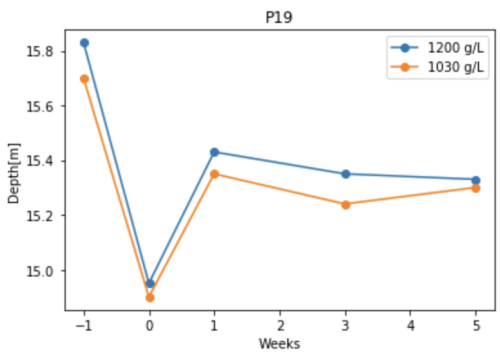

Figure 449: Rheotune data for point P19.

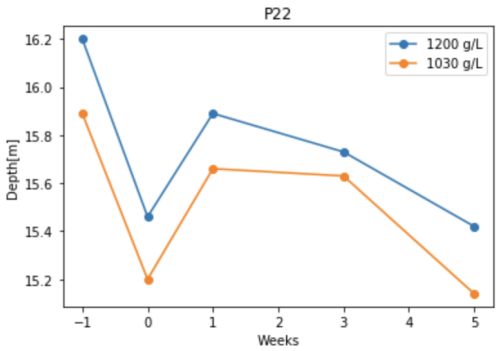

Figure 450: Rheotune data for point P22.

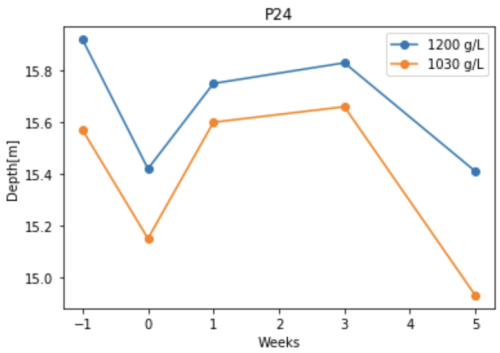

Figure 451: Rheotune data for point P24.

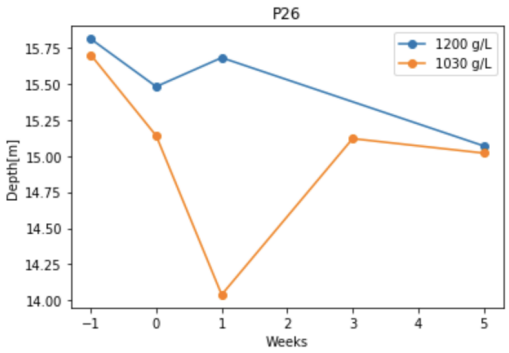

Figure 452: Rheotune data for point P26.

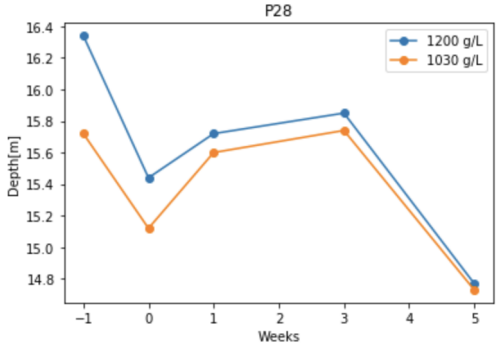

Figure 453: Rheotune data for point P28.

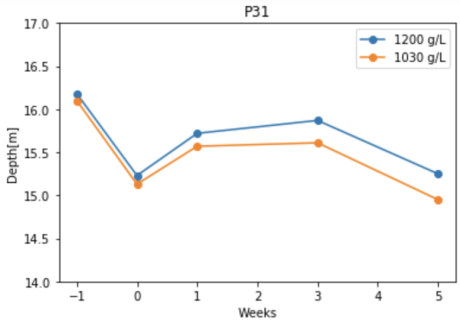

Figure 454: Rheotune data for point P31.

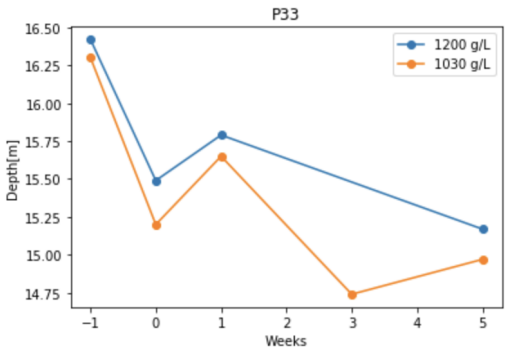

Figure 455: Rheotune data for point P33.

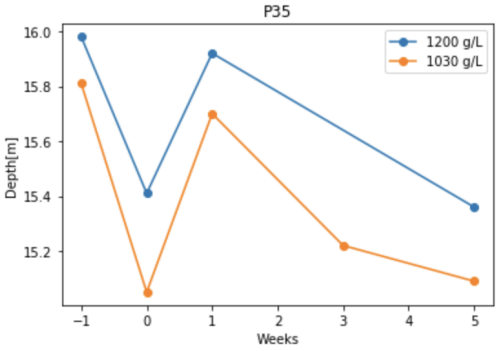

Figure 456: Rheotune data for point P35.

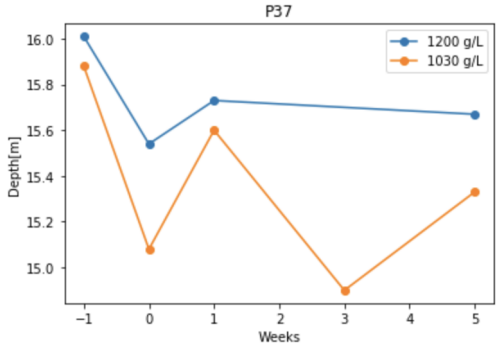

Figure 457: Rheotune data for point P37.

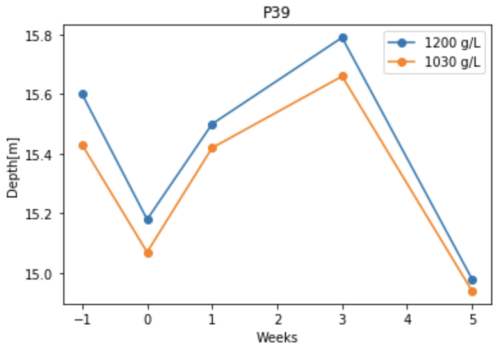

Figure 458: Rheotune data for point P39.

Silas: Water Injection Dredging

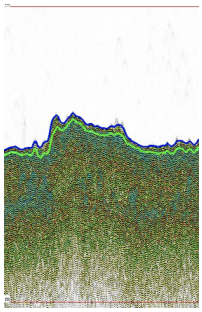

(a) Week47: Reference situation

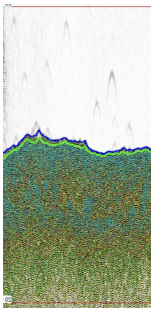

(b) Week 48: Pilot week

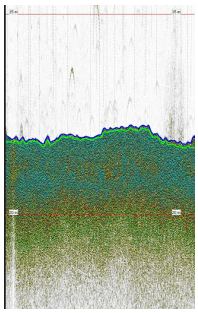

(c) Week 49: Monitor week 1

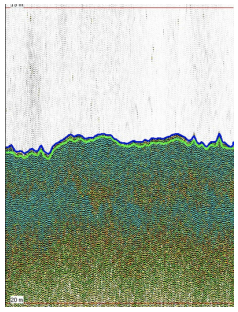

(d) Week 50: Monitor week 2

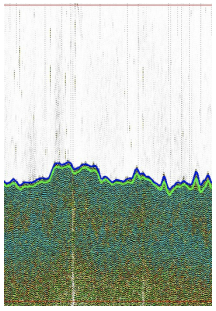

(e) Week 51: Monitor week 3

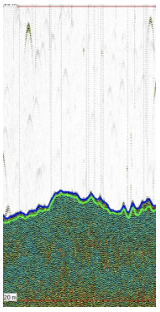

(f) Week 52: Monitor week 4

Figure 459: Silas data for the fine sand sediments, with a great depth and low current velocities circumstances. The blue line represents the 1030 g/L layer and the green line represents the 1200 g/L layer.

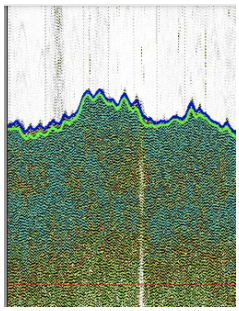

(g) Week 1: Monitor week 5

Figure 459: Silas data for the fine sand sediments, with a great depth and low current velocities circumstances. The blue line represents the 1030 g/L layer and the green line represents the 1200 g/L layer.

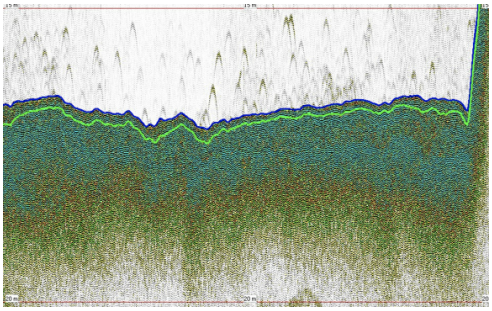

(a) Week47: Reference situation

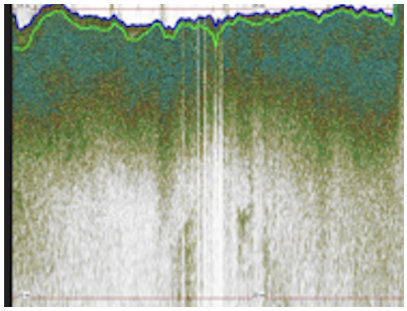

(b) Week 48: Pilot week

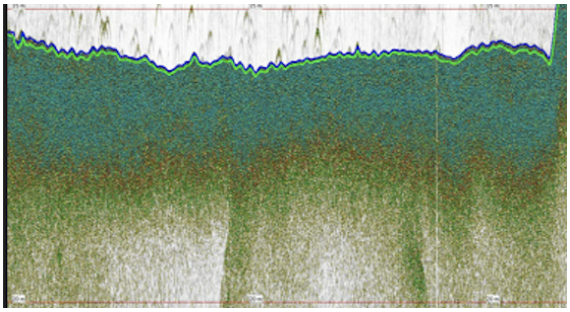

(c) Week 49: Monitor week 1

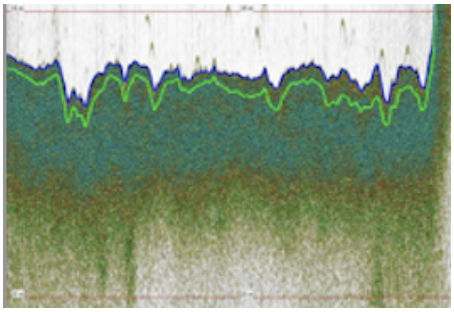

(d) Week 51: Monitor week 3

Figure 460: Silas data for the medium silt sediments, with a medium depth in the pocket area and high current velocities circumstances. The blue line represents the 1030 g/L layer and the green line represents the 1200 g/L layer.

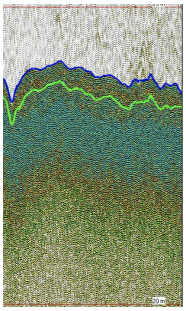

(a) Week 47: Reference situation

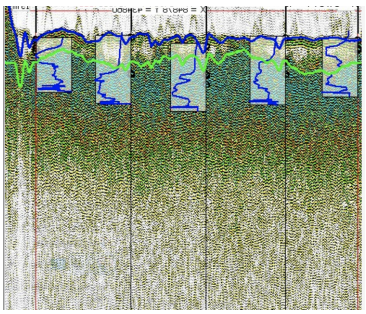

(b) Week 48: Pilot week

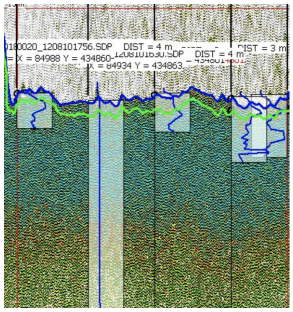

(c) Week 49: Monitor week 1

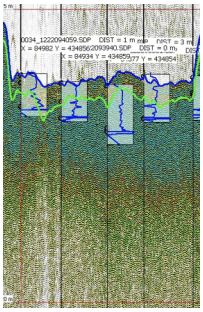

(d) Week 51: Monitor week 3

Figure 461: Silas data for the medium silt sediments, with a medium depth and high current velocities circumstances. The blue line represents the 1030 g/L layer and the green line represents the 1200 g/L layer.

Rheotune: Underwater Plough

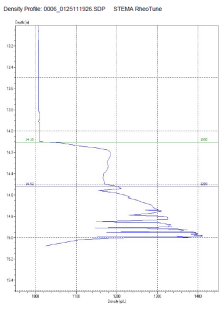

(a) Week 4: Reference situation

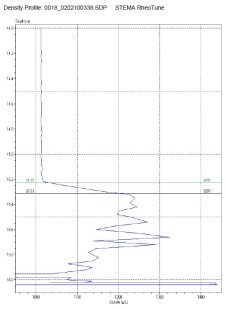

(b) Week 5: Pilot week

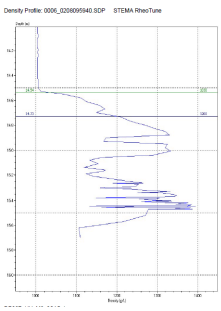

(c) Week 6: Monitor week 1

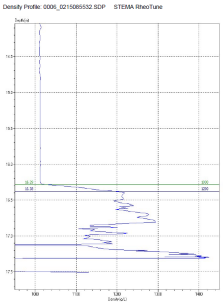

(d) Week 7: Monitor week 2

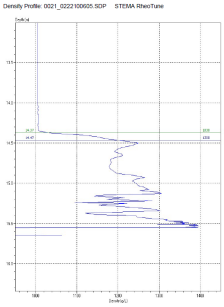

(e) Week 8: Monitor week 3

Figure 462: Rheotune data for the underwater plough.

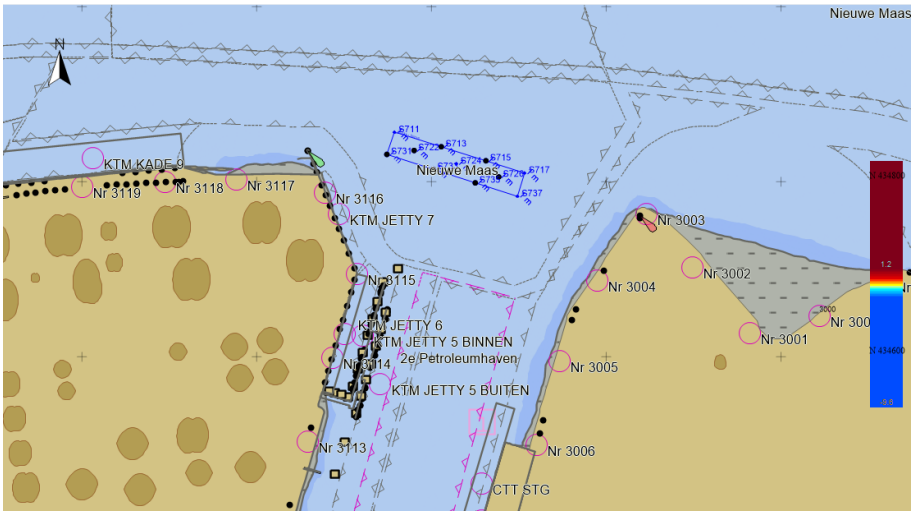

Figure 463: Location of the Rheotune for the estuary of the 2nd Petroleumhaven and the Koolekade.

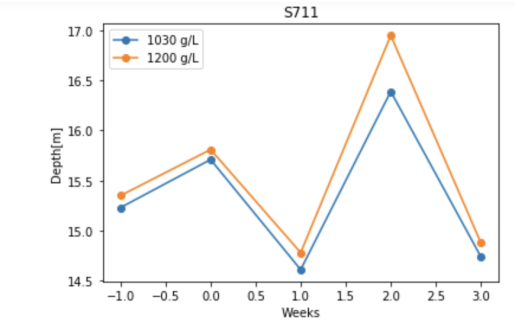

Figure 464: Rheotune data for point S711.

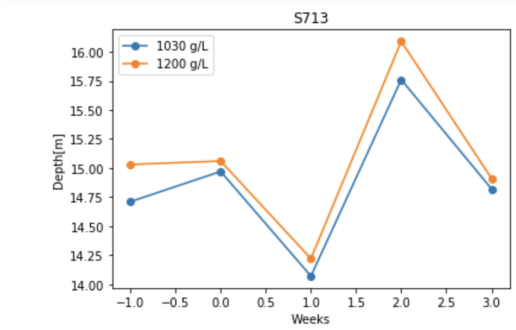

Figure 465: Rheotune data for point S713.

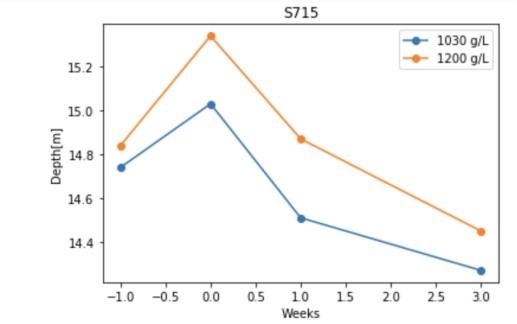

Figure 466: Rheotune data for point S715.

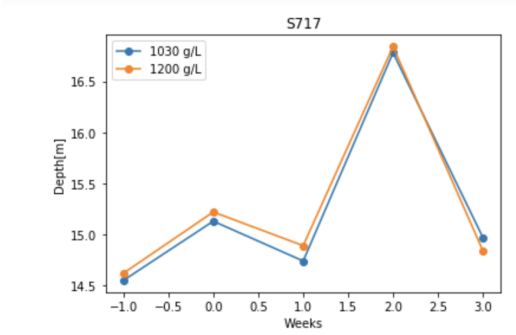

Figure 467: Rheotune data for point S717.

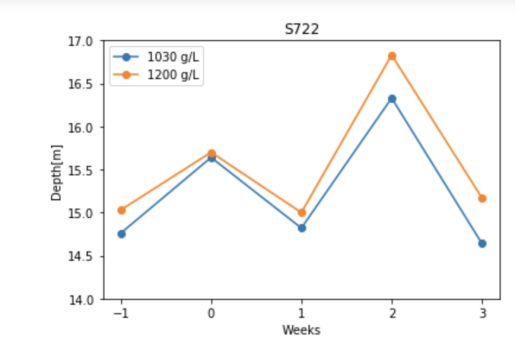

Figure 468: Rheotune data for point S722.

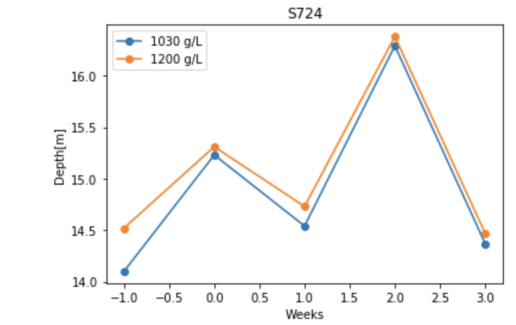

Figure 469: Rheotune data for point S724.

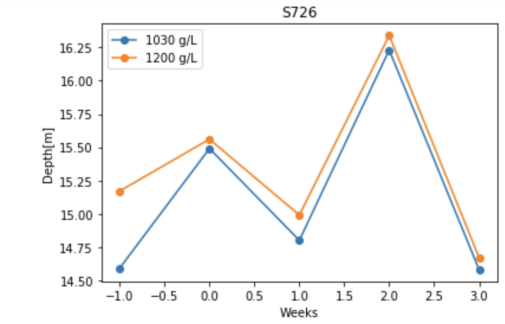

Figure 470: Rheotune data for point S726.

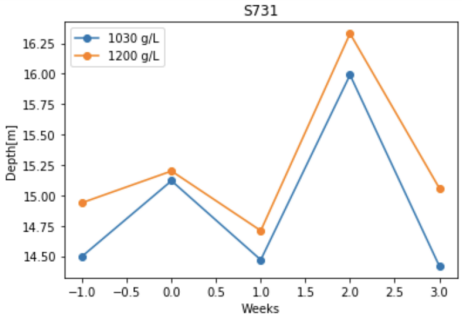

Figure 471: Rheotune data for point S731.

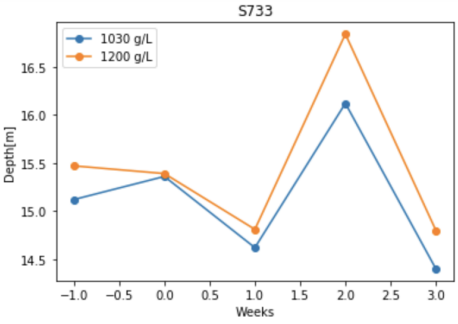

Figure 472: Rheotune data for point S733.

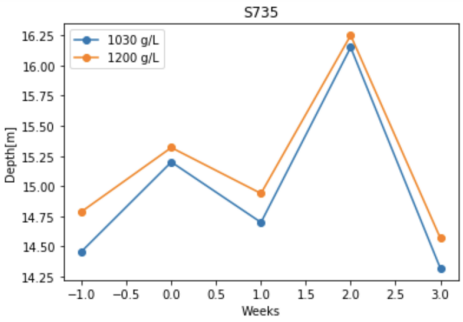

Figure 473: Rheotune data for point S735.

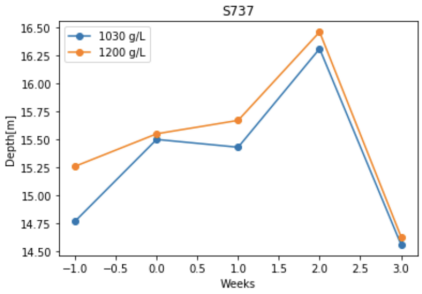

Figure 474: Rheotune data for point S737.

Silas: Underwater Plough

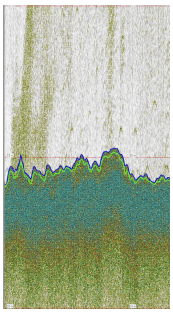

(a) Week 4: Reference situation

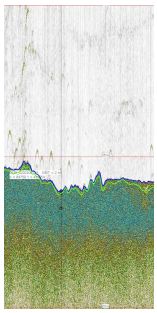

(b) Week 5: Pilot week

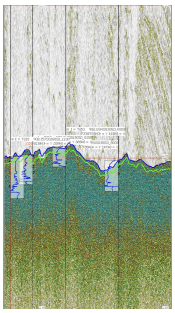

(c) Week 6: Monitor week 1

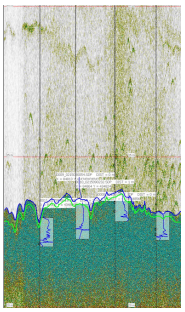

(d) Week 7: Monitor week 2

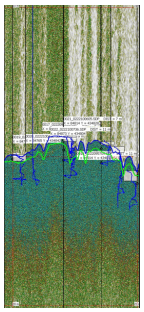

(e) Week 8: Monitor week 3

Figure 475: Silas data for the medium silt sediments, with a medium depth and high current velocities circumstances. The blue line represents the 1030 g/L layer and the green line represents the 1200 g/L layer.

Appendix VII: Depth maps during monitoring weeks

In this appendix, the depth figures before the pilot, during the pilot and for the monitoring weeks can be found. The data were extracted with a Multibeam Echosounder. The data is loaded with QINSy and the profiles are made.

Tiamat

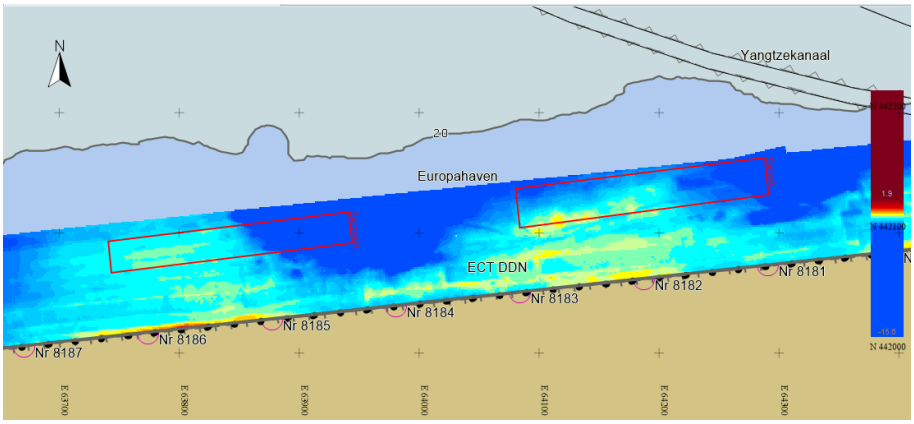

Figure 476: Europahaven before dredging with the Tiamat.

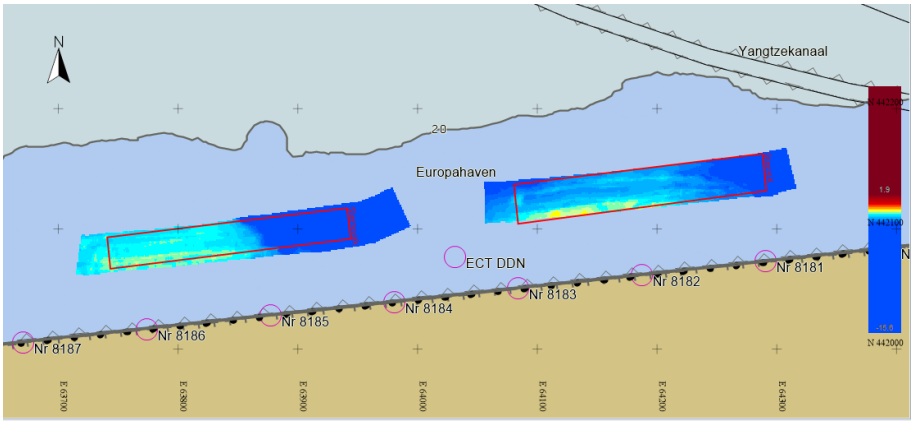

Figure 477: Europahaven pilot week Tiamat day 1 (17-10-2022).

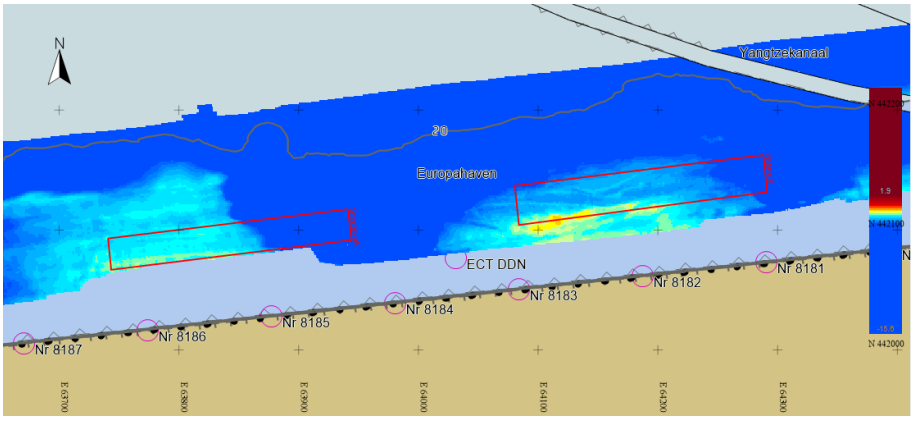

Figure 478: Europahaven pilot week Tiamat day 2 (18-10-2022).

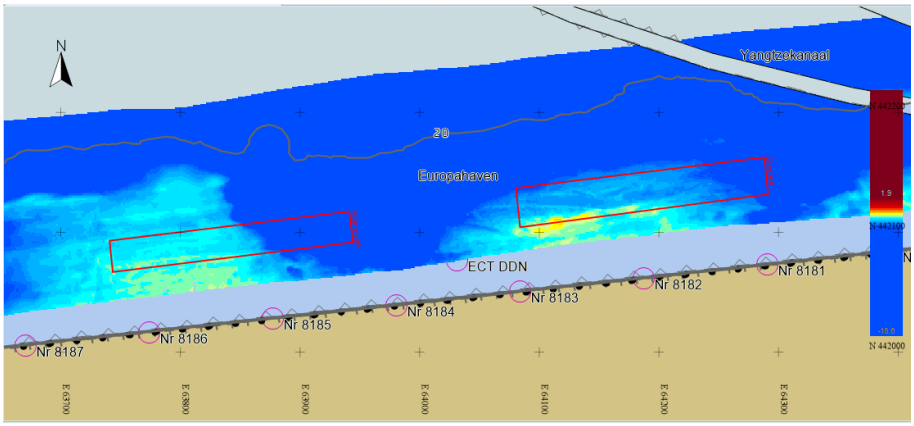

Figure 479: Europahaven Tiamat monitor week 1 (week 43).

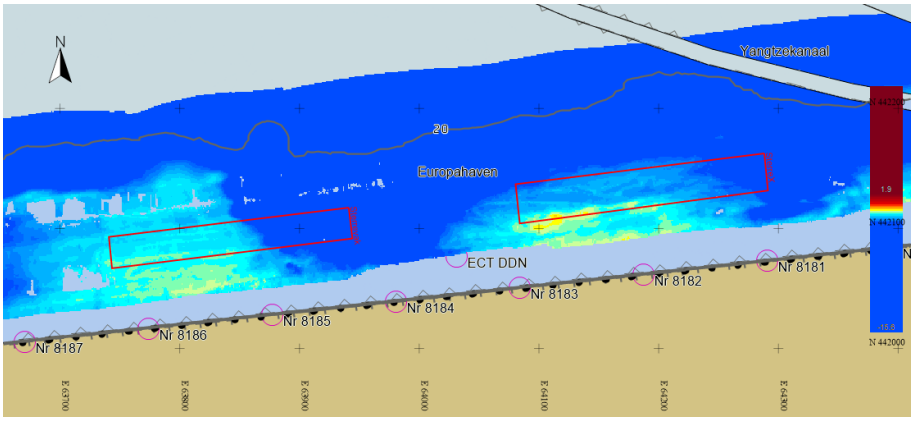

Figure 480: Europahaven Tiamat monitor week 2 (week 44).

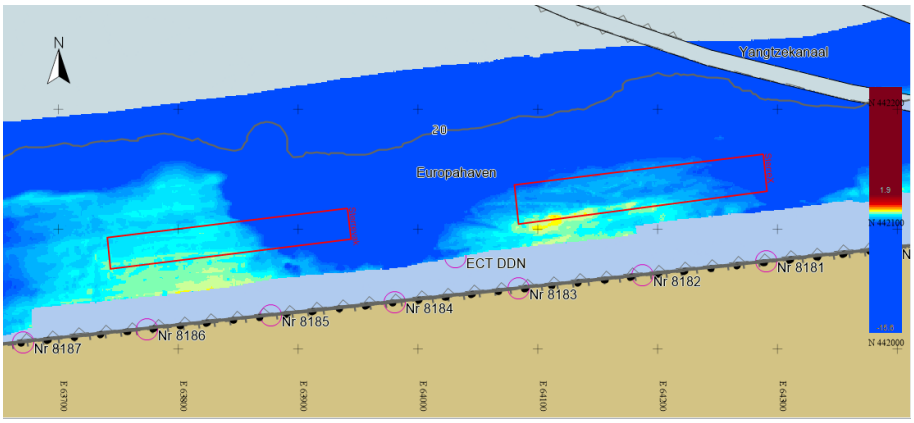

Figure 481: Europahaven Tiamat monitor week 3 (week 45).

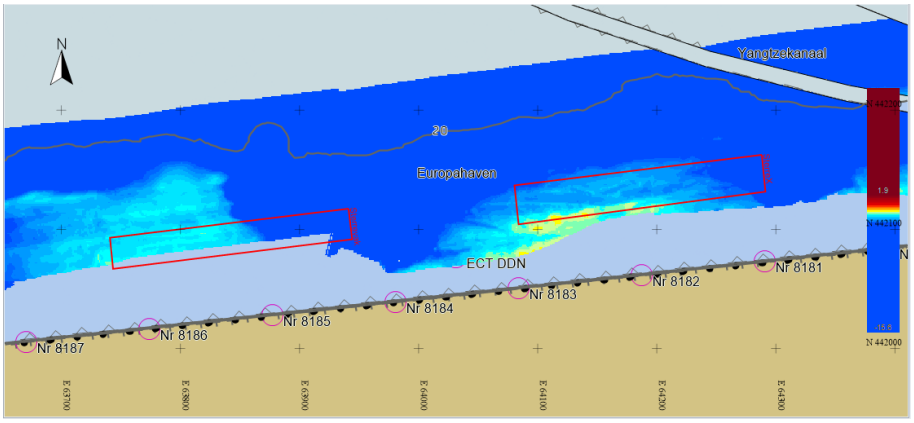

Figure 482: Europahaven Tiamat monitor week 4 (week 46).

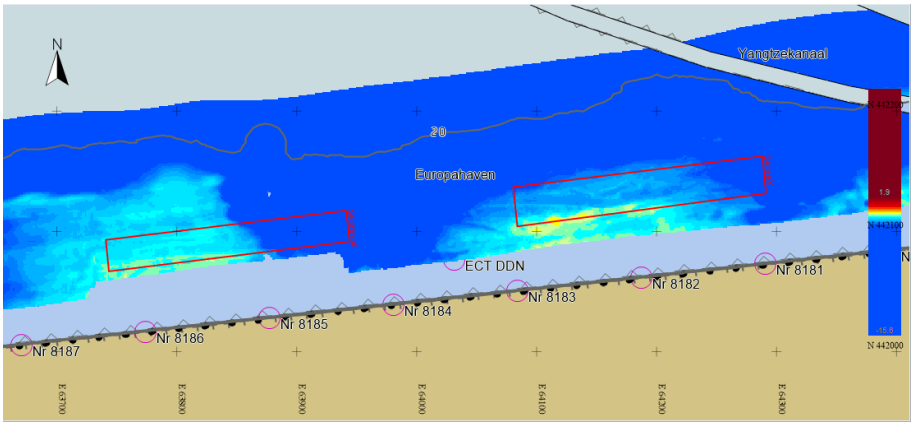

Figure 483: Europahaven Tiamat monitor week 5 (week 47).

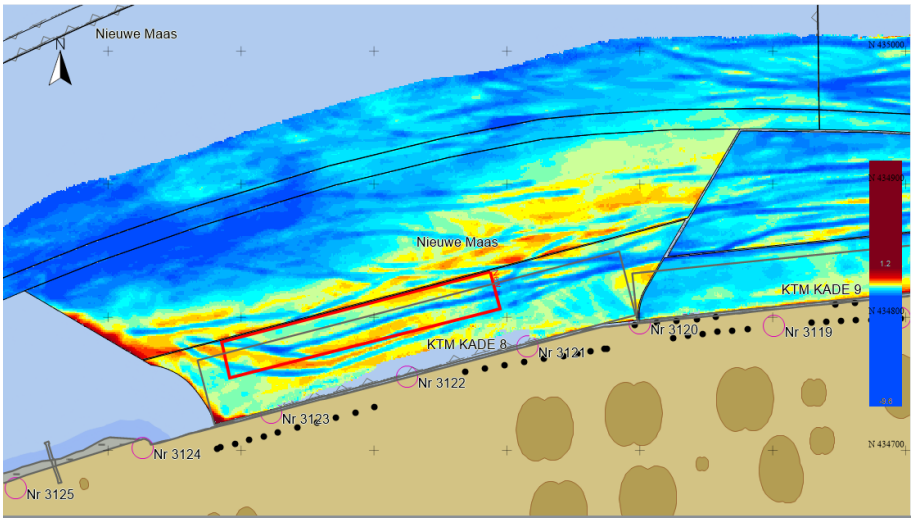

Figure 484: Koolekade before dredging with the Tiamat.

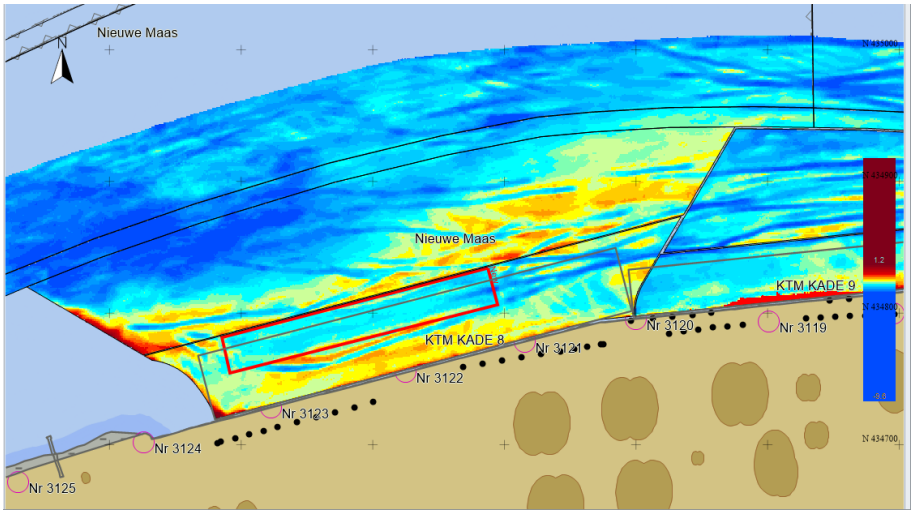

Figure 485: Koolekade pilot week Tiamat.

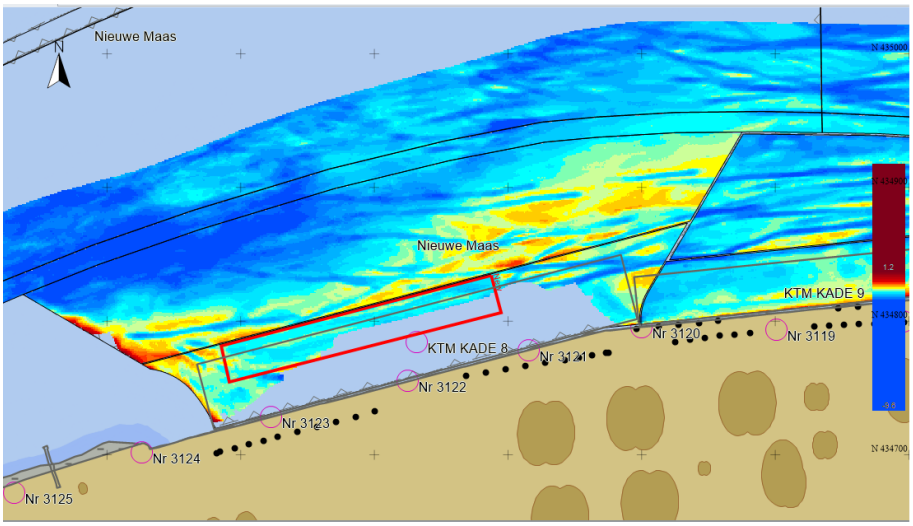

Figure 486: Koolekade Tiamat monitor week 1 (week 43).

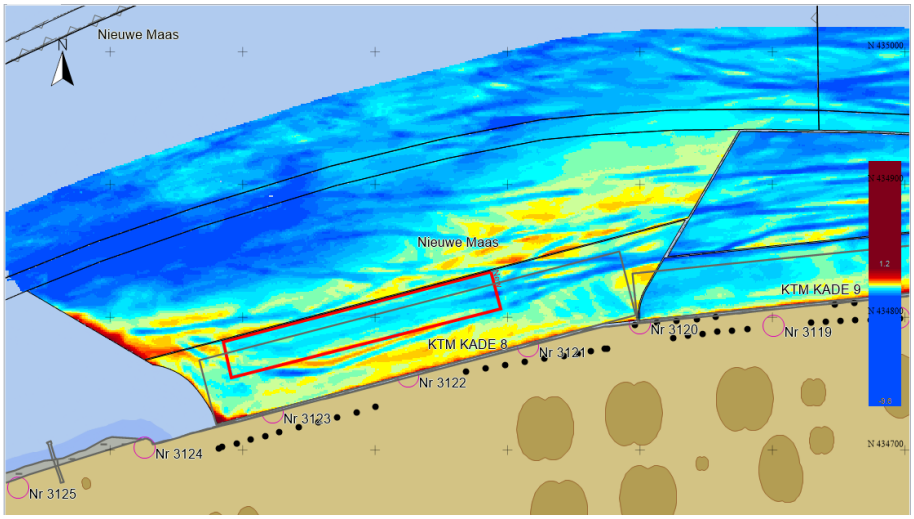

Figure 487: Koolekade Tiamat monitor week 2 (week 44).

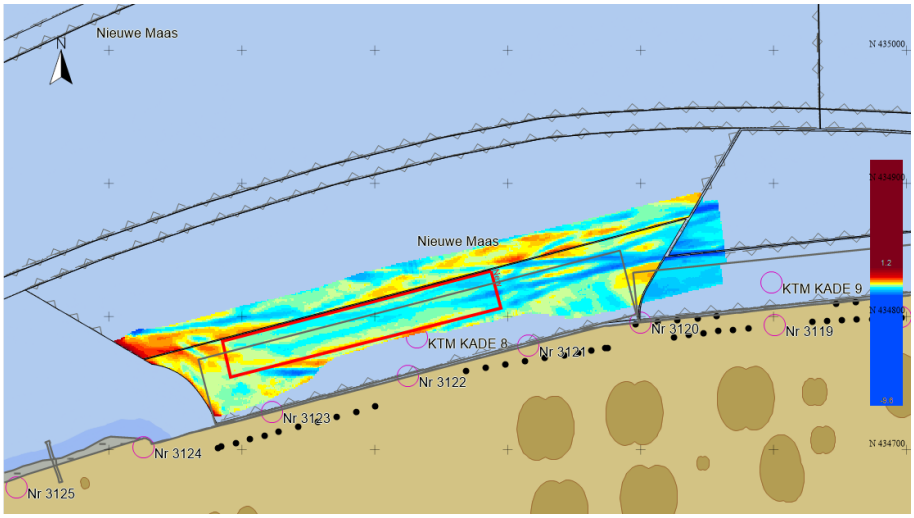

Figure 488: Koolekade Tiamat monitor week 3 (week 45).

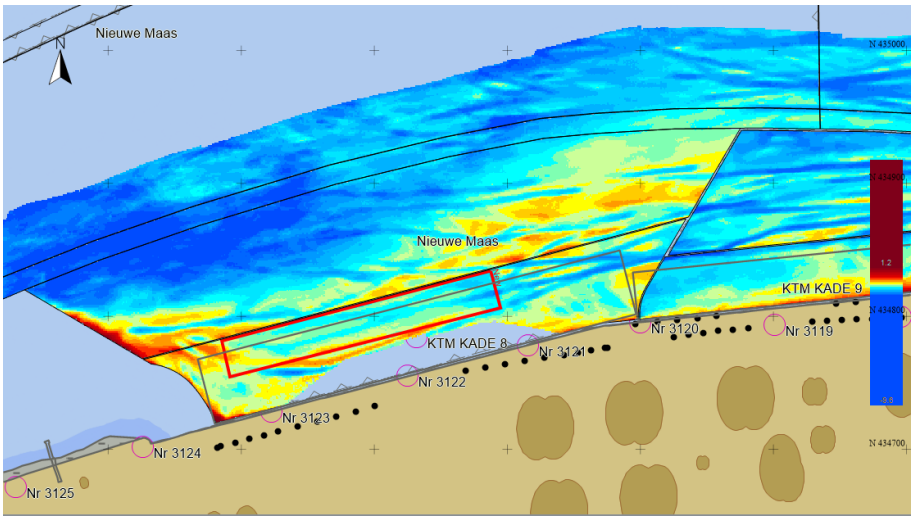

Figure 489: Koolekade Tiamat monitor week 4 (week 46).

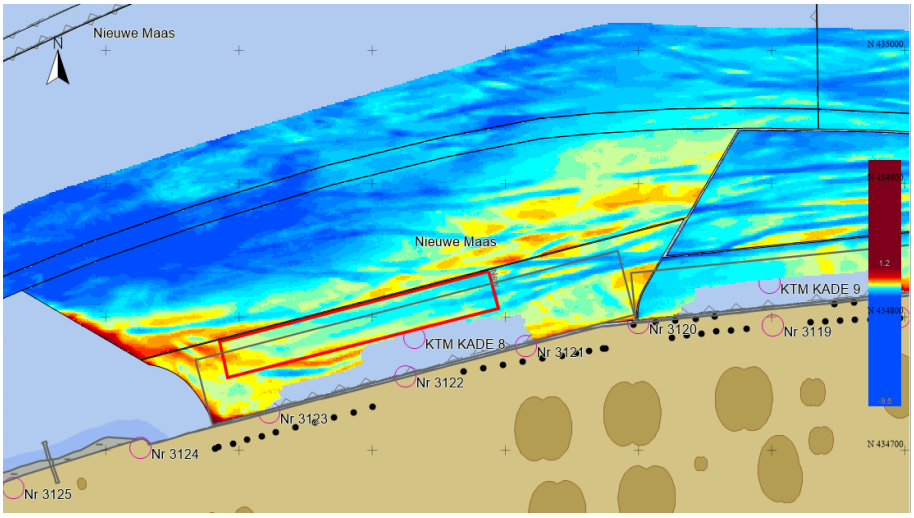

Figure 490: Koolekade Tiamat monitor week 5 (week 47).

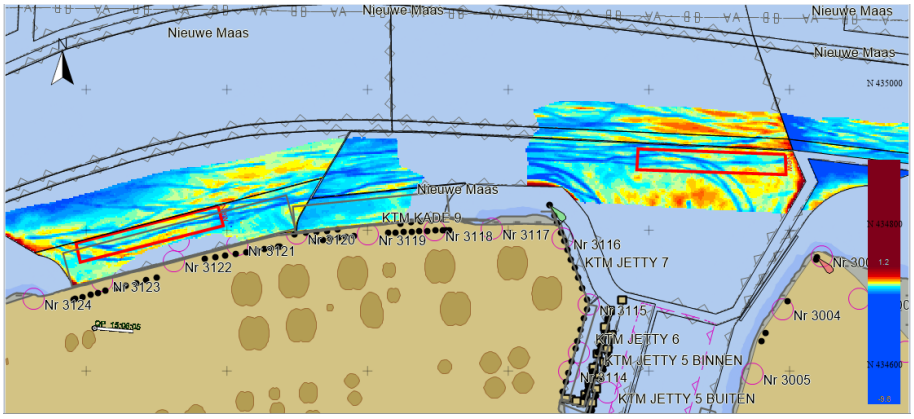

Figure 491: Estuary 2nd Petroleumhaven before dredging with the Tiamat.

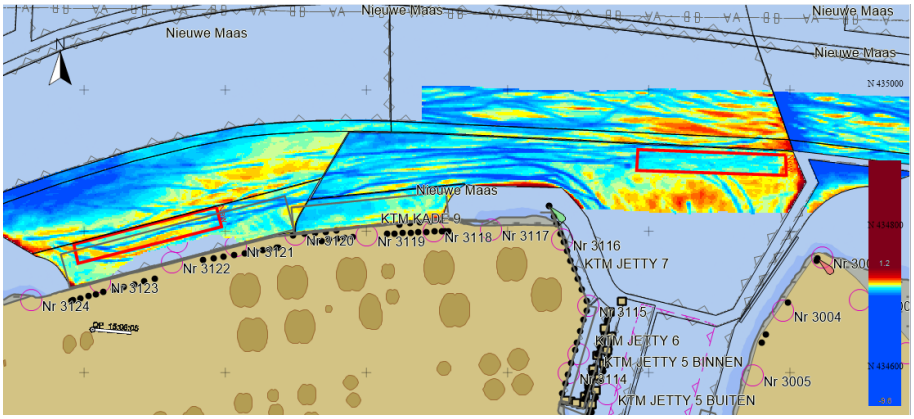

Figure 492: Estuary 2nd Petroleumhaven pilot week Tiamat day 1 (19-10-2022).

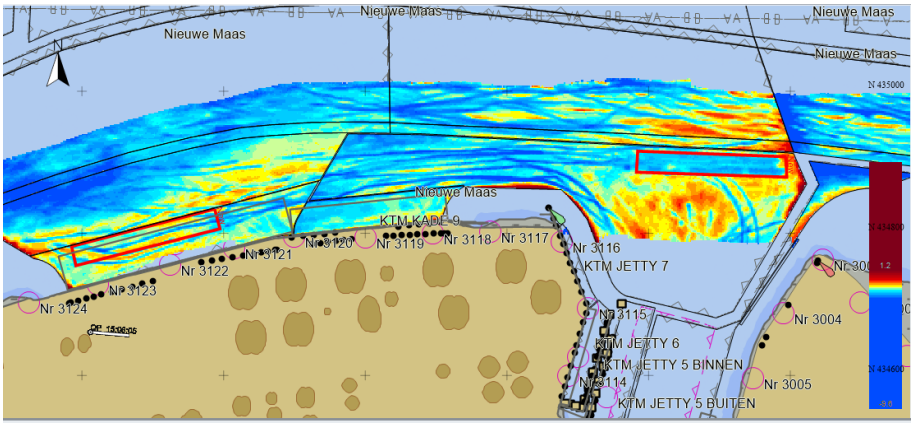

Figure 493: Estuary 2nd Petroleumhaven pilot week Tiamat day 2 (20-10-2022).

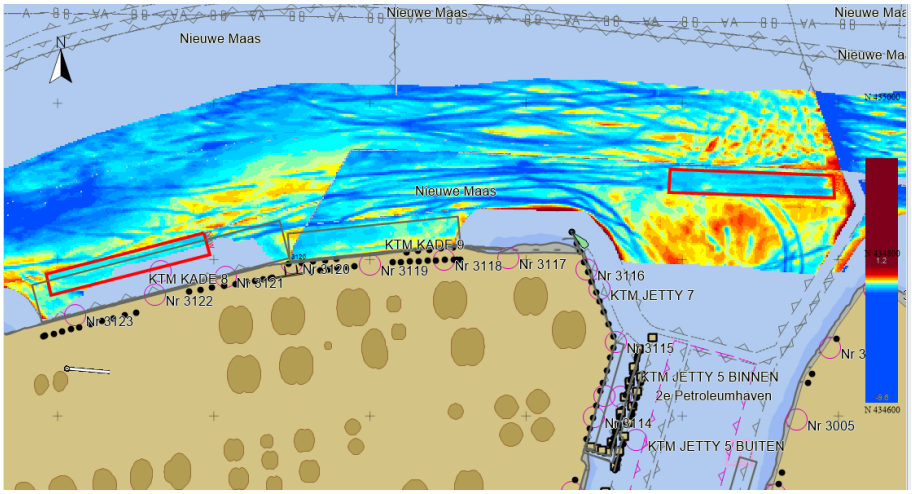

Figure 494: Estuary 2nd Petroleumhaven Tiamat monitor week 1 (week 43).

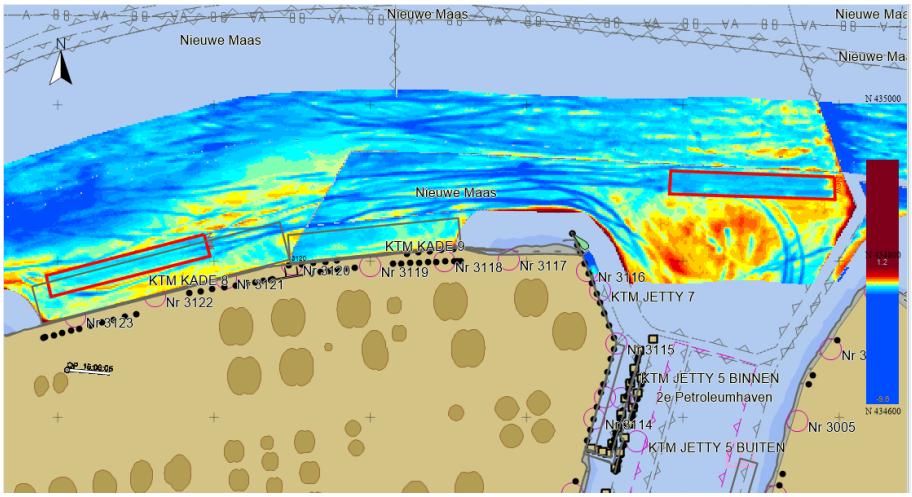

Figure 495: Estuary 2nd Petroleumhaven Tiamat monitor week 2 (week 44).

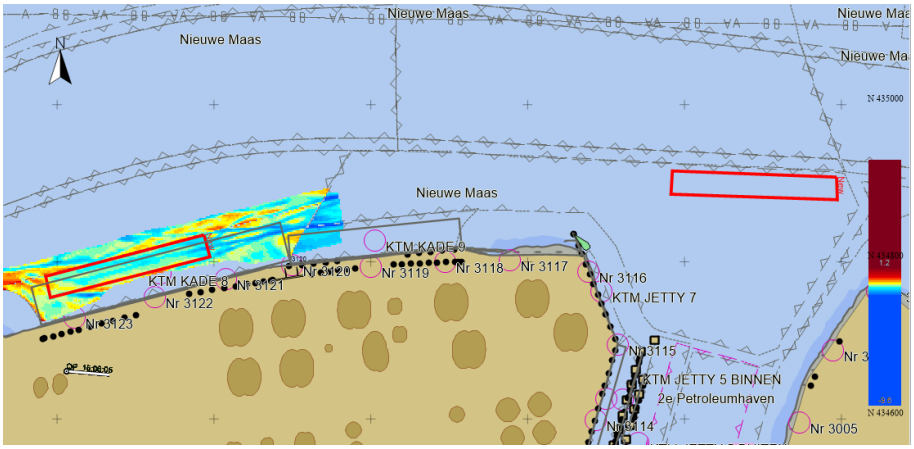

Figure 496: Estuary 2nd Petroleumhaven Tiamat monitor week 3 (week 45).

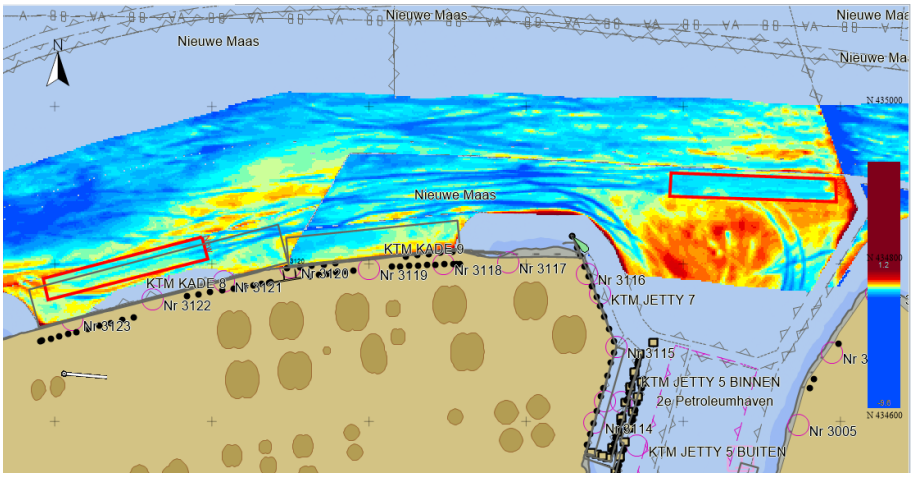

Figure 497: Estuary 2nd Petroleumhaven Tiamat monitor week 4 (week 46).

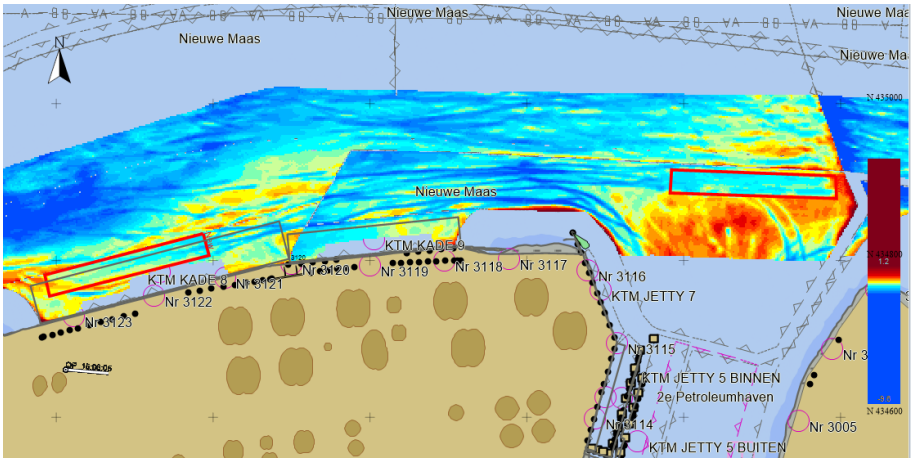

Figure 498: Estuary 2nd Petroleumhaven Tiamat monitor week 5 (week 47).

Water Injection Dredging

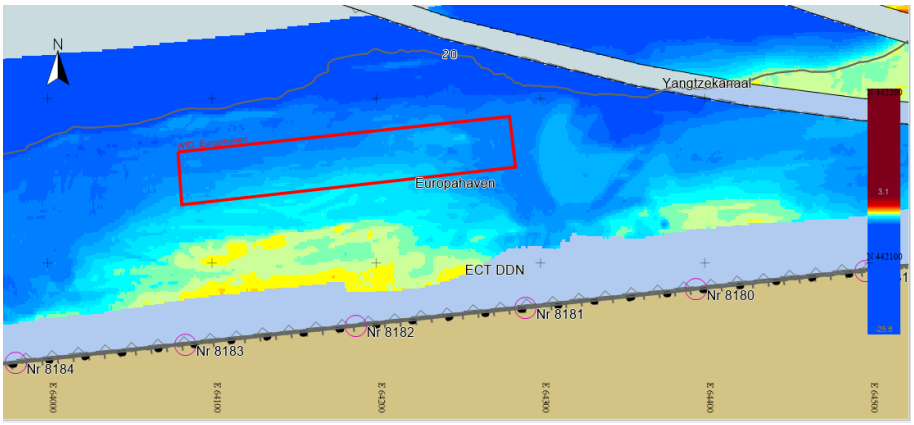

Figure 499: Europahaven before dredging WID.

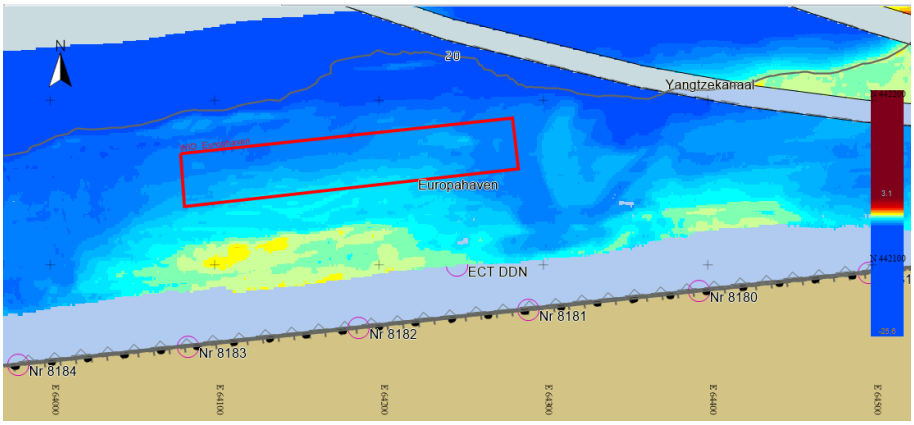

Figure 500: Europahaven pilot week WID.

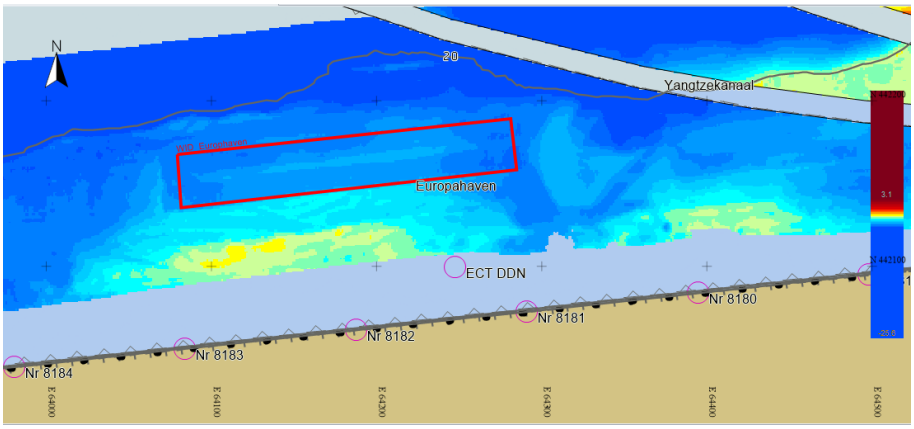

Figure 501: Europahaven WID monitor week 1 (week 49).

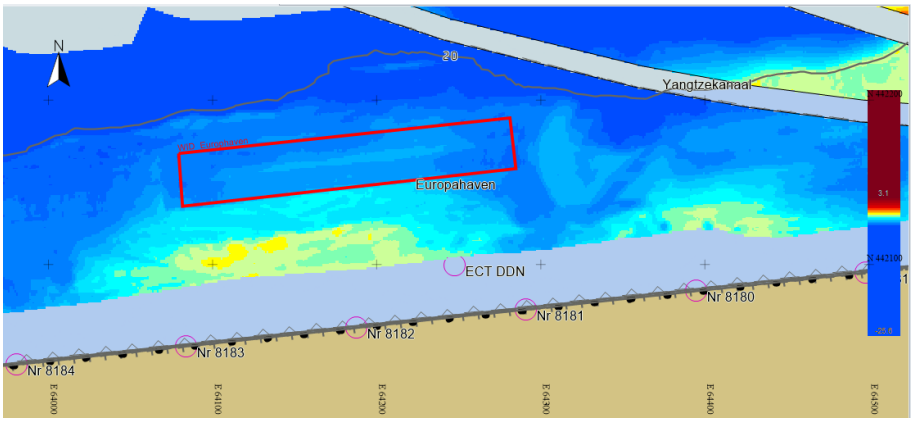

Figure 502: Europahaven WID monitor week 3 (week 51).

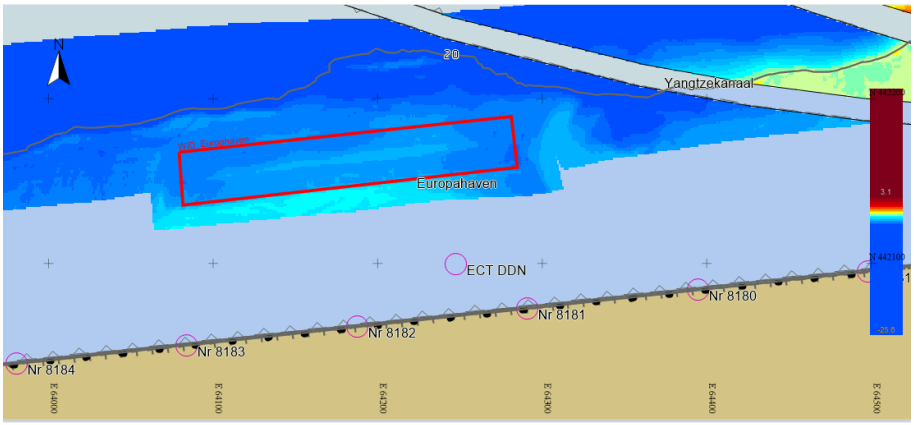

Figure 503: Europahaven WID monitor week 4 (week 52).

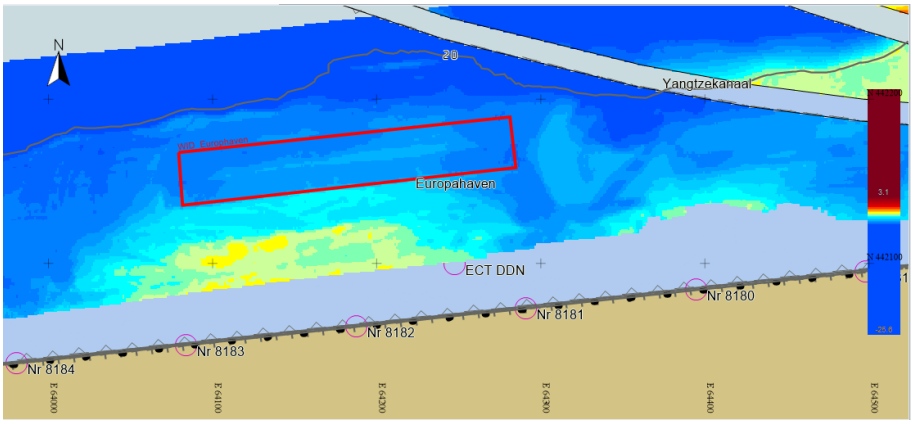

Figure 504: Europahaven WID monitor week 5 (week 1).

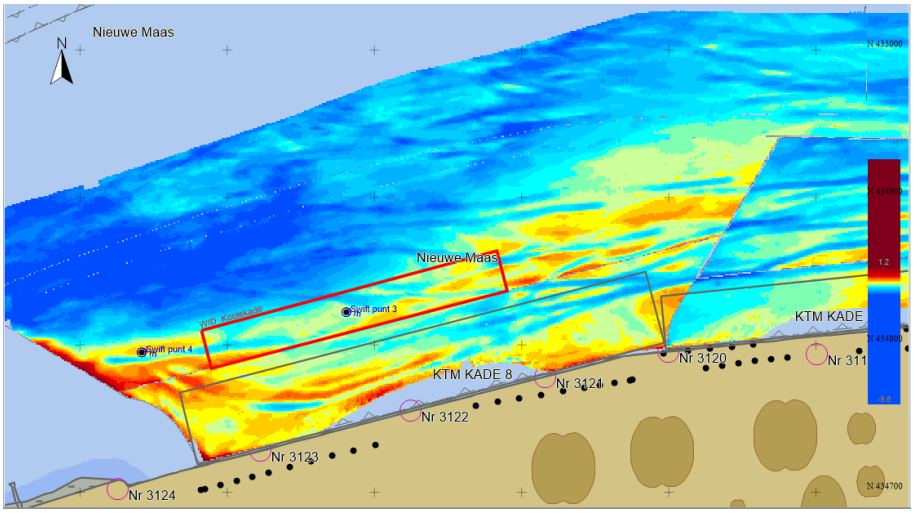

Figure 505: Koolekade before dredging WID.

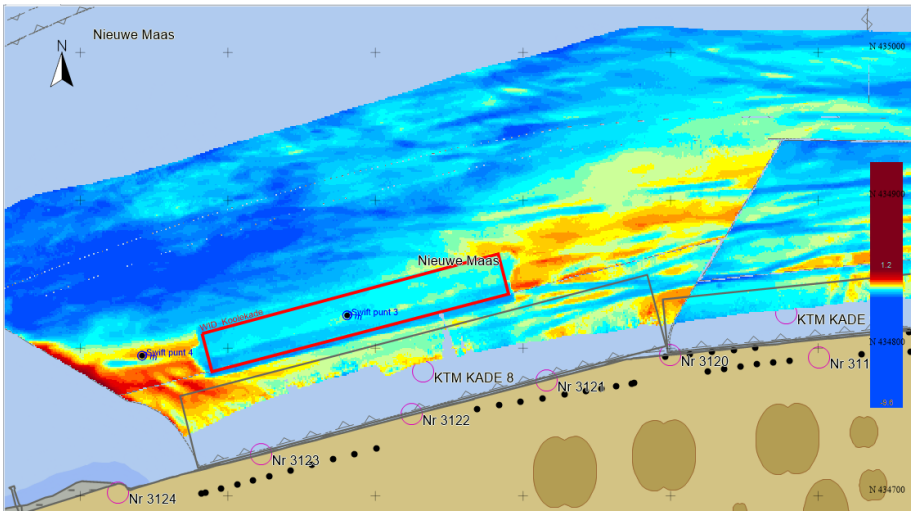

Figure 506: Koolekade pilot week WID.

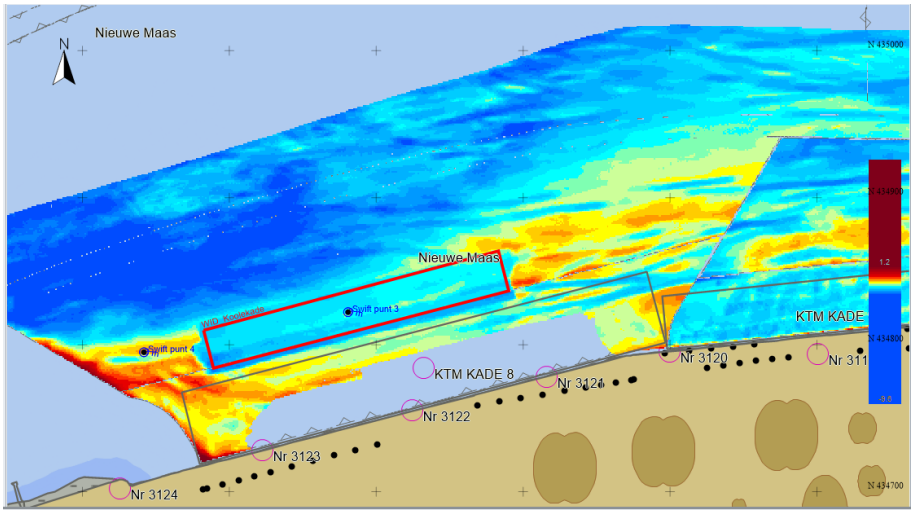

Figure 507: Koolekade WID monitor week 1 (week 49).

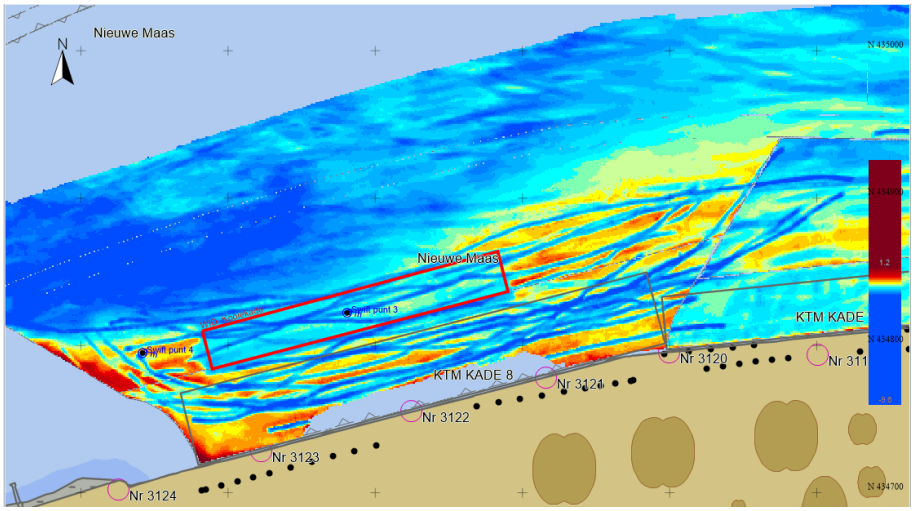

Figure 508: Koolekade WID monitor week 3 (week 51).

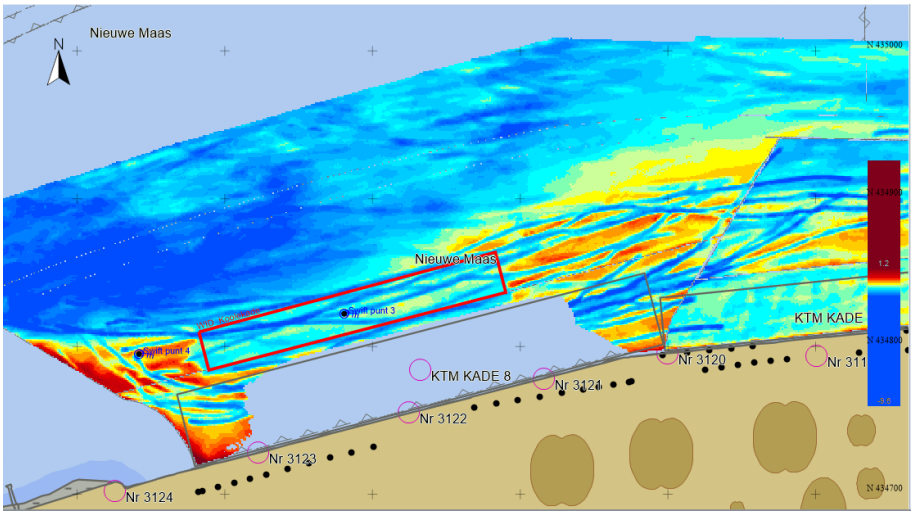

Figure 509: Koolekade WID monitor week 5 (week 1).

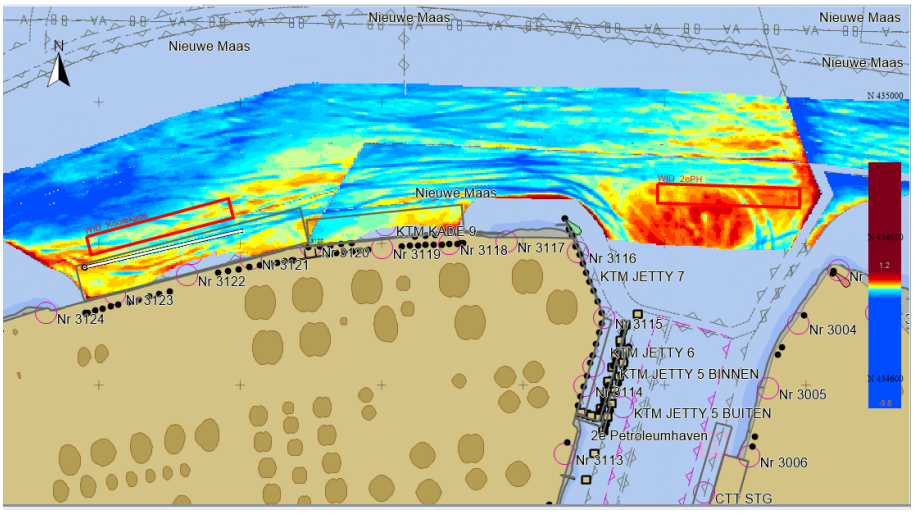

Figure 510: Estuary 2nd Petroleumhaven before dredging WID.

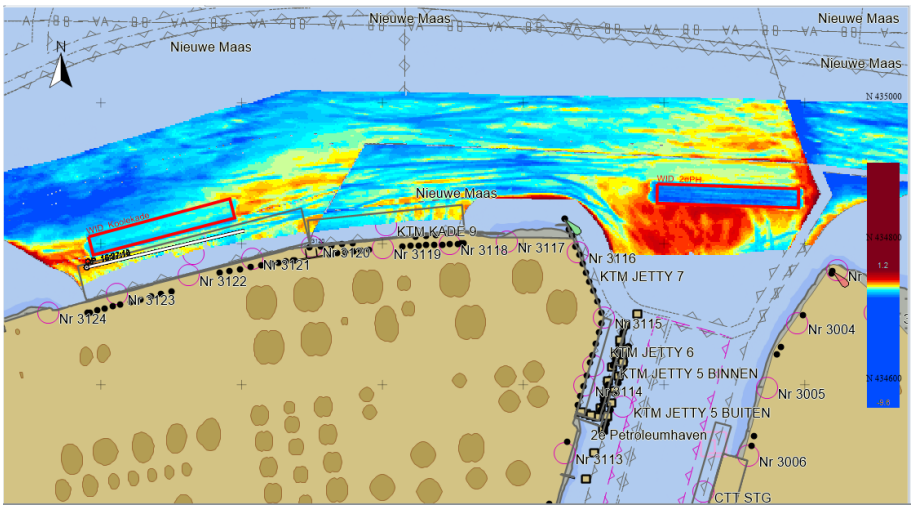

Figure 511: Estuary 2nd Petroleumhaven pilot week WID.

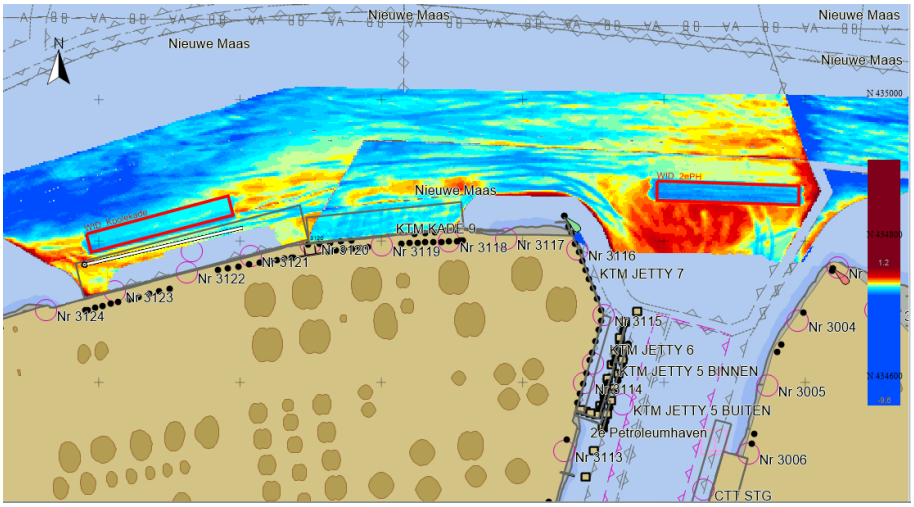

Figure 512: Estuary 2nd Petroleumhaven WID monitor week 1 (week 49).

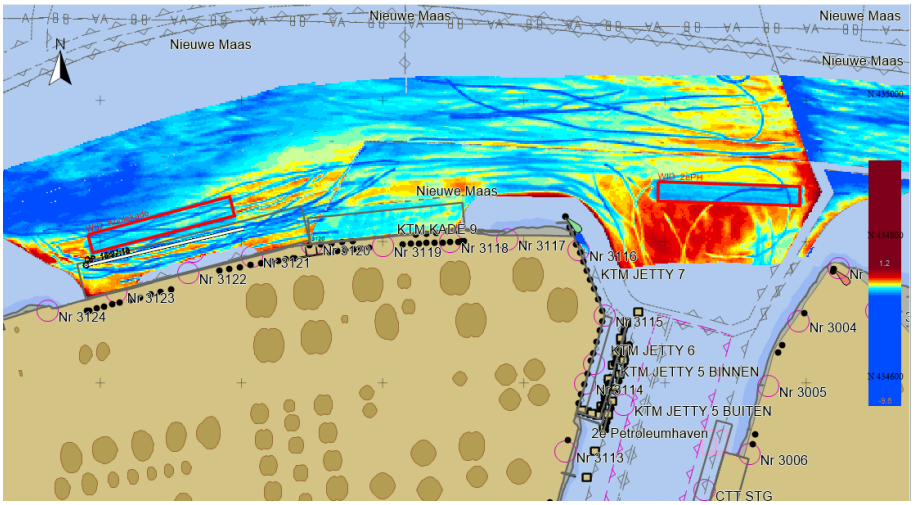

Figure 513: Estuary 2nd Petroleumhaven WID monitor week 3 (week 51).

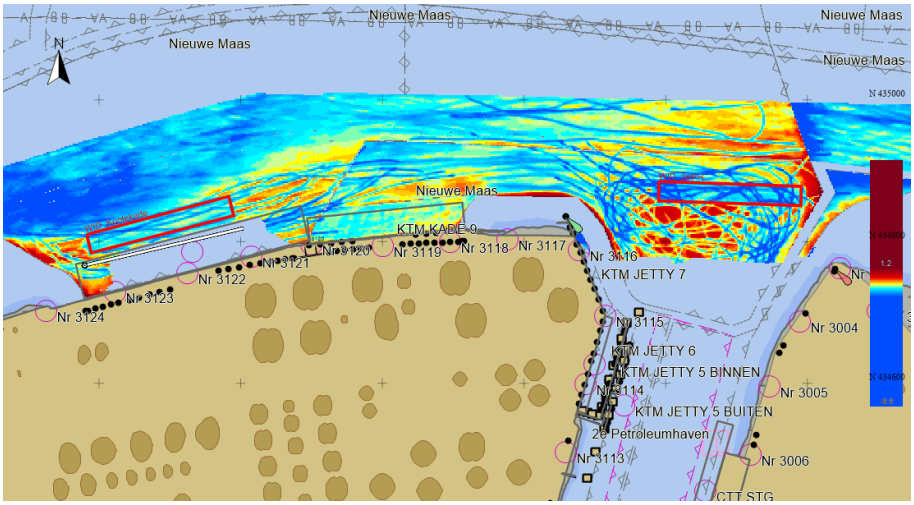

Figure 514: Estuary 2nd Petroleumhaven WID monitor week 5 (week 1).

Underwater plough

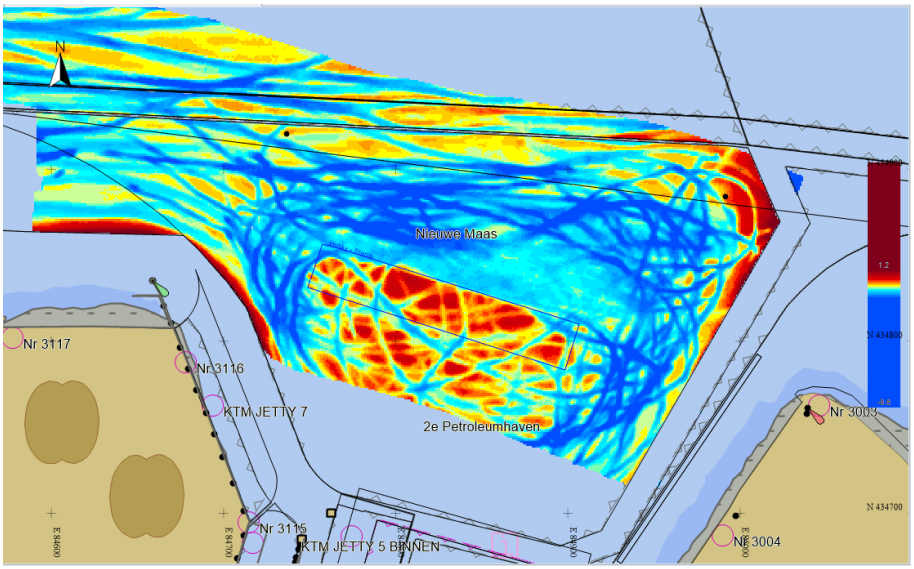

Figure 515: Reference data (week 4).

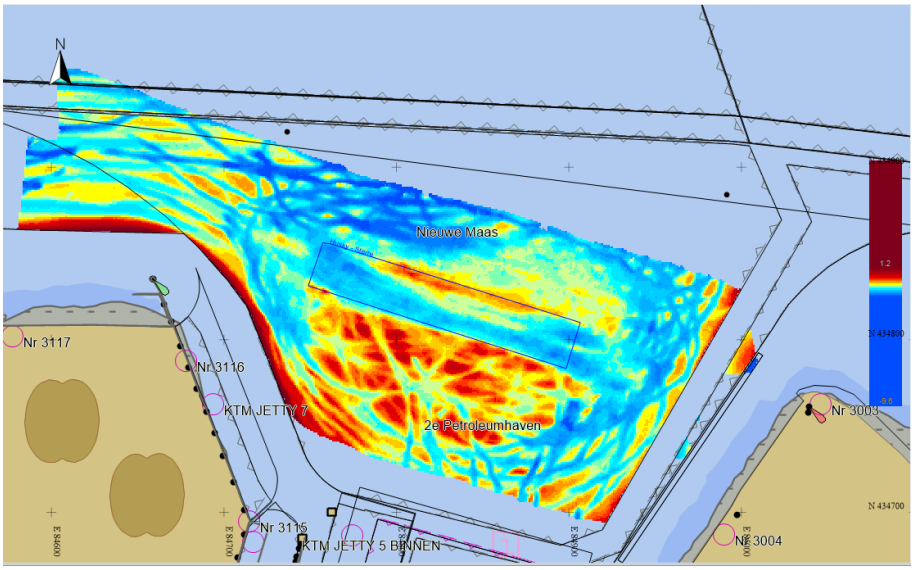

Figure 516: Pilot week (week 5).

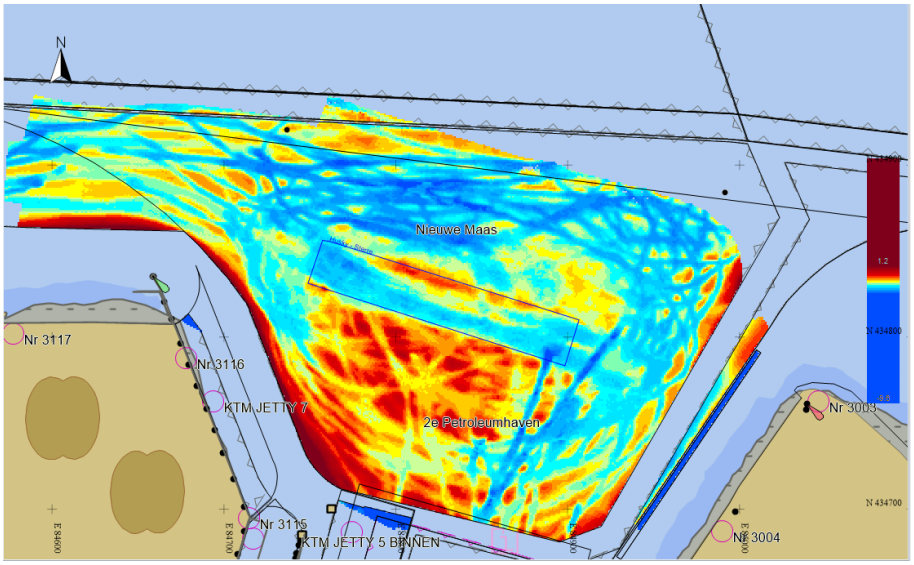

Figure 517: Monitor week 1 (week 6).

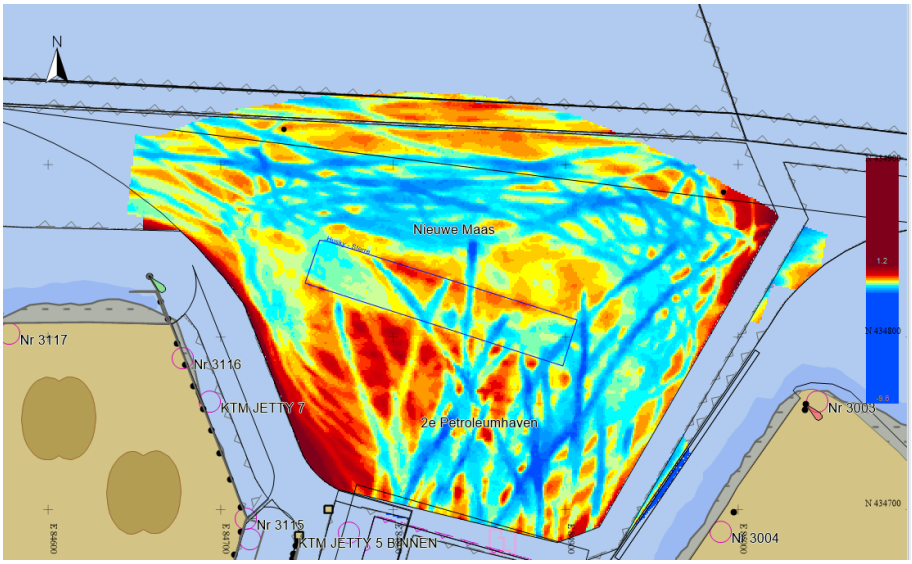

Figure 518: Monitor week 2 (week 7).

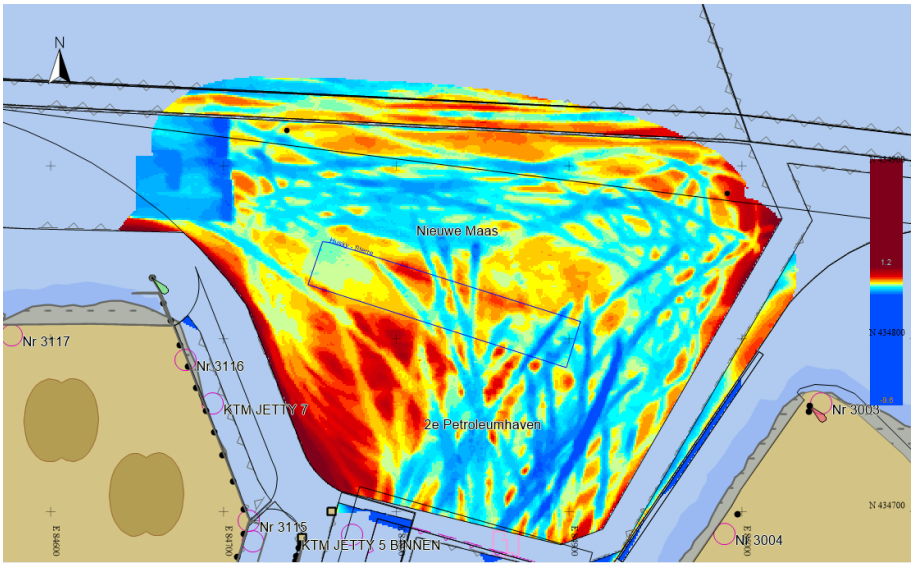

Figure 519: Monitor week 3 (week 8).

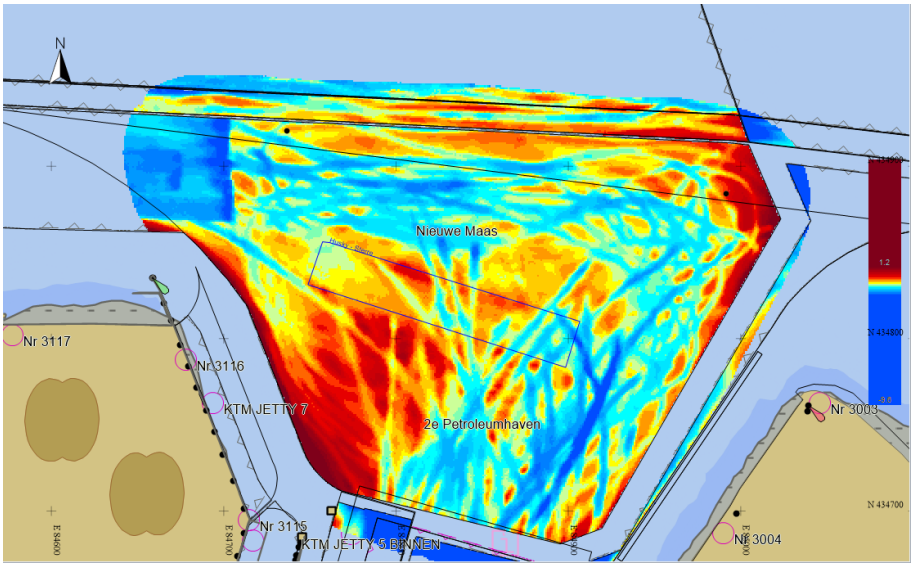

Figure 520: Monitor week 4 (week 9).

Appendix VIII: Calculations

The calculations can be found in this appendix.

Minimal current velocity

Europahaven

The following parameters are the same for the Europahaven left and right areas. Engineering Toolbox and My agriculture information bank are used to determine the density of the particles. The parameters for the EH are shown in table 9.

Parameter	**Value**	**Unit**
D_{peak}	209	μm
Depth where the pipe brings the sediments	14	m
ρ_s	2659	g/L
ρ_w	1010	g/L
Temperature water	16.3	$^\circ$ Celcius
η	0.00105	Pa·s

Table 9: The parameters for EH.

With equation 6 the settling velocity is calculated.
$u_{settling}$=$\frac{(209 \cdot 10^{-6})^2 \cdot 9.81 \cdot (2659-1010)}{18 \cdot 0.00105}$ = 0.037 m/s

The settling velocity with equation 6 is checked by calculating the settling velocity again using the turbidity profiles. In table 10 the parameters from the turbidity profiles are given.

Day	**Time [minutes]**	**Depth [m]**	**Turbidity [NTU]**
17 October	116	-4	20.773
17 October	132	-20.38	19.98
18 October	175	-6.15	19.78
18 October	182	-15.50	22.414

Table 10: The parameters from the vertical turbidity profiles for EH right area.

$u_{settling1710}$=$\frac{20.38-4}{(132-116) \cdot 60}$=0.017 m/s
$u_{settling1810}$=$\frac{15.50-6.15}{(182-175) \cdot 60}$=0.022 m/s

The settling velocity is in the same order as the settling velocity calculated using equation 6. But there are differences due to other assumptions. For this calculation, the vertical turbidity profiles

are used at one location.

In table 11, the parameter from the vertical turbidity profiles for EH left area can be found.

Day	**Time [minutes]**	**Depth [m]**	**Turbidity [NTU]**
17 October	5	-7.49	15.67
17 October	31	-20.72	15.18

Table 11: The parameters from the vertical turbidity profiles for EH left area.

$u_{settling1710}$=$\frac{20.72-7.49}{(31-5)\cdot 60}$=0.0086 m/s

The settling velocity calculated using equation 6 is significantly larger than the settling velocity determined from the turbidity profiles. This disparity can be attributed to the presence of two peaks in the PSD, as depicted in figure 15. One peak is in the coarser sediments, while the other peak is in the finer particles. Finer particles are more easily transported, and since the Swift Turbidity is situated in the outgoing tidal stream, it is likely that finer particles are causing the turbidity at the location. Furthermore, it has been confirmed through analysis of the PSD before and after that, the coarser sediments have shifted to deeper areas of the region, this means that the finer sediments are in the tidal outgoing stream. Since the settling velocity for finer particles is lower, this could account for the differences observed between the calculated settling velocity using equation 6, which is based on the density of fine sand from the peak in coarser sediments, and the settling velocity determined from the turbidity profiles.

In the case of Europahaven, directing particles towards the Beerkanaal, where the currents are stronger, can be useful. The water depth in this area of approximately 3 meters above the bed is necessary, it allows the particles to be easily transported by the strong currents. Also, the distance from the middle of the pilot area to the middle of the Beerkanaal is taken. For the next calculations the settling velocity calculated with equation 6, Stoke's Law, is used. In table 12 the distances for EH can be found.

Parameter	**Value**	**Unit**
Depth	14-3=11	m
Distance left area	1718	m
Distance right area	1374	m

Table 12: Distance parameters for EH.

The time it takes for the particle to reach the depth is: $\frac{11}{0.037}$=294.22 s.
This will give a minimal current velocity for the right area of $\frac{1374}{294.22}$=4.67 m/s.
And a minimal current velocity for the left area of $\frac{1718}{294.22}$=5.83 m/s.

Koolekade

In table 13 the parameters for KK can be found. Engineering Toolbox and My agriculture information bank are used to determine the density of the particles.

Parameter	**Value**	**Unit**
D_{peak}	14	μm
Depth where the pipe brings the sediments	12	m
ρ_s	2837	g/L
ρ_w	1010	g/L
Temperature water	14.9	$^\circ$ Celcius
η	0.00102	Pa·s

Table 13: The parameters for KK.

With equation 6 the settling velocity is calculated.
$u_{settling}=\frac{(14\cdot10^{-6})^2\cdot9.81\cdot(2837-1010)}{18\cdot0.00102}$ = 0.00019 m/s

Again to check the value of the settling velocity calculated with equation 6, the settling velocity is also calculated using the vertical turbidity profiles. In table 14 the parameters from the vertical turbidity profiles can be found.

Day	**Time [minutes]**	**Depth [m]**	**Turbidity [NTU]**
21 October	67	-6.77	256.06
21 October	257	-14.48	218.44

Table 14: The parameters from the vertical turbidity profiles for KK.

$u_{settling2110}=\frac{14.48-6.77}{(257-67)\cdot60}$=0.00067 m/s
The settling velocity determined from the turbidity profiles is in the same order as the settling velocity calculated using equation 6, but the turbidity-derived settling velocity is slightly higher. This may be due to the fact that the turbidity in this location was spread throughout the water column, making it more challenging to determine where the plume had settled using vertical turbidity profiles.

In the case of the Koolekade, directing particles towards the estuary of the Botlek, where the currents are stronger, can be useful. The water depth in this area of approximately 3 meters above the bed is necessary, it allows the particles to be easily transported by the strong currents. Also the distance from the middle of the pilot area to the middle of the estuary of the Botlek is taken. For the next calculations the settling velocity calculated with equation 6, Stoke's Law, is used. In table 15 the parameters of the distance for KK can be found.

Parameter	Value	Unit
Depth	12-3=9	m
Distance	3463	m

Table 15: Distance parameters for KK.

The time it takes for the particle to reach the depth is: $\frac{9}{0.00019}$ =47038.41 s.
This will give a minimal current velocity for the right area of $\frac{3463}{47038.41}$= 0.074 m/s.

Estuary of the 2nd Petroleumhaven

In table 16, the parameters for PH can be found. Engineering Toolbox and My agriculture information bank are used to determine the density of the particles.

Parameter	Value	Unit
D_{peak}	13.8	μm
Depth where the pipe brings the sediments	12	m
ρ_s	2837	g/L
ρ_w	1010	g/L
Temperature water	14.9	° Celcius
η	0.00102	Pa·s

Table 16: The parameters for PH.

With equation 6 the settling velocity is calculated.
$u_{settling}$=$\frac{(13.8\cdot10^{-6})^2\cdot9.81\cdot(2837-1010)}{18\cdot0.00102}$ = 0.00019 m/s

Again to check the value of the settling velocity calculated with equation 6, the settling velocity is also calculated using the vertical turbidity profiles. In table 17 the parameters from the vertical turbidity profiles can be found.

Day	Time [minutes]	Depth [m]	Turbidity [NTU]
19 October	53	-8.04	40.82
19 October	141	-13.25	42.72
20 October	14	-6.21	121.34
20 October	184	-14.97	121.85

Table 17: The parameters from the vertical turbidity profiles for PH.

$u_{settling1910}$=$\frac{13.25-8.04}{(141-53)\cdot60}$=0.00099 m/s
$u_{settling2010}$=$\frac{14.97-6.21}{(184-14)\cdot60}$=0.00086 m/s

The settling velocity determined from the turbidity profiles is in the same order as the settling velocity calculated using equation 6, but the turbidity-derived settling velocity is slightly higher. This may be due to the fact that the turbidity in this location was higher and spread out further into the waterway due to high currents, making it more challenging to determine where the plume had settled using vertical turbidity profiles.

In this case, directing particles toward the estuary of the Botlek, where the currents are stronger, can be useful. The water depth in this area of approximately 3 meters above the bed is necessary, it allows the particles to be easily transported by the strong currents. Also, the distance from the middle of the pilot area to the middle of the estuary of the Botlek is taken. For the next calculations the settling velocity calculated with equation 6, Stoke's Law, is used. In table 18 the distances parameters for PH can be found.

Parameter	**Value**	**Unit**
Depth	12-3=9	m
Distance	4374	m

Table 18: Distance parameters for PH.

The time it takes for the particle to reach the depth is: $\frac{9}{0.00019}$= 48411.56 s.
This will give a minimal current velocity for the right area of $\frac{4374}{48411.56}$= 0.090 m/s.

Boundary conditions of the Tiamat

The parameters are the parameters for the boundary conditions of the Tiamat and can be found in table 19. Engineering Toolbox and My agriculture information bank are used to determine the density of the particles.

Parameter	**Value**	**Unit**
D_{peak}	195	μm
D_{peak}	210	μm
Depth where the pipe brings the sediments	14	m
ρ_s	2659	g/L
ρ_w	1010	g/L
Temperature water	16.3	$^\circ$ Celcius
η	0.00105	Pa·s

Table 19: Distance parameters for the boundary conditions.

With equation 6 the settling velocity is calculated.
$u_{settling195}$=$\frac{(195\cdot10^{-6})^2\cdot9.81\cdot(2659-1010)}{18\cdot0.00105}$ = 0.033 m/s

$u_{settling210}$=$\frac{(210 \cdot 10^{-6})^2 \cdot 9.81 \cdot (2659-1010)}{18 \cdot 0.00105}$ = 0.038 m/s
For this case we take the Europahaven, directing particles towards the Beerkanaal, where the currents are stronger, which can be useful. The water depth in this area of approximately 3 meters above the bed is necessary, it allows the particles to be easily transported by the strong currents. Also, the distance from the middle of the pilot area to the middle of the Beerkanaal is taken, the distances can be found in table 20.

Parameter	**Value**	**Unit**
Depth	14-3=11	m
Distance right area	1374	m

Table 20: Distance parameters for the boundary conditions in EH.

The time it takes for the particle of 195 μm to reach the depth is: $\frac{11}{0.033}$=337.98 s.
The time it takes for the particle of 210 μm to reach the depth is: $\frac{11}{0.038}$=291.42 s.
Taking the distance for the Europahaven as an example for 195 μm, the minimal current velocity needs to be: $\frac{1374}{337.99}$=4.06 m/s
Taking the distance for the Europahaven as an example for 210 μm, the minimal current velocity needs to be: $\frac{1374}{291.42}$=4.71 m/s
More general, for 195 μm the minimal current velocity in m/s needs to be $0.0030 \cdot distanceinmeters$.
More generally, for 210 μm the minimal current velocity in m/s needs to be $0.0034 \cdot distanceinmeters$.

Tiamat maximum production rate

For calculating the maximum production rate when using the Tiamat more often the production rates of Harwich Haven Authority (HHA) are used. With the slope of the production rate graph. First, their production rate needed to be calculated. HHA calculated the production rate with equation 9:

$$Actualproduction = nettoproduction + accretion \tag{9}$$

The production rate used for the Port of Rotterdam is also used to calculate the net production rate for Harwich Haven Authority. However, the Port of Rotterdam experiences significantly lower sedimentation per hour, which can be ignored when calculating the production rate. This can also be seen from the Multibeam depth profiles over time, which show only a small increase in depth during monitor weeks, indicating minimal sedimentation. However, to use the data of Harwich Haven Authority, the production rate must be calculated in the same way as for the Port of Rotterdam. Therefore, the net production rate is calculated and used to create the graph. The slopes are calculated and can be found in table 21.

Between days	**Slope** [m^3/day]
1 and 7	1864.71/7=266.39
7 and 11	(2181-1864.71)/4=79.04
11 and 18	(8769.5-2181)/7=941.21

Table 21: Slope in the production rate graph for Harwich per day.

The dredging time per day for Harwich Haven Authority was 10 hours. For calculating the slope for the Port of Rotterdam the slope from Harwich Haven Authority needs to be divided by 10 hours, this can be found in table 22.

Between days	**Slope** [m^3/OH]
1 and 7	26.46
7 and 11	79.07
11 and 18	941.21

Table 22: Slope in the production rate graph for Harwich per hour.

Then the following point in the graph for the Port of Rotterdam is calculated and can be found in table 23.

Day	**Production rate** [m^3/OH]
7	26.46 * 5 + 321.09 = 454.09
11	7.91 * 4 + 454.29 = 485.93
18	94.12 * 7 + 485.93 = 1144.77

Table 23: Production rates for the Port of Rotterdam calculated using the data of Harwich.

Appendix IX: Tracks

In this appendix, the tracks of the Barney with the Tiamat and the tracks of the Mersey with the WID can be found. This information is used to determine whether one area is better dredged than another area. This is also used to brighten up uneven dredging profiles.

Tracks with the Tiamat

First, tracks of the Barney with the use of the Tiamat are displayed in the areas.

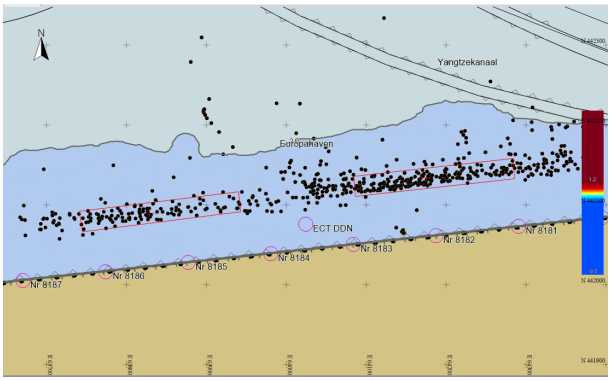

(a) Tracks of the Barney (Tiamat) at EH.

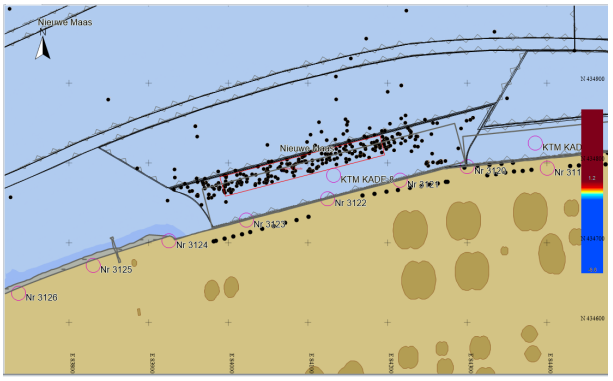

(b) Tracks of the Barney (Tiamat) at KK.

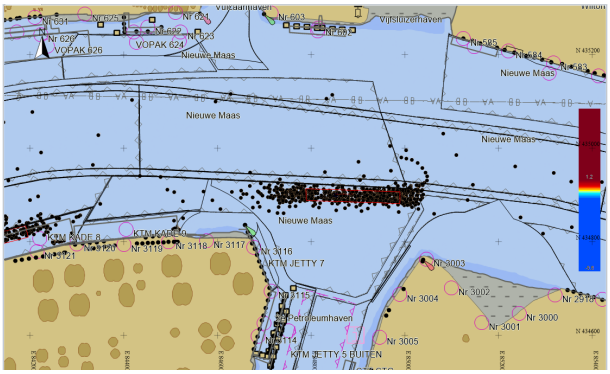

(c) Tracks of the Barney (Tiamat) at PH.

Figure 521: Dredging tracks of the Tiamat in the areas.

The density of dots in a given location indicates the frequency of dredging activity in that area. A comparison of the two Europahaven locations reveals that the right area displays a greater density of dots than the left area, as it was dredged for a longer period of two days. The region located in at PH exhibits the highest concentration of dots, likely due to the fact that it was dredged for the longest duration and with greater precision across the entire pilot area. The EH was the location

where the pilot started and the Tiamat staff needed to become acquainted with the work area. After the EH feedback was provided and the other dredging days of the pilot were conducted with even greater efficiency.

Tracks with the WID

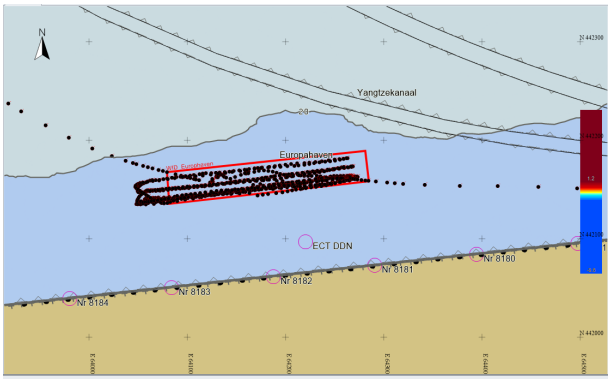

(a) Tracks of the Mersey (WID) at EH.

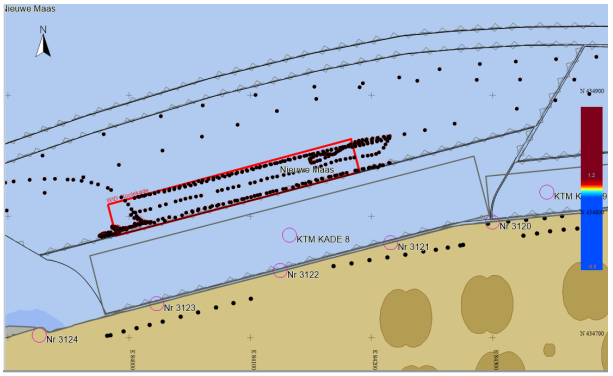

(b) Tracks of the Mersey (WID) at KK.

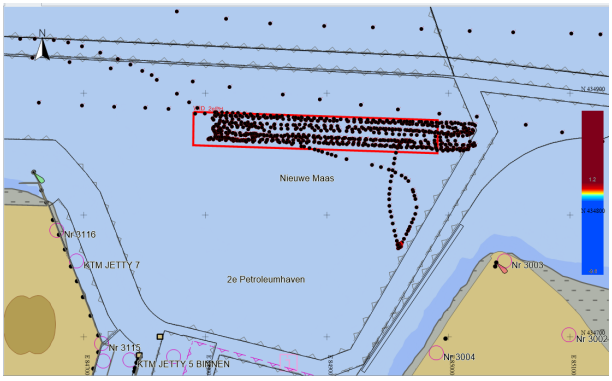

(c) Tracks of the Mersey (WID) at PH.

Figure 522: Dredging tracks of the Water Injection Dredger in the areas.

Again, the density of the dots in a given location indicates the frequency of dredging activity in that area. Comparing the K with the other two locations reveals a lower density of the dots. This is because the location is done for a shorter time. It appears from the data that the dredging activity in the EH may have resulted in a shift of the dredged area towards the left.

Appendix X: Technical drawing of the Tiamat

Here a technical drawing with some specifications of the Tiamat can be found.

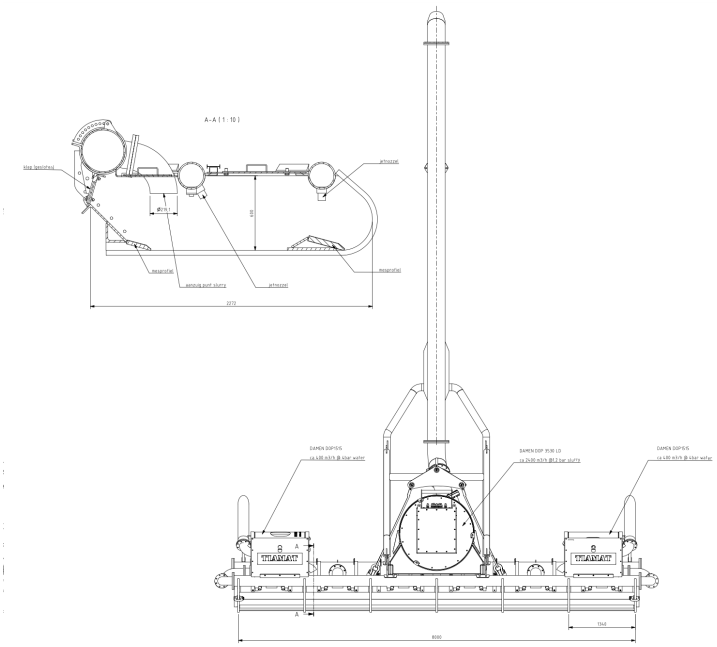

Figure 523: Technical drawing of the Tiamat (de Haas, 2022)